EVALUATION OF THE SEISMIC RESPONSE OF GENTLE SLOPES IN SOFT CLAY

Cristian Yair Soriano Camelo

Tese de Doutorado apresentada ao Programa de Pós-graduação em Engenharia Civil, COPPE, da Universidade Federal do Rio de Janeiro, como parte dos requisitos necessários à obtenção do título de Doutor em Engenharia Civil.

Orientadores: Marcio de Souza Soares de Almeida
Maria Cascao Ferreira de Almeida

Rio de Janeiro
Maio de 2021

EVALUATION OF THE SEISMIC RESPONSE OF GENTLE SLOPES IN SOFT CLAY

Cristian Yair Soriano Camelo

TESE SUBMETIDA AO CORPO DOCENTE DO INSTITUTO ALBERTO LUIZ COIMBRA DE PÓS-GRADUAÇÃO E PESQUISA DE ENGENHARIA DA UNIVERSIDADE FEDERAL DO RIO DE JANEIRO COMO PARTE DOS REQUISITOS NECESSÁRIOS PARA A OBTENÇÃO DO GRAU DE DOUTOR EM CIÊNCIAS EM ENGENHARIA CIVIL.

Orientadores: Marcio de Souza Soares de Almeida
                       Maria Cascao Ferreira de Almeida

Aprovada por: Prof. Marcio de Souza Soares de Almeida
                       Prof. Maria Cascão Ferreira de Almeida
                       Prof. Amir Kaynia
                       Prof. Bernardo Caicedo
                       Prof. Gopal Madabhushi
                       Prof. Mauricio Ehrlich

RIO DE JANEIRO, RJ – BRASIL
MAIO DE 2021

Acknoledgments

Resumo da Tese apresentada à COPPE/UFRJ como parte dos requisitos necessários para a obtenção do grau de Doutor em Ciências (D.Sc.)

AVALIAÇÃO DA RESPOSA SÍSMICA DE TALUDES SUAVES EM ARGILA MOLE

Cristian Yair Soriano Camelo

Maio/2021

Orientadores: Marcio de Souza Soares de Almeida
Maria Cascao Ferreira de Almeida

Programa: Engenharia Civil

Esta tese examina a resposta sísmica de taludes suaves com ângulos de inclinação de três e seis graus em argila mole mediante ensaios centrífugos e modelagem numérica. Desenvolveu-se uma metodología de preparação de modelos para a simulação de perfis uniformes e um perfil considerando a presença de uma camada fraca de argila. Os ensaios centrífugos foram feitos no Schofield Centre, Universidade de Cambridge, sendo os modelos submetidos a uma aceleração centrífuga de 60g e os sismos aplicados mediante uma mesa vibratória embarcada. Ensaios de caracterização em vôo da resistência não drenada e da velocidade de onda cisalhante foram feitos empregando T-bar e Air Hammer, respectivamente. Os modelos centrífugos foram submetidos a uma série de carregamentos dinâmicos com diferentes amplitudes e conteúdos de frequência, com a resposta monitorada com acelerômetros, transdutores de poro pressão e transdutores de deslocamento. Dados complementares foram obtidos a partir de velocimetría por imagem de partículas (PIV). Os resultados dos ensaios centrífugos foram utilizados para a calibração de modelos numéricos em OpenSees simulando colunas de solo 3-D e um modelo constitutivo dinâmico, não linear. Finalmente, uma série de simulações numéricas foram feitas para avaliar a resposta de taludes submarinos representativos da Bacía de Campos, no sudeste brasileiro. Os efeitos de fatores como a inclinação do talude e a espessura da camada de solo foram considerados para fornecer informações referentes ao comportamento de taludes submarinos durante eventos sísmicos.

EVALUATION OF THE SEISMIC RESPONSE OF GENTLE SLOPES IN SOFT CLAY

Cristian Yair Soriano Camelo

May/2021

Advisors: Marcio de Souza Soares de Almeida
Maria Cascao Ferreira de Almeida

Department: Civil Engineering

This thesis examines the seismic response of gentle slopes in soft clay through centrifuge experiments and numerical modeling. A series of centrifuge tests considering slope angles of 3 and 6 degrees was performed on kaolin clay models. A model preparation methodology was developed to simulate uniform soil profiles and to consider the presence of a soft weak layer. The centrifuge experiments were carried out at the Schofield Centre, University of Cambridge, using models tested at an acceleration of 60g, and the earthquake ground motions were applied with a shaking table. In-flight characterization of the undrained shear strength and shear wave velocities was achieved by means of T-bar and air hammer tests. The centrifuge models were subjected to a series of input motions with different amplitudes and frequency content, and the response was monitored using accelerometers, pore pressure sensors and displacement transducers. Complementary data were obtained using particle image velocimetry (PIV). The centrifuge test data were utilized to calibrate numerical models in the software OpenSees using three-dimensional soil columns and a dynamic nonlinear constitutive model. Finally, a series of numerical simulations was performed to evaluate the seismic response of submarine slopes representative of the offshore Campos Basin in southeastern Brazil. The influences of slope inclination and depth to bedrock were addressed to provide insight into the performance of submarine slopes under various seismic events typical of intraplate areas.

Contents

List of Figures

xvii

List of Tables

Nomenclature

ABBREVIATIONS

AHD	Air Hammer
$COPPE$	Instituto Alberto Luiz Coimbra de Pós-Graduação e Pesquisa de Engenharia
CPT	Cone Penetration Test
ESB	Equivalent Shear Beam
$GEBCO$	General Bathymetric Chart of the Oceans
HPC	Hinged Plate Container
$LMC2$	Laboratório Multiusuário em Modelagem Centrífuga
$LVDT$	Linear Variable Differential Transformer
$PEER$	Pacific Earthquake Engineering Research
$PIMY$	Pressure Independent Multiyield
PIV	Particle Image Velocimetry
PPT	Pore Pressure Transducer
RSN	Record Sequence Number
$UFRJ$	Universidade Federal do Rio de Janeiro
SF	factor of safety

SYMBOLS

g	gravity acceleration (m/s^2)
N	model scale factor
t	time (s)
K_0	Coefficient of at-rest earth pressure
PI	Plasticity Index (%)
σ'_v	Vertical effective stress (kPa)
x_i, y_i	PIV marker coordinates (pixels)
X_i, Y_i	PIV marker coordinates (m)

V	Normalized penetration rate of the T-bar
v	T-bar penetration velocity (mm/s)
D	T-bar diameter (mm)
c_v	Coefficient of consolidation (mm^2/s)
OCR	Overconsolidation Ratio
K	Normalized strength parameter
m	Power constant
s_u	Undrained shear strength (kPa)
$T_{sr}[n]$	Cross-correlation function
ΔZ_{ij}	Distance between accelerometers (m)
Δt_{ij}	Arrival time between accelerometers (s)
G_0	Initial shear modulus (kPa)
V_s	Shear wave velocity (m/s)
ρ	soil density
T	elastic site period (s)
PGA	Peak Ground Acceleration (g)
PSA_0	5% damped pseudo acceleration response spectra at the surface of the model (g)
PSA_b	damped pseudo acceleration response spectra at the base of the model (g)
z	Depth coordinate (m)
τ	Shear stress (kPa)
$\ddot{u}$	Absolute horizontal acceleration (m/s^2)
$\bar{u}$	Bedrock horizontal displacement (m)
G_{sec} , G	Secant shear modulus (kPa)
D	Damping (%)
γ_{sat}	Saturated unit weight (kN/m^3
f_{max}	Maximum frequency (Hz)
λ_{min}	Minimum wavelength (m)
h_{max}	Maximum allowable size of a mesh element
$[C]$	Viscous damping matrix
$[M]$	Mass matrix
a_0, a_1	Rayleigh damping coefficients
D_b	Bracketed duration (s)
D_s	Significant duration (s)
AI	Arias intensity (%)
m	Power constant
M	Earthquake magnitude
H	Depth to bedrock (m)

Chapter 1

Introduction

1.1 Problem statement and motivation

The study of deep-water continental slopes is widely motivated by the hydrocarbon industry and, recently, by the development of renewable sources of energy. With this development, a series of offshore geohazards have been identified and defined. The Norwegian Geotechnical Institute (NGI, 2005) defines offshore geohazards as local and regional conditions that may lead to accidental events affecting life, health, the environment or assets. Geohazards include slope instability and mass movements, seismic hazards and phenomena associated with pore pressure. Infrastructure projects are not risk free: risk can be managed, minimized, shared, transferred or accepted, but it cannot be ignored (Latham, 1994).

Among the offshore geohazards, submarine landslides represent a widespread phenomenon around the world, varying from large-scale landslides (Embley, 1980; O´Leary, 1996, Mosher *et al.*, 2004; Vanneste *et al.*, 2006) to minor scale instabilities (Lastras *et al.*, 2004; L´Hereux *et al.*, 2012). The unique features of submarine landslides include their significant volume of mass movements and large travel distances at very gentle slopes (Gue, 2012). Part of the overall risk assessment in offshore oil and gas projects involves understanding the various geotechnical-geological processes that generate hazardous conditions, particularly seismic-induced landslides. Recognizing the importance of the seismic stability of submarine slopes, researchers have made significant contributions to understand the dynamic behavior of submarine slopes, mechanisms of earthquake-induced deformations in slopes, liquefaction and cyclic mobility during seismic events (Prior, 1984; Hampton *et al.*, 1996; Locat Lee, 2000; Biscontin *et al.*, 2004, Kvalstad *et al.*, 2005; Coulter, 2005; Biscontin *et al.*, 2006).

Despite previous and ongoing research on seismic stability of submarine slopes, some areas still need further research and attention, particularly the behavior of gentle slopes (with inclination angles from 1° to 5°, according to Masson *et al.*, 2006) under seismic loading.

Centrifuge modelling is a well-established approach to investigating geotechnical problems when the soil conditions are difficult, the constitutive models for the soils are not defined or the loading is unusual or extreme (Madabhushi, 2014). This research uses centrifuge modelling to study the seismic response of gentle slopes in soft clay under seismic loading.

Regarding the Brazilian context, recent studies performed at COPPE-UFRJ centrifuge laboratory (LMC2) and supported by Petrobras, have focused on various topics such as: occurrence of hydroplaning and turbidity currents (Acosta *et al.*, 2017; Pelissaro, 2018; Hotta *et al.*, 2019), on the seismic response of clayey submarine canyons representative of Brazilian offshore conditions (Tarazona, 2019; Tarazona *et al.*, 2020) and also on the assessment of seismic hazards on the continental margin of southeastern Brazil (Borges *et al.*, 2019).

A gap in knowledge was identified during the development of this thesis. Specifically the seismicity in Brazil and its effects on the response of submarine gentle slopes, particularly in the offshore Campos Basin. This region represents a significant pole in the Brazilian economy and is one of the most prolific oil-producing basins (Cobbold *et al.*, 2001). The Campos Basin is located in the Southeastern margin, offshore the states of Rio de Janeiro (RJ) and Espirito Santo (ES), covering an area of around 100,000 km^2 (Castro and Picolini, 2015).

The submarine physiography of the Campos Basin comprises four physiographic provinces (Figure 1.1): continental shelf, continental slope, São Paulo plateau and continental rise of slope (Almeida and Kowsmann, 2015). From the physiographic features of the Campos Basin, the continental slope has a wide range of declivities ranging from 0 to 10 degrees with the highest values associated to the presence of submarine canyons (Figure 1.2). The São Paulo plateau can be defined as a horizontal area from a regional point of view with declivities ranging between 0 degrees to 2 degrees (Figure 1.2). Considering the geomorphology of the Campos Basin, this research aims at studying the slopes with a low gradient (gentle slopes), distributed across extended areas.
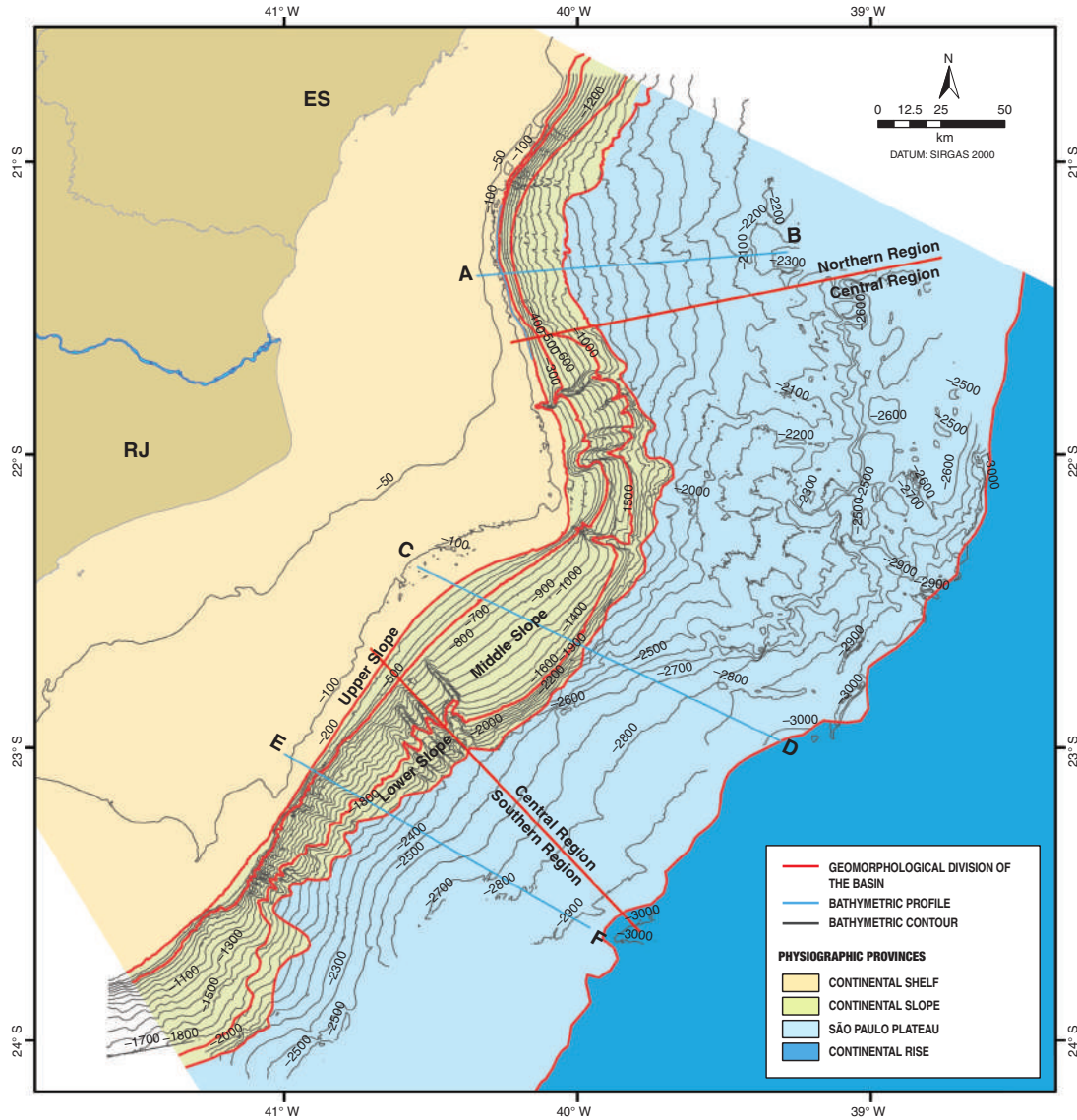
Figure 1.1: Bathymetry chart of Campos Basin with physiographic province boundaries (Almeida and Kowsmann, 2015)
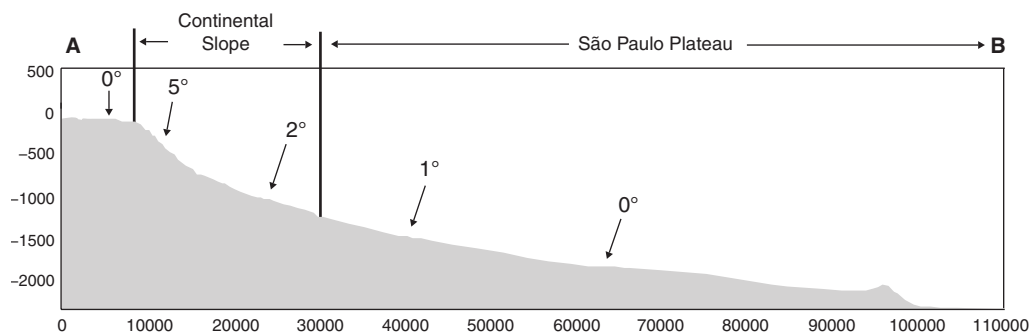
Figure 1.2: Bathymetric profiles and declivities of the northern region (A-B), central region (C-D) and southern region (E-F) of the Campos Basin. (Almeida and Kowsmann, 2015)
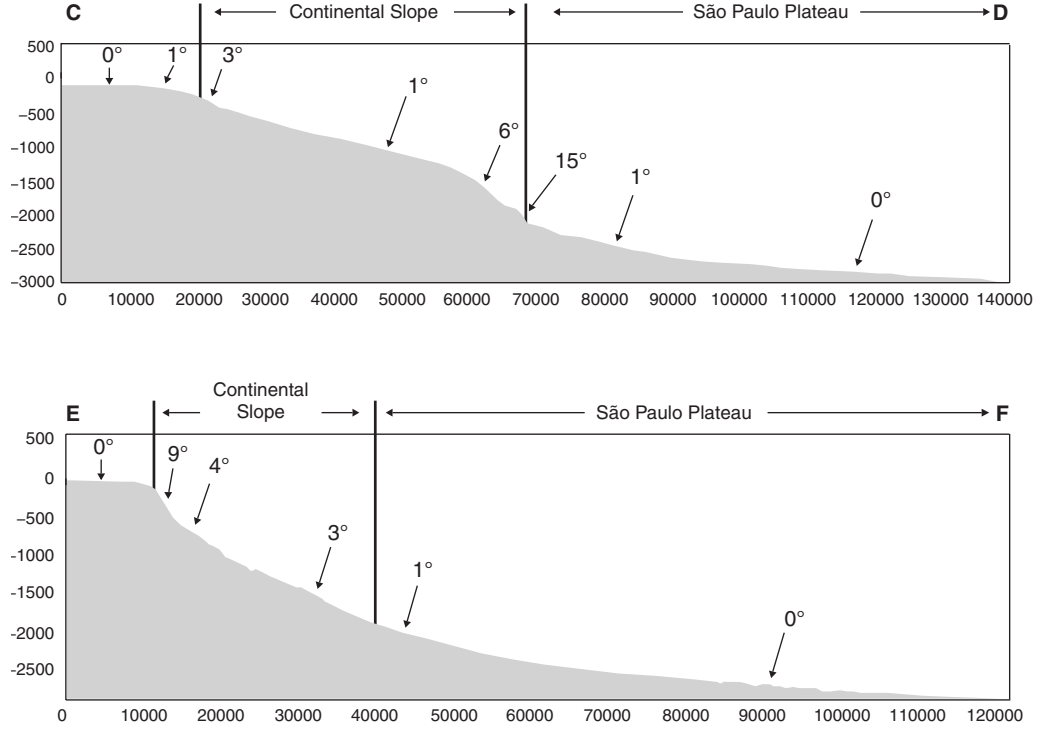
Figure 1.2: Bathymetric profiles and declivities of the northern region (A-B), central region (C-D) and southern region (E-F) of the Campos Basin. (Almeida and Kowsmann, 2015) (*cont.*)

In terms of the seismic hazards in the area of interest, Brazil is in a large mid-plate region of low to moderate seismicity. As previously stated, offshore geohazards, including earthquakes, cannot be ignored. As a result, notable efforts have been made in recent years to improve instrumental monitoring of earthquakes, to research and review historical seismicity and to update seismic hazard estimates (Borges *et al.*, 2019). The experimental results from the centrifuge tests performed allowed the calibration and validation of numerical models as a baseline for parametric studies. The parametric studies included representative parameters of the offshore Campos Basin, such as the topography and soil parameters such as the undrained shear strength and shear wave velocities, fundamental inputs for seismic site response analyses. Seismic hazards and input ground motions were additionally included in the parametric analyses using the mean uniform hazard response spectra for the Campos Basin, developed by Borges *et al.* (2019).

1.2 Objective

The primary objective of this work is to present a research program on the physical modelling of the seismic behavior of gentle slopes in clay, considering uniform profiles and a particular scenario, including a weak layer since these are typical features in offshore environments. The experimental results will be inputs for the calibration

4

of numerical models, resulting in a parametric study applied to the seismic response of submarine slopes in the offshore Campos Basin.

1.2.1 Specific objectives

In light of the problem statement and motivation, this research has been structured around the following objectives:

(i) To develop a model preparation technique to simulate the seismic behavior of a gentle slope in clay under seismic loading using a laminar container.

(ii) To describe and analyze the seismic response of gentle slopes based on the measured data obtained from the instrumentation installed in the model, particularly horizontal displacements and accelerations at different depths in the slopes.

(iii) To perform a parametric study on the response of submarine slopes in the offshore Campos Basin using soil strength, slope topography and seismicity parameters representative of the region of interest. Parameters such as slope inclination and depth to bedrock are considered in the analyses.

1.3 Outline of the thesis

This thesis is presented in eight chapters as follows:

Chapter 1: Introduction
A description of the problem is presented, and the scope of the work is briefly outlined.

Chapter 2: Literature review
A literature review of the general features of submarine slopes, offshore geotechnical risks, submarine landslides and physical modelling principles is presented. The chapter ends with a review of experimental and numerical studies related to the seismic response of clays.

Chapter 3: Materials and methods
An introduction to the facilities, equipment, instrumentation and model preparation techniques used to perform the centrifuge tests is presented. Details of the development methodology for particle image velocimetry (PIV) are also presented in this chapter.

Chapter 4: Evaluation of the seismic response of gentle slopes in clay using centrifuge experiments

A series of centrifuge tests were carried out to investigate the seismic behavior of gentle slopes in clay. The chapter explains and presents in detail the results of two centrifuge tests performed on two uniform profile slopes: 3 degrees and 6 degrees. The chapter also presents a comparison of the response of both models in terms of surface displacements and amplification and attenuation of peak ground accelerations (PGA).

Chapter 5: Seismic centrifuge modelling of a gentle slope of layered clay, including a weak layer.

This chapter presents a model preparation methodology to simulate the seismic behavior of a gentle slope in soft clay with the presence of a weak layer. The results of the associated centrifuge test are presented in terms of displacements and accelerations at different depths. A discussion of the experimental results is also presented.

Chapter 6: Numerical modelling of a gentle slope in soft clay

This chapter presents the calibration of a numerical model based on the data from a centrifuge test simulating the seismic response of a uniform slope profile. The chapter discusses the strain rate effects in clay and their potential effects on the seismic response of the physical and numerical models. The chapter closes with the results of a series of additional numerical simulations using the parameters of the baseline model calibrated using data from the centrifuge experiments. The slope angle was varied in those numerical models, and displacement-time histories and permanent displacements at various slope angles were compared.

Chapter 7: Seismic response of submarine gentle slopes in the offshore Campos Basin, southeastern Brazil

This chapter presents a series of parametric numerical analyses of the seismic response of gentle slopes. Geotechnical parameters and input ground motions representative of the offshore Campos Basin in southeastern Brazil were used in the calculations. Additionally, the results and interpretations of the models are provided.

Chapter 8: Conclusions and recommendations for future research studies

The key findings of the research are described and summarized. The implications of this thesis are discussed, and recommendations are outlined for future work in this area.

1.4   Chapter 1 references

ACOSTA, E., TIBANA, S., ALMEIDA, M.S.S., AND SABOYA, F., 2017, "Centrifuge modeling of hydroplaning in submarine slopes," Ocean Engineering, Vol. 129, No.1, pp. 451–458

ALMEIDA, A.G., AND KOWSMANN, R.O., 2015, "Geomorphology of the continental slope and São Paulo Plateau," In: Kowsmann, R.O., editor. Geology and Geomorphology. Rio de Janeiro: Elsevier. Habitats, Vol. 1, p. 33-66.

BISCONTIN, G. AND PESTANA, J.M., 2006, "Factors affecting seismic response of submarine slopes," Natural Hazards and earth systems sciences, Vol. 6, .pp.97-107

BISCONTIN, G., PESTANA, J.M., AND NADIM, F., 2004, "Seismic triggering of submarine slides in soft cohesive soil deposits," Marine Geology, Vol. 203, pp. 341-354.

BORGES, R.G., ASSUMPÇAO, M.S., ALMEIDA, M.C.F., AND ALMEIDA, M.S.S., 2020, "Seismicity and seismic hazard in the continental margin of southeastern Brazil," J. Seismol, Vol.24, pp. 1205-1224.

CASTRO, R.D., AND PICOLINI, J.P. 2015, "Main features of the Campos Basin regional geology," In: Kowsmann, R.O., editor. Geology and Geomorphology. Rio de Janeiro: Elsevier. Habitats, Vol. 1, pp. 1-12.

COBBOLD, P.R, MEISLING, K.E., AND MOUNT, VAN.S, 2001, "Reactivation of an Obliquely Rifted Margin, Campos and Santos Basins, Southeastern Brazil," AAPG Bulletin, Vol. 85, No.11, pp. 1925–1944.

COULTER, S.E., 2005, "Seismic initiation of submarine slope failures using physical modeling in a geotechnical centrifuge", M.Eng Thesis, Memorial University of Newfoundland.

EMBLEY, R.W., 1980, "The role of mass transport in the distribution and character of deep-ocean sediments with special reference to north Atlantic," Marine Geology , Vol.38, pp.23-50.

GUE, C. S., 2012, "Submarine landslides simulation using centrifuge modelling," PhD thesis, University of Cambridge.

HAMPTON, M.A., LEE, H.J., AND LOCAT, J., 1996, "Submarine Landslides," Reviews of Geophysics, Vol.34, No.1, pp. 33-59.

HOTTA, M.M., ALMEIDA, M.S.S., PELISSARO, D.T., OLIVEIRA, J.R.M.S., TIBANA, S., BORGES, R.G.B, 2019, "Centrifuge tests for evaluation of submarine-

mudflow hydroplaning and turbidity currents," International Journal of Physical Modelling in Geotechnics, Vol. 20, No. 4, pp 239-253.

KVALSTAD, T.J., ANDRESEN, L., FORSBERG, C.F., BRYN, P., AND WANGEN, M., 2005, "The Storegga slide: evaluation of triggering sources and slide mechanics," Marine and Petroluem Geology, Vol. 22, pp. 245-256.

LASTRAS, G., CANALS, M., URGELES, R., DE BATIST, M., CALAFAT, A.M., AND CASAMOR, J.L., 2004, "Characterisation of the recent BIG95 debris flow deposit on the Ebro margin, Western Mediterranean Sea, after a variety of seismic reflection data," Marine Geology, Vol.213, No.1, pp.235–255

LATHAM, M., AND GREAT BRITAIN. DEPARTMENT OF THE ENVIRONMENT, 1994, "Constructing the team: Joint review of procurement and contractual arrangements in the United Kingdom construction industry ; final report, July 1994", London: HMSO.

L'HEUREUX, J.S., LONGVA, O., STEINER, A., HANSEN, L., VARDY, M., VANNESTE, M., HAFLIDASON, H., BRENDRYEN, J., KVALSTAD, T., FORSBERG, C., CHAND, S., AND KOPF, A., 2012, "Identification of weak layers and their role for the stability of slopes at Finneidfjord, Northern Norway," In: Yamada, Y., Kawamura, K., Ikehara, K., Ogawa, Y., Urgeles, R., Mosher, D., Chaytor, J., Strasser, M. (Eds.), Submarine Mass Movements and Their Consequences. Springer, Netherlands, pp.321-330.

LOCAT, J. AND LEE, H.J., 2000, "Submarine landslides: Advances and Challenges," Proceedings of the 8th International Symposium on Landslides, Cardiff, UK, 2000. Also published in the (2002) Canadian Geotechnical Journal, Vol.39, pp. 193-212.

MADABHUSHI, S.P.G., 2014, "Centrifuge Modelling for Civil Engineers," In: CRC Press (eds.), London, New York

MASSON, D.G., HARBITZ, C.B., WYNN, B., PEDERSEN, G., AND LOVHOLT, F., 2006, "Submarine landslides: processes, triggers and hazard prediction," Philosophical Transactions of the Royal Society A. M. Vol.364, pp. 2009-2039.

MOSHER, D.C., MONAHAN, P.A., BARRIE, J.V., COURTNEY, R.C., 2004, "Coastal submarine failures in the Strait of Georgia, British Columbia: Landslides of the 1946 Vancouver Island earthquake," J Coast Res. Vol. 20, pp.277–291.

NORWEGIAN GEOTECHNICAL INSTITUTE, (NGI), 2005, "Offshore geohazards. Summary report for research institution-based strategic project 2002-2005", NGI report no.20021023-2.

O'LEARY, D.W., 1996, "The timing and spatial relations of submarine canyon erosion and mass movement on the New England continental slope and rise," in: Gardner, J.V., Field, M.E., and Twichell, D.C., eds., Geology of the United States Seafloor: The view from GLORIA, Cambridge Univ. Press, Cambridge UK, pp. 47–58.

PELISSARO, D. T., 2018, "Modelagem Centrífuga de um Fluxo de Detritos Submarinos," M.Sc dissertation, Federal University of Rio de Janeiro, Rio de Janeiro, Brazil.

PRIOR, D.B.,1984, "Subaqueous landslides," Proceedings of the IV International Symposium on Landslides, Toronto, Vol. 1, pp.179-196.

TARAZONA, S.F.M, 2019, "Evaluation of seismic site response of submarine canyons," D.Sc thesis, Federal University of Rio de Janeiro, Rio de Janeiro, Brazil.

TARAZONA, S.F.M., ALMEIDA, M.C.F., BRETSCHNEIDER, A., ALMEIDA, M.S.S., ESCOFFIER, S., AND BORGES, R.G, 2020, "Evaluation of seismic site response of submarine clay canyons using centrifuge modelling," International Journal of Physical Modelling in Geotechnics, Vol.20, No. 4 pp. 224-238.

VANNESTE, M., MIENERT, J., AND BÜNZ, S., 2006, "The Hinlopen Slide: Agiant, submarine slope failure on the northern Svalbard margin, Arctic Ocean," Earth and Planetary Science Letters, Vol.245, No.1-2, pp.373–388

Chapter 2

Literature Review

2.1 Introduction

This chapter introduces some of the features and characteristics of submarine landslides, as well as the classification systems available in the literature. Further in this chapter, the triggering mechanisms of submarine landslides are introduced with particular emphasis on earthquakes. Some of the principles of dynamic centrifuge modeling are presented jointly with a review of the model containers in dynamic centrifuge experiments. Experimental and numerical works by other researchers are additionally included in this chapter to portray a general picture of the seismic behavior of soft clays.

2.2 Submarine landslides

Submarine landslides belong to the group of potential offshore geohazards. According to the Norwegian Geotechnical Institute (NGI, 2005), offshore geohazards are defined as local and regional site conditions that may lead to failure or accidental events affecting life, health, environment, or assets. Figure 2.1 summarizes the potential offshore geohazards, highlighting submarine landslides as they are the subject of interest of this research. As stated by Masson *et al.* (2006), landslide terminology could be imprecise, particularly in the submarine environment. In this work, analogically to Masson *et al.* (2006) a landslide will be defined as a generic term that encloses all the forms of submarine slope failure independent of the process.
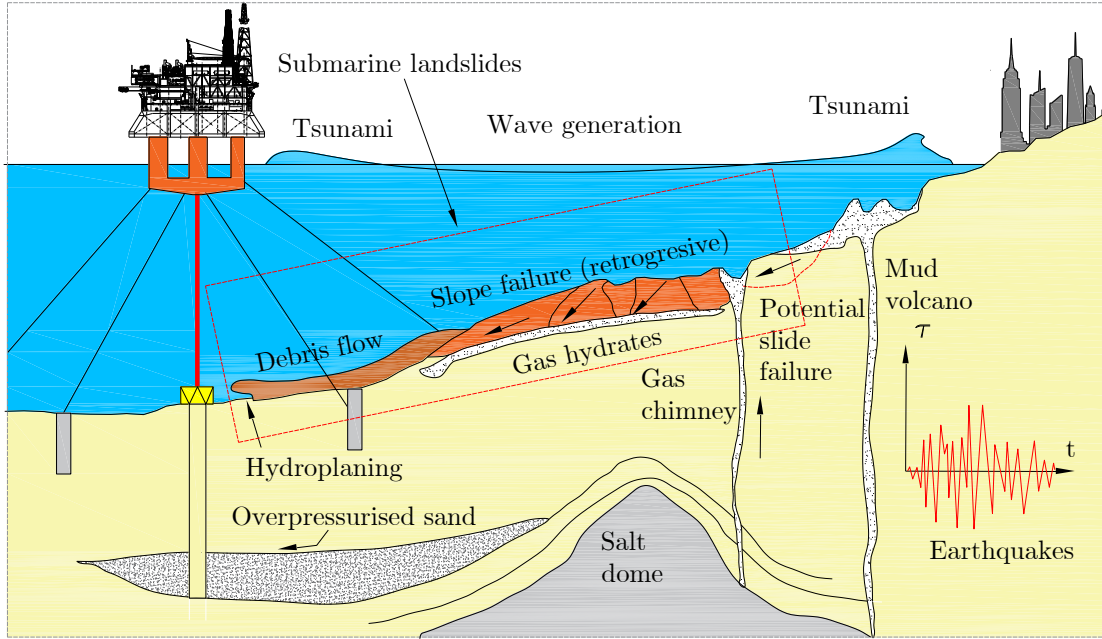
Figure 2.1: A summary of offshore geohazards (modified after NGI, 2005).

As the exploration of renewable and non-renewable sources of energy intensified and expanded to deep offshore continental slopes, new unknown aspects began to appear, like the geotechnical and geological soil conditions and their interaction with the subsea developments (e.g., subsea wells, pipelines, foundations for floating structures, cables, monopiles for wind turbines). Among the potential offshore geohazards, submarine landslides have gained particular attention with the development and improvement of surveying techniques of the seafloor (Locat and Lee, 2000).

To have insight into the behavior of submarine landslides, it is helpful, to begin by identifying the type of constitutive materials of submarine slopes. From the evidence of submarine landslides, a broad range of materials is involved, varying from rocks, soils, muds, and a mixture of them (Locat and Lee, 2000). Loose cohesionless sediments that may strain soften when loaded during seismic events have been linked with landslides produced by flow liquefaction (McKenna *et al.*, 1992; Lade, 1993; Christian *et al.*, 1997). Fine materials, typically normally consolidated to lightly overconsolidated soft clays in layers ranging from few meters to hundreds of meters have been associated with large-scale submarine landslides in gentle slopes, also associated with seismic loading (Frydman *et al.*, 1988; Puzrin *et al.*, 1997; Leynaud and Mienert, 2003). Huhnerbach *et al.* (2004) compiled a database of 260 slope failures from diverse tectonic environments in the North Atlantic based on previously published data sets to establish relationships between parameters and their potential importance. A trend between the length of the landslide and the materials

was observed; long slides were associated to soft, fluid materials, meanwhile, short landslides implied the presence of more stiff sediments.

Another relevant parameter to be considered in the study of submarine landslides is the geometry of the slopes. Submarine slopes on open continental margins are the result of a process of parallel sedimentation over large areas. This causes a condition to produce large submarine landslides, for example, the Storegga Slide, an event that occurred about 8,200 years ago, which involved around 3,000 km2 of material volume affecting an area of 90,000 km2 (Kvalstad *et al.*, 2005). From the historical records and compilations of submarine landslide features, a trend between the slope inclination, frequency of landslides, and large-scale failures was observed (Figure 2.2). Huhnerbach *et al.* (2004) concluded that the largest landslides occur on the lowest slopes (with angles as low as 1°). According to Masson *et al.* (2006) the largest submarine landslides occur on open continental margins of low gradient (1° to 5°) and oceanic island flanks. Although many of the landslides won't necessarily lead to tsunamis, they represent a potential threat to cables and other seabed infrastructure.
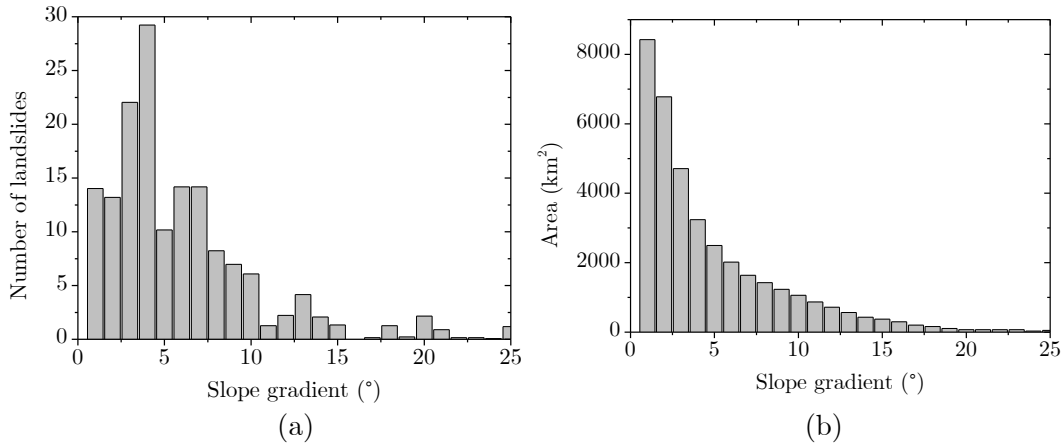
Figure 2.2: (a) Number of landslides on the eastern continental slope of North America; (b) Distribution of slope gradients and area affected in slopes on the eastern North American slope (adapted from Masson *et al.*, 2006).

2.3   Classification and characteristics of Submarine landslides

High-resolution mapping of continental margins and fjords have systematically revealed that submarine landslides represent a widespread phenomenon around the world, varying from large-scale landslides (Embley, 1980; O´Leary, 1996; Piper *et al.*, 1999; Laberg *et al.*, 2003; Mosher *et al.*, 2004; Solheim *et al.*, 2005; Vanneste *et*

al., 2006; Krastel *et al.*, 2012) to instabilities in a minor scale (Lastras *et al.*, 2004; L´Heureux *et al.*, 2012).

Landslides may be submarine (offshore) or subaerial (onshore). In both cases, they share many similarities but significant differences as well (Hampton *et al.*, 1996). According to Hutchinson (1968), mass movements exhibit significant variability, being affected by geology, climate, and topography, and a rigorous classification is rarely possible. Hampton (1972) described submarine landslides in terms of three stages: slide, debris flow, and turbidity currents with transitions between stages in terms of the strength of the flowing soil. Since the 1970s, different categorization systems have been published, including those of Zaruba and Mencl (1969), Varnes (1978), Brunsden (1979), Selby (1982), and Mulder and Cochonat (1996). From the classification systems, a notable one is the proposed by the International Society for Soil Mechanics and Geotechnical Engineering (ISSMGE) Technical Committee on Landslides (WP/WLI, 1993). This classification framework presents five types of landslides with subgroups applicable to submarine landslides, including turbidity currents (Figure 2.3).
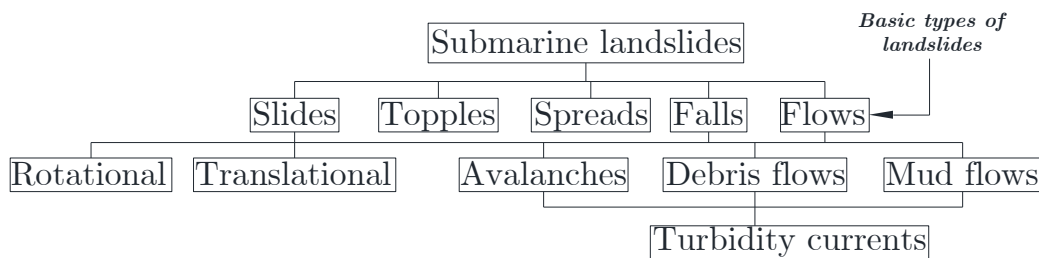
Figure 2.3: Classification of submarine landslides (adapted from ISSMGE Technical Committee on Landslides, TC-11)

2.4   Causes of submarine landslides

Submarine landslides occur when shear stresses exceed the available strength of the materials of the slope (Locat and Lee, 2002). Masson *et al.* (2006) suggested that the factors possible contributors to the initiation of submarine landslides can be broadly grouped into two types: (1) those related to the geological characteristics of the landslide material (e.g., overpressure due to rapid deposition or the presence of weak layers); and (2) factors driven by transient external events (e.g., earthquakes). A brief list of examples of submarine landslides and their triggering factors is presented in Table 2.1.

Table 2.1: Examples of documented submarine landslides
(Adapted from Masson *et al.*, 2006)

Triggering Factor	Examples	References
Earthquakes	Grand Banks	Fine *et al.* (2005)
Hurricanes – cyclic loading	Missisipi delta	Prior and Coleman (1982)
Oversteeping slopes	Nice; Canary Islands	Assier-Rzadkiewicz *et al* (2000).
Underconsolidation (overpressure)	Missisipi delta	Prior and Coleman (1982)
Parallel weak layers	East Coast US; Storegga; West Africa	O´Leary (1991); Hafliadson *et al.* (2003); Bryn et al (2005)
Gas hydrate dissociation	East Coast US, Storegga	Sultan *et al.* (2003)
Sea level change	Madeira Abyssal Plain	Weaver and Kujipers (1983)

The initiation of submarine landslides is associated to the environment in which they occur. Hampton *et al.* (1996) designated five environments as submarine landslide territory: (i) fjords, (ii) active river deltas on the continental margin, (iii) submarine canyon-fan systems, (iv) the open continental slope, and (v) oceanic volcanic islands and ridges. In all the cases is either an increase of gravitational driving stresses, a decrease in resisting forces or a combination of both. Hampton *et al.* (1996) compiled the potential elements that can lead into submarine landslides and showed how they affect the factor of safety of a slope (SF) (Figure 2.4).

$$SF = \frac{\sum Resisting\ Forces}{\sum Gravitational\ Forces}$$

Reducing the Strength	Increasing the Stresses
Earthquakes	Earthquakes
Wave loading	Wave loading
Tidal changes	Tidal changes
Sedimentation	Sedimentation
Gas	Erosion
Weathering	Diapirs

Figure 2.4: Causes of submarine landslides (adapted from Hampton *et al.*, 1996)

To study the safety factor, geotechnical information in terms of the available resisting forces (undrained shear strength) is required. Borges *et al.* 2015 compiled data from seafloor geometry and seafloor mechanical properties to develop regional maps of static safety factors for the evaluation of susceptibility for submarine shallow translational slides on the slope and São Paulo Plateau of Campos Basin. Figure 2.5 presents the location of a set of geotechnical boreholes of the Petrobras/Cenpes database.
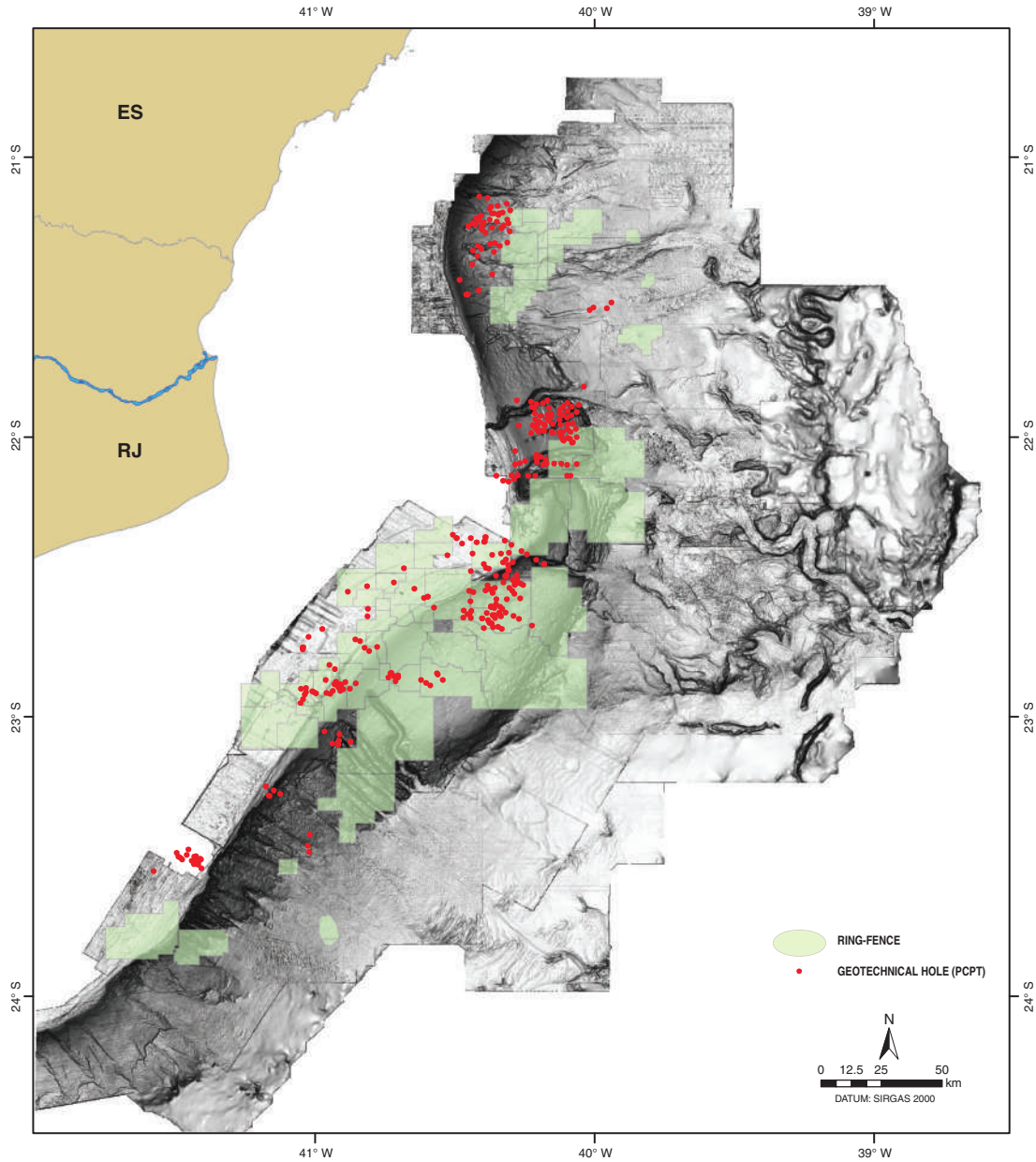
Figure 2.5: Location of piezocone tests on the Campos Basin, in green contour of Petrobras oil fields (Borges *et al.*, 2015)

Figure 2.6 shows examples undrained shear strength profiles from two boreholes to illustrate the range of undrained shear strength of the soil deposits at the Campos Basin. Borehole GT-212 taken at Espadarte Field at UTM coordinates 354,370 m E and 7,483,541 m N and Borehole GT-500 at Marlim Sul Field at UTM coordinates 376,414 m E and 7,413,150 m N. From the profiles it can be observed an increasing pattern with depth with values close to zero near the surface. Figure 2.7 shows the the undrained shear strength from a borehole executed in the central region of the continental slope in which a weak layer was evidenced at depths between 28 m and 33 m. Details about a methodology to simulate a weak layer using a geotechnical centrifuge are presented by Soriano *et al.* 2019.
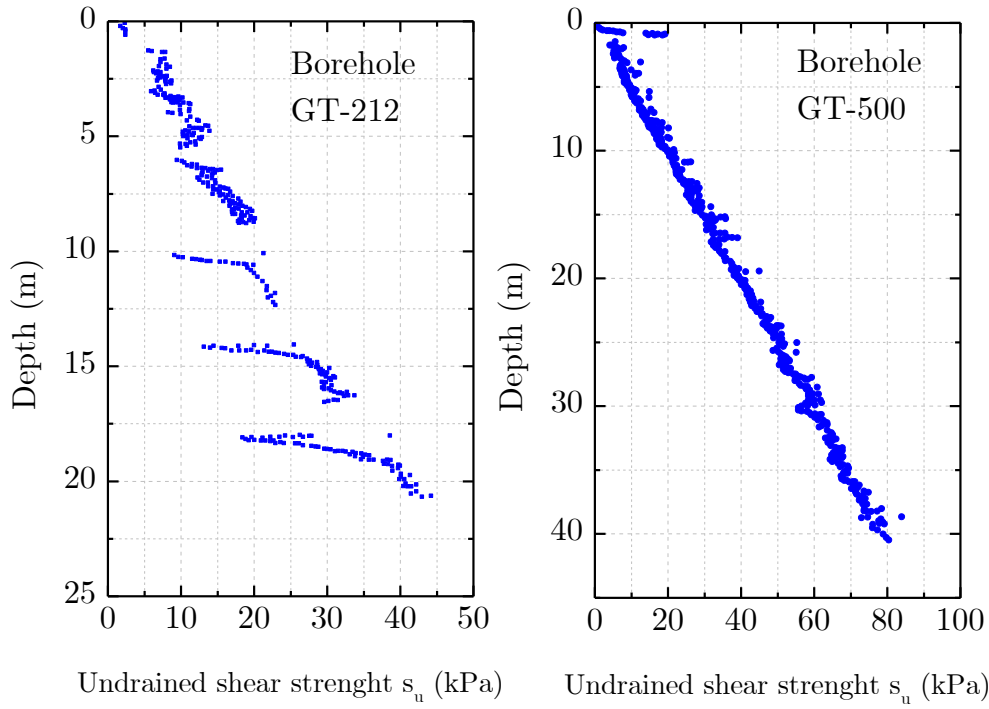
Figure 2.6: Undrained shear strength profiles on borehole at the Campos Basin (adapted from Borges *et al.*, 2015)
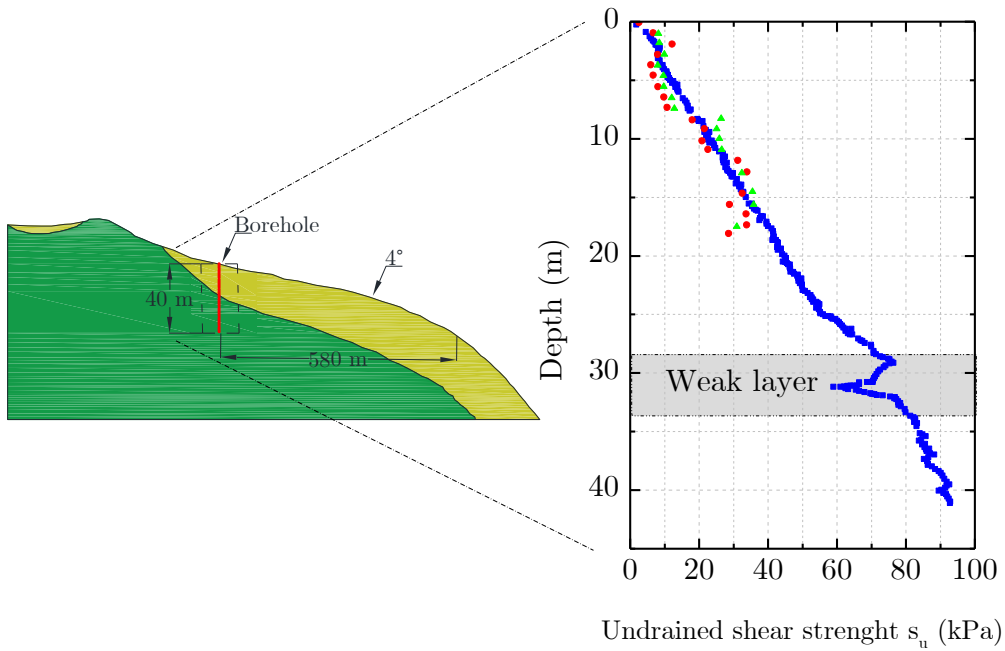
Figure 2.7: Detail of undrained shear strength profile and weak layer from a borehole at the offshore Campos Basin (adapted from Soriano *et al.*, 2019)

2.4.1 Earthquakes

Earthquakes as a trigger of submarine landslides have been recognized and studied by various researchers (Prior, 1984; Hampton *et al.*, 1996; Locat and Lee, 2000;

16

Biscontin *et al.*, 2004; Kvalstad *et al.*, 2005; Coulter, 2005, Biscontin and Pestana, 2006; Gue, 2012). The primary consequence of earthquakes on the instability of submarine slopes is a combined effect on the reduction of the shear strength of the soil deposit and the increase of the shear stresses. During an earthquake, there is a propagation of shear waves from the bedrock to the soil inducing cyclic shear stresses (Evans, 1995). In a submarine slope, even for very slight inclinations, a static shear stress is imposed on the slope (Biscontin and Pestana, 2006). When superimposed the previous static shear stresses with the dynamic shear stress in conjunction with gravitational and hydraulic forces, the available shear strength of the soil is exceeded leading to slope failure.

One known example of earthquake-induced submarine landslides is the sequence of events that occurred after the Grand Banks earthquake of November 18th, 1929, about 280 km south of Newfoundland (Piper *et al.*, 1999; Fine *et al.*, 2005; Mulder and Cochonat, 1996). By means of SAR (Système Acoustique Remorquè) high resolution, sidescan sonar, seismic reflection profiles, and field observations, Piper *et al.* (1999) described a series of failures in the continental slope. Around the epicenter of the 1929, Grand Banks earthquake a series of retrogressive rotational failures were followed by debris flows and turbidity currents triggered by numerous small thin-skinned failures. An illustrative drawing from Piper *et al.* (1999) is reproduced in Figure 2.8 to describe the interaction between the pre-existing relief and its role in the transition from failures to the development of debris flows and turbidity currents on the St. Pierre submarine slope during the occurrence of the 1929 Grand Banks earthquake. This is also a clear example of a process of formation of submarine slopes and it is one of the factors that engineering projects should deal with.
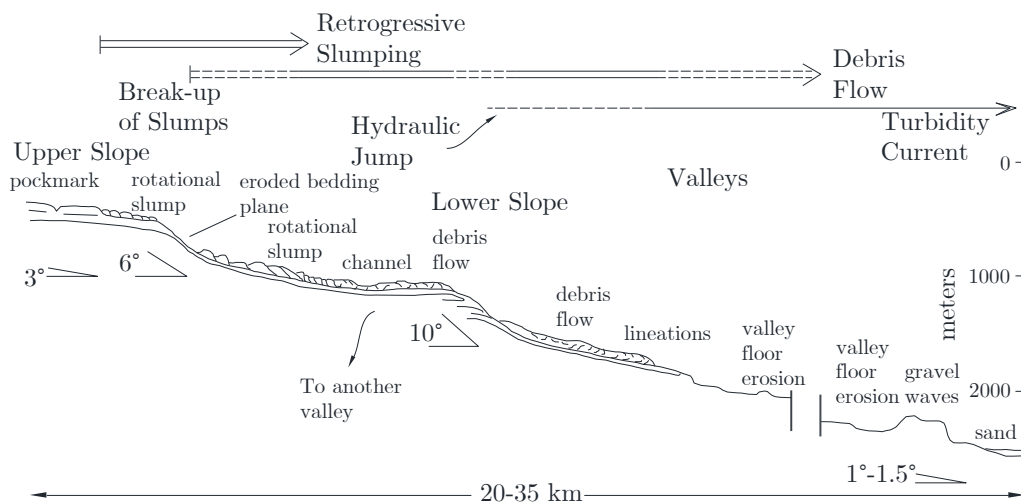
Figure 2.8: Interpretative diagram adapted from Piper *et al.* (1999) showing the sequence of sediments facies developed downslope of the Grand Banks margin

17

2.4.2 Sedimentation

The accumulation of sediments as a trigger mechanism of submarine landslides has been described by Lee *et al.* (2007). When sedimentation occurs rapidly, new weight is added to the slope. A rapid increase occurs in the pore pressures, followed by their delayed dissipation (delayed shear strength development). Then, the shear stress acting downslope increases more rapidly pushing the slope toward failure.

An example of sediment accumulation as a trigger for submarine slopes is the Mississippi Delta. Coleman *et al.* (1993) examined the mechanisms responsible for submarine landslides in this region. Particularly in the Bird Foot delta of the Mississippi river system, where sediments consist of the product rapidly deposited clays with extremely high-water content, organic matter, and elevated concentration of gasses. As previously mentioned, the rapid deposition leads to a delayed pore pressure dissipation throughout low permeability clays and silts, leading to elevated pore pressures as the sediments accumulate. Pore pressure measurements in the area indicated pressures exceeding the hydrostatic pressures and, in some cases, approaching to the pressures produced by the weight of the water column above and the overlying sediment. This condition was defined by Coleman *et al.* (1993) as *underconsolidation*.

2.4.3 Gas and gas hydrates related effects

Triggering mechanisms related to gas can be divided into two types: gas hydrates and free gas. Newton *et al.* (1980) noted that free gas is present in the subsurface and can accumulate in permeable horizons producing high-pressure gas pockets. These gas pressures may act as a loading mechanism affecting the shear strength and/or increasing the driving forces on the soil.

Gas hydrates are unique compounds consisting of an ice-like substance composed of gas, most commonly methane, trapped with water molecules (Nixon and Grozic, 2007). The formation and decomposition of gas hydrates are believed to influence the mechanical properties of sediments. According to Paull *et al.* (2000), the processes associated with the formation and decomposition of gas hydrate can cause the strengthening of sediments in which gas hydrate grows and the weakening of sediments in which gas hydrate decomposes. When gas hydrates become unstable, there occurs a decomposition into water plus gas. This process of transformation of solids into liquid and gas may produce a decrease in the shear strength of the sediments making them more prone to failure.

Various studies have investigated the possible connection between slope failures

and the presence of gas hydrates (Kvenvolden, 1993, 1999; Mienert *et al.*, 2005; Jung and Vogt, 2004; Vogt and Jung, 2002; Sultan *et al.*, 2004a, 2004b). Sultan *et al.* (2003) developed a theoretical model of the thermodynamic chemical equilibrium of gas hydrates in sediment. The model was adopted in a back-analysis of the Storegga slide on the Norwegian margin. The results showed that the melting of gas hydrates can be associated with the origin of a retrogressive failure in the Storegga slope.

2.4.4   Presence of weak layers

Weak layers can represent a significant role in the development of many submarine landslides. Different studies related to submarine mass movements suggested the presence of weak layers as one of the reasons for the initiation of submarine landslides (O'Leary, 1991; Haflidason *et al.*, 2003; Bryn *et al.*, 2005a, 2005b; Solheim *et al.*, 2005; Locat and Lee, 2009).

According to Locat *et al.* (2014), a weak layer can be defined as a layer (or band) consisting of sediment or rock that has strength potentially or sufficiently lower than that of adjacent units (strength contrast) to provide a potential focus for the development of a surface of rupture. Shear strength contrast between weak layers and bordering layers of about 50% is not uncommon (L'Hereux *et al.*, 2012; Steiner *et al.*, 2012; Rodriguez-Ochoa *et al.*, 2015).

A weak layer can follow stratigraphic horizons, but this is not a requirement. From the definition proposed by Locat *et al.* (2014), weak layers can be divided into two groups: inherited and induced (Figure 2.9).
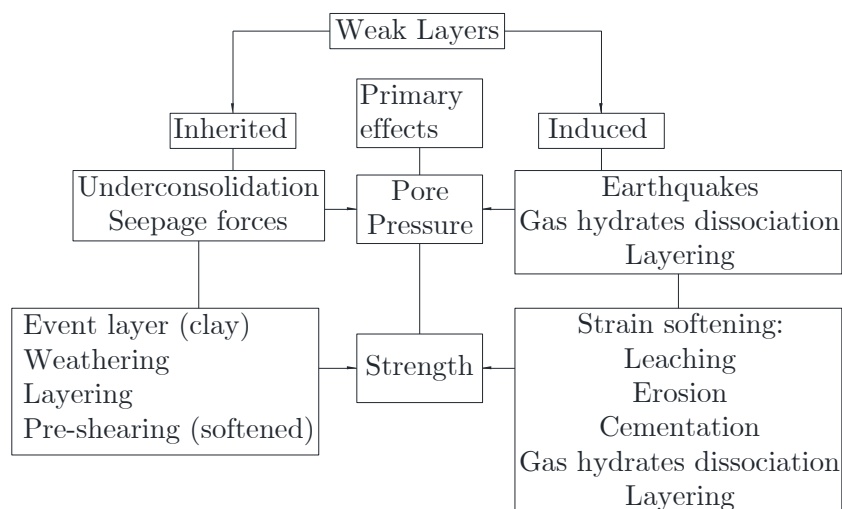
Figure 2.9: Sedimentological classification for weak layers
(Adapted from Locat *et al.*, 2014)

From the classification of weak layers proposed by Locat *et al.* (2014) some definitions were also presented:

-"*Inherited weak layers*": appear when the shear strength was already low before landslide occurrence. Examples of inherited weak layers are those that have developed as part of older landslides, long term weathering (resulting in a reduction of the shear strength of the sediment) and the presence of joints or aligned pockmarks that may reduce the shear strength at the head of a potential landslide.

- "*Induced weak layers*": are the result of a strength reduction during the slide process. External forces such as earthquakes, gas hydrates dissociation or strain softening behavior are some of the factors responsible of the process involved in the formation of an induced weak layer.

The understanding of many aspects of submarine landslides, including the location and deduction of weak layers, is commonly based on hypotheses, observation, and interpretation (Masson *et al.*, 2010). Few recent exceptions that included direct sampling, like the Storegga slide (Kvalstad *et al.*, 2005), the Nice airport failure (Dan *et al.*, 2007) and submarine landslides in fjords (Hansen *et al.*, 2011; L'Heureux *et al.*, 2012; Levesque *et al.*, 2004). An example of the various factors involved in the Finneidfjord landslide (L'Hereux *et al.*, 2012) is presented in Figure 2.10. The scheme shows how the low-permeability weak layers affect the general land-fjord groundwater flow and how they further control the stability of slopes along the steep foreshore slopes (L'Hereux *et al.*, 2012).
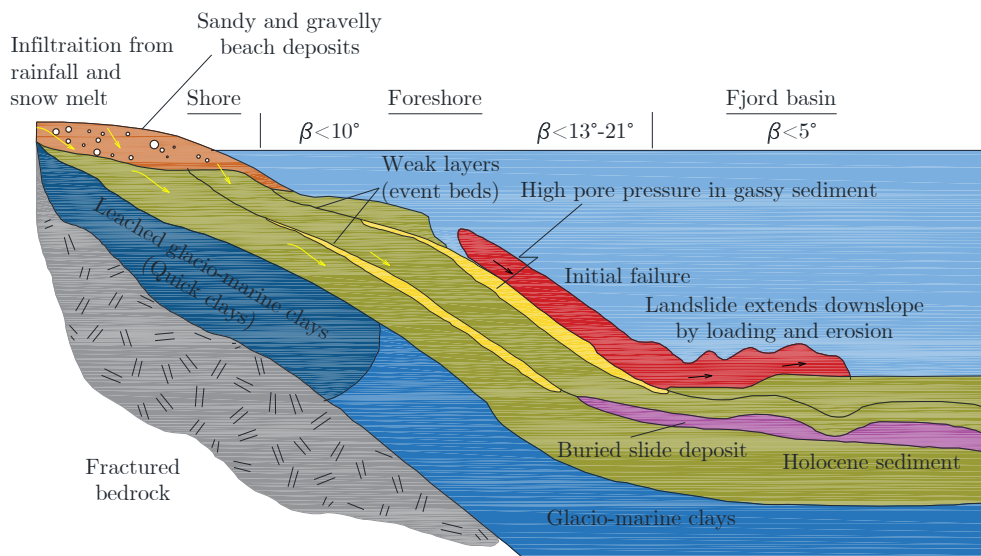
Figure 2.10: Schematic representation of the near shore setting at Finnefjord and factors affecting the stability of slopes (Adapted from L´Hereux *et al.*, 2012).

2.5 Physical modelling in geotechnical engineering

The physical modeling technique has become a significant tool to investigate numerous geotechnical engineering problems, characterized for their complex soil and loading conditions. In physical modeling, two approaches can be adopted: (*i*) full-scale tests ($1g$), and (*ii*) centrifuge tests, under higher gravity accelerations (Ng). The work introduced in this thesis is an application of dynamic centrifuge modeling, then a brief overview of the basic principles of centrifuge modeling and scaling laws will be introduced in the current section. In addition, a description of two types of model containers and their application in dynamic centrifuge experiments is also presented given their relevance in the development of the tests presented in this thesis.

2.5.1 Basic principles of centrifuge modelling and scale laws

The key premise in centrifuge modeling is to test a $1/N$ scale model of a prototype in the enhanced gravity field of a geotechnical centrifuge. In a centrifuge, the radial acceleration field is increased by the same geometric factor N relative to earth's gravity field, g (Madabhushi, 2014). With this technique, stresses and gravity-dependent processes may be correctly reproduced. According to Joseph *et al.* (1988), three assumptions must be satisfied to guarantee the model performance is like the prototype behavior:

(i) The model is a correct scaled version of the prototype.

(ii) The $1/N$ scaled model when subjected to an ideal N times g gravity field behaves like the prototype at $1g$.

(iii) The centrifuge produced that ideal gravity field.

The relationship between the behavior of the centrifuge model and the prototype is explained by the scale laws. The background for the development of the conventional scale laws in centrifuge modeling is described by Taylor (1995). Madabhushi (2014) presented a list of the scaling laws divided into "*slow*" and "*dynamic*" events and their corresponding definition (Table 2.2). A problem is defined as "*slow*" when the inertial effects in the direction normal to gravity field can be neglected. Examples of slow events are the flow of groundwater in soil (consolidation) or the slow application of lateral loads to piles or retaining walls. On the other hand, a "*dynamic*" event is when the inertial effects cannot be neglected. This is the case of the loading produced by an earthquake, in which polarized shear waves that propagate vertically throughout the soil can cause damage to the structures placed above the

ground surface. Other examples of dynamic events are the effects of blast and wind loading on structures.

Table 2.2: Scaling laws for "slow" and dynamic events (Madabhushi, 2014)

	Parameter	Scaling law Model/Prototype	Units
General scaling laws ("slow" events)	Length	$1/N$	m
	Area	$1/N^2$	m^2
	Volume	$1/N^3$	m^3
	Mass	$1/N^3$	$Nm^{-1}s^2$
	Stress	1	Nm^{-2}
	Strain	1	-
	Force	$1/N^2$	N
	Bending moment	$1/N^3$	Nm
	Work	$1/N^3$	Nm
	Energy	$1/N^3$	J
	Seepage velocity	N	ms^{-1}
	Time (consolidation)	$1/N^2$	s
Dynamic events	Time (dynamic)	$1/N$	s
	Frequency	N	s^{-1}
	Displacement	$1/N$	m
	Velocity	1	ms^{-1}
	Acceleration/ Acceleration due to gravity (g)	N	ms^{-2}

2.5.2 Strain rate effects

In centrifuge modeling, small-scale models are subjected to increasing acceleration levels to match a particular prototype stress level. Since the physical models tested in the centrifuge are smaller than the prototype by a scale factor, N, events like earthquakes will occur more rapidly in the model than in the prototype (Sathialingam and Kutter, 1989). In dynamic centrifuge testing, in the simulation of earthquakes, the time is scaled by a factor equal to N. This means that the rate of change of stresses and strains occur N-times faster in the model than in the prototype.

The dynamic response of soils has been associated with the strain rate. Sheahan *et al.* (1996), from a set of consolidated-undrained triaxial compression tests at strain rates varying between $1x10^{-5}$ %/s and 0.01%/s, observed that the peak shear strength of normally consolidated and lightly overconsolidated Boston blue clay increased around 5% to 12% per log cycle of strain rate. Lefebvre and LeBoeuf (1987) presented the results of a series of monotonic and cyclic triaxial tests carried out to investigate the influence of strain rates and loading cycles on the undrained shear strength of sensitive clays from eastern Canada. For a range of strain rates between 1 *times* 10^{-5}%/s to 1%/s, an increase in undrained shear

strength of 7% to 14% per log cycle was found. Almeida and Marques (2003) described the geotechnical properties of very soft Brazilian clay (Sarapui clay) by means of laboratory and *in situ* tests. For the Sarapui clay it was reported an average increase of 15% in s_u per logarithm cycle of strain rate. Yi *et al.* (2020) discussed the loss of similitude in the strain rate between model and prototype and its effects on the installation of anchors in centrifuge tests. The discrepancy was identified in the anchor embedment depth due to strain-rate-related modeling errors. Afacan (2014) and Afacan *et al.* (2019) applied strain rate corrections for the numerical modeling of soft clays under large strains (2% to 10%). The peak strain rate in the centrifuge experiments conducted at 57g was 6,600%/s resulting in rate corrections that increased the monotonic strength of the clay in the order of 115%. Sathialingam and Kutter (1989) summarized the results of some investigations of the effect of strain rate on monotonic properties of cohesive soils. The results are compiled in Figure 2.11 and additional data is shown from recent research works (Afacan 2014; Afacan *et al.*, 2019 for San Francisco Bay mud). For reference, the 10% per log increase line shows that some data falls below this pattern (Olson and Parola, 1967, Cheng, 1980), and depending on the strain rate, the effects are higher on the increase of the monotonic undrained shear strength. It is important to mention that the data presented in Figure 2.11 corresponds to various cohesive soils and the behavior may vary from soil to soil.
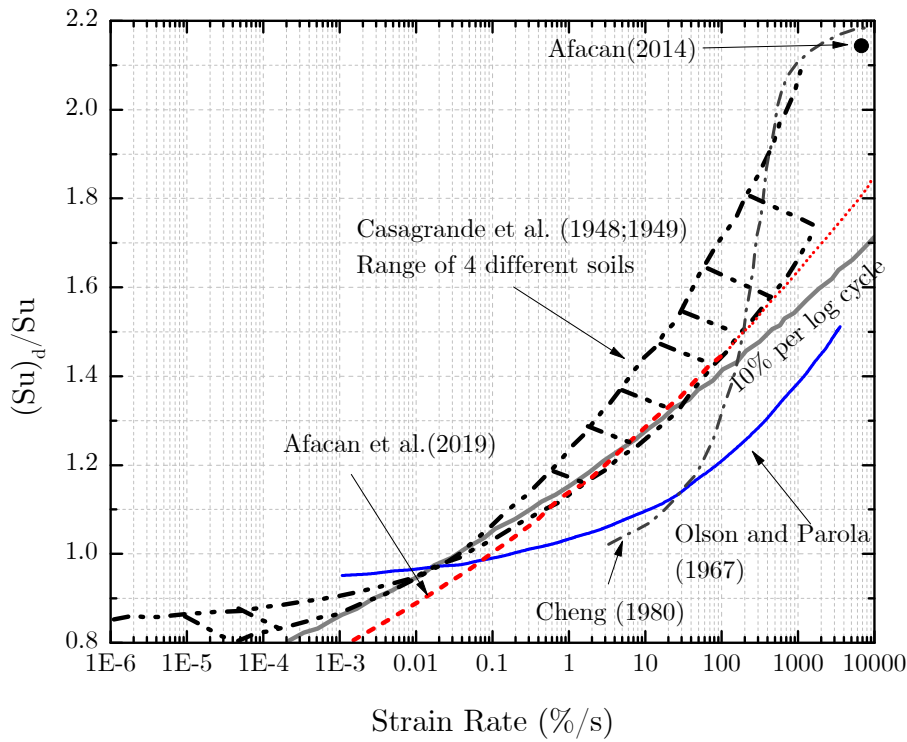
Figure 2.11: Comparison of some of the results reported by different authors regarding the strain rate effects on the strength of cohesive soils (Adapted from Kutter, 1982 and updated with data from Afacan 2014; Afacan *et al.*, 2019).

23

2.5.3 Model containers in dynamic centrifuge tests

In centrifuge testing, the space available to simulate real situations is limited, then, the model needs to be enclosed within finite boundaries delimited by a model container (Teymur, 2002). In dynamic centrifuge modeling, for some problems, like site response, liquefaction, or soil-structure interaction it is required to simulate prototype deposits of infinite lateral in the direction parallel to shaking. Then, to properly reproduce an infinite soil deposit, the boundaries of the model container should not influence the behavior of the soil (Fiegel *et al.*, 1994). Steedman and Zeng (1995) discussed some of the effects that a model container may produce on the stress field, on the strain field, or on the propagation of seismic waves throughout the soil. Various containers have been developed and used throughout the last three decades and design considerations for model containers applied to dynamic centrifuge modeling have been proposed (Whitman and Lambe, 1986; Campbel *et al.*, 1991; Schofield and Zeng, 1992; Steedman and Zeng, 1995). Bhattacharya *et al.* 2012 listed the following criteria that a model container must satisfy:

(i) Maintain stress and strain similarity in the model and prototype.

(ii) Guarantee the propagation of the base shaking throughout the upper soil layers, without significant energy transfer between the soil and the model container.

(iii) The model container should be watertight for saturated tests.

(iv) The model container end and side walls should be stiff enough to guarantee a K_0 condition during consolidation.

Based on the kind of problem to be studied and the selection of the design considerations, various types of model containers have been developed. Depending on the class of model container, the design considerations are achieved to a varying degree. Bhattacharya *et al.* (2012) identified six types of model containers for carrying out seismic soil-structure interactions at $1g$ (shaking table experiments) and Ng (centrifuge testing):

1. Rigid containers

2. Rigid container with flexible boundaries

3. Equivalent Shear Beam (ESB) containers

4. Laminar containers

5. Active boundary containers

Particular attention is given in this literature review to the Equivalent Shear Beam and to the Laminar Container as most of the experimental research on the seismic behavior of clays in centrifuge testing has been performed employing these types of boxes.

Equivalent Shear Beam (ESB) containers are designed to minimize the boundary effects by matching the deflections and natural frequency of an ideal prototype soil layer (Zeng and Schofield, 1996). A typical ESB container consists of a stack of large frames separated by thick rubber aiming to achieve the same dynamic response as the soil inside it. Figure 2.12 shows a schematic representation of an ESB model container and the deflections achieved by the soil and the container. Madabhushi (2014) pointed out the limitations of the ESB box in two areas. Firstly, the shear stiffness of the soil changes with the shear strain; for instance, during liquefaction, large strains may occur, and the boundaries of the model container will no longer match the stiffness of the soil. Secondly, the lateral deformations of the soil can be limited, then ESB containers are not suitable for lateral spreading problems.

Figure 2.12: Schematic representation of an Equivalent Shear Beam Container (adapted from Bhattacharya *et al.*, 2012).

Several design approaches have been applied in the development of ESB model containers, some examples of model ESB model containers are reported in the literature (Zeng and Schofield, 1996; Madabhushi *et al.*, 1998; Brennan and Madabhushi, 2002; Lee *et al.*, 2013). Figure 2.13 shows the ESB model containers used at the Schofield Centre, University of Cambridge (Zeng and Schofield, 1996; Brennan and Madabhushi, 2002).

Dimensions
Depth = 200 mm
Length 560 mm
Width= 250 mm

Dimensions
Depth = 427 mm
Length=673 mm
Width= 253 mm
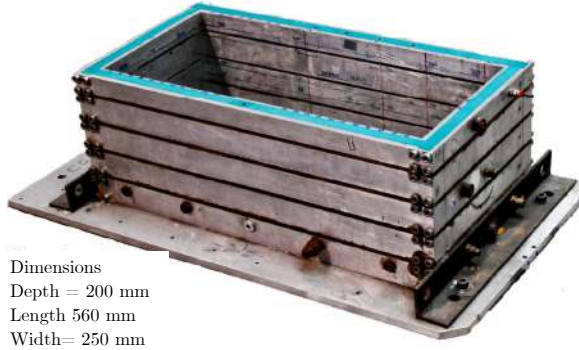
Figure 2.13: Examples of Equivalent Shear Beam containers used in centrifuge testing at the Schofield Centre, University of Cambridge.

To overcome the limitations of the ESB model containers, particularly for large strain problems (liquefaction), laminar containers are used. One of the design principles of laminar containers is to minimize its lateral stiffness, then the deformations of the soil-box system are governed by the soil (Madabhushi, 2014). Laminar containers are built by rectangular frames stacked with bearings in between, allowing relatively free movement of the soil and the frames during shaking (Figure 2.14). The design principles and construction details used for the development of a laminar container at Renssealer Polytechnic Institute (RPI) were documented by Van Laak *et al.* (1994). Emphasis in the design of RPI laminar container was given to maintain a constant cross-section during shaking, to allow settlements of the soil during consolidation, to maximize the number of vertical layers (laminae), and to minimize the mass of the laminar frames. A view of the laminar container used at the Schofield Centre, University of Cambridge (Brennan and Madabhushi, 2006) is shown in Figure 2.15.

Ring

Bearing

Base

Laminar container   Deformation of laminar container
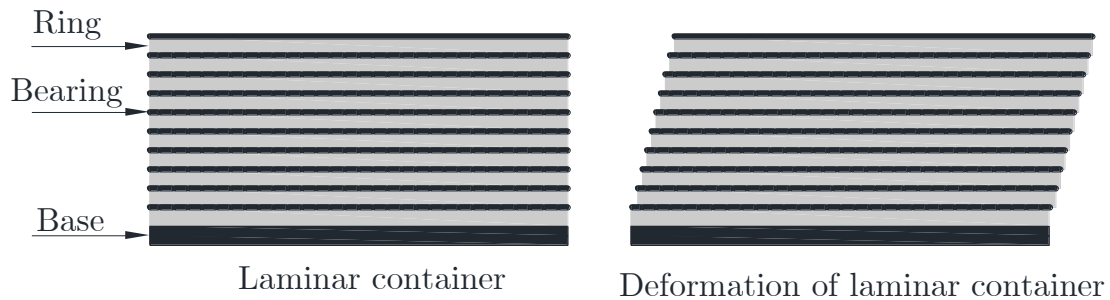
Figure 2.14: Schematic representation of a laminar container.

26

Dimensions
Depth = 226 mm
Length 500 mm
Width= 250 mm

Figure 2.15: A view of the laminar container used at the Schofield Centre, University of Cambridge. .

Brennan and Madabhushi (2006) compared the behavior of the laminar container with the ESB box, both built at Cambridge. For that purpose, models in dry sand were subjected to a sequence of earthquakes and the performance of the models was compared in terms of readings of accelerations at the box center and near the boundaries. From the results, both containers showed similar acceleration traces and transfer functions at the center and near the boundaries. The laminar container indicated a trend to exaggerate soil modes due to the finite inertia of the rings. Meanwhile, the ESB container presented a trend to attenuate soil modes due to its own dynamic vibration. Both model containers have their own advantages and disadvantages, and the selection depends on the type of problem to be studied.

Since the laminar container of the Schofield Centre, University of Cambridge was employed in the development of the tests presented in this thesis (Figure 2.15), a gap was observed in terms of the experience in using this model container for experiments in clay. Most of the studies found in the literature are related to seismic studies in sands (Lanzano *et al.*, 2012; Brennan *et al.*, 2006; Tricarico, 2016; Garcia-Torres and Madabhushi, 2019). This lead to propose and develop a new model preparation procedure, to include the use of clay in a laminar container.

2.6 Previous work on the seismic response of clays

This section presents a compilation of studies related to the dynamic response of soft clays or submarine clay deposits. The research works reported here are based on centrifuge modeling, numerical modeling, or a combination of both approaches.

From the literature review, a limited number of researches are related to the cen-

trifuge modelling of submarine slopes. Two of the references reported in this section are related to soft clays for 1D onshore conditions (Afacan *et al.*, 2013; Rayhani and El Naggar, 2007) they are relevant for this research as part of their modelling and analyses approaches are used in this thesis. From the few of the geotechnical centrifuge modelling works that explicitly mention applications to offshore clays there are the publications of Zhou *et al.* 2017 and Tarazona *et al.* 2020.

Biscontin and Pestana (2006) addressed the relevance of different factors on the response of submarine slopes during seismic loading. A parametric analysis was performed including variables as the slope angle (0°, 2.5°, 5°, and 10°), input ground motion characteristics, presence of weak layers, and depth to bedrock (20 m, 100m, and 500 m). The computer program AMPLE2000 (Pestana and Nadim, 2000) was used in the analyses; it was designed to solve the propagation of 1D shear waves in a flat or inclined ground profiles. Together with AMPLE2000, a constitutive model called SIMPLEDSS (Pestana *et al.*, 2000) was implemented. The advantage of the SIMPLEDSS model is the capability to simulate the development of excess pore pressures and the accumulation of shear strains during cyclic shearing. The soil profile properties were defined to represent the behavior of nearly normally consolidated and medium plasticity clays. The analyses indicated the effects of the local site conditions on the propagation of the ground motions throughout the soil profile. High-frequency content was filtered or deamplified by the deep soft soil deposits, while response amplification was observed at larger periods, specifically near the elastic period and the degraded natural period of the ground profile. Even small slope inclinations (lower than 5°) showed they cannot be ignored in the analyses. The slope effects are reflected in the accumulation of strains and in the permanent displacements at the end of the earthquakes. The thickness of the soil deposit revealed that deeper deposits are better than shallow deposits in terms of earthquake energy dissipation. Larger strains and higher pore pressure ratios were predicted for the shallower deposits. The presence of weak layers on the analyses showed they became slip surfaces leading to the failure of the slope.

Rayhany and El Naggar (2007) performed centrifuge tests at an acceleration level of 80g to study the dynamic response of soft clays and seismic soil-structure interaction. The experiments were carried out using an ESB container and applying a set of earthquakes with different frequency and amplitude content. To simulate soft and medium-stiff clay profiles, it was utilized an artificial clay known as "glyben" consisting of mixtures of sodium bentonite powder and glycerin. By means of vane shear tests, the strengths obtained for the soft clay and the medium-stiff clay were about 30 kPa and 60 kPa, respectively. The dynamic response of the models was monitored by means of accelerometers and displacement transducers at differ-

ent depths. As general conclusions, the authors reported a reasonable agreement between the measured dynamic soil properties with empirical relations published in the literature. From seismic site response analyses, adopting a nonlinear approach, it was observed a good agreement between the numerical simulations and the experimental data. This was a significant observation that confirmed the applicability of the glyben material for simulating soft soils in centrifuge testing. From spectral analyses performed, it was observed that the amplification and the predominant frequencies in the surface accelerations were reduced with increasing earthquake intensity. These effects were explained by the degradation of the soil stiffness and evolution of the damping as the earthquake amplitude increased.

Afacan *et al.* (2013) presented a centrifuge modeling study of site response in soft clay over a broad range of shear strains. Two centrifuge models were built using San Francisco Bay mud, selected for its presence in a seismically active region and a good characterization of its dynamic soil properties in other studies. A Hinged Plate Container (HPC) was used for the first time in the test sequence. The HPC follows a similar principle as the laminar container in the concept of exhibiting a near-zero shear stiffness, then the model stiffness is controlled by the soil. A wide range of input motions was applied to the centrifuge models: scaled versions of earthquake recordings, small amplitude sine sweeps and small amplitude sine waves. After the centrifuge tests, the HPC performance was evaluated by comparing the recordings of the accelerometers at the center of the model with the accelerations measured at the boundary of the container. The acceleration response spectra for a ground motion measured near the surface and on the container ring at the same depth exhibited identical values, indicating its suitability for site response modeling. The data were interpreted to obtain measured modulus reduction and damping curves that were compared with empirical models. A modest misfit was observed in the modulus curves; however, a significant scatter was exhibited because of the complex shapes of the hysteresis loops from broadband excitations. A significant aspect observed in the experiments performed was at the large-strain response in which shear stresses exceeding the monotonic shear stress were mobilized by factors in the order of 1.5 to 2.0.

Kaynia and Saygili (2014) developed predictive models for the permanent displacement and shear strains of infinite offshore slopes subjected to ground motions of various amplitudes. The predictive models were developed using the computer program QUIVER_SLOPE (Kaynia, 2011). The constitutive models also considered strain-softening to simulate the behavior of sensitive clays. Realistic soil profiles were defined using reference parameters based on lab test data. The analyses considered slope angles ranging between 3° and 12° and soil thicknesses of 40 m, 70

m, and 100 m. The predictive models revealed that larger displacements and shear strains occurred in the sensitive clay models for all geometry and earthquake conditions when compared with the models that not considered the sensitivity of the clay. Other comparisons of the predictive model were performed with 2D Finite Element analyses, the results compared well; however, some overestimations were observed in the shear strains from the results of the predictive model.

Zhou *et al.* (2017a) described a series of dynamic centrifuge tests, followed by numerical simulations to assess the behavior of deep offshore clay profiles when subjected to earthquakes. The clay profile simulated in the centrifuge tests consisted of slightly overconsolidated clay with a prototype depth of 44.4 m. The ground profile was built in a Flexible Shear Beam (FSB) model container that offers a natural low frequency, aiming to minimize the lateral stiffness contribution of the container to the soil layer. Ground motions with different frequency contents and amplitudes, ranging from step waves, sine sweeps, and scaled real earthquakes were applied as input motions to the models. The results of the centrifuge tests showed that for the high input motions, low amplification ratios of peak ground acceleration were observed. A consistent trend was observed for the displacement amplification, in which a large displacement response occurs under the strong base shakings. The data from the centrifuge test were additionally utilized to calibrate the parameters of a numerical model simulating the 1-D site response of the centrifuge test in DEEPSOIL program. With the validation of the numerical model methodology, 1-D site response analyses were performed in a synthetic clay deposit with different thicknesses. Two key implications were raised from the study: one demonstrates the importance of use depth varying input motions to the nonlinear dynamic analysis of offshore structures, and the second states that nonlinearity produces significant attenuation of accelerations in soft clay profiles under large ground motions.

Zhou *et al.* (2017b) evaluated the strain-softening effects on the development of submarine landslides. By means of undrained compression tests on reconsolidated samples of soft sensitive clay, a constitutive model was proposed. QUIVER_SLOPE code (Kaynia, 2011) was used to implement the constitutive model, and response analyses of gentle infinite slopes were conducted. The parametric study consisted of applying harmonic loads and real earthquakes to slopes of 3°, 6°, and 9° with different disturbance degrees and a constant thickness of 30 m. From the laboratory experiments used as input of the constitutive model, it was observed that undisturbed sensitive clay presented a higher stiffness when compared with the disturbed samples consolidated at the same stress level. The numerical simulations from QUIVER_SLOPE revealed the marked effects on the site response and permanent displacements on submarine clay slopes. At shallow depths, it was observed

a strain localization over a thin layer, which explains the large displacements at the seabed submarine clay slopes. It was also suggested the importance of coupling soil disturbance degree and depth with the slope angle and earthquake intensity in engineering design for situations in which the previous loading induced disturbance in the soils.

Tarazona *et al.* (2020) examined the ground response of submarine canyons representative of the submarine geomorphology of south-eastern Brazil. A set of centrifuge tests were carried out on kaolin clay with canyon slope angles between 15° and 45° using an ESB model container. The model preparation aimed to simulate a soft clay profile with a prototype depth of 15.2 m. The clay was instrumented with accelerometers, pore pressure transducers (PPTs), displacement transducers, and bender elements. The models were subjected to sinusoidal motions with increasing amplitude, a real earthquake (Emilia, 2012, Mw=5.9), and an artificial motion generated with parameters of the seismic activity in southeastern Brazil. From the experimental results, it was concluded that a satisfactory agreement was observed between the characterization of the soil in terms of the undrained shear strength and shear wave velocity with well-known empirical relationships. Topographic effects were observed, especially for the 45-degrees canyon with significant amplification for the lowest amplitude input motion. The topographic amplification was affected by the non-linear effects produced by the higher intensity motions.

2.7   Final remarks

Through the available literature from historical case studies of submarine slopes, a set of triggering mechanisms have been identified. In this research, special attention is directed to earthquakes, as failure mechanism of submarine slopes .

To simulate the complexity of geotechnical problems, centrifuge modeling is a reliable and established research tool that can help to clarify the seismic behavior of submarine slopes under earthquakes. Well-established principles and scaling laws for slow, static and dynamic problems have been developed for centrifuge testing.

The selection of the model containers for dynamic centrifuge testing is a primary consideration. Depending on the model container, several boundary conditions can be imposed to the soil models. In most cases, the investigations performed have been related to the seismic behavior of sands. An area in which there is a lack of research into the use of laminar containers for clay models.

31

From the previous works on the behavior of clays under seismic loading, a gap in the experimental simulation of submarine slopes with small inclinations (less than 5 degrees) was identified. A similar problem was investigated by means of numerical modeling (Biscontin and Pestana, 2006; Kaynia and Saygili, 2014, Zhou *et al.*, 2017b). The centrifuge experiments in clays are related to the simulation of flat ground profiles or to higher inclination slopes (submarine canyons) (Rayhany and El Naggar, 2007; Afacan *et al.*, 2013; Zhou *et al.*, 2017a; Tarazona *et al.*, 2020).

2.8   Chapter 2 references

AFACAN, K.B., BRANDENBERG , S.J., AND STEWART, P.J., 2013, "Centrifuge modeling studies of site response in soft clay over wide strain range," Journal of Geotechnical and Geoenvironmental Engineering, Vol.140, No.2, pp. 1-13.

AFACAN, K., 2014, "Evaluation of Nonlinear Site Response of Soft Clay Using Centrifuge Models," PhD dissertation, University of California, Los Angeles, USA.

ALMEIDA, M.S.S., AND MARQUES, M.E.S., 2003," The behaviour of Sarapui soft organic clay," In: Invited Paper for the International Workshop on Characterisation and Engineering Properties of Natural Soils. Characterisation and Engineering properties of Natural Soils. Vol.1, pp.477-504

ASSIER-RZADKIEWICZ, S., HEINRICH, P., SABATIER, P. C., SAVOYE, B. AND BOURILLET, J. F. 2000, "Numerical modelling of a landslide-generated tsunami: the 1979 Nice event Pure," Appl. Geophys. Vol.157, pp. 1717–1727.

BHATTACHARYA, S., LOMBARDI, D., DIHORU, L, DIETZ, M.S. AND CREWE, C.A., 2012, "Model container design for soil–structure interaction studies Role of seismic testing facilities in performance-based earthquake engineering," Springer, The Netherlands, pp.135-158

BISCONTIN, G. AND PESTANA, J.M., 2006, "Factors affecting seismic response of submarine slopes," Natural Hazards and earth systems sciences, Vol.6, pp.97-107.

BISCONTIN, G., PESTANA, J.M., AND NADIM, F., 2004, "Seismic triggering of submarine slides in soft cohesive soil deposits," Marine Geology, Vol.203, pp. 341-354.

BORGES, R.G., LIMA, A.C., AND KOWSMANN, R.O. 2015, "Areas susceptible to landsliding on the continental slope," In: Kowsmann, R.O., editor. Geology and Geomorphology. Rio de Janeiro: Elsevier. Habitats, Vol.1. pp. 99-136

BRENNAN, A.J., AND MADABHUSHI, S.P.G., 2002, "Effectiveness of vertical drains in mitigation of liquefaction," Soil Dynamics and Earthquake Engineering, Vol.22, No.9–12, pp.1059-1065.

BRENNAN, A. J., MADABHUSHI, S. P. G., AND HOUGHTON, N. E., 2006, "Comparing Laminar and Equivalent Shear Beam (ESB) Containers for Dynamic Centrifuge Modeling," Proceedings of the 6th International Conference on Physical Modelling in Geotechnics, 6th ICPMG '06, Hong Kong, pp. 171–176.

BRUNSDEN, D., 1979, "Mass movements" Processes in Geomorphology C. Embleton, J. Thornes (Eds.), Arnold, London (1979), pp. 130-186

BRYN, P., BERG, K., FORSBERG, C.F., SOLHEIM, A., AND KVALSTAD, T.J., 2005a, "Explaining the Storegga slide," Mar. Pet. Geol. Vol.22, pp.11-19.

BRYN, P., BERG, K., STOKER, M.S., HAFLIDASON, H., AND SOLHEIM, A., 2005b, "Contourites and their relevance for mass wasting along the Mid-Norwegian Margin," Mar. Pet. Geol. Vol.22, pp.85-96.

CAMPBELL, D., J. A .. CHENEY, AND B.L. KUTTER, 1991, "Boundary Effects 10 Dynamic Centrifuge Model Tests, " Centrifuge 91, Ko and McLean (eds.), Balkema, Rotterdam, pp. 441-448.

CASAGRANDE, A. AND SHANNON, W. L.,1949, "Strength of Soils under Dynamic Loads," Transactions, ASCE, Vol. 114.

CASAGRANDE, A., AND SHANNON, W.L., 1948, "Stress-deformation and strength characteristics of soils under dynamic loads." Proc. 2nd ICSMFE. Volume V. Rotterdam, The Netherlands, pp.29-34.

CHENG, R. Y. K., 1980, "Effect of Shearing Strain Rate on the Undrained Strength of Clays," Laboratory Shear Strength of Soils, ASTM, STP No.740, pp. 243-253.

CHRISTIAN, H.A., WOELLER, D.J., ROBERTSON, P.K., AND COURTNEY, R.C., 1997, "Site investigation to evaluate flow liquefaction slides at Sand Heads, Fraser River delta," Canadian Geotechnical Journal, Vol.34, pp.384-397

COLEMAN, J.M., PRIOR, D.B., GARRISON, L.E., AND LEE, J., 1993, "Slope failures in an area of high sedimentation rate: Offshore Missisipi River delta," in: Submarine Landslides: selected studies in the U.S. Exclusive Economic Zone, edited by Schwab, W.C., Lee, H.J., and Twichell, D.C., US. Geol. Surv.

PBull., 2002, pp.79-91.

COULTER, S.E., 2005, "Seismic initiation of submarine slope failures using physical modeling in a geotechnical centrifuge", M.Eng Thesis, Memorial University of Newfoundland.

DAN, D., SULTAN, N., AND SAVOYE, B. ,2007, "The 1979 nice harbour catastrophe revisited: trigger mechanism inferred from geotechnical measurements and numerical modeling," Mar Geol. Vol.245, pp.40–64.

EMBLEY, R.W., 1980, "The role of mass transport in the distribution and character of deep-ocean sediments with special reference to north Atlantic," Marine Geology , Vol.38, pp.23-50.

EVANS, N.C., 1995, "Stability of Submarine Slopes". Geo Report No 47. Hong Kong Government. Geotechnical Engineering Office.

FIEGEL G. L., HUDSON M., IDRISS I. M., KUTTER B. L. AND ZENG, X., 1994, "Effect of model containers on dynamic soil response," Proceedings of the international centrifuge conference, pp.145–150.

FINE, I. V., RABINOVICH, A. B., BORNHOLD, B. D., THOMSON, R. E. AND KULIKOV, E. A., 2005, "The Grand Banks landslide-generated tsunami of November 18, 1929: preliminary analysis and numerical modelling," Mar. Geol. Vol. 215, pp. 45–57.

FRYDMAN, S., TALESNICK, M., ALMAGOR, G., AND WISEMAN, G., 1988, "Simple shear testing for the study of the earthquake response of clay from the Israeli continental slope," Mar. Geotechnol., Vol. 7, pp.143-171.

GARCÍA-TORRES, S., AND MADABHUSHI, G.S.P., 2019, "Performance of vertical drains in liquefaction mitigation under structures," Bulletin of Earthquake Engineering, Vol. 17, pp. 5849–5866.

GUE, C. S., 2012, "Submarine landslides simulation using centrifuge modelling," PhD thesis, University of Cambridge.

HAFLIDASON, H., SEJRUP, H. P., BERSTAD, I. M., NYGARD, A., RICHTER, T., LIEN, R. AND BERG, K., 2003, "A weak layer feature on the northern Storegga slide escarpment," In:European margin sediment dynamics (ed. J. Mienert P. P. E. Weaver), pp.55–62. Berlin, Germany: Springer.

HAMPTON, M.A. 1972., "The role of subaqueous debris flows in generating turbidity currents," Journal of Sedimentary Petrology, Vol. 42, pp.775–793.

HAMPTON, M.A., LEE, H.J., AND LOCAT, J., 1996, "Submarine Landslides," Reviews of Geophysics, Vol.34, No.1, pp. 33-59.

HANSEN, L., L'HEUREUX J-S., AND LONGVA, O., 2011, "Turbiditic, clay-rich event beds in fjord-marine deposits caused by landslides in emerging clay deposits – palaeoenvironmental interpretation and role for submarine mass-wasting," Sedimentology Vol.58, pp.890–915.

HUHNERBACH, V., MASSON, D. G., AND COSTA PROJECT PARTNERS, 2004, "Landslides in the north Atlantic and its adjacent seas: an analysis of their morphology, setting and behaviour," Mar. Geol. Vol.213, pp. 343–362.

HUTCHINSON J.N.,1968, "Mass movement" In: Geomorphology. Encyclopedia of Earth Science, Springer, Berlin, Heidelberg.

JOSEPH, P.J., EINSTEIN, H.H., AND WHITMAN, R.V., 1988, A' Literature Review of Geotechnical Centrifuge Modeling with Particular Emphasis on Rock Mechanics," Engineering Services Laboratory Air Force Engineering Services Center Tyndall Air Force Base, Florida

JUNG, W.Y., AND VOGT, P.R. 2004, "Effects of bottom water warming and sea level rise on Holocene hydrate dissociation and mass wasting along the Norwegian-Barents Continental Margin," Journal of Geophysical Research, Vol.109, B06104

KAYNIA, A.M., 2011, "QUIVER_SLOPE – numerical code for one-dimensional seismic response of slopes with strain softening behaviour," NGI report 20071851-00-79-R.

KAYNIA, A.M., AND SAYGILI G., 2014, "Predictive Models for Earthquake Response of Clay and Sensitive Clay Slopes," In: Ansal A. (eds) Perspectives on European Earthquake Engineering and Seismology. Geotechnical, Geological and Earthquake Engineering, Vol.34. Springer.

KRASTEL. S., WYNN, R.B., GEORGIOPOULOU, A., GEERSEN, J., HEN-RICH, R., MEYER, M., AND SCHWENK, T., 2012, "Large-scale mass wasting on the northwest African continental margin: Some general implications for mass wasting on passive continental margins," In: Yamada Y, Kawamura K, Ikehara K, Ogawa Y, Urgeles R, Mosher D, Chaytor J, Strasser M (eds) Submarine mass movements and their consequences. Advances in natural and technological hazards research 31, Springer, Dordrecht, pp. 189–199.

KVALSTAD, T.J., ANDRESEN, L., FORSBERG, C.F., BRYN, P., AND WANGEN, M., 2005, "The Storegga slide: evaluation of triggering sources and slide mechanics," Marine and Petroluem Geology, Vol.22, pp.245-256.

KVENVOLDEN, K.A., 1993, "Gas hydrates-geological perspective and global climate change," Reviews of Geophysics, Vol.31, pp.173-187

KVENVOLDEN, K.A., 1999, "Potential effects of gas hydrate on human welfare," In: Proceedings of the National Academy of Sciences of the United States of America, Vol.96, pp.3420-3426.

L'HEUREUX, J.S., LONGVA, O., STEINER, A., HANSEN, L., VARDY, M., VANNESTE, M., HAFLIDASON, H., BRENDRYEN, J., KVALSTAD, T., FORSBERG, C., CHAND, S., AND KOPF, A., 2012, "Identification of weak layers and their role for the stability of slopes at Finneidfjord, Northern Norway," In: Yamada, Y., Kawamura, K., Ikehara, K., Ogawa, Y., Urgeles, R., Mosher, D., Chaytor, J., Strasser, M. (Eds.), Submarine Mass Movements and Their Consequences. Springer, Netherlands, pp.321-330.

LABERG, J. S., VORREN, T. O., MIENERT, J., HAFLIDASON, H., BRYN, P. AND LIEN, R, 2003, "Preconditions leading to the Holocene Traenadjupet slide, offshore Norway," in: Submarine mass movements and their consequences (ed. J. Locat J. Mienert), Dordrecht, Netherlands: Kluwer Academic Publishers, pp. 247–254.

LADE, P.V., 1993, "Initiation of static instability in the submarine Nerlerk berm," Canadian Geotechnical Journal, Vol.30, pp.895–904

LANZANO, G., BILOTTA, E., RUSSO, G., SILVESTRI, F., AND MADAB-HUSHI, S.P.G., 2012, "Centrifuge Modeling of Seismic Loading on Tunnels in Sand," Geotechnical Testing Journal, Vol.35, No.6, pp. 854-869.

LASTRAS, G., CANALS, M., URGELES, R., DE BATIST, M., CALAFAT, A.M., AND CASAMOR, J.L., 2004, "Characterisation of the recent BIG95 debris flow deposit on the Ebro margin, Western Mediterranean Sea, after a variety of seismic reflection data," Mar Geol. Vol.213, No.1/4, pp.235–255

LEFEBVRE, G., AND LEBOEUF, D., 1987, "Rate Effects and Cyclic Loading of Sensitive Clays." J. Geotec. Geoenviron. Eng., Vol.113, No.5, pp.476-489.

LEE, H. J., J. LOCAT, P. DESGAGNÉS, J. PARSON, B. MCADOO, D. ORANGE, P. PUIG, F. WONG, P. DARTNELL, AND É. BOULANGER, 2007, "Submarine mass movements on continental margins, in Continental-Margin Sedimentation: From Sediment Transport to Sequence Stratigraphy," (Special Publication 37 of the IAS), edited by C. A. Nittrouer et al., pp. 213–274, Blackwell Publishing, Malden, MA, USA.

LEE, S-H., CHOO, Y-W., AND KIM, D-S., 2013, "Performance of an equivalent shear beam (ESB) model container for dynamic geotechnical centrifuge tests," Soil Dynamics and Earthquake Engineering, Vol. 44, pp.102-114.

LEVESQUE, C., LOCAT, J., URGELES, R., AND LEROUEIL, S., 2004,

"Preliminary overview of the morphology in the Saguenay Fjord with a particular look at mass movements," In: Proceedings of the 57th Canadian geotechnical conference, Quebec, Session Vol.6, pp.23–30.

LEYNAUD, D., AND MIENERT, J., 2003, "Slope stability assesment of the Traenadjupet slide area offshore the mid-norwegian margin," Submarine Mass Movements and Their Consequences, pp.255-265.

LOCAT, J. AND LEE, H.J., 2000, "Submarine landslides: Advances and Challenges," Proceedings of the 8th International Symposium on Landslides, Cardiff, UK, 2000. Also published in the (2002) Canadian Geotechnical Journal, Vol.39, pp. 193-212.

LOCAT, J., AND LEE, H.J., 2002," Submarine landslides: Advances and challenges", Can. Geotech. J., Vol.39, pp.193–212.

LOCAT, J., AND LEE, H., 2009, "Submarine mass movements and their consequences: an overview," In: Sassa Kyoji, C.P. (Ed.), Landslides e Disaster Risk Reduction, pp.115-142.

LOCAT, J., LEROUEIL, S., LOCAT, A., AND LEE, H., 2014, "Weak Layers: Their definition and classification from a geotechnical perspective," Submarine Mass Movements and Their Consequences, Advances in Natural and Technological Hazards Research, Vol.37, pp.3-11.

MADABHUSHI, G., 2014, "Centrifuge Modelling for Civil Engineers," In: CRC Press (eds.), London, New York.

MADABHUSHI, S.P.G, BUTLER, G, AND SCHOFI ELD, A.N., 1998, "Design of an Equivalent Shear Beam (ESB) container for use on the US Army," In: Kimura, Takemura (eds) Centrifuge. Balkema, Rotterdam

MASSON, D.G., HARBITZ, C.B., WYNN, B., PEDERSEN, G., AND LOVHOLT, F., 2006, "Submarine landslides: processes, triggers and hazard prediction," Philosophical Transactions of the Royal Society A. M. Vol.364, pp.2009-2039.

MASSON, D.G., WYNN, R.B., AND TALLING, P.J., 2010, "Large landslides on passive continental margins: processes, hypotheses and outstanding questions," In: Mosher DC *et al.* (eds) Submarine mass movements and their consequences. Advances in natural and technological hazards research, Vol.28, pp.153–16.

MCKENNA, P.A., LUTERNAUER, J.L., AND KOSTASCHUK, R.A, 1992, "Large scale mass-wasting events on the Fraser River delta front near Sand Heads, British Columbia," Canadian Geotechnical Journal, Vol.29, pp.151-156.

MIENERT, J., VANNESTE, M., BUNZ, S., ANDREASSEN, K., HAFLIDA-

SON, H., AND SEJRUP, H.P., 2005, "Ocean warming and gas hydrate stability on the mid-Norwegian margin at the Storegga Slide," Marine and Petroleoum Geology, Vol.22, pp.233-244.

MOSHER D.C., MONAHAN P.A., AND BARRIE J.V., 2004, "Coastal submarine failures in the Strait of Georgia, British Columbia: Landslides of the 1946 Vancouver Island earthquake," J Coast Res. Vol.20, pp.277–291.

MULDER, T. AND COCHONAT, P., 1996, "Classification of offshore mass movements," Journal of sedimentary research, Vol.66, No.1, pp.43-57.

NEWTON, R.S., CUMMINGHAM, R.C., AND SCHUBERT, C.E., 1980, "Mud volcanoes and pockmarks: seafloor engineering hazards or geologic curiosities". In: Proceedings - Annual Offshore Technology Conference, Houston, USA, pp. 425-435.

NIXON, M.F., AND GROZIC, J.L.H., 2007, "Submarine slope failure due to gas hydrate dissociation: a preliminary quantification," Canadian Geotechnical Journal, Vol.44, pp.314-325.

NORWEGIAN GEOTECHNICAL INSTITUTE, (NGI), 2005, "Offshore geohazards. Summary report for research institution-based strategic project 2002-2005", NGI report no.20021023-2.

O'LEARY, D. W., 1991, "Structure and morphology of submarine slab slides: clues to origin and behaviour," Mar. Geotech. Vol.10, pp.53–69.

O'LEARY, D.W., 1996, "The timing and spatial relations of submarine canyon erosion and mass movement on the New England continental slope and rise," in: Gardner, J.V., Field, M.E., and Twichell, D.C., eds., Geology of the United States Seafloor: The view from GLORIA, Cambridge Univ. Press, Cambridge UK, pp.47–58.

OLSON, R.E., AND PAROLA, J.F., 1967, "Dynamic shearing properties of compacted clay," Int. Symp. Wave Prop. Dyn. Prop. Earth Mater. ASCE (1967), pp.173-182

PAULL, C.K., USSLER, W., AND DILLON, W., 2000, "Potential Role of Gas Hydrate Decomposition in Generating Submarine Slope Failures," Natural Gas Hydrate in Oceanic and Permafrost Environments, pp.149-156. Kluwer Academic Publishers.

PESTANA, J. M., BISCONTIN, G., NADIM, F., AND ANDERSEN, K. H., 2000, "Modeling cyclic behavior of lightly overconsolidated clays in simple shear," Soil Dynamics and Earthquake Engineering, Vol.19, pp.501–519.

PESTANA, J. M. AND NADIM, F., 2000. Nonlinear site response analysis of submerged slopes, Tech. Rep. UCB/GT/2000-04, Department of Civil and Environmental Engineering.

PIPER, D. J. W., COCHONAT, P., AND MORRISON, M. L. 1999, "The sequence of events around the epicentre of the 1929 Grand Banks earthquake: initiation of debris flows and turbidity currents inferred from sidescan sonar," Sedimentology Vol.46, pp.79–97.

PRIOR, D.B.,1984, "Subaqueous landslides," Proceedings of the IV International Symposium on Landslides, Toronto, Vol.1, pp.179-196.

PRIOR, D. B. AND COLEMAN, J. M. 1982, "Active slides and flows in underconsolidated marine sediments on the slope of the Mississippi delta," In: Marine slides and other mass movements (ed. S. Saxov J. K. Nieuwenhuis), pp. 21–49. New York, NY: Plenum Press.

PUZRIN, A., FRYDMAN, S., AND TALESNICK, M., 1997, "Effect of degradation on seismic response of Israeli continental slope". J. Geotech. Geoenviron. Eng., Vol.123, pp.85-93.

RAYHANI, M AND EL NAGGAR, M.H., 2007, "Centrifuge modeling of seismic response of layered soft clay," Bulletin of Earthquake Engineering, Vol. 5, No. 4, pp 571-589.

RODRÍGUEZ-OCHOA, R., NADIM, F., AND HICKS, M.A., 2015, "Influence of weak layers on seismic stability of submarine slopes," Marine and Petroleum Geology, Vol.65, pp.247-268.

SATHIALINGAM, N., AND KUTTER, B., 1989, "The Effects of High Strain Rate and High Frequency Loading on Soil Behavior in Centrifuge Model Tests," NCEL Contract Report.

SCHOFIELD, A.N., AND X. ZENG, 1992, "Design and Performance of an Equivalent Shear Beam Container for Earthquake Centrifuge Modelling," Cambridge Univ. Eng. Dept. Report CUED/DSOILS/TR245.

SELBY, M.J.,1982, "Rock mass strength and the form of some inselbergs in the central namib desert," Earth Surf. Process. Landforms, Vol.7, pp.489-497

SHEAHAN, T.C., LADD, C.C,. AND GERMAINE, J.T., 1996, "Rate-dependent undrained shear behavior of saturated clay," J. Geotech. Eng., ASCE, Vol.122, No.2, pp.99-108.

SOLHEIM, A., BRYN, P., SEJRUP, H.P., MIENERT, J., AND BERG, K., 2005, "Ormen Lange e an integrated study for the safe development of a deep-water gas field within the Storegga slide complex, NE Atlantic continental margin; executive summary," Mar. Pet. Geol. Vol.22, pp.1-9.

SORIANO, C., ANDRADE, R.B., TARAZONA., S.F.M, ALMEIDA., M.S.S., ALMEIDA, M.C.F., OLIVEIRA, J.R.M., AND TREJO, P., 2019, "Simulation of a Weak Layered Profile Using a Geotechnical Centrifuge," Proceedings of the XVI Pan-American Conference on Soil Mechanics and Geotechnical Engineering (XVI PCSMGE), Cancun, México, pp.477-484.

STEINER, A., L'HEUREUX, J.S., KOPF, A., VANNESTE, M., LANGE, M., AND HAFLIDASON, H., 2012, "An in-situ free-fall piezocone penetrometer for characterizing soft and sensitive clays at Finneidfjord, northern Norway," In: Yamada, Y., Kawamura, K., Ikehara, K., Ogawa, Y., Urgeles, R., Mosher, D., Chaytor, J., Strasser, M. (Eds.), 5th International Symposium on Submarine Mass Movements and Their Consequences. Springer, Dordrecht, Kyoto, Japan, pp.99-109.

STEEDMAN, R., AND ZENG, X., 1995, "Chapter: Dynamics," Geotechnical Centrifuge Technology (ed. RN Taylor), Blackie Academic Professional, London.

SULTAN, N., COCHONAT, P., CANALS, M., CATTANEO, A., DENNIELOU, B., HAFLIDASON, H., LABERG, J.S., LONG, D., MIENERT, J., TRINCARDI, F., URGELES, R., VORREN, T.O., AND WILSON, C., 2004a, "Triggering mechanisms of slope instability processes and sediment failures on continental margins: a geotechnical approach," Marine Geology, Vol.213, pp.291-321.

SULTAN, N., COCHONAT, P., FOUCHER, J.P., AND MIENERT, J., 2004b, "Effect of gas hydrates melting on seafloor slope stability," Marine Geology, Vol.231, pp.379-401.

SULTAN, N., COCHONAT, P., FOUCHER, J. P., MIENERT, J., HAFLI-DASON, H. AND SEJRUP, H. P., 2003, "Effect of gas hydrates dissociation on seafloor slope stability," In: Submarine mass movements and their consequences (ed. J. Locat J. Mienert), pp.103–111. Dordrecht, Netherlands: Kluwer Academic Publishers

TAYLOR, R. N., 1995, "Geotechnical centrifuge technology," London: Blackie Academic Professional.

TARAZONA, S.F.M., ALMEIDA, M.C.F., BRETSCHNEIDER, A., ALMEIDA, M.S.S., ESCOFFIER, S., AND BORGES, R.G, 2020, "Evaluation of seismic site

response of submarine clay canyons using centrifuge modelling," International Journal of Physical Modelling in Geotechnics, Vol.20, No.4 pp. 224-238.

TEYMUR, B., 2002., "The Significance of Boundary Conditions in Dynamic Centrifuge Modelling," PhD thesis, University of Cambridge, Cambridge, UK.

TRICARICO, M., MADABHUSHI, G.S.P., AND AVERSA, S., 2016, "Centrifuge modelling of flexible retaining walls subjected to dynamic loading," Soil Dynamics and Earthquake Engineering, Vol.88, pp.297-306.

VAN LAAK, P, TABOADA, V, DOBRY, R., AND ELGAMAL, A.W., 1994, "Earthquake centrifuge modelling using a laminar box," Dynamic geotechnical testing, ASTM STP 1213. American Society for Testing and Materials, Philadelphia, Vol.2, pp.370–384.

VANNESTE, M., MIENERT, J., AND BÜNZ, S., 2006, "The Hinlopen Slide : Agiant, submarine slope failure on the northern Svalbard margin, Arctic Ocean," Earth and Planetary Science Letters, Vol.245, No.1-2, pp.373–388.

VARNES D.J., 1978, "Slope movement and types and processes," In: Landslides: Analysis and Control. Edited by R.L. Schuster and R.J. Krizek. Transportation Research Board, National Academy of Science, Washington, Special Report, Vol.176, pp.11–33.

VOGT, P.R., AND JUNG, W.Y., 2002, "Holocene mass wasting on upper non-polar continental slopes-due post-glacial ocean warming and hydrate dissociation," Geophysical Research Letters, Vol.29, No.9, pp.55-1 – 55-4.

WEAVER, P. P. E. AND KUIJPERS, A., 1983, "Climatic control of turbidite deposition on the Madeira Abyssal plain," Nature, Vol.306, pp.360–363

WHITMAN, R.V., AND LAMBE, P.C., 1986, "Effect of boundary conditions upon centrifuge experiments using ground motion simulation," Geotech Test J Vol.9, No.2, pp.61–71.

WP/WLI (International Geotechnical Societies UNESCO Working Party on World Landslide Inventory), 1993, "Multilingual Landslide Glossary", BiTech Publishers Ltd.

YI, J.T., CAO, M.Y., LIU, Y., AND ZHANG, L., 2020, "Insight into centrifuge modelling errors in predicting embedment depths of dynamically installed anchors". Canadian Geotechnical Journal. Vol.57, No.11, pp. 1796-1804.

ZARUBA Q. AND MENCL V., 1969, "Landslides and their control", Elsevier, New York.

ZENG X, AND SCHOFIELD, A.N., 1996, "Design and performance of an equivalent-shear-beam container for earthquake centrifuge modelling," Geotechnique, Vol.46, No.1, pp.83–102.

ZHOU, Y-G., CHEN, J., CHEN, Y-M., KUTTER, B., ZHENG, B, WILSON, D., STRINGER, M., AND CLUKEY, E., 2017a, " Centrifuge modeling and numerical analysis on seismic site response of deep offshore clay deposits," Engineering Geology, Vol.227, pp.54-68.

ZHOU, Y., CHEN, J., CHEN, Y, SHE, Y., KAYNIA, A.M., HUANG, B., AND CHEN, Y-M., 2017b, "Earthquake response and sliding displacement of submarine sensitive clay slopes," Engineering Geology, Vol.227, pp.69-83.

Chapter 3

Materials and methods

3.1 Introduction

This chapter outlines the physical modelling techniques employed to investigate the seismic behaviour of gentle slopes in soft clay as presented in Chapter 4 and Chapter 5. Details of the equipment, instrumentation, and materials are first introduced. Next, details of model preparation techniques and the testing program are explained. Reference is made to the development of a methodology of Particle Image Velocimetry developed to obtain displacements at different depths of the model as a complementary source of data.

3.2 Testing Equipment

3.2.1 The Phillip Turner centrifuge

To simulate the target stresses and strains to be experienced by the prototype, it is necessary to increase the gravity field of a scaled-down model by a factor of N. This was achieved by using the Turner Beam Centrifuge at the Schofield Centre, the University of Cambridge (shown in Figure 3.1 and described in detail by Schofield, 1980). The centrifuge consists of a beam-like structure that rotates about a central axis. The models are carried at one end and a counterweight at the other, both are placed on a swing platform. The nominal diameter of the centrifuge is 10 m with a working radius of 4.125 m. The maximum centrifugal acceleration that can be achieved by the Turner beam centrifuge is 150 times the earth's gravity (150g) with a payload of 1 ton at this operational level. The alignment of the model vertical direction with the radial direction of the centrifuge can be defined as the swing up, and it takes place at an acceleration level of about 10 g when the centrifuge is spinning at around 45 RPM (Figure 3.2). The centrifuge tests in this research were performed at an acceleration of 60g corresponding to 116 RPM.

Figure 3.1: A view of the Turner Beam Centrifuge at the Schofield Centre – University of Cambridge.
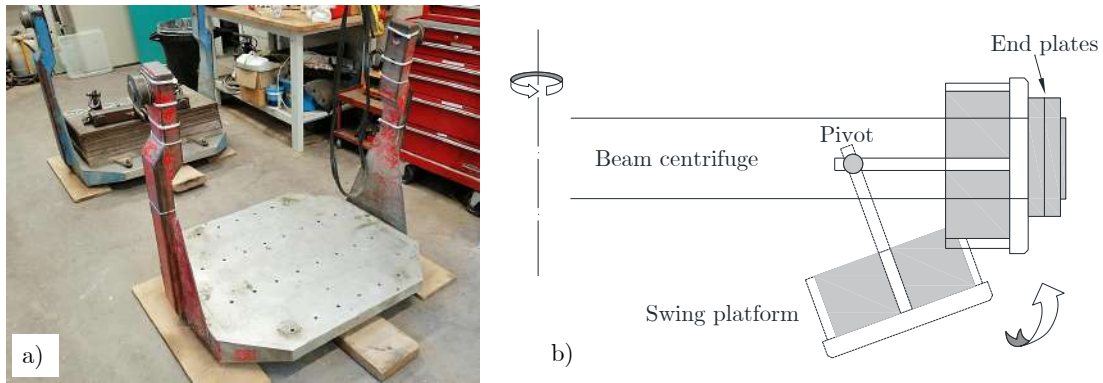
Figure 3.2: a) Swing up platforms for model and counterweights. b) Swing-up of the centrifuge model at the end of one arm (adapted from Madabhushi, 2014).

3.2.2   Servo-Hydraulic actuator

Earthquakes were simulated in-flight using the Servo-Hydraulic actuator, described in detail by Madabhushi *et al.* (2012). The energy necessary to shake the centrifuge models is accumulated in hydraulic fluid compressed to high pressures (20 MPa-30 MPa). To simulate a given earthquake, the flow of the high-pressure oil is controlled by a servo-valve which can open proportional to the earthquake signal (Madabhushi, 2014). The advantage of the servo-hydraulic actuator is the capability to simulate real earthquake loads over a broad range of amplitude and frequency content. The input motions are defined in terms of displacement-time histories. Next, the desired acceleration-time history is converted using a MAT-LAB script into a displacement-time history by double integration. A view of the servo-hydraulic actuator is presented in Figure 3.3.

Figure 3.3: Servo-hydraulic earthquake actuator.

3.2.3 Laminar model container

The problem investigated in this research consisted of semi-infinite sloping grounds in soft clay. Under these conditions, large deformations are expected, and a laminar container was utilized (Figure 3.4). This box is built by a series of rectangular frames (laminae) that are separated by cylindrical bearings to minimize the friction between the laminations. The laminar model container was designed to have "zero" lateral stiffness, then the lateral deformations of the model are driven by the soil mass. The plan area is 500 mm x 250 mm and the depth 300 mm. The weight of an individual lamination with the cylindrical bearings is 2.1 kg. To maintain the alignment and stiffness of the container in the transverse direction, T-sections connected by gantries are installed. The gantries are additionally used for supporting model instrumentation (i.e., T-bar actuator, model wiring). To prevent leakage of water, an inner rubber membrane is installed.

Dimensions
B=500 mm
L=250 mm
H = 300 mm
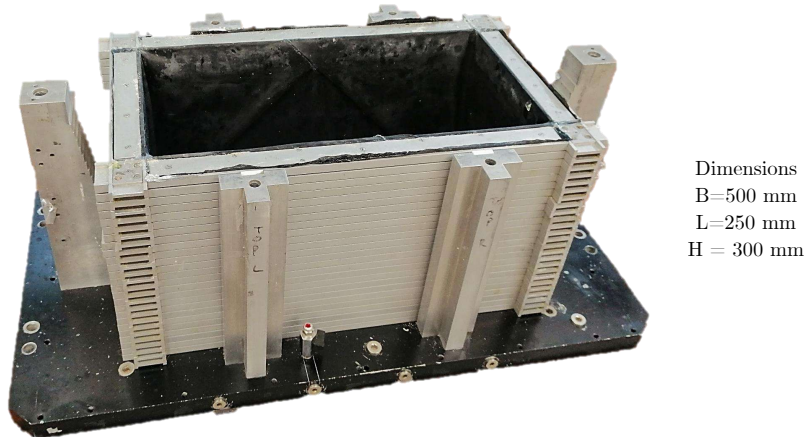
Figure 3.4: Laminar model container.

3.3 Instrumentation

3.3.1 Accelerometers

In the centrifuge tests, miniature piezoelectric accelerometers type A/23 manufactured by D.J. Birchall Ltd. (now DJB Instruments) were utilized to measure the accelerations at different depths of the models. One of the features of the piezoelectric accelerometers employed is their lightweight design, one accelerometer weights around 5 grams. The coupling between the device and the soil is usually good and true soil acceleration can be measured (Madabhushi, 2014). The frequency response of the piezo accelerometers is in the range of 5Hz to 2kHz. Below 5Hz, the response of these instruments is poor, and it has implications when performing numerical integration. Brennan *et al.* 2005 discussed the importance of filtering data at high and low frequency to eliminate drift errors during integration to obtain velocities and accelerations for this type of accelerometers. Figure 3.5 shows a view and the dimensions of a miniature piezo accelerometer.
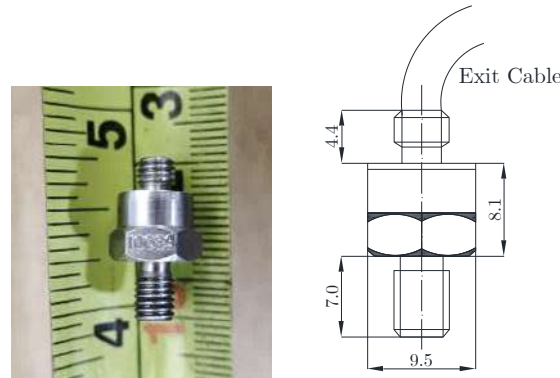
Figure 3.5: Birchall type A/23 piezo-electric accelerometer (dimensions in mm).

The accelerometers were calibrated before and after use in the centrifuge using a Bruel Kjael Type 4291 accelerometer calibrator that can precisely apply ±1 g acceleration. The calibration factor is obtained in the units of g/V. Typical calibration constants are between 6g/V and 10g/V (Knappet, 2006).

3.3.2 Linear Variable Differential Transformers (LVDTs)

Complementary measurements of displacements were conducted using LVDTs placed at specific locations outside the laminar container to measure lateral displacements (Figure 3.6). The LVDTs are calibrated before and after use in the centrifuge by applying known displacements and registering the output voltage. Typical calibration constants for the LVDTs used in this research (Reference DC15

manufactured by Solartron) are between 3.5 mm/V and 4.0 mm/V. As mentioned by Madabhushi (2014), LVDTs are reliable instruments and are used in most centrifuge tests. One of the applications of the LVDTs in the current experimental program was also calibration/validation of the PIV measurements of displacements.
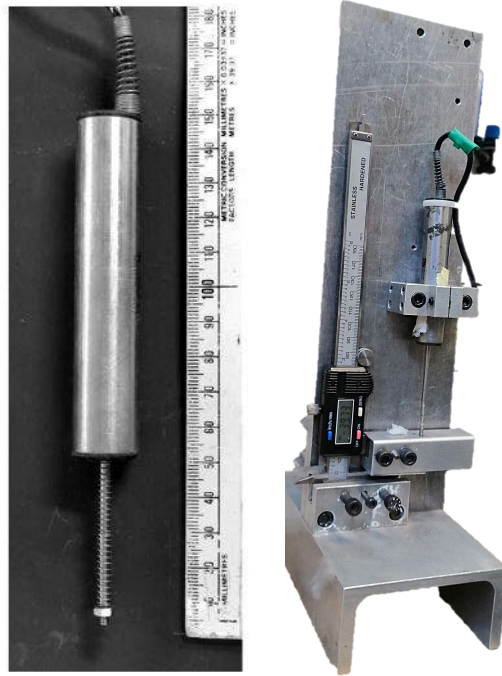
Figure 3.6: A view of a Linear Variable Differential Transformer and application of known displacements for calibration.

3.3.3 Pore pressure transducers (PPTs)

Pore pressure transducers were used as part of the measurements to monitor the behavior of the model during the swing up, consolidation, and application of the earthquakes. Specifically, miniature PPTS manufactured by Druck were installed in the centrifuge models. The calibration of the PPTs is executed by applying known water pressures and registering the output voltage, the calibration factors obtained are in units of kPa/V. Figure 3.7 shows a view of a miniature PPT and a schematic diagram of its components.
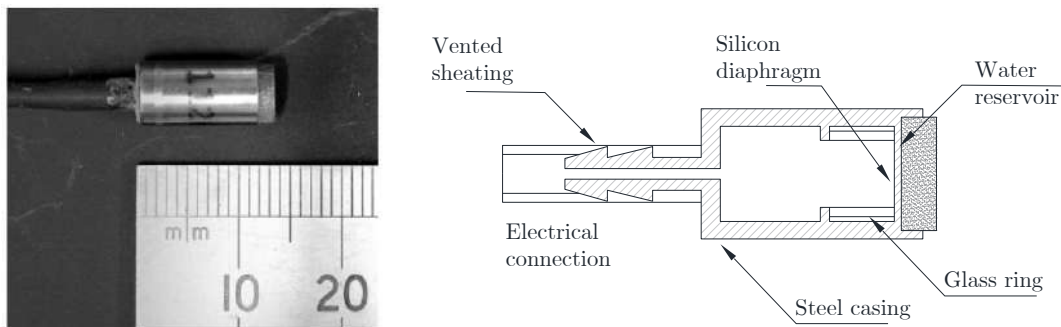
Figure 3.7: A typical PPT transducer and schematic diagram of its components.

3.3.4   In-flight characterization instruments

A miniature T-bar penetrometer and an Air Hammer (AHD) were used to carry out in-flight characterization of the undrained shear strength and shear wave velocities of the soil profile, respectively. The T-bar used was 40 mm long with a 4 mm diameter, and it was designed to measure only the tip resistance avoiding friction by means of a shaft as shown in Figure 3.8. The tip resistance is measured by a miniature load cell with a capacity of 50 N. Shear wave velocity characterization was performed by means of an air hammer that consists of a small brass tube with a pellet inside (Figure 3.8). By applying alternating high pressures at the ends, the pellet inside strikes the ends of the hammer producing shear waves that propagate throughout the model. By identifying the arrival times of the shear waves recorded by the accelerometers at various depths, the shear wave velocities can be determined. Further details about the Air Hammer were described by Ghosh and Madabhushi (2002).
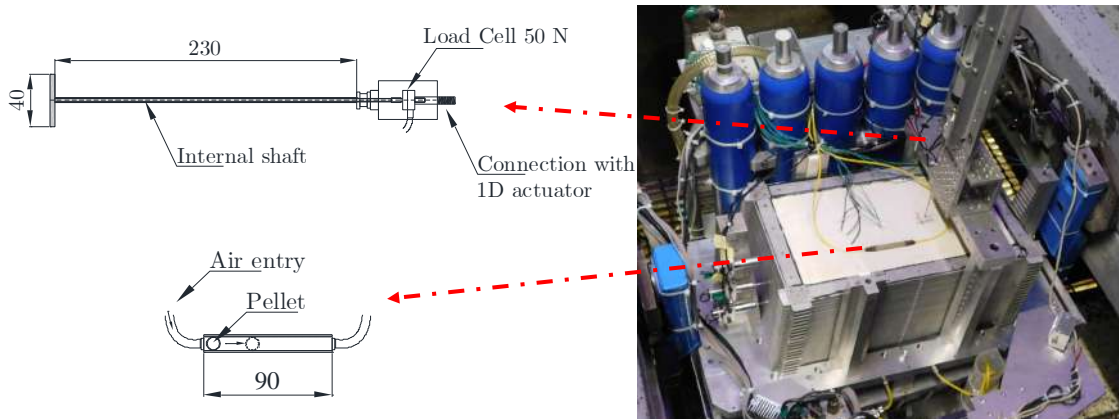
Figure 3.8: Schematic drawings of the T-Bar and Air Hammer and installation in a centrifuge model (dimensions in mm).

3.3.5   High-speed camera

The experiments presented in this thesis employed Particle Image Velocimetry (PIV) to monitor the lateral displacements of the model at specific depths. For that purpose, a high-speed camera developed to record fast processes in confined spaces was employed (MotionBLITZ EoSens mini2 produced by Mikrotron). The resolution of the pictures captured by the camera is linked to the recording frame rate. For example, at a maximum resolution of 1696 pixels by 1710 pixels it is possible to record images at a frame rate of 523 Hz. A view of the camera employed in the centrifuge tests is shown in Figure 3.9.

Figure 3.9: A view of a high-speed camera (MotionBLITZ EoSens mini2).

3.3.6 Materials

The soil used in the experiments was Speswhite kaolin, a well-documented material with comparative data sets available, widely used in research projects involving physical modelling (Almeida, 1984; Kim, 1996; Williamson, 2014; Lau, 2015). Table 3.1 presents some of the Speswhite Kaolin properties published in the literature.

Table 3.1: Published properties of Speswhite Kaolin clay.

Property	Lau (2015)	Vardanega et al. (2012)	Stewart (1992)	Phillips (1988)	Almeida (1984)	Clegg (1981)
Liquid Limit, LL(%)	63.0	62.6	61.0	64.0	69.0	69.0
Plastic Limit, PL (%)	30.0	29.6	27.0	31.0	38.0	38.0
Plasticity Index, PI (%)	33.0	33.0	34.0	33.0	31.0	31.0
Specific Gravity, Gs	2.60	-	2.60	-	2.70	2.61
Slope of unload- reload line (κ)	0.039	0.039	0.044	-	-	-
Slope of normal consolidation line (λ)	0.220	0.220	0.205	0.187	-	0.210-0.310

3.4 Model preparation techniques

The centrifuge tests carried out simulated the behavior of gentle slopes in soft clay. Two types of profiles were defined in the development of the models identified in this work as uniform profile and weak layer profile. Both types of models have in common the initial stages of consolidation and the last stages consisting of the installation of the model container around the clay profiles and placing of the instrumentation. The weak layer model profile will be explained in detail in this section, as the uniform profile can be considered a "simplified" version of this methodology as it required fewer stages for the model preparation.

The weak layer profile was developed to simulate a strength contrast between neighbouring layers of about 25%. The soil profile consisted of three layers, then, different consolidation pressures were applied. The selection of the consolidation pressures was aimed to reproduce a strength profile typical of marine clays like that encountered at the seabed of the Offshore Campos Basin, south-eastern Brazil

(Fagundes *et al.*, 2012). The model soil profile was built from reconstituted clay, as previously mentioned, the laminar container at the Schofield Centre has been used extensively for liquefaction and lateral spreading problems in sand. One of the fundamental aspects of the preparation of models in clay is the consolidation of the soil. This requires the use of an impermeable container and strong enough to handle the pressures to the clay during consolidation (K_0 condition). In a laminar container, the soil body is placed within a rubber bag or a latex membrane for saturated models. For the construction of a layered profile in clay, an extension is required and an inner rubber bag that can be easily damaged during the application of the consolidation pressures, leading to leakages, and the generation of additional drainage paths. To sort out the mentioned practical issues, a strong box, or consolidation container was designed with the same internal dimensions as the laminar container (500 mm length x 250 mm width), but deeper (500 mm), aiming to produce samples of clay between 250 mm and 300 mm in height at the end of consolidation. The sides of the consolidation container can be easily detached, and complete slices of consolidated clay can be removed with minimal disturbance, enabling the simulation of the target layered soil profile as described below. To build the three-layer slope soil profile, the model preparation was divided into stages:

1. The kaolin powder was mixed with water at a 120 % water content employing a clay mixer under vacuum to remove air bubbles from the clay. Once mixed the slurry, it was poured into the consolidation container with draining interfaces at the top and the base of the clay. A piston was placed on top of the clay slurry and it was left to consolidate for one day. The additional consolidation pressures were applied in stages using a computer-controlled consolidation rig (Figure 3.10).

<div align="center">(a)   (b)</div>

Figure 3.10: a) Pouring of the clay at a water content of 120%; b) Consolidation in a computer-controlled consolidation rig.

2. The top and bottom layers of the clay were first consolidated by applying a maximum consolidation pressure of σ'_{vmax}= 250 kPa (Figure 3.11). The load was applied in steps starting from 0.7 kPa, corresponding to the pressure applied by the piston and increased doubling the pressures until reaching 250 kPa. The consolidation lasted twelve days, and it was stopped when the settlements stabilized in 48 hours. Figure 3.12 presents the settlement-time curve of the first block of clay, roughly, the height of the clay at the end of consolidation (250 mm) and for the pressures applied was half of the initial height (500 mm).
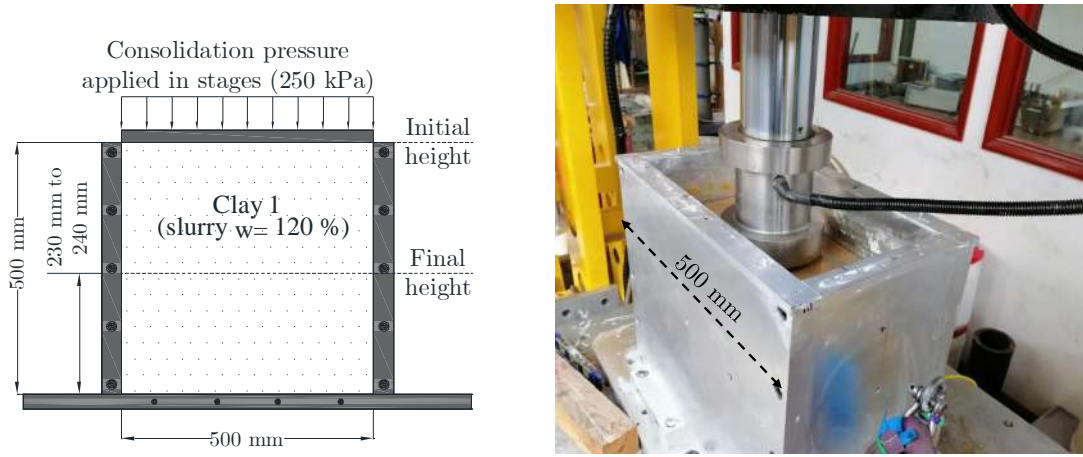
Figure 3.11: Detail of consolidation of the clay.
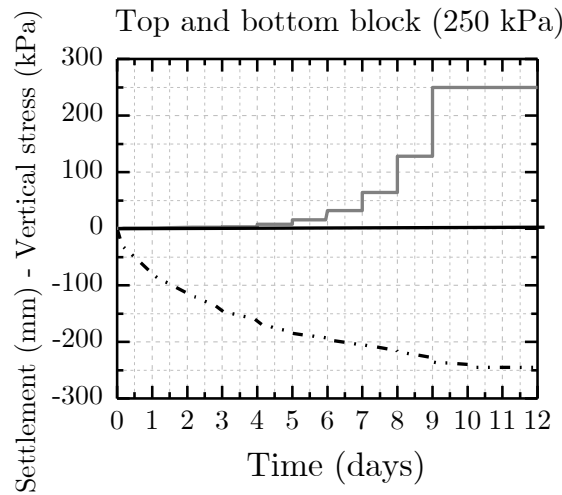
Figure 3.12: Settlement-consolidation curves for the clay used in the centrifuge test - Block 1.

3. The sides of the consolidation container were removed; the resultant block was split by cutting off the top 80 mm and keeping the remaining 150 mm in the same position. The top block was stored in a humidity chamber and protected to avoid loss of moisture (Figure 3.13).
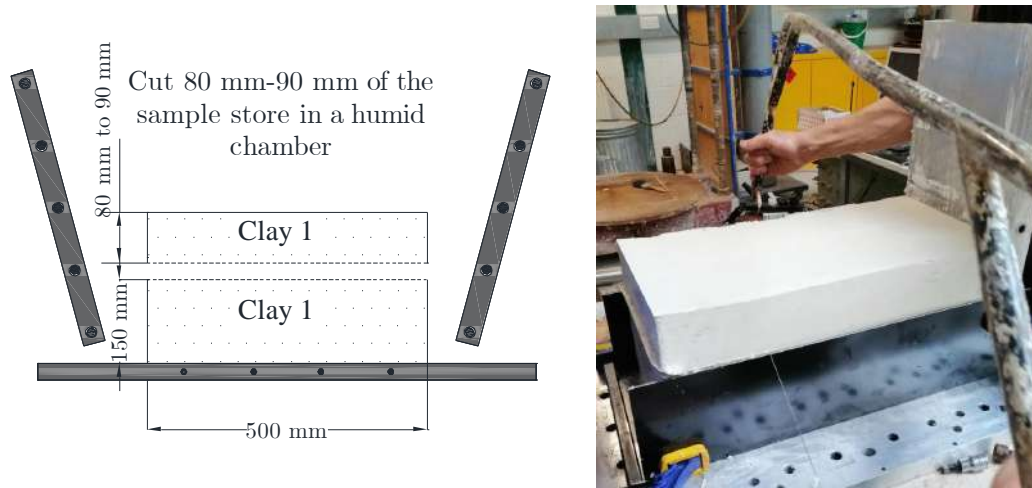
Figure 3.13: Detail of cut of a block of clay to prepare a layered profile.

4.The sides of the consolidation container were reassembled, and a new layer of slurry was poured in top of the block of consolidated clay that remained (Figure 3.14), then, a maximum consolidation pressure σ_{vmax}= 125 kPa was applied in stages (Figure 3.15).
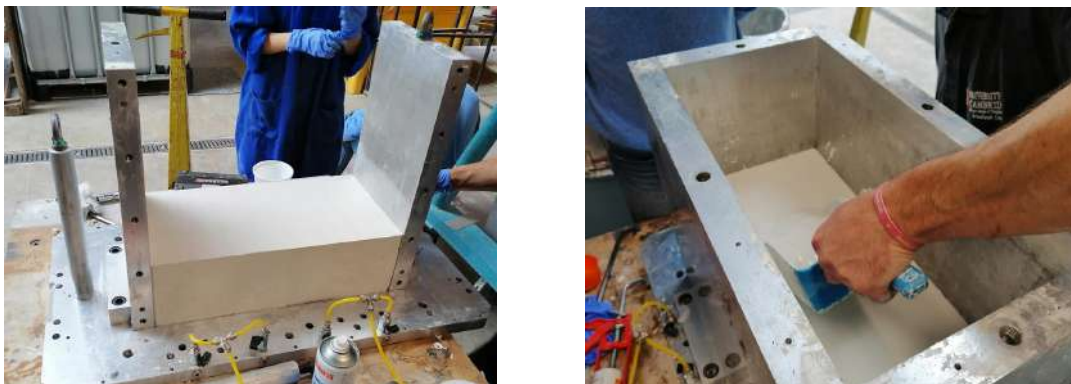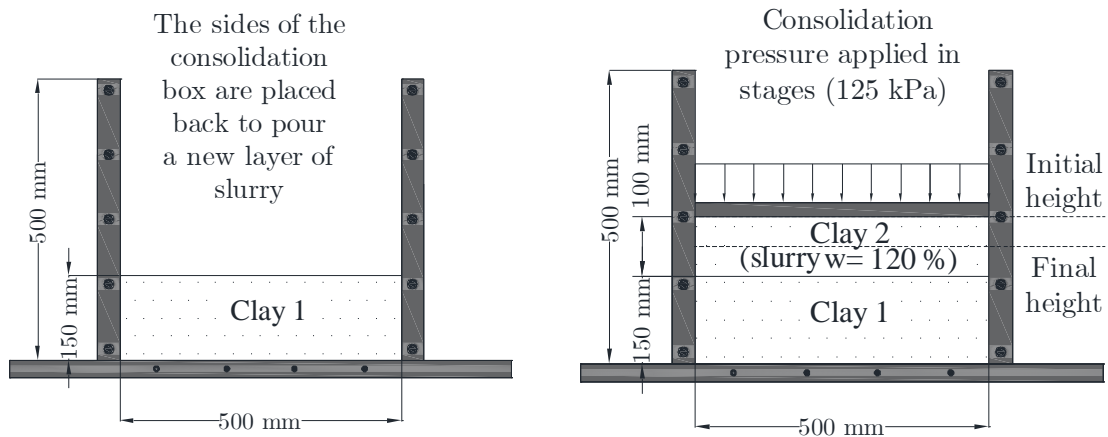
Figure 3.14: Pouring of clay and container preparation for a softer clay layer.
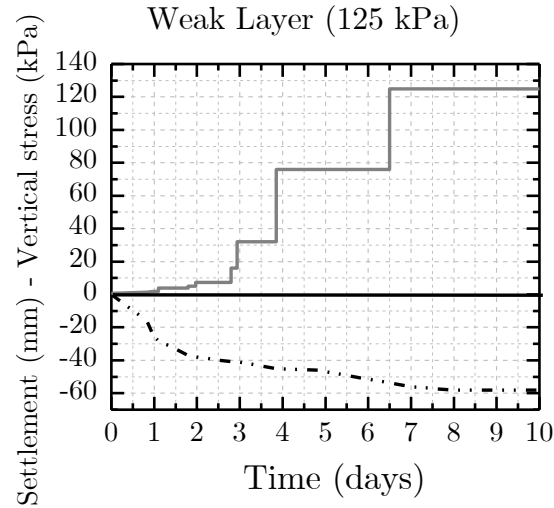
Figure 3.15: Settlement-consolidation curves for the clay used in the centrifuge test - Block 2.

5. At the end of consolidation of the second layer, the previously stored top layer was positioned on top, and a σ_{vmax} = 125 kPa pressure was applied to the three-layer clay bed for two days to ensure continuity between layers. This continuity was checked after the centrifuge test by cutting transverse slices of clay (Figure 3.16).
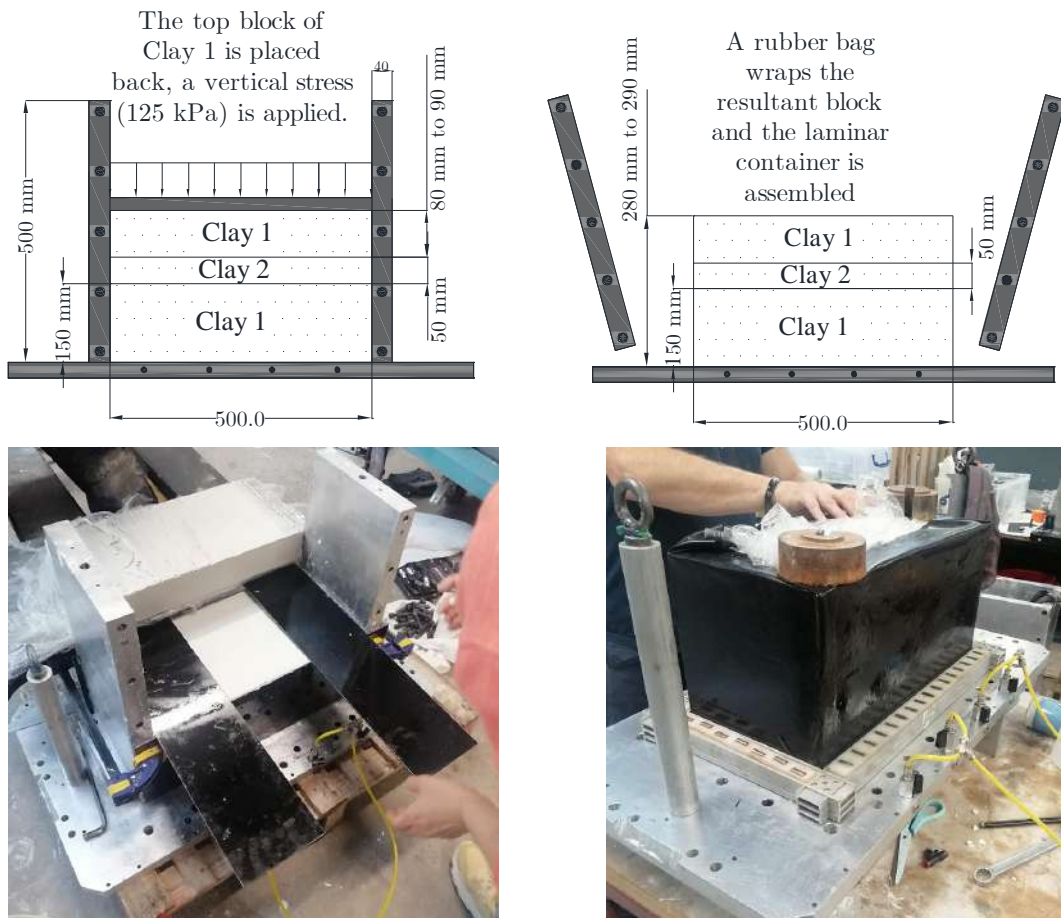
Figure 3.16: End of consolidation and preparation of the clay for installation of the laminar container.

Once assembled the laminae around the clay, the instrumentation was installed. The piezo accelerometers and the PPTs were placed by excavating boreholes with small pipes, removing the clay, and positioning the instruments with a probe for installation at specific depths (Brennan *et al.*, 2006a). Figure 3.17 presents a general view of the centrifuge models and Figure 3.18 one of the models in the servo-hydraulic actuator.

To summarize the model preparation methodology, Table 3.2 presents the model preparation stages and the time spent on each one, the total time for the test presented in this chapter was 27 days, or roughly 1 month. It is worth to mention that monitoring of the time involved in the various stages in an experiment is useful to prepare more accurate schedules in an experimental testing program.

Table 3.2: Model preparation stages

Stage	Time (days)
Preparation of the consolidation container	1
Consolidation - block 1 of kaolin ($\sigma_v = 250$ kPa)	12
Consolidation - block 2 of kaolin ($\sigma_v = 125$ kPa)	10
Re-consolidation the of three-layer profile	2
Installation of the laminar container around the clay	1
Installation of instruments	1
Total	**27**
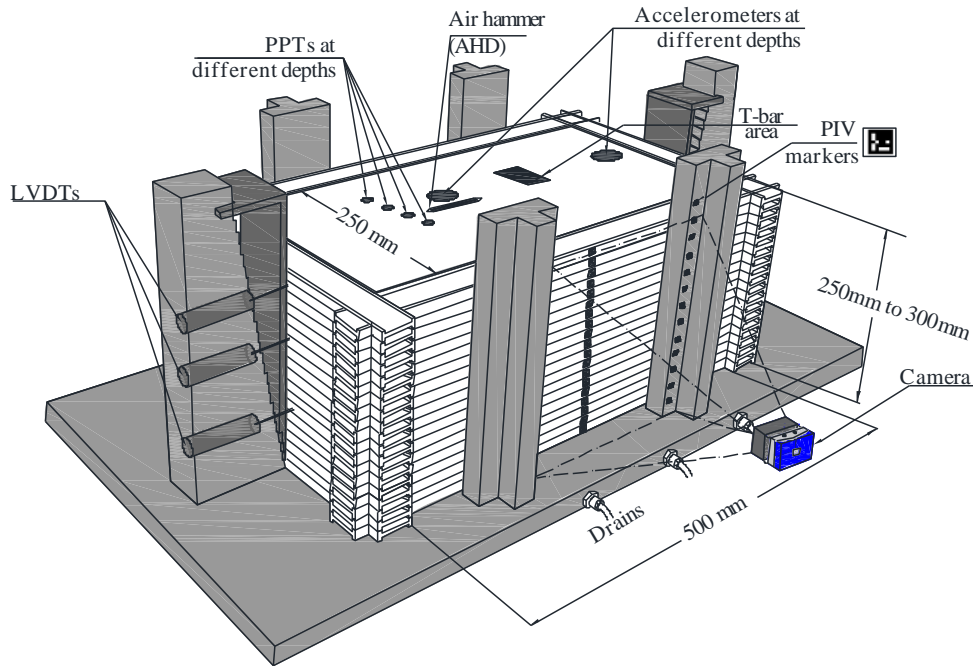
Figure 3.17: A general view of the setup of the centrifuge experiments and instrumentation setup.

54

1	PPTs
2	Accelerometers
3	T-bar
4	Gantry
5	High-speed camera
6,7	Lights
8	LVDTs
9	AHD
10,11	Junction box
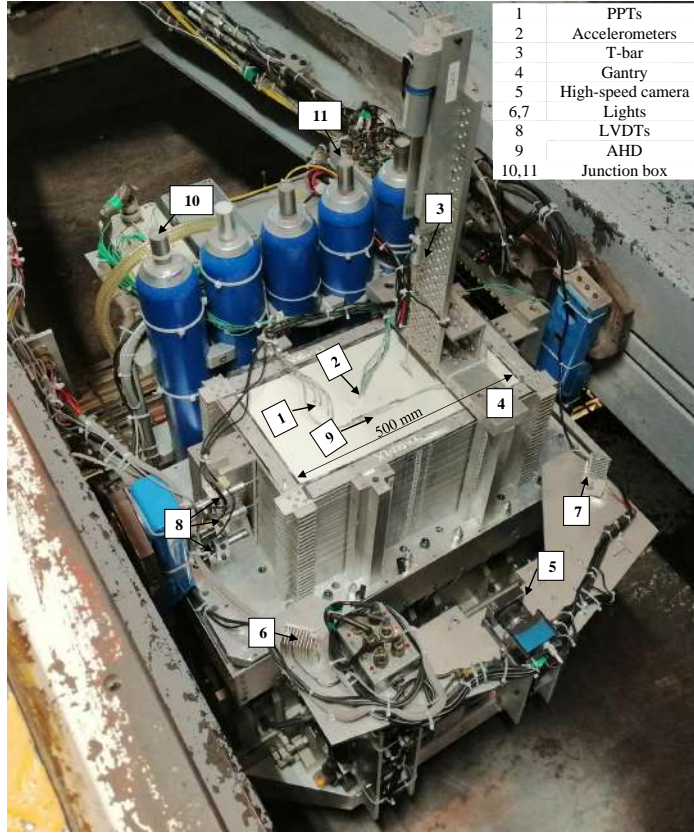
Figure 3.18: A View of a model in the centrifuge.

Considering that after unloading the clay, there would be a reduction in the effective stress prior to centrifuge testing commencing, the clay was held under a suction of around -60 kPa. This was done by connecting a vacuum pump to the drains located at the base of the model container (Figure 3.17) allowing for a continuous application of negative pressure until the moment prior to the centrifugal acceleration of the model in the centrifuge. The applied suction of -60 kPa was below the air entry value to prevent the occurrence of cavitation. A range of pressures of the same order (-60 kPa to -70 kPa) was used by Garala *et al.* 2020 for the preparation of a model in clay during the unloading phase of consolidation. Given the short time in which the suction was applied to the model, no considerable effects were expected in terms of the saturation of the clay. As part of the experimental setup, water content samples were taken at different depths across the clay profile at the end of the centrifuge test. Figure 3.19 presents an example of the sampling of a column of clay and water content profiles taken from tests belonging to the same experimental testing program consisting on simulating layered soil profiles. It can be observed a consistency between the results of the experiments, for reference the water content of the centrifuge experiment presented in this chapter is labelled as "Weak layer test 1" in Figure 3.19(b). The data labeled "Weak layer test 2" is from a test in which it was aimed to simulate a softer clay layer by applying a pre-consolidation pressure in

the weak layer of 75 kPa. The data series labelled "Sand layer test 1" is from a test in which a sand layer was installed between two clay layers consolidated at 250 kPa. The average water content and degree of saturation of the clay were around 53% and 100 % respectively, confirming that during the centrifuge test the clay was in a saturated condition. Some differences can be observed between the water content profile of the experiment identified as "Weak layer test 1", it could be attributable to the sampling methodology between experiments. To verify the homogeneity of the soil profile, tomography studies may be useful for similar testing programs.
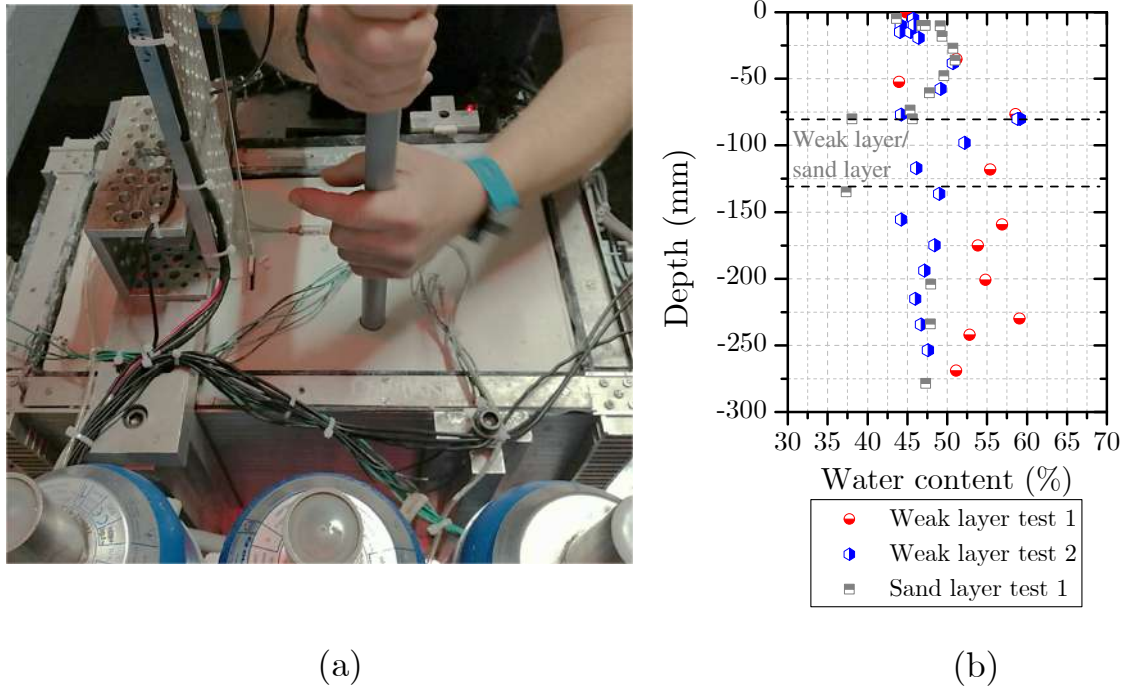
Figure 3.19: Water content after centrifuge test(a) sampling; (b) water content profiles of tests in the same experimental program.

3.5 Particle Image Velocimetry (PIV) analysis setup

PIV analysis was adopted in the experiments as an additional source of data, particularly for the measurements of displacements at different depths of the model. For the experiments, the high-speed camera presented previously was set to record images with a resolution of 1504 pixels by 1050 pixels, resulting in a frame rate of 953 Hz. The camera was triggered to record 15 percent of the total frames via an external signal, and the remaining percentage to record the earthquake itself. The recording time for dynamic events in the centrifuge is of the order of a few seconds; for the current test 1.4 seconds was sufficient to record a total of 1354 photos (or frames) per earthquake.

Once the laminar container was assembled and the instruments installed, ArUco markers (Garrido-Jurado *et al.*, 2014) were glued to each lamina. Two sets of markers were used, the first set, labelled as "Fixed column", (Figure 3.20) was attached to the vertical, rigid columns that act as a boundary and support for the laminar container in the transverse direction. The displacement of the elements of the "Fixed column" is related to the displacement of the shaking table, enabling tracking of the input motion. The second set of markers, labelled as "Displacement markers" (Figure 3.20), was installed in the laminae of the container and used to track the displacement of the mass of soil at different depths. The three LVDTs installed on the side of the container were also used for comparison with and validation of the displacements tracked by the PIV method.
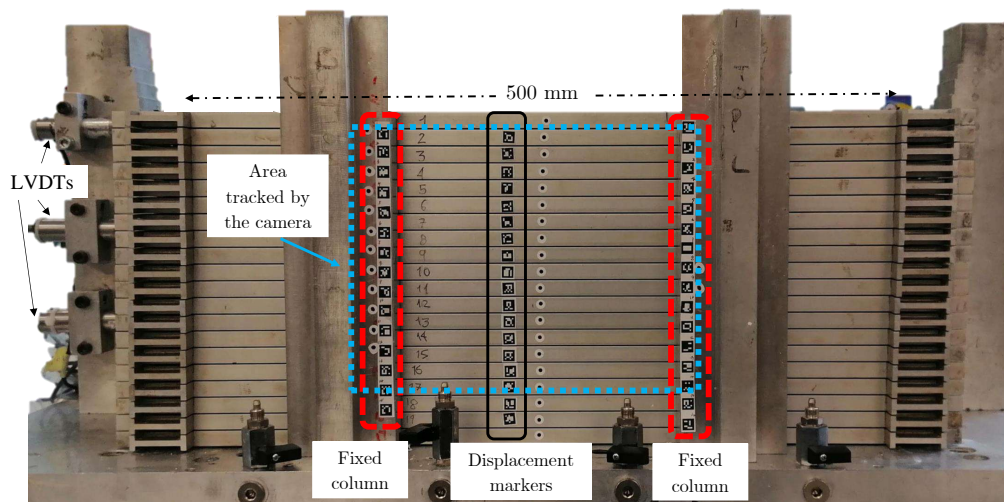
Figure 3.20: Location and sets of markers for PIV.

Blender is an open-source software package for many purposes related to 2D and 3D animation (Hess, 2010). Among its functionalities, there is a module for motion tracking that enables tracking of markers during a photo or video sequence. Options such as marker size, tracking area, correlation between matched and source image and tracking methodologies are available. Blender uses a tracker with subpixel precision following a brute-force search with subpixel refinement. For the current test, a correlation coefficient of 0.95 and a tracking method called "Location only", which looks for changes in translation of the markers, was used.

The tracking process begins by assigning initial coordinates to the markers to be tracked, in a frame the coordinates are in pixel units in the horizontal and vertical directions. This is performed by defining a pattern area with a size equivalent to the dimensions of the marker. Next, a search area is established in which Blender will look for the position of the marker in the following frames. The definition of the pattern area and the search area is shown in Figure 3.21(a). The

search area was assigned to the markers based on their expected displacements during each earthquake motion, this area can be increased in case one of the markers moves beyond the defined range. After tracking the markers, the results were generated in terms of frame number, and the horizontal and vertical coordinates of each marker in pixels. Before the test, a checkerboard was placed in front of the camera in the same plane as the markers to associate real coordinates to the coordinates of the markers in the photos (1 pixel was equivalent to approximately 0.18 mm in model scale). Figure 3.21 (b) shows the coordinate system for a photo in pixels and the corresponding equivalence in millimetres.
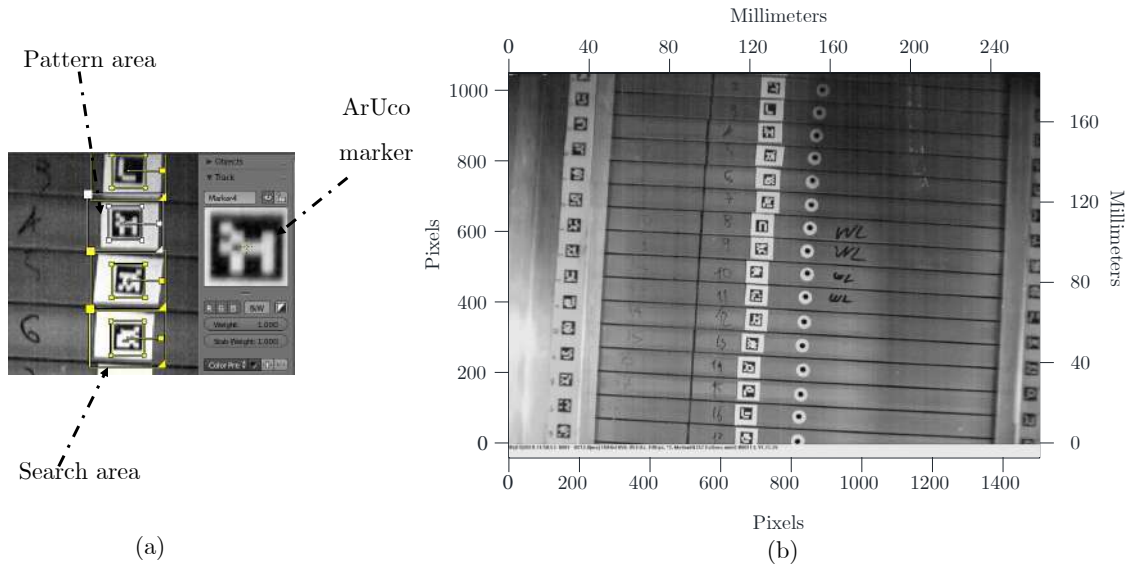
Figure 3.21: Tracking of markers: a) screenshot of Blender, pattern and search area definition; b) photo in pixels and scaled in millimetres.

An example of the tracking of one marker is presented in Figure 3.22. The coordinates of each marker (x_i, y_i) after being tracked are in units of pixels and presented frame by frame with a total of 1354 frames tracked in a period of 1.4 s (frame rate 953 Hz) as previously discussed. According to the camera settings and position, an area of 1504 pixels by 1050 pixels covering 15 out of 23 laminations of the model container. The scaling between pixel units and distance units is performed using a known length employing a checkerboard, as mentioned above, then a relationship of a 1-pixel equivalent to approximately 0.18 mm in model scale was obtained. Finally, each coordinate of the marker is expressed in prototype units (X_i, Y_i), the time step is obtained from the sampling frequency and the variation of the horizontal displacement is plotted with time. Since the displacements occur in the downslope orientation, there was no variation of displacements in the y (vertical) direction (also for the boundary condition imposed by the laminar container), however, the methodology can be applied to problems in which is necessary to track displacements also in this direction.
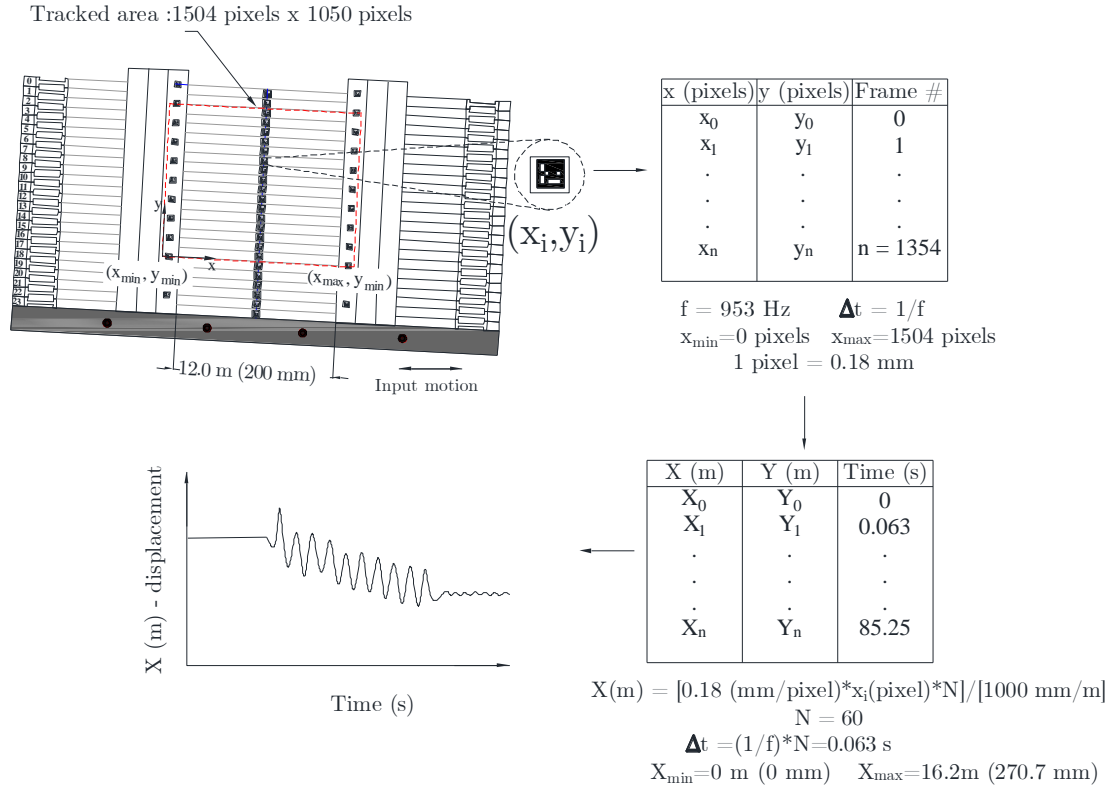
Figure 3.22: Example of tracking of a marker (model units in parenthesis).

3.6   Test procedure

After model preparation had been complete, the servo-hydraulic actuator and counterweight were loaded onto the centrifuge. Next, the model itself was loaded onto the servo-hydraulic actuator. The model was tilted by the desired inclination by utilizing wedges placed along its base. At that time, the wires of the instruments were connected to the junction boxes on the servo-hydraulic actuator and cable-tied into place.

Pre-flight checks were carried out including the response of the air-hammer, the readings of the instruments, the response of the high-speed camera with the light system, the setup of the data acquisition system, and the pressures available in the accumulators of the servo-hydraulic actuator to fire the earthquakes.

The swing-up of the model consisted of increments of 10g until reaching the acceleration level for the test (60g). The bottom drains of the model were closed during the centrifuge test, then no extra water could enter or leave during the test.

Air hammer tests (AHT) were performed at the different stages of the spinning up of the model and between the shaking events as a method to estimate the shear wave velocities within the soil profile in flight. The accelerometers were used to capture the arrival times generated by the air hammer placed on top of the clay (Figure 3.17), further details about the air hammer test are presented by Ghosh and Madabhushi (2002). To perform air hammer tests, it is imperative to have a very fast data acquisition system (Madabhushi, 2014), then a high sampling frequency of 30 kHz was set in the data acquisition system.

Pore pressures and displacements of the model were monitored during the swing up to check the response of the model during the increasing acceleration field. During this stage, the data acquisition system was set to record samples at a rate of 120 Hz. Once the target acceleration level was achieved, the model was maintained in flight for 40 minutes before the application of the earthquakes to increase the total stresses and redistribute the pore pressures and effective vertical stresses, a similar methodology was reported by Garala *et al.* 2020. The following stage consisted of a T-bar penetrometer test (Stewart and Randolph, 1991) and an additional air hammer test. The T-bar was pushed into the clay at a rate of approximately 2mm/s and at a sampling frequency of 6kHz.

Once the in-flight characterization took place, the model was subjected to the selected earthquakes, consisting of sinusoidal motions, and scaled real earthquakes to cover a broad range of frequencies. Specific details of the input motions applied are presented in the following chapter. For the earthquakes, a sampling frequency of 6 kHz was utilized. Simultaneously with the application of the earthquakes, the high-speed camera and light system were triggered to start recording once the model was subjected to the earthquakes.

After data acquisition was complete, the centrifuge was slowed and stopped; the process was monitored and recorded by the LVDTs and PPTs at a sampling rate of 120 Hz. The actuator was then blocked up to hang level and the model was examined, measured, photographed and samples to quantify the water content were taken

3.7   Final remarks

The proposed model preparation enabled the simulation of uniform and layered soil profiles in clay. The instrumentation implemented in the centrifuge experiments has been extensively employed in dynamic centrifuge testing, so reliable response

and measurements can be expected. The installation of the instrumentation and the consolidation steps varies according to the research institution. The time intervals of each loading step during consolidation followed the experience of using Speswhite kaolin over the last 40 years.

The proposed PIV setup aimed to obtain complementary information about displacements and, indirectly, the acceleration measurements at different depths. This methodology could be applied in comparable testing programs involving the use of laminar containers. In the following chapters the use of the techniques described here is applied with reference to three centrifuge tests: two investigating the seismic response of slopes in uniform profiles and one examining the response of a slope with a weak layer.

3.8   Chapter 3 References

ALMEIDA, M.S.S., 1984, "Stage constructed embankments on soft clays," PhD thesis, Cambridge University, Cambridge, UK.

BRENNAN, A. J., MADABHUSHI, S. P. G., AND COOPER, P., 2006a, "Dynamic centrifuge testing of suction caissons in soft clay," Proceedings of the 6th International Conference on Physical Modelling in Geotechnics, 6th ICPMG '06, Hong Kong, pp.625-630.

BRENNAN, A. J., THUSYANTHAN, N. I. AND MADABHUSHI, S. P. G., 2005, "Evaluation of shear modulus and damping in dynamic centrifuge tests," Journal of Geotechnical and Geoenvironmental Engineering, Vol.131, No.12, pp.1488–1498.

CLEGG, D. 1981. Model piles in stiff clay. Ph.D. thesis, Cambridge University, Cambridge, UK.

FAGUNDES, D.F., RAMMAH, K.I., ALMEIDA, M.S.S., PEQUENO, J., OLIVEIRA, J.R.M.S., AND BORGES, R.G, 2012, "Strength Behaviour Analysis of an Offshore Brazilian Marine Clay." Proceedings of the ASME 2012 31st International Conference on Ocean, Offshore and Arctic Engineering, Rio de Janeiro, Brazil, Vol.4, pp.1-9.

GARALA, T. K., MADABHUSHI, G., AND DI LAORA, R., 2020, "Experimental investigation of kinematic pile bending in layered soils using dynamic centrifuge modelling," Geotechnique, pp. 1-16.

GARRIDO-JURADO, S., MUÑOZ-SALINAS, R., MADRID-CUEVAS, F., AND MARÍN-JIMÉNEZ, M., 2014, "Automatic generation and detection of highly reliable fiducial markers under occlusion," Pattern Recognition, Vol.47,

pp.2280–2292.

GHOSH, B., AND MADABHUSHI, S.P.G., 2002, "An efficient tool for measuring shear wave velocity in the centrifuge." Proceedings of the International Conference on Physical Modeling in Geotechnics: ICPMG'02, pp.119-124.

HESS, R., 2010, "Blender Foundations: The Essential Guide to Learning Blender 2.6", Focal Press.

KIM, S. H., 1996, "Model Testing and Analysis of Interactions between Tunnels in Clay," Ph.D. thesis, University of Oxford, Oxford, UK.

HESS, R., 2010, "Blender Foundations: The Essential Guide to Learning Blender 2.6", Focal Press.

KNAPPETT, 2006, "Piled foundations in liquefiable soils: accounting for axial loads," PhD thesis, Cambridge University, Cambridge, UK

LAU, B. H. ,2015, "Cyclic behaviour of monopile foundations for offshore wind turbines in clay," PhD thesis, University of Cambridge, Cambridge, UK.

MADABHUSHI, S.P.G., 2014, Centrifuge modelling for civil engineers, CRC Press, Boca Raton.

MADABHUSHI, S.P.G., HAIGH, S.K., HOUGHTON, N.E., AND GOULD, E., 2012, "Development of a servo hydraulic earthquake actuator for the Cambridge Turner beam centrifuge". International Journal of Physical Modelling in Geotechnics, Vol.12, pp.77-88.

PHILLIPS, N., 1988, "Centrifuge lateral pile tests in clay. Tasks 2 and 3," A report by Exxon Production Research Corp.

SCHOFIELD, A.N., 1980, "Cambridge Centrifuge Operations," Géotechnique, Vol .30, No.3, pp.227-268.

STEWART, D., 1992, "Lateral loading on piles due to simulated embankment construction." PhD thesis, The University of Western Australia.

STEWART, D.P AND RANDOLPH, M.F., 1991, "A new site investigation tool for the centrifuge," Proceedings of the International Conference on Centrifuge Modeling –Centrifuge'91, Boulder, Colorado, pp.531-538

VARDANEGA, P.J., LAU, B.H., LAM, S.Y., HAIGH, S.K., MADABHUSHI, S.P.G, AND BOLTON, M.D., 2012, "Laboratory measurement of strength mobilisation in kaolin: link to stress history", Geotechnique Letters, Vol.2, pp.9-15.

WILLIAMSON, M., 2014. Tunnelling effect on bored piles in clay. PhD thesis. University of Cambridge, United Kingdom.

Chapter 4

Evaluation of the seismic response of gentle slopes in clay using centrifuge experiments

4.1   Introduction

Two centrifuge tests were conducted to investigate the effects of the inclination on the seismic response of gentle slopes. The first model consisted of a slope with an inclination of three degrees and the second model simulated a slope with a six-degrees angle. Both models were built under similar conditions. In this chapter a detailed characterization of the seismic response of a three-degrees slope test is performed, as it is the baseline model for the calibration of the numerical model presented in Chapter 6. Then a summary of the results of a six-degrees slope test is also shown to compare the response of both models in terms of surface displacements and accelerations.

4.2   Three-degrees slope test

Figure 4.1 presents the experimental setup of the three-degree slope model instrumented with nine accelerometers, four pore-pressure transducers, three LVDTs, an Air Hammer, and a setup (actuator, load cell, support gantry) to perform in-flight T-bar tests. The centrifuge test was conducted under a centrifugal acceleration of 60g. The clay was consolidated in steps using a strongbox, starting from 0.7 kPa and increased by doubling the pressures until reaching 1000 kPa. The consolidation took place at 1g in a computer controlled consolidation rig, the process lasted 21 days and it was stopped until settlements were stabilized within 48 hours.

The following are the stages of the experiment:

(i) Pre-flight checks

(ii) Swing up to 60g: 10h and AHT, 20g and AHT, 30g and AHT, 40g and AHT, 50g and AHT, 60g and AHT.

(iii) Consolidation for 40 minutes at 60g (Figure A.1 in Appendix A), followed by an AHT.

(iv) T-bar test.

(v) Earthquakes: EQ1, EQ2, EQ3, EQ4, EQ5 (refer to Section 4.2.2 - Shaking events).

(vi) Swing down

(vii) Post-test investigations.
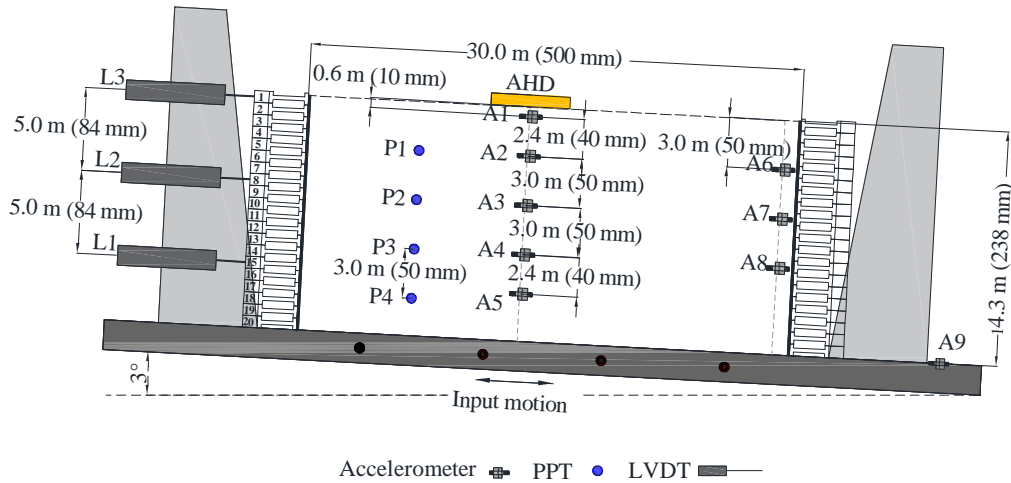
Figure 4.1: Instrumentation layout of three-degrees slope model.

4.2.1 In-flight characterization

The in-flight characterization of the soil profile was done by means of Air-Hammer and T-bar tests. Figure 4.2a shows the undrained shear strength (s_u) profile measured in flight at an acceleration level of 60g before the application of the earthquakes. The T-bar used was 40 mm wide with a 4mm diameter, and was pushed into the clay at a rate of approximately 2 mm/s. For clays, normalized velocities (V) greater than 10 are likely to be undrained (Oliveira *et al.*, 2011; Randolph and Gourvenec, 2011), for the current test V=114, therefore ensuring that the T-bar penetrometer test was performed at an undrained rate. The normalized penetration rate, V (after Finnie and Randolph, 1994) is defined as:

$$V = \frac{vD}{c_v} \tag{4.1}$$

where,

v= penetration velocity of the T-bar, 2mm/s,

D= diameter of the T-bar, 4mm

c_v coefficient of consolidation of the kaolin, 4.29 mm^2/min (0.07 mm^2/s) (Chow *et al.*, 2020).

The *OCR* profile (Figure 4.2b) was back-calculated using the well-known stress history relationship (Wroth, 1984):

$$s_u = K\sigma'_v(OCR)^m \rightarrow OCR = \left[\left(\frac{s_u}{\sigma'_v} * \frac{1}{K}\right)\right]^{\frac{1}{m}} \tag{4.2}$$

where,

K= normalized strength parameter,

σ'_v= effective vertical stress in kPa,

OCR= overconsolidation ratio,

m= power constant in the equation,

The values of K and m have been reported by several authors (Almeida, 1984; Springman, 1989; Sharma and Bolton, 1996). The OCR profile was calculated based on the parameters presented by Zhang *et al.* (2011) (K=0.23, m=0.62).
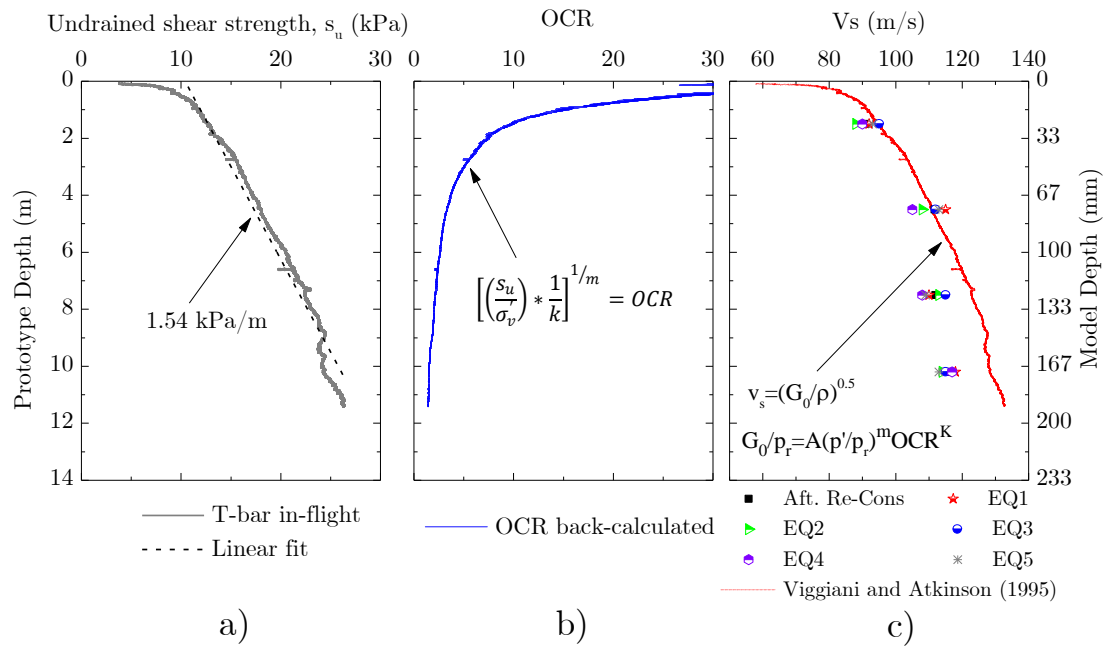
Figure 4.2: Clay model properties: (a) Undrained shear strength profiles, (b) stress history, (c) shear wave velocity profile.

The observed s_u from the centrifuge test is in reasonable agreement with in-situ measured profiles (Chapter 2, section 2.4 Figure 2.6). For instance, at a depth of 10 m, the s_u is around 25 kPa, a slightly larger value as the displayed in Figure 2.6 (20 kPa) from boreholes at the Campos Basin.

The shear wave velocities from the Air Hammer test were calculated by obtaining the arrival time of the shear waves generated by the Air Hammer placed on top of the clay (AHD in Figure 4.1). The travel times can be determined by two methods: peak to peak and cross-correlation (Marshall *et al.*, 2018). The peak-to-peak method uses the first two peaks as the travel time (Ghosh and Madabhushi, 2002). Whereas the cross-correlation performs a point-wise multiplication to determine where two signals are best aligned. Two correlated discrete signals denoted as $s[k]$ and $r[k]$ with a cross-correlation function $T_{sr}[n]$ can be defined as (Rabiner and Gold, 1975):

$$T_{sr}[n] = \sum_{m=-\infty}^{\infty} s[m]r[m+n] \qquad (4.3)$$

Where the parameter n is an integer between positive and negative infinity. The time shift between the correlated signals is obtained at the maximum value of the cross-correlation function. Figure 4.3 shows a schematic representation of a typical arrival of shear waves at different depths with the corresponding response of the accelerometers. The time difference between the first peaks of the signals is the arrival time (Δt_{ij}). With the arrival time obtained either by cross correlation or by the peak-to-peak method, the shear wave velocity is calculated with the known depth of the accelerometers. For the current tests, the arrival time was determined by cross correlation as it avoids complications with picking the first peak from the signals.

The shear wave velocity profile was calculated using the small-strain stiffness correlation based on the Viggiani and Atkinson (1995) equation:

$$\frac{G_0}{p_r} = A \left(\frac{p'}{p_r}\right)^M OCR^k \qquad (4.4)$$

where:
G_0= initial shear modulus in kPa,
p'= mean effective stress in kPa,

p_r= reference pressure equivalent to 1 kPa,

OCR= overconsolidation ratio (see Eq. 4.2)

A, k, M =correlated parameters.

The selection of the correlated parameters (A, k, M) was based on the Plasticity Index of the clay (PI=33%). The relationship between the plasticity index and the parameters is presented in Viggiani and Atkinson (1995). For the current research, A=950, k=0.24, and M=0.8. The shear wave velocity (V_s) was calculated in terms of the initial shear modulus (G_0) and the soil density (ρ) expressed as the total unit weight divided by gravity:

$$V_s = \sqrt{\frac{G_0}{\rho}} \qquad (4.5)$$

Figure 4.2c displays the points of shear wave velocity obtained by means of the Air Hammer test at different stages of the test: after re-consolidation of the clay and between shaking events (identified as EQ1 to EQ5). From the results, a reasonable agreement can be observed between the shear wave velocities estimated by means of the Air Hammer test and the profile calculated from the OCR profile.
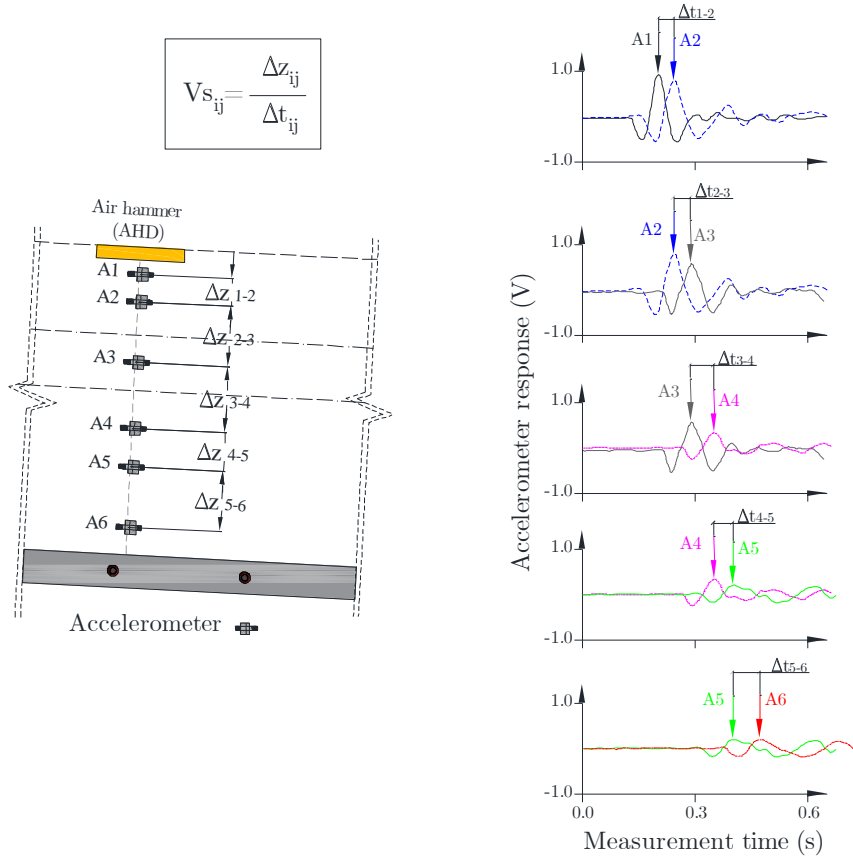
Figure 4.3: Schematic representation of the arrival time for the calculation of the shear wave velocity between accelerometers.

The elastic site period of the soil profile was estimated from the continuous profile extending the shear wave velocity values back calculated from the OCR profile (Figure 4.2c) to the depth of the model (14.3 m). The weighted average of shear wave velocity method was applied (Dobri et al. 1976), for that purpose, the profile was subdivided in sub-layers of 0.10 m and using equation 4.6 an elastic site period of 0.5 s was initially estimated.

$$T = \frac{4H^2}{\sum_{i=1}^{n} V_i H_i} \tag{4.6}$$

where:

T = elastic site period (s)

H = thickness of the soil profile (m)

V_i = shear wave velocity of the corresponding layer (m/s)

H_i = thickness of the sub-layer (m)

Is worth to mention that although weighted average of shear wave velocities is a widely used method, it has a poor physical background (Sawada, 2004). An approach using the measured data is the identification of the first peak of an experimental transfer function, associated to the fundamental frequency of the site, as explained in section 4.2.3.

4.2.2   Shaking events

The three-degrees slope model was subjected to five earthquakes. Three consisted of sinusoidal motions with a driven frequency of 1Hz (EQ1, EQ4, EQ5), a low amplitude and broad frequency motion (EQ2) , and a scaled real motion (EQ3 - Kobe earthquake, 1995). During the application of the earthquakes, the transducer data was recorded at a sampling frequency of 6 kHz. Figure 4.4 and Figure 4.5 present the input motions with their corresponding frequency content. The input motions are defined in this research as the accelerations measured at the base of the model (accelerometer A9 in Figure 4.1). The data are presented in terms of prototype scale.

The input motions identified as sinusoidal (EQ1, EQ4, EQ5) are not completely smooth and from the frequency content, higher harmonics are observed. From the frequency content of the input motions displayed in Figure 4.4 and Figure 4.5, additional harmonics can be observed, particularly evident in the sinusoidal motions. As discussed by Brennan *et al.* 2005 the load applied by the shaking table to the laminar box is not necessarily single frequency. Then, the higher

harmonics reflect part of the vibration of the shaker and transmitted to the model container, therefore, they can be considered as real loading components and cannot be considered as noise.
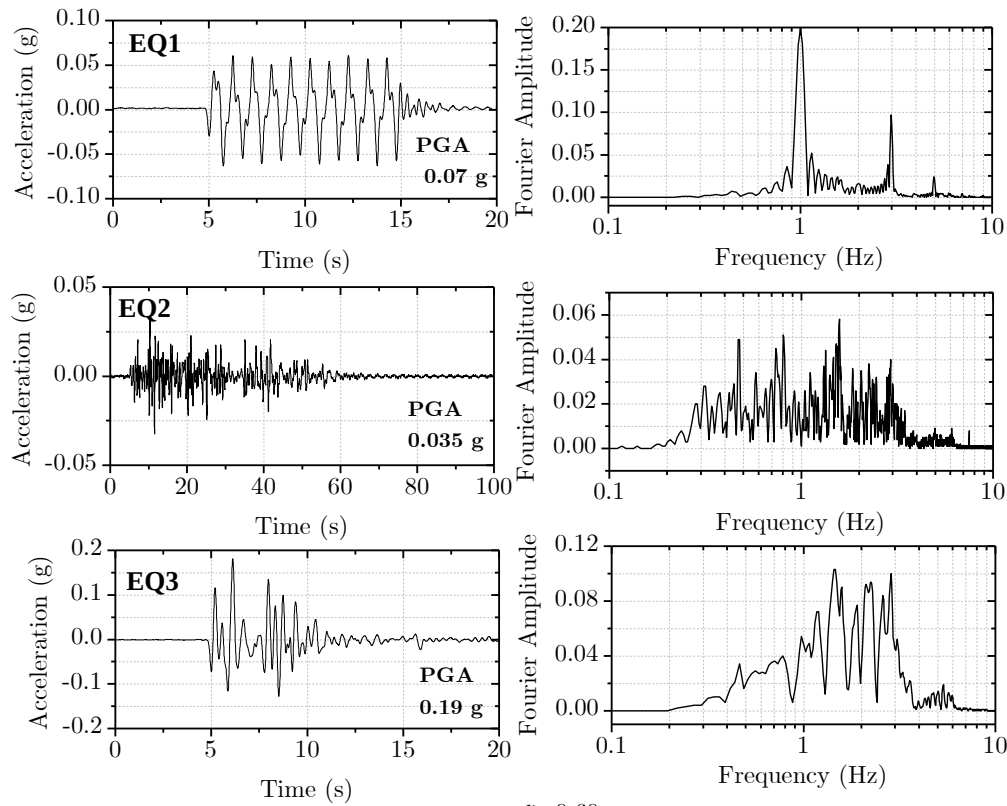
Figure 4.4: Three-degrees slope test: input motions EQ1, EQ2, EQ3 and frequency contents (prototype scale).
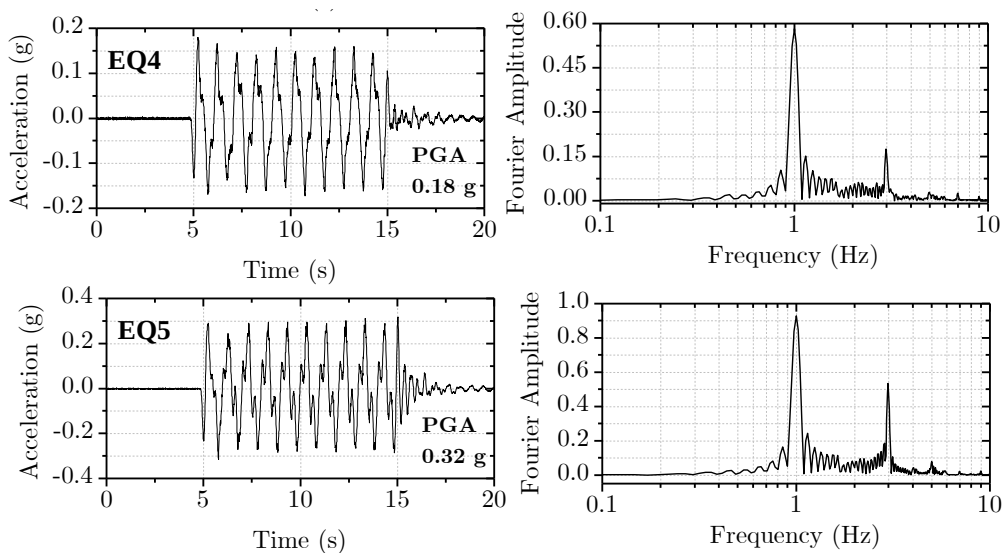
Figure 4.5: Three-degrees slope test: input motions EQ4, EQ5 and frequency contents (prototype scale)

4.2.3 Experimental transfer function

An important practice for ground response analysis is the use of transfer functions, which display how the frequencies from the input motions are amplified or deamplified by the soil deposit. A transfer function can be understood as a filter that acts on an input signal leading to an output signal.

In theory, for shear wave propagation, throughout a layered deposit, the frequency near the site's natural frequency will be amplified significantly (Kramer, 1996). An experimental transfer function was calculated using the accelerometer at the base of the model (A9 in Figure 4.1) and at the surface (A1 in Figure 4.1) for the lowest amplitude and broader frequency content ground motion (EQ2). From the transfer function presented in Figure 4.6, a peak was identified at 1.65 Hz or in terms of period at 0.6 s. This result differs from the elastic site previously calculated (0.5 s). Therefore, the shear wave velocity profile back-calculated from the OCR requires an adjustment to better reflect the elastic site period. This was confirmed by preliminary numerical simulations that evidenced a shift in the peak of the transfer function when using the shear wave velocity profile presented in Figure 4.3(c). A discussion of the adjustment of the shear wave velocity profile is presented in Chapter 6. Then, from the adjustments in the shear wave velocity profile and the measured transfer function, an elastic site period of 0.6 s was obtained for this model.
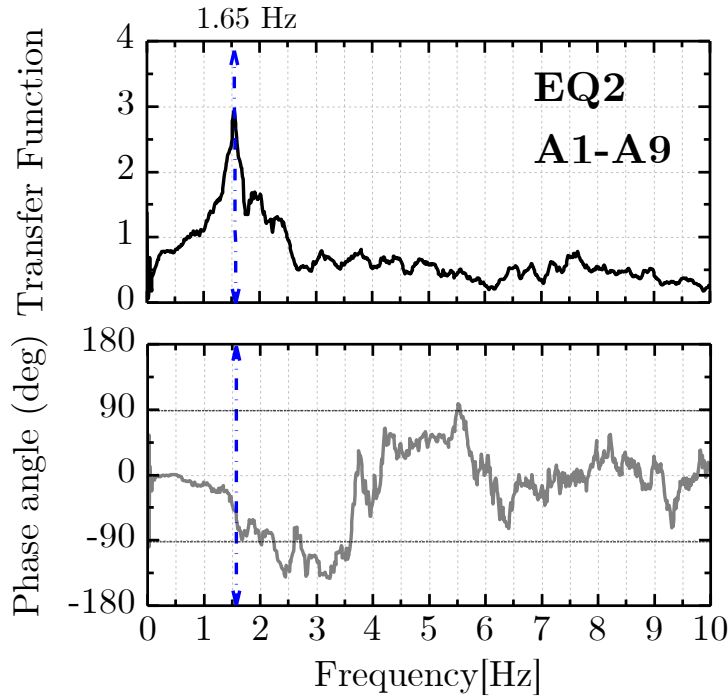
Figure 4.6: Measured transfer function for the 3-degrees slope test

4.2.4   Test results: Lateral displacement-time histories

For reference, Figure 4.7 presents the location of the LVDTs employed to measure the lateral displacements displayed in Figure 4.8 and Figure 4.9. The results include PIV measurements and the corresponding input ground motions. It can be observed the largest displacement-time histories at the surface of the slope as measured by LVDT L3. As expected, the amplitude of the displacements increased as the input motion intensity increased. Lateral displacements during the earthquake EQ2 are not shown as they were not noticeable. The results measured by the PIV and the LVDTs indicate an excellent agreement. Then, the displacements at different depths can be monitored by this method, and data from malfunctioning LVDTs can be recovered. For example, LVDT L1 detached from the side of the laminar container, then, no response was registered by this instrument. Secondary analyses with the PIV are introduced in the following chapter including the calculation of approximated acceleration-time histories by a double derivative of the displacements obtained by PIV as an additional source of data to construct a continuous profile of peak ground accelerations.

From Figure 4.7 it can be observed a particular behavior in terms of the lateral displacements. Although the PGA of EQ1 was smaller (0.07g) than the PGA of EQ3 (0.19 g) larger lateral displacements occurred during the application of the first input motion. This is attributed to the number of significant cycles of the sinusoidal motion, in this case 10, on the other hand, the EQ3 has less significant cycles. This means that the sinusoidal motion had a greater effect on the accumulation of seismic displacements on the slope.
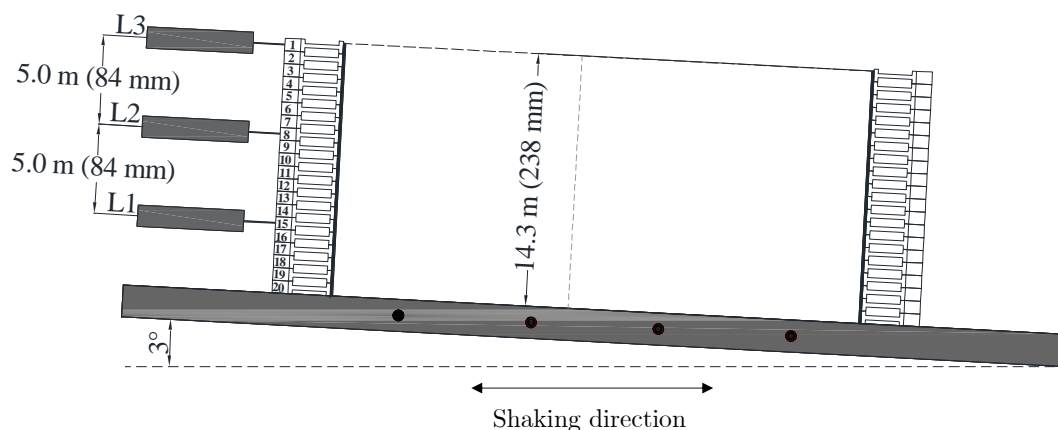
Figure 4.7: Location of LVDTs: three-degrees slope test
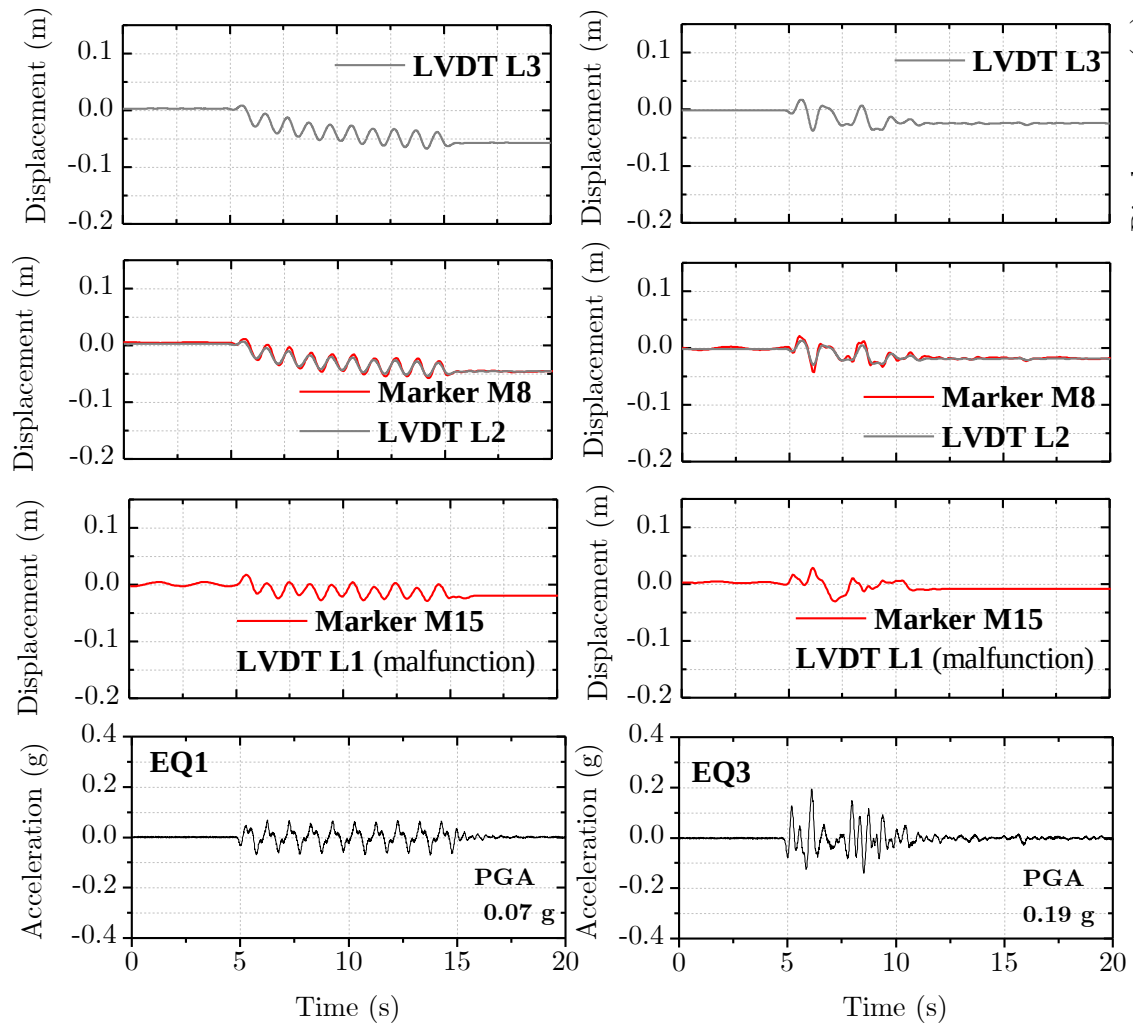
Figure 4.8: Three-degrees slope test: recorded displacement-time histories for EQ1 and EQ3
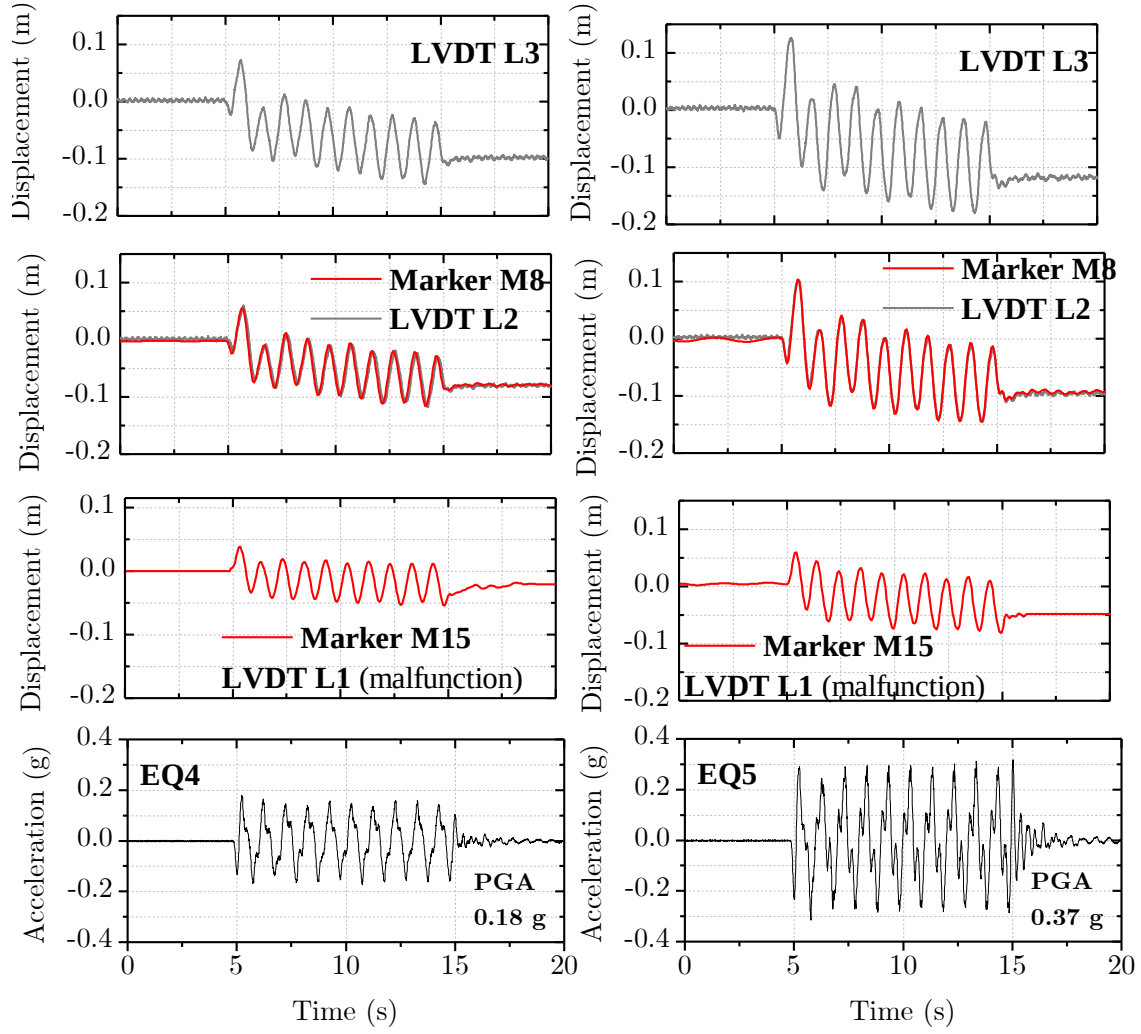
Figure 4.9: Three-degrees slope test: recorded displacement-time histories for EQ4 and EQ5

4.2.5 Test results: Acceleration-time histories

The acceleration-time histories at different depths for the earthquakes applied to the model are presented in Figure 4.10. The results are presented in prototype scale. The raw data from the accelerometers were filtered using a fourth-order Butterworth type filter with a bandpass between 20 Hz and 450 Hz in terms of model scale. The selected range of frequencies was defined to remove the low frequencies that produce a drift in the accelerometer signal and the high frequencies associated with electrical noise. Altogether, the instruments presented a good response, except accelerometer A5 at 11.4 m depth that displayed an irregular response during earthquakes EQ1, EQ2 and EQ3.
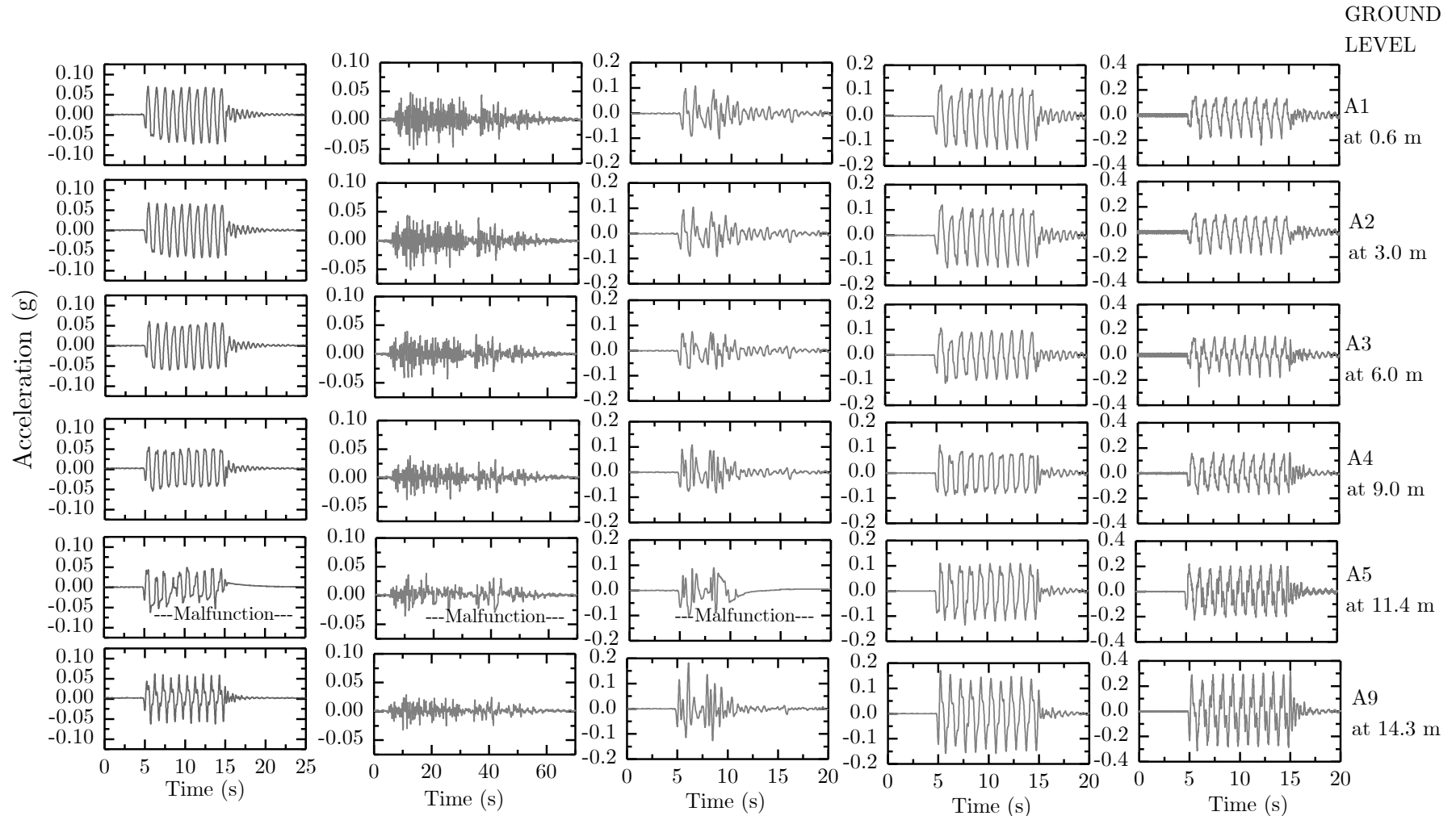
Figure 4.10: Three-degree slope test: recorded acceleration-time histories

4.2.6 Test results: Excess pore pressure measurements

Figure 4.11 presents the response of the pore pressure transducers at different depths during and after the application of the earthquakes. On balance, PPT P4 at 12 m depth was the only one that registered an increasing pattern in the excess pore pressures through the shaking events with values ranging between 3 kPa and 6 kPa. PPTs P2 and P3 exhibited residual pore pressures after the earthquakes showing an increasing trend with time. The pore pressure transducer installed at the surface (P1) did not present any noticeable response during earthquakes EQ1 and EQ2 and the instrument presented malfunction (no response) in the course of the last two earthquakes. The results of the dynamic pore pressures show one of the limitations of the current experimental testing program. From the scale of the pore pressure measurements, it can be said that the pore pressures did not present a significant variation during and after the application of the earthquakes. Given the model preparation methodology, it was not contemplated to install instruments during the consolidation of the clay to avoid damage to the wiring of the instruments themselves. The pore pressure transducers were installed at the end of consolidation by excavating small boreholes removing the clay, positioning the instruments at the desired depths and back-filling the space with slurry. These results suggest that there may not be adequate contact between the clay and the PPTs.
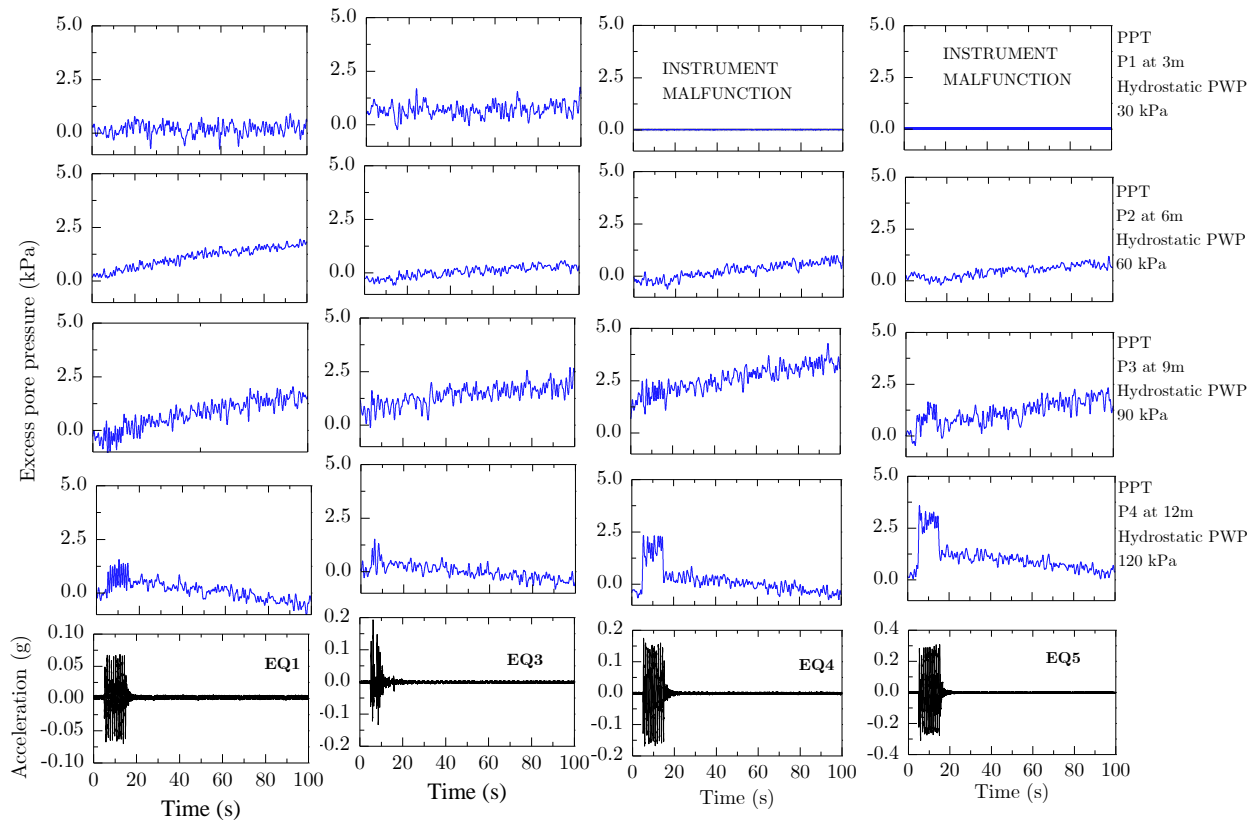
Figure 4.11: Three-degrees slope test: recorded excess pore pressures

75

4.2.7 Peak ground accelerations and permanent lateral displacements

The slope response was evaluated by means of permanent lateral displacements at the end of each input motion, peak ground accelerations (PGA), spectral response spectra (5%-damping) at the base and near the surface, and the ratios between the response spectra. The permanent displacements are defined here as the displacements at the end of the earthquakes (Figure 4.12). For comparison purposes, it must be pointed out that the displacements were plotted for each earthquake by resetting them to zero prior to that earthquake.
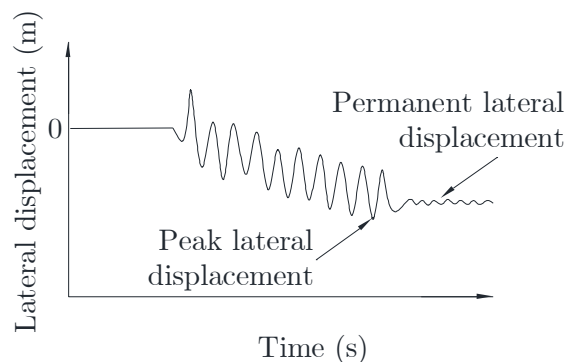
Figure 4.12: Schematic definition of peak and permanent lateral displacements

Figure 4.13 presents the permanent horizontal displacements and PGA profiles obtained after the application of the earthquakes to the model. The values of EQ2 are not presented in the figure as no noticeable displacements were obtained. The permanent horizontal displacement profiles shown in Figure 4.13a were obtained from PIV measurements and from the LVDTs (permanent horizontal displacements at the top of the slope recorded by LVDT L3).

Figure 4.13b shows the PGA variation with depth, the data were acquired from two sources, the continuous line profiles from PIV using the second derivative of the displacements at the depths of the markers and the individual points were obtained from the accelerometer measurements. The permanent displacement pattern, as expected displays an increase from the bottom to the top. It should be noticed that, earthquake EQ1, a sinusoidal motion with an amplitude of PGA=0.07 g, produced larger displacements than EQ3, a scaled real motion with a PGA=0.19g. In terms of the PGA profiles, an attenuation pattern was observed for earthquakes EQ3, EQ4, and EQ5. The results shown in the PGA profiles in Figure 4.13b show a good agreement between the PIV approximations and the measurements from the accelerometers. This was also observed in the centrifuge model that included a weak layer as explained in Chapter 5.

76
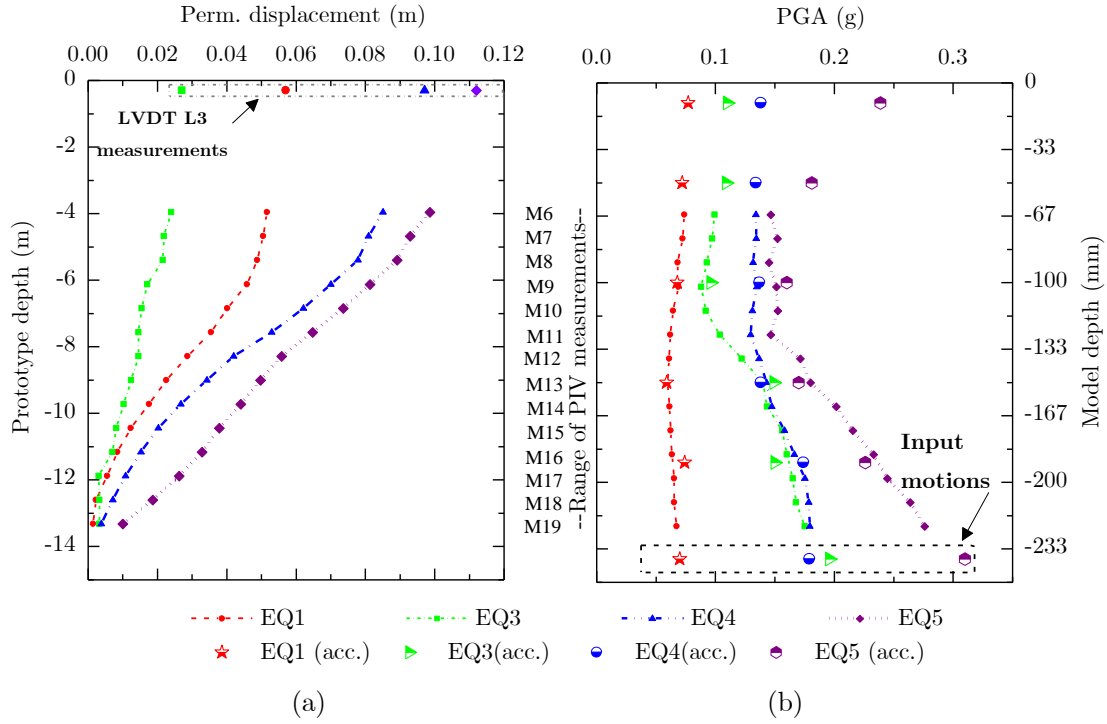
Figure 4.13: Three-degree slope response profiles: (a) permanent displacements; (b) PGA.

Figure 4.14 presents the 5% damped pseudo acceleration response spectra of the earthquakes applied to the model at the base (PSA_b) and those at the surface (PSA_0). Figure 4.15 shows the spectral amplifications defined as the ratio of the 5% damped pseudo acceleration (PSA) response spectra of the recorded ground surface and container base motions:

$$Response\ Spectra\ ratio = \frac{PSA_0}{PSA_b} \tag{4.7}$$

Some trends can be identified from the results:

(i) For periods T< 0.1 s the response spectra ratios are relatively flat with amplification values associated to the amplitude of the input motion. EQ1 and EQ2, the weakest motions (in terms of the PGA) presented response spectra ratios larger than 1.0 (amplification). The stronger motions EQ3, EQ4, and EQ5 produced response spectra ratios of smaller than 1.0 (attenuation).

(ii) From earthquakes EQ1 and EQ2, it was observed a peak near the elastic site period (0.6 s - refer to section 4.2.3). For the larger earthquakes, EQ3, EQ4, and EQ5, a shift in the peak response was observed and may be explained by nonlinear effects resulting from the stiffness reduction of the soil and the increasing damping as the soil is sheared.

(iii) For increasing periods larger than the elastic site period (0.6 s - refer to section 4.2.3), the response spectra ratios exhibit a trend of increasing values except for the lowest amplitude motion (EQ2) that presents a reverse pattern.
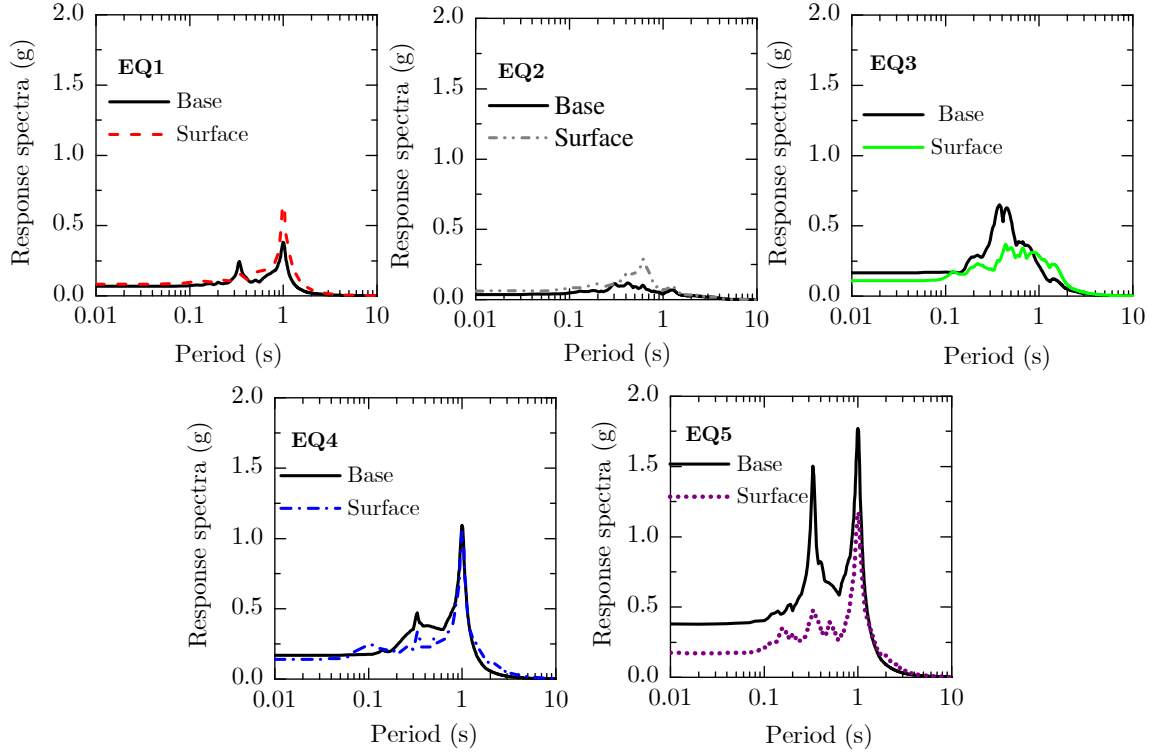
Figure 4.14: Acceleration response spectra for the base and surface of the model for the applied ground motions
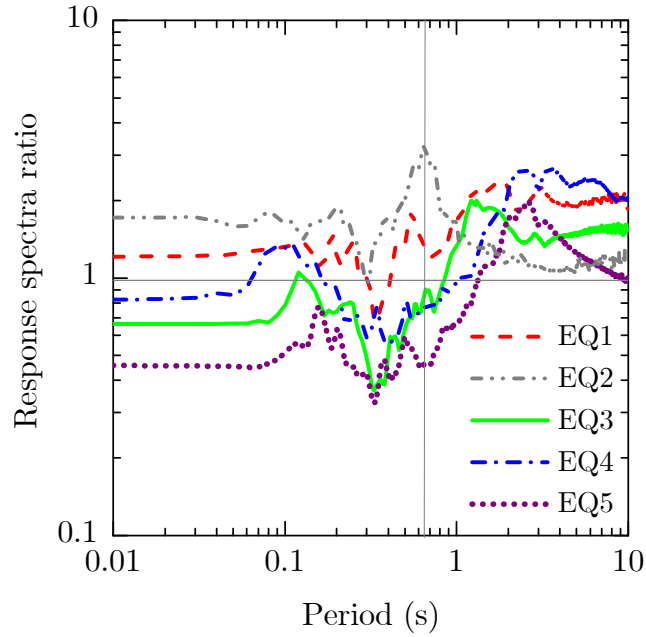
Figure 4.15: Response spectra ratios (amplification factors) for the applied ground motions

4.2.8 Model container performance

Boundary effects in dynamic centrifuge testing of the laminar container used at the Schofield Centre have been previously studied for 1-D conditions for models in sand (Brennan *et al.*, 2006). However, no information related to the boundary effects for models in clay is available. In this research, the performance of the laminar model container has been evaluated by comparing the 5% damped spectral accelerations at the center of the model and near the walls of the model container.

Two ground motions were selected for the evaluation of the boundary effects in the response of the model; a low-intensity motion with a broad frequency content, and a high-intensity motion that induced relatively larger strains in the clay. The 5% damped response spectra of the accelerations at the central column of the soil model (A2, A3, A4) were compared with the response from accelerometers at the same depths (A6, A7, A8), but close to the container wall. The spectral accelerations are shown in Figure 4.16. It can be observed that the response of the accelerometers at the central column and near the boundaries are essentially identical at all periods. This indicates the laminar container produced appropriate boundary conditions for the simulation of an infinite slope model.
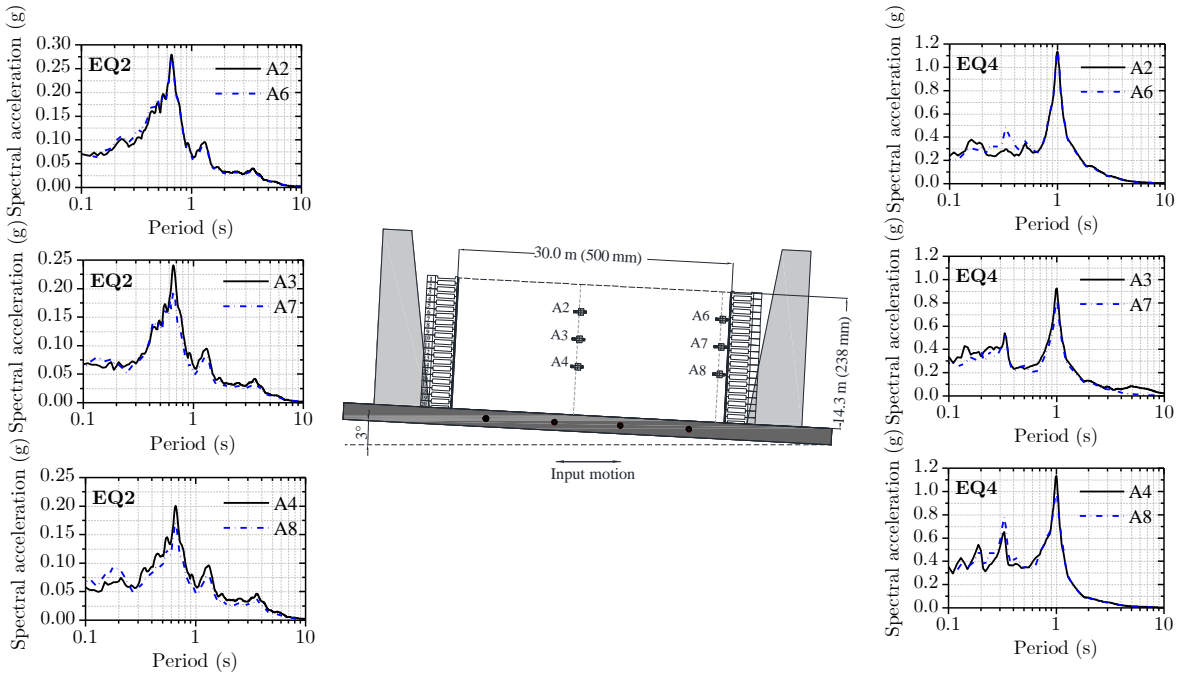
Figure 4.16: Evaluation of model container boundary effects

79

4.2.9 Identification of the soil dynamic properties from the centrifuge test

Complementary information in terms of the dynamic characterization of the clay can be obtained from the experimental results of the centrifuge test. Particularly, using the recorded accelerations during the applied earthquakes, modulus reduction and damping data points were calculated. The methodology employed followed the approach proposed by Zeghal *et al.* (1995) and adapted by Brennan *et al.* (2005) to centrifuge tests to obtain shear stress and strain histories from accelerometers placed in a downhole array.

- Evaluation of centrifuge shear stress and strain histories

To obtain the experimental modulus and damping data points to be compared with empirical relationships (Darendelli, 2001; Vucetic and Dobri, 1991), the first stage is the evaluation of the shear stress-time and strain-time histories. Assuming an infinite slope approximation, the seismic response of the model can be considered a one-dimensional site response problem (Biscontin and Pestana, 2006). Having said that, a one-dimensional shear beam idealization can be used to describe the seismic lateral response (Zeghal *et al.*, 1994):

$$\frac{\partial \tau}{\partial z} = \rho \ddot{u}, with\ boundary\ conditions\ u(h,t) = \bar{u},\ and\ \tau(0,t) = 0 \qquad (4.8)$$

where,
t=time (s),
z= depth coordinate (m),
$\tau(0,t)$= horizontal shear stress (kPa),
$\ddot{u}=\ddot{u}(z,t)$=absolute horizontal acceleration (m/s^2),
$u=u(z,t)$= absolute horizontal displacement (m),
$\bar{u}=\bar{u}(t)$=input (or bedrock) horizontal displacement (m),
ρ=mass density,
h=site depth.

Figure 4.17, presents a site with accelerometers in a downhole array. From the shear beam equation, the shear stress τ at any depth z can be expressed as the integration of the density ρ times the acceleration $\ddot{u}$:

$$\tau(z,t) = \int_0^z \rho \ddot{u} dz \qquad (4.9)$$
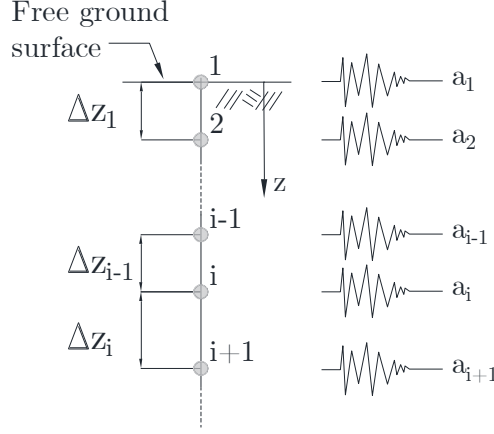
Figure 4.17: Site discretization of accelerometers in a downhole array (Adapted from Zeghal *et al.*, 1995)

Using linear interpolation between downhole accelerations, the discrete version of the shear stress at a level z_i can be expressed using a second-order accurate expression (Zeghal and Elgamal, 1994):

$$\tau_i\left(t\right)\sum_{k=1}^{i-1}\rho\frac{\ddot{u}_k + \ddot{u}_{k+1}}{2}\Delta z_k, i = 2, 3, \ldots \tag{4.10}$$

where,
$z_i =$level associated to subscript i (Figure 4.17),
$\tau_i = \tau\left(z_i, t\right)=$shear stress at level i (kPa),
$\ddot{u}_i = \ddot{u}\left(z_i, t\right) =$ acceleration at level i (m/s^2),
$\Delta z_k=$ spacing interval (Figure 4.17).

Shear strains can be calculated using a second order expression if three accelerometers are stacked in a soil column:

$$\gamma_i\left(t\right) = \frac{1}{\Delta z_{i-1} + \Delta z_i}\left[\left(u_{i+1} - u_i\right)\frac{\Delta z_i}{\Delta z_{i-1}}\right] \tag{4.11}$$

where,
$u_i=u(z_i, t)=$ absolute displacement (from double integration of the corresponding acceleration-time histories).

For the calculation of the stress and strain histories appropriate data filtering needs to be performed. Brennan *et al.* 2005 illustrated the effects of high and low frequency noise that produce drift errors during the integration of

the accelerations to obtain displacements. A bandpass filter was employed with frequencies between 20 Hz and 450 Hz (model scale) to remove the mentioned noise at high frequency and drifts from the low-frequency range.

- Shear modulus and hysteretic damping data points

From the calculated shear stresses and shear strains at specific depths, hysteretic loops were obtained. Figure 4.18a shows an example of hysteresis loops at mid-depth of the slope obtained from the application of earthquake EQ4. It can be observed that the loops do not start from zero in the shear stress axis, this is due to model inclination. The shear stress-strain histories were influenced by the presence of a driving static shear stress component induced by gravity. This static stress can be expressed as $\tau_s = \rho g z sin(\alpha)$ where, ρ is the soil density, g the gravity acceleration, z depth in which the stresses and strains are calculated and α the slope inclination angle. In addition, the stress-strain loops present a displacement in the horizontal axis as they reflect the accumulation of strains in the downslope direction as the shaking occurs. Figure 4.18b shows a typical hysteresis loop and the equations for the calculation of the modulus G_{sec} or G and damping (D) experimental data points.
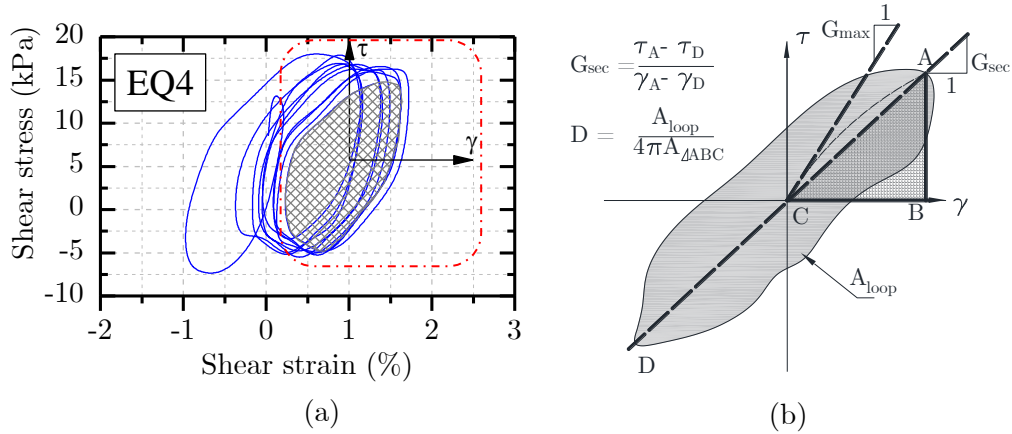
Figure 4.18: Schematic representation of a stress-strain loop and calculation of secant modulus and hysteretic damping.

The depths selected for the calculation of the shear modulus(G_{sec} or G) correspond to the accelerometers A2, A3, and A4 in Figure 4.1. The obtained shear modulus were normalized by the maximum shear modulus, also defined as small-strain modulus G_{max}, calculated as:

$$G_{max} = \rho V_s^2 \tag{4.12}$$

where,

V_s= measured shear wave velocity (using the adjusted profile, see Chapter 6)

ρ= soil density

Figure 4.19 shows the normalized secant modulus (divided by the maximum shear modulus) for all the shaking events. The data points are plotted together with the empirical curves developed by Darendelli (2001) and Vucetic and Dobri (1991). The empirical curves were extended to large strains (10%) by using the GQ/H model (Groholski *et al.*, 2015) that applies a quadratic equation to achieve a target shear strength at large strains. The modulus degradation data points show a reasonable agreement with the empirical curves. Damping values show a significant scatter and present values higher than the published curves. This behaviour is similar to other investigations that have used 1-D array data to obtain modulus degradation and damping curves for centrifuge tests (Brennan *et al.*, 2005; Afacan *et al.*, 2013; Zhou *et al.*, 2017; Tarazona *et al.*, 2020) and for field studies (Elgamal *et al.*, 2001; Tsai and Hashash, 2009).
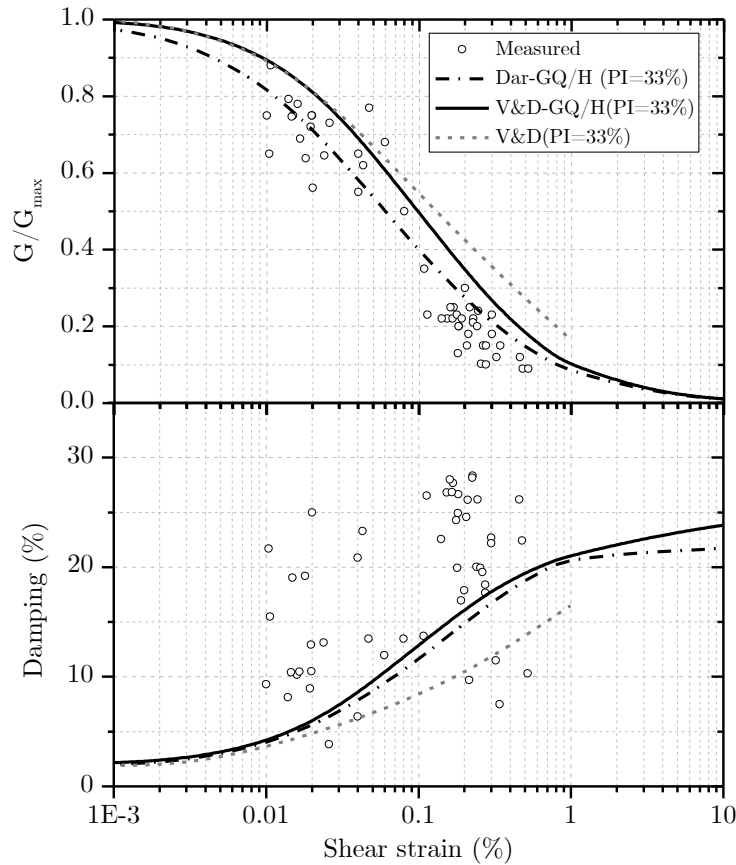
Figure 4.19: Normalized shear modulus and damping data points and empirical curves

4.3 Six-degrees slope test

For comparison purposes a summary of the measured response of a six-degrees slope built under similar conditions as the previously presented centrifuge test. The sample was consolidated in stages reaching a maximum pre-consolidation pressure of 1,000 kPa, the model preparation and instrument installation followed the same procedures of the previous tests to guarantee repeatability of the experiment. The model was instrumented with eight accelerometers, four pore pressure transducers, and three LVDTs (Figure 4.20). During the test, a problem with the camera setup did not allow capturing images to perform PIV analysis. The centrifuge test was performed at an acceleration level of 60 g, with increments of 10 g. The consolidation time was the same as the three-degrees slope test (40 minutes), a plot of the excess pore pressures monitoring during the swing up of the model is shown in Appendix A (Figure A.2).
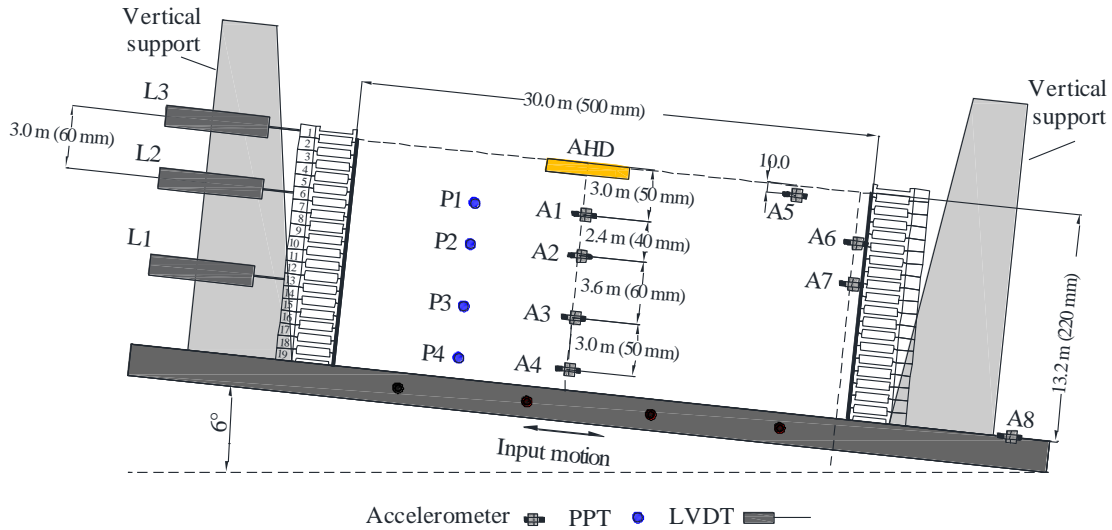
Figure 4.20: Instrumentation layout of six-degrees slope model.

The undrained shear strength profile measured from the in-flight characterization is shown in Figure 4.21a. It can be observed a reasonable agreement between undrained shear strength profiles of the six-degrees and the three-degrees tests, both simulating soft clay conditions ($s_u < 30$ kPa). The OCR contour presented in Figure 3.15b was back-calculated in a similar manner as the previous test, and it was employed as input for the calculation of the shear wave velocity profile using the Viggiani and Atkinson (1995) equation. The shear wave velocity profile was complemented with data points from the Air Hammer using the pairs of accelerometers A1-A2, A2-A3, and A3-A4 in Figure 4.20. Some differences can be observed between

the air hammer test data points. As pointed by McCullog *et al.* 2007, uncertainties are involved during air hammer tests, such as the location of the instruments, given the permanent deformations that occur during testing. Then, the observed differences could be attributed to the uncertain locations of the accelerometers after the shaking events.
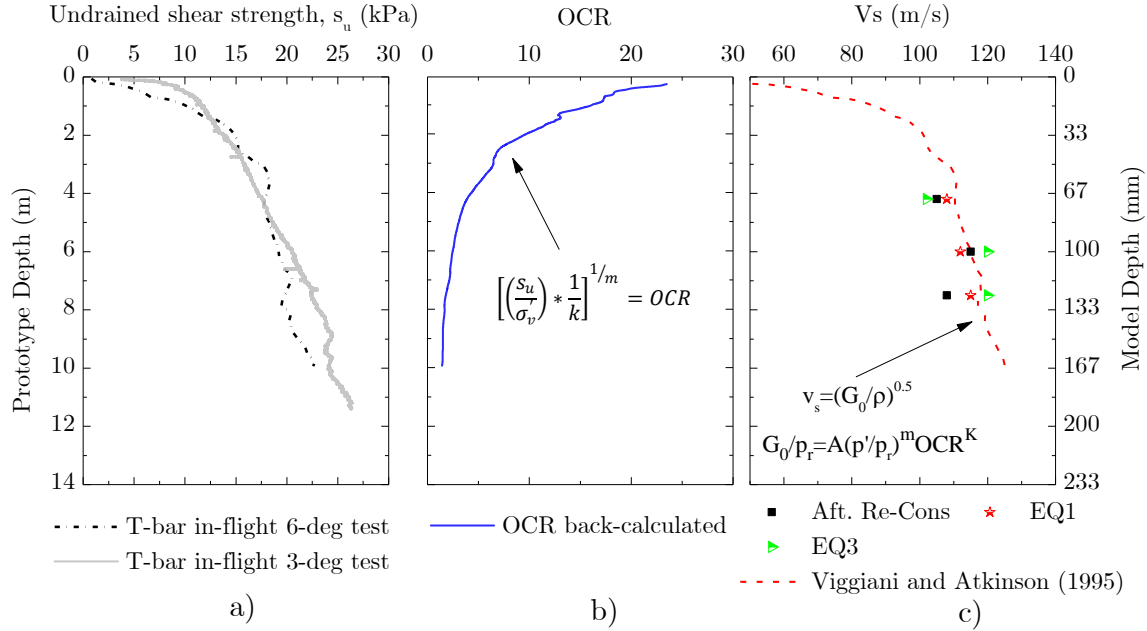
Figure 4.21: Clay model properties: (a) Undrained shear strength profiles, (b) stress history, (c) shear wave velocity profile.

4.3.1 Shaking events

Figure 4.22 and Figure 4.23 present the earthquakes applied to the six-degrees model, consisting of sinusoidal motions, and two real and scaled motions.
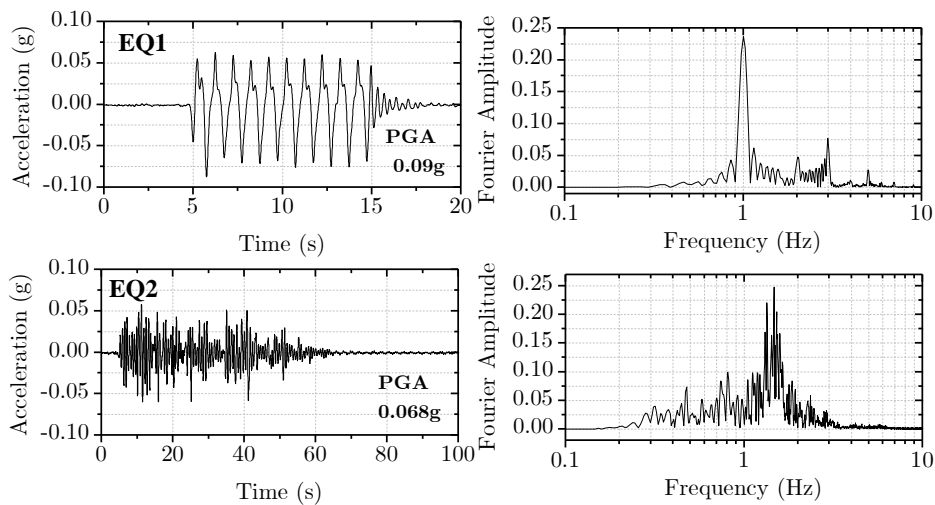
Figure 4.22: Six-degrees slope test: input motions EQ1, EQ2, EQ3 and frequency content (prototype scale).
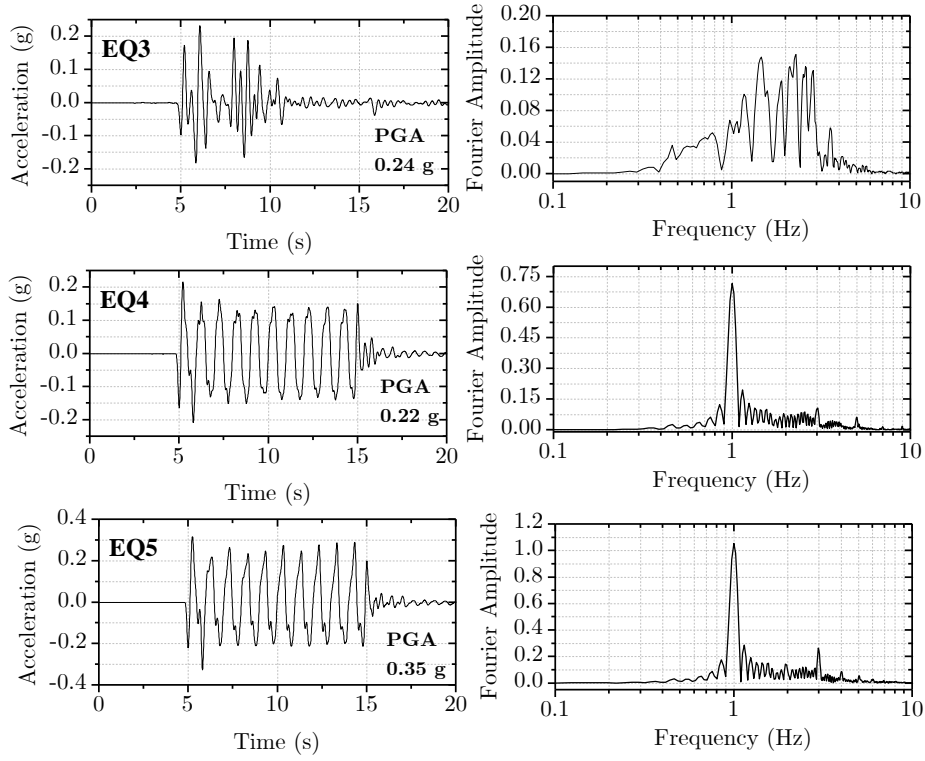
Figure 4.23: Six-degrees slope test: input motions EQ3, EQ4, EQ5 and frequency content (prototype scale).

The earthquakes applied are reasonably similar as the applied in the three-degrees slope test. However slight differences in the PGA values were observed. In more detail Table 4.1 displays a comparison of some of the features of the input motions applied to both models, all the values are presented in terms of prototype scale. Overall, the input motions applied to the six-degrees model present slightly larger PGA values, similar significant duration and similar predominant periods when compared with the input motions applied to the three-degrees slope model.

Table 4.1: Input motions characteristics for both models

Input Motion	Type	Duration (s) D_{5-95}		Predominant period (s)		PGA (g)	
		3-deg	6-deg	3-deg	6-deg	3-deg	6-deg
EQ1	Sinusoidal	9.3	9.3	1.0	1.0	0.07	0.09
EQ2	Imperial Valley (scaled)	48.7	43.7	0.5	0.7	0.04	0.07
EQ3	Kobe (scaled)	4.9	4.8	0.4	0.4	0.19	0.24
EQ4	Sinusoidal	9.5	9.6	1.0	1.0	0.18	0.22
EQ5	Sinusoidal	9.8	9.5	1.0	1.0	0.32	0.35

86

4.3.2 Test results: displacement time -histories

Figure 4.24 presents for reference the location of the LVDTs employed to measure the lateral displacements shown in Figure 4.25 and Figure 4.26. The results of LVDT L1 are not displayed as the instrument detached from the model container and no response was recorded. The largest permanent lateral displacements occurred at the surface as measured by LVDT L3 ranging between 0.15 m for EQ3 and 0.50 m for EQ5 (Figure 4.25 and Figure 4.26). In a similar manner as the three-degree slope test, larger displacements occurred during and after the application of EQ1 (sinusoidal, PGA=0.09 g) when compared with EQ3 (Kobe scaled, PGA=0.24 g). For both tests, the largest permanent displacements occurred after earthquake EQ5, the largest amplitude input motion.
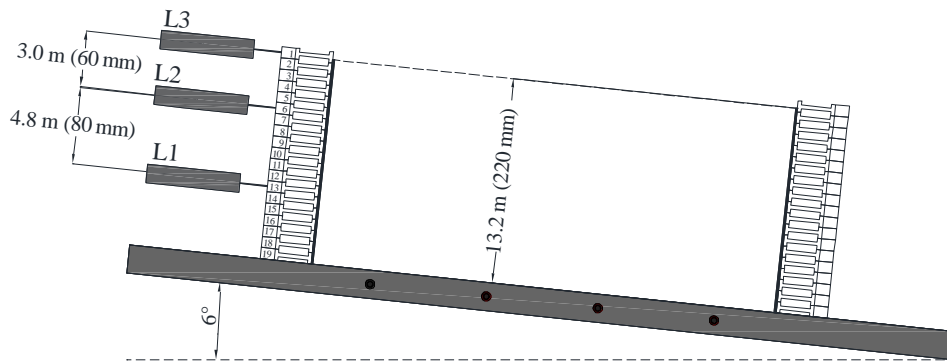
Figure 4.24: Location of LVDTs: six-degrees slope test
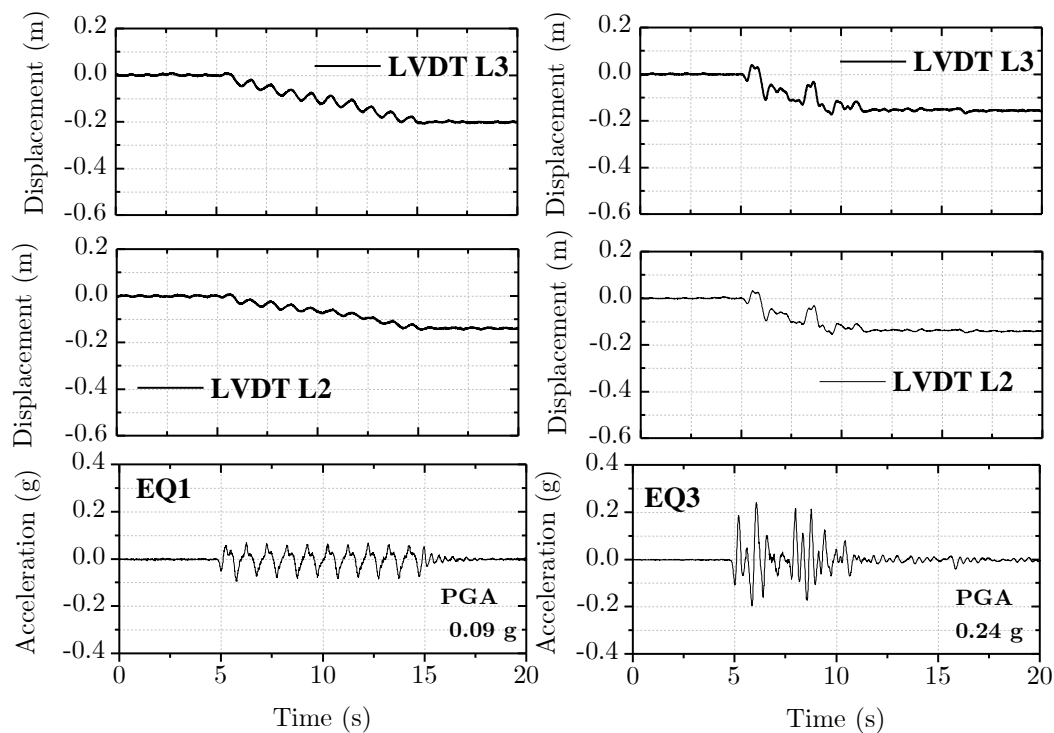
Figure 4.25: Six-degrees slope test: recorded displacement time-histories for EQ1 and EQ3

87
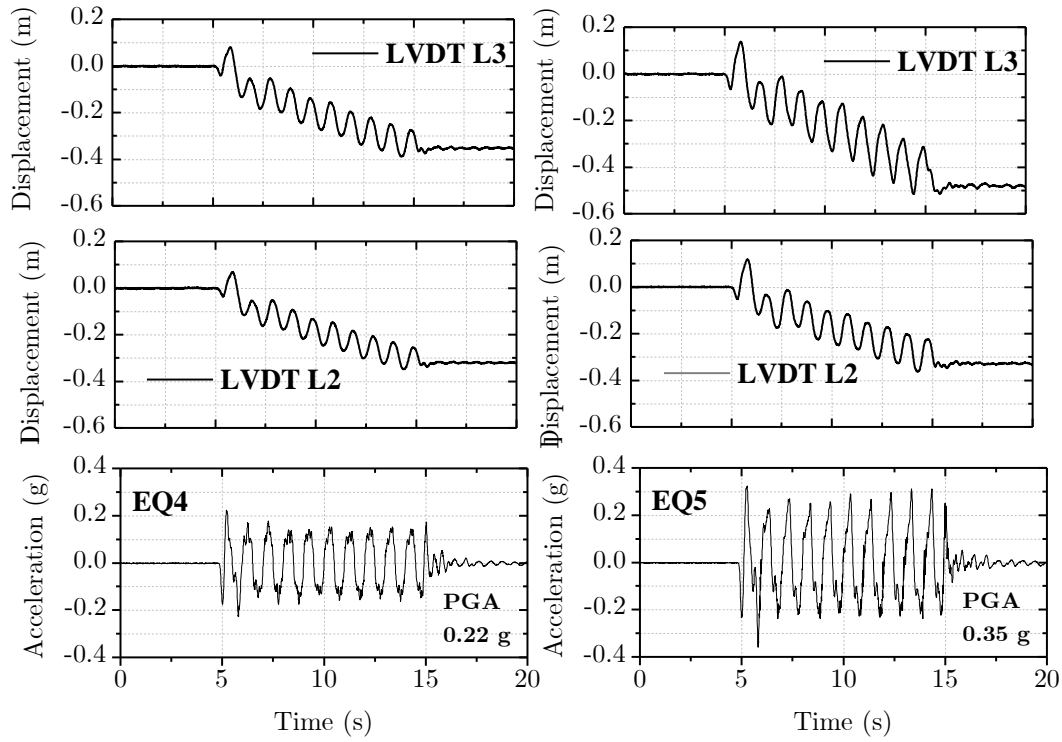
Figure 4.26: Six-degrees slope test: recorded displacement time-histories for EQ4 and EQ5

4.3.3   Test results: acceleration time-histories

The acceleration-time histories recorded by the installed accelerometers are shown in Figure 4.27. Overall, a good response of the instruments was observed. During earthquake EQ5, several peaks were recorded by accelerometers A5, A1, and A2. This means that after the second cycle of the sinusoidal motion, some of the laminae reached the limits of the box and impacted against the vertical supports of the container. This means larger displacements beyond the limits of the box may have occurred during the application of input motion EQ5.
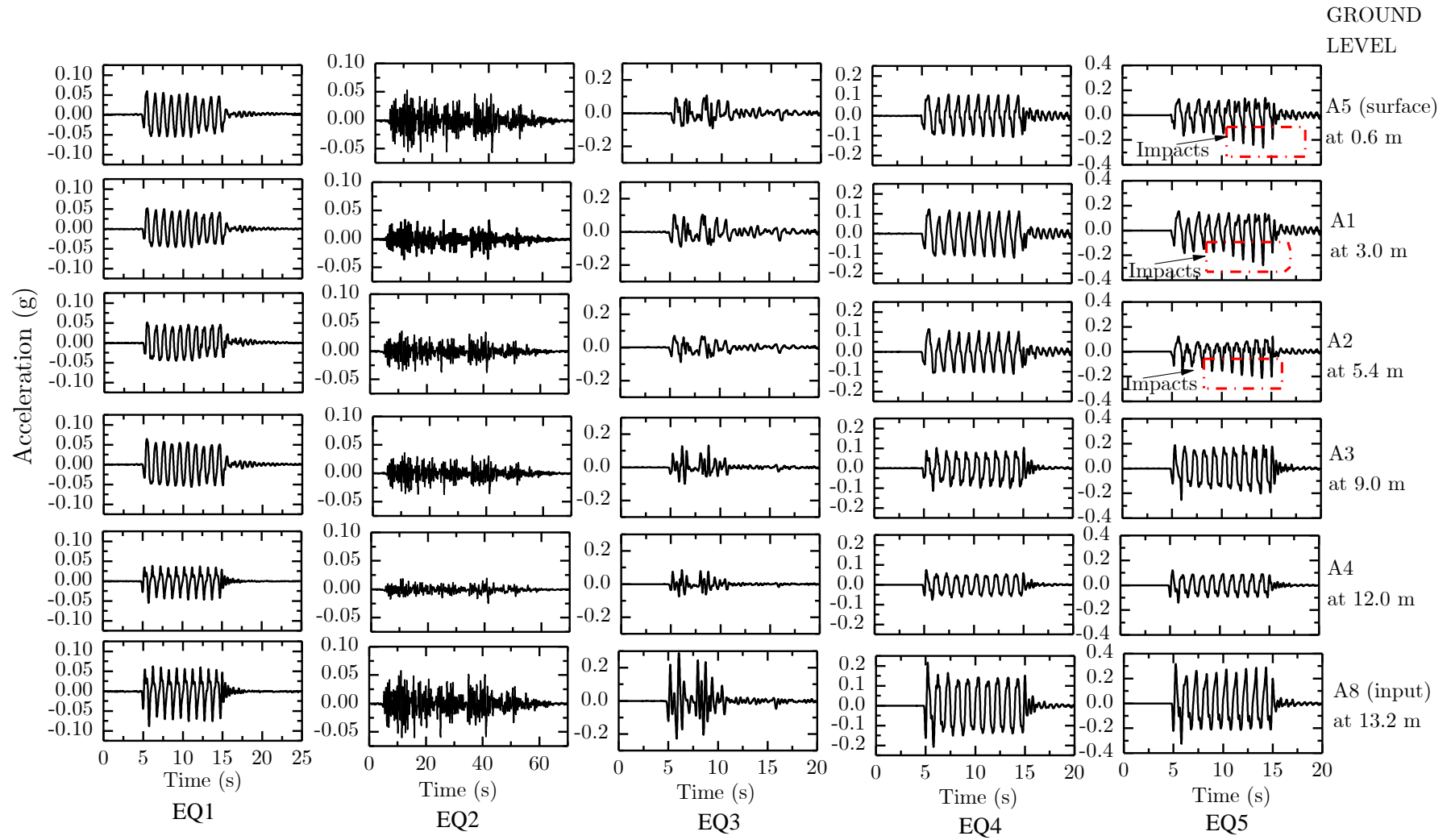
Figure 4.27: Six-degrees slope test: recorded acceleration time-histories

4.3.4 Test results: excess pore pressure measurements

Excess pore pressure measurements are shown in Figure 4.28. The values were displayed to start from zero before the earthquakes to compare the response of the instruments at different depths. From the results, PPT P2 at 3 m depth recorded rising values of excess pore pressures as the amplitude of the earthquake was increased, followed by a dissipation. Regarding the response of the remaining pore pressure transducers, PPTs P1, P3, P4, the recorded pore pressures did not follow a trend as PPT P2. Observing the scale of the pore pressures measured by PPTs P1, P3 and P4, it can be stated that the pore pressures did not showed a notable variation during and after the application of the earthquakes, in a similar manner as the three-degree slope centrifuge test. This raises again the question about using a different PPT installation method to guarantee a better coupling between the instrument and the clay during all the stages of the model preparation, including consolidation.
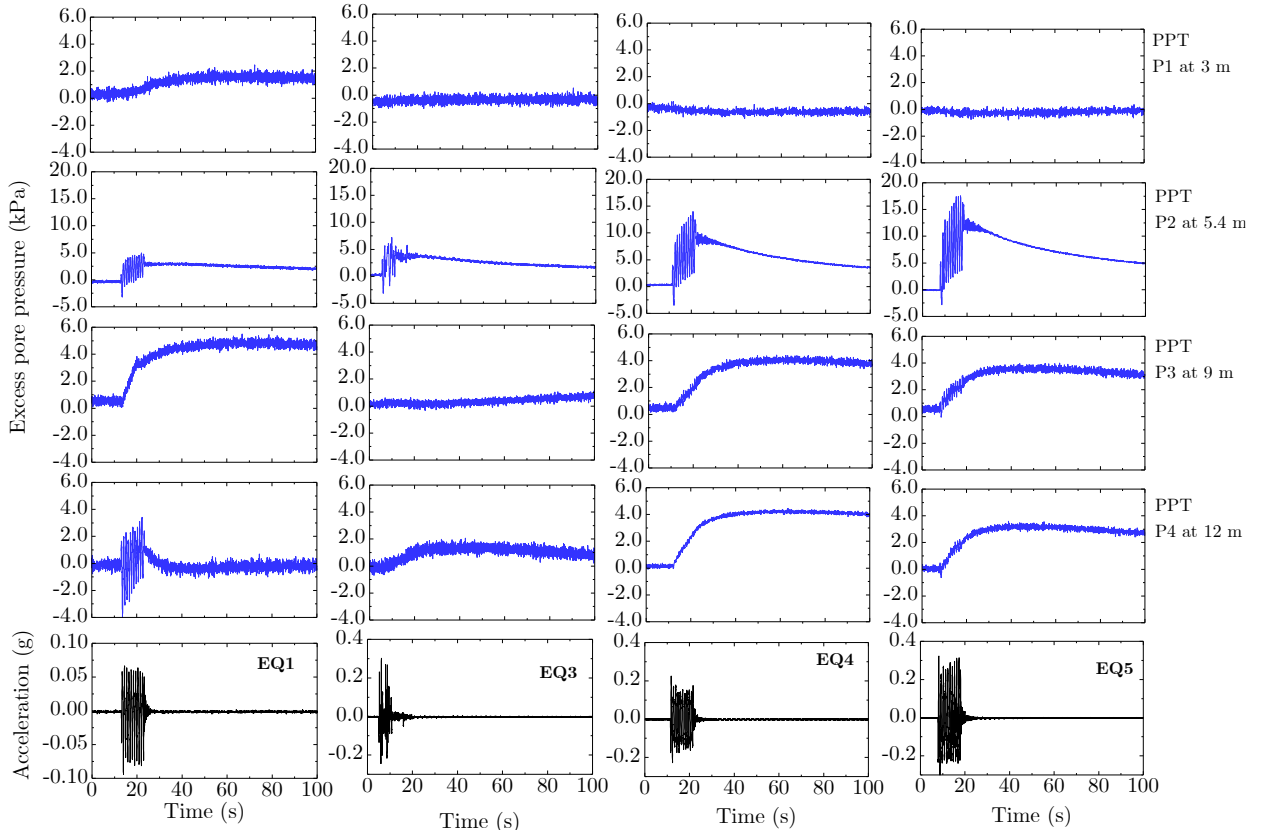
Figure 4.28: Six-degrees slope test: recorded excess pore pressures

4.4 Evaluation of slope inclination effects on the measured responses

4.4.1 Effect of slope angle on lateral permanent displacements

Figure 4.29 depicts the comparative response of the slopes in terms of lateral displacements. For all the cases, as comparison criteria, the permanent lateral displacements at the surface of the slope are presented, as they represent the region in which larger displacements occurred.

Figure 4.29a shows the relationship between the PGA at the base and permanent displacements. It can be observed that as the PGA of the sinusoidal input motions (EQ1, EQ4 and EQ5) increased, the permanent displacements also increased, with more significant displacements obtained for the six-degrees slope. As previously explained, the input motion EQ3 consisted of a scaled real motion (Kobe earthquake, 1995), with a larger PGA when compared with EQ1, a sinusoidal motion. From the results, it was observed that the sinusoidal motion was more detrimental than the real scaled motion due to the number of significant cycles of the sinusoidal motion that lead to a larger accumulation of lateral displacements.

Figure 4.29b presents the relationship between the slope angle and the measured permanent displacements. From Figure 4.29 the average of the displacements measured for the three-degrees slope is 0.09 m, and the average of the six-degrees slope, is 0.30 m, evidencing that even for a small increase of the slope angle, the effect of the permanent displacements is noticeable.

A direct comparison of displacement time-histories is provided in Figure 4.29c. According to Biscontin and Pestana (2006), when the ground is inclined, even by small angles, static shear stresses act on the slope. This stress produces a remarkable effect on the dynamic behavior of the slope, then, an accumulation of displacements will occur in the downslope direction, regardless of the characteristics of the earthquake.
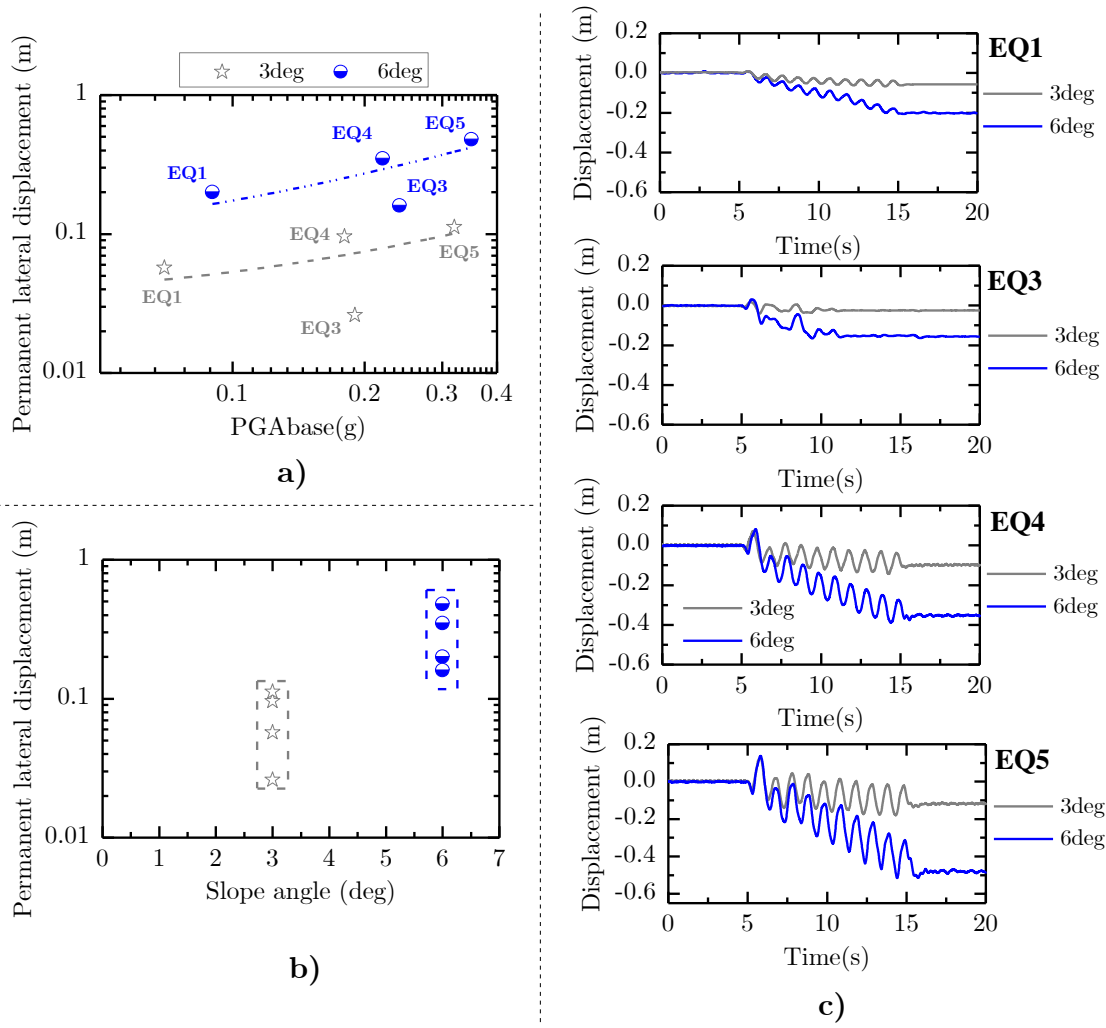
Figure 4.29: Influence of slope inclination on permanent displacements: a) in terms of PGA at the base; b) in terms of the slope angle; c) Displacement time-histories for three- and six-degrees slopes.

4.4.2 Effect of slope angle on amplification of PGA

The results obtained from the centrifuge experiments allowed to extract supplementary information related to the topographic effects on the amplification of PGA at the surface, for the case of gentle slopes in clay. Figure 4.30a shows the amplification/attenuation characteristics of PGA at the surface of the slopes. The results are compared with the trend presented by Stewart and Liu (2000) that developed empirical relationships to predict amplification factors as a function of surface geology. The reference figure used for comparison from the work of Stewart and Liu (2000) corresponded to regression results from field observations for lacustrine/marine geology sites. Is worth to mention that the regressions developed by Stewart and Liu (2000) do not make reference to the topography of the sites and it is employed here as a reference to compare the measured response with studies based on field observations. The results illustrate a similar trend with the low boundary of the empirical relationship. With an attenuation pattern of PGA

as the slope angle was increased. Data from earthquake EQ5 from the six-degree slope test was not displayed in the figure, due to the peaks that occurred during the last cycles of the sinusoidal motion, product of impacts of the lamination with the boundary of the laminar box as previously discussed.

The second way of comparison of the amplification-attenuation pattern of the slopes is presented in terms of Amplification Factors as displayed in Figure 4.30b. For comparison with the empirical predictions, the amplification ratios were calculated from the 5% response spectra at the base and at the surface implementing the spectral accelerations at T=0.01 s. The results show a tendency of the amplification factors to reduce as the amplitude of the input motion was increased (Stewart and Liu, 2000; Suetomi *et al.*, 2004; Zhou *et al.*, 2017). The fitting curves from the centrifuge tests present an offset as the slope angle was increased with a trend to exceed the lower boundary prediction of Stewart and Liu (2000).
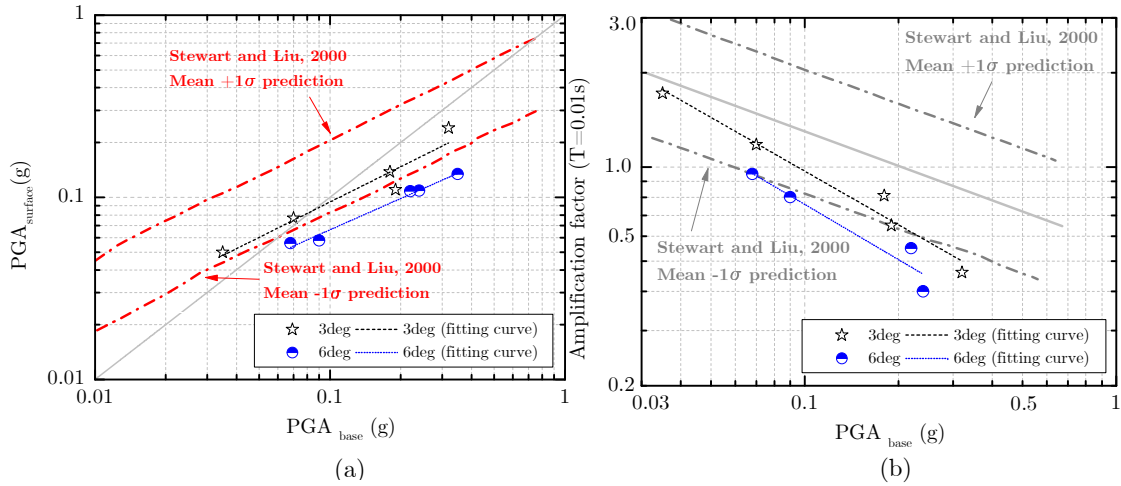
Figure 4.30: . Influence of slope inclination on the amplification-attenuation of base accelerations: a) base and surface accelerations; b) amplification factor of base accelerations for three and six-degrees slopes.

4.5   Final remarks

The measured responses of two centrifuge tests, simulating 3-degree and 6-degree infinite slopes, were presented. A detailed characterization of the first model was presented, as it is used as a reference for the calibration of a numerical model presented in Chapter 6. In general terms, the instruments registered a reliable response in both tests, allowing the researchers to obtain base and surface accelerations and surface displacements. From the analysis of PPTs, a clear trend was not observed in the measured excess pore pressures. One explana-

tion could be associated with the installation methodology of the transducers. Given the model preparation, it was not possible to guarantee perfect contact between the PPTs and the clay, which would be ideally achieved if they were installed at the beginning or at least during the last stages of consolidation of the clay.

Using the additional analyses performed in the 3-degree slope test, the container performance was evaluated by comparing the 5% damping response spectra of accelerations measured at similar depths at the center and near the boundary of the laminar box. The responses essentially gave the same results, showing excellent performance by the laminar container for models in clay. This opens the possibility to use this type of container for models in clay under a wider range of strains than can be achieved using the ESB box at the Schofield Centre.

The models presented in this chapter were prepared under similar conditions, and the input motions applied, despite their small differences, allowed a direct comparison of the response of the slopes in terms of permanent displacements at the surface and with regard to amplification or attenuation of the base accelerations.

4.6   Chapter 4 references

ALMEIDA, M.S.S., 1984, "Stage constructed embankments on soft clays," PhD thesis, Cambridge.

AFACAN, K.B., BRANDENBERG, S.J., AND STEWART, P.J., 2013, "Centrifuge modeling studies of site response in soft clay over wide strain range," Journal of Geotechnical and Geoenvironmental Engineering, Vol.140, No.2, pp. 1-13.

BISCONTIN, G., AND PESTANA, J., 2006, "Factors affecting seismic response of submarine slopes," Natural Hazards and Earth System Science, Vol.6, No.1, pp.97-107.

BRENNAN, A. J., MADABHUSHI, S. P. G., AND HOUGHTON, N. E., 2006, "Comparing laminar and equivalent shear beam (ESB) containers for dynamic centrifuge modelling," In C. W. W. Ng, L. M. Zhang, Y. H. Wang (Eds.), Physical modelling in geotechnics: 6th ICPMG '06: proceedings of the Sixth International Conference on Physical Modelling in Geotechnics–6th ICPMG'06, Hong Kong, 4-6 August 2006, Vol.1-2, pp.171-176.

BRENNAN, A. J., THUSYANTHAN, N. I. AND MADABHUSHI, S. P. G., 2005, "Evaluation of shear modulus and damping in dynamic centrifuge tests," Journal of

Geotechnical and Geoenvironmental Engineering, Vol.131, No.12, pp.1488–1498.

CHOW, J.K., WANG, Y., LUI, H.L., AND HUANG, E., 2020, "Determination of consolidation parameters based on the excess pore water pressure measurement using a newly developed U-oedometer," Acta Geotechnica, Vol.15, pp.2665-2680.

DARENDELI, M. B., 2001, "Development of a New Family of Normalized Modulus Reduction and Material Damping Curves," Ph.D. thesis, University of Texas, Austin, TX, USA.

DOBRI, R., OWEIS, I., AND URZUA, A., 1976, "Simplified procedures for estimating the fundamental period of a soil profile," Bulletin of the Seismological Society of America. Vol.66, No.4, pp.1293-1324.

ELGAMAL, A., LAI, T., AND YANG, Z., 2001, "Dynamic Soil Properties, Seismic Downhole Arrays and Applications in Practice," In: Proceedings International Conferences on Recent Advances in Geotechnical Earthquake Engineering and Soil Dynamics. Vol.6, 85 p., San Diego, California, March.

FINNIE, I. M. S., AND RANDOLPH, M. F., 1994, "Punch-Though and liquefaction induced failure on shallow foundations on calcareous sediments," Proceeding International Conference on Behaviour of Off-Shore Structures – BOSS '94, Boston, Vol.1, pp.217-230.

GHOSH, B., AND MADABHUSHI, S. P. G., 2002, "An efficient tool for measuring shear wave velocity in the centrifuge."Proc. Int. Conf. on Phys.Modelling in Geotechnics, R. Phillips, P. J. Guo, and R. Popescu, eds.,Balkema, Rotterdam, Netherlands, pp.119–124.

GROHOLSKI, D.R., HASHASH, Y.M.A., MUSGROVE, M., HARMON, J., AND KIM, B., 2015, "Evaluation of 1-D non-linear site response analysis using a general quadratic/hyperbolic strength- controlled constitutive model," 6th International Conference on Earthquake Geotechnical Engineering, Vol.1–4 November 2015, Christchurch, New Zealand.

KRAMER, S. L., 1996, Geotechnical Earthquake Engineering, New Jersey, Prentice Hall.

MARSHALL, A., HERON., C., AND CUI, G., 2018, "Shear wave velocity: comparison between centrifuge and triaxial based measurements," Physical Modelling in Geotechnics – Mc Namara *et al.* (Eds.), Taylor Francis Group, London.

MCCULLOUGH, N., DICKENSON, S., SCHLECHTER, S., AND BOLAND, J., 2007,"Centrifuge Seismic Modeling of Pile-Supported Wharves." Geotechnical Testing Journal. Vol.30, No.5, pp. 349-359.

OLIVEIRA, J.R.M.S., ALMEIDA, M.S.S., MOTTA, H.P.G., AND ALMEIDA M.C.F, 2011, "Influence of penetration rate on penetrometer resistance," Journal of Geotechnical and Geoenvironmental Engineering, Vol.137, pp. 695-70.

RABINER, L.R., AND GOLD, B., 1975, "Theory and application of digital signal processing," Englewood Cliffs, NJ, Prentice Hall, Inc.

RANDOLPH, M., AND GOURVENEC, S., 2011, Offshore Geotechnical Engineering. 1 ed. Oxon, Spon Press.

SAWADA, S., 2004, " A simplified equation to approximate natural period of layered ground on the elastic bedrock for seismic design of structures," in: 13th World Conference on Earthquake Engineering,Vancouver, Canada.

SHARMA, J.S., AND BOLTON, M.D., 1996, "Centrifuge modeling of an embankment on soft clay reinforced with geogrid," Geotextiles and Geomembranes, Vol.14, No.1, pp.1-17.

SPRINGMAN, S.M., 1989, "Lateral loading on piles due to simulated embankment construction," PhD thesis, Cambridge University, Cambridge, UK

STEWART, J.P., AND LIU, A.H., 2000, "Ground motion amplification as a function of surface geology," Proc. SMIP2000 Seminar on Utilization of Strong Motion Data, California Strong Motion Instrumentation Program, Sacramento, California, pp.1–22.

SUETOMI, I., ISHIDA, E., ISOYAMA, R., AND GOTO, Y., 2004, "Amplification factor of peak ground motion using average shear wave velocity of shallow soil deposits," 13th World Conference on Earthquake Engineering, Canada.

TARAZONA, S.F.M., ALMEIDA, M.C.F., BRETSCHNEIDER, A., ALMEIDA, M.S.S., ESCOFFIER, S., AND BORGES, R.G, 2020, "Evaluation of seismic site response of submarine clay canyons using centrifuge modelling," International Journal of Physical Modelling in Geotechnics, Vol.20, No.4, pp.224-238.

TSAI, C.-C., AND HASHASH, Y. M. A., 2009, "Learning of Dynamic Soil Behavior from Downhole Arrays" Journal of Geotechnical Geonvironmental Engineering, Vol.135, n.6, pp.745-75.

WROTH, C.P., 1984, "The Interpretation of in Situ Soil Test," Geotechnique, Vol.34, pp. 449-489. University, Cambridge, UK.

VIGGIANI, G., AND ATKINSON, J.H., 1995, "Stiffness of fine-grained soil at very small strains," Geotechnique, Vol.45, No.2, pp.249-265.

VUCETIC, M., AND DOBRY, R., 1991, "Effect of Soil Plasticity on Cyclic Response", Journal of Geotechnical Engineering, Vol.117, No.1, pp. 89-107.

ZEGHAL, M., AND ELGAMAL, A.-W, 1994, "Analysis of Site Liquefaction Using Earthquake Records", Journal of Geotechnical Engineering, Vol.120, No.6, pp.996-1017.

ZEGHAL, M., ELGAMAL, A.-W., AND TANG, H.T., 1995, "Lotung downhole array. II: Evaluation of Soil Nonlinear properties ", Journal of Geotechnical Engineering, Vol.121, No. 4, pp.363–378.

ZHANG C, WHITE, D., AND RANDOLPH, M., 2011, "Centrifuge modeling of the cyclic lateral response of a rigid pile in soft clay," Journal of Geotechnical and Geoenvironmental Engineering, Vol.137, No.7, pp.717–729.

ZHOU, Y-G., CHEN, J., CHEN, Y-M., KUTTER, B., ZHENG, B, WILSON, D., STRINGER, M., AND CLUKEY, E., 2017, " Centrifuge modeling and numerical analysis on seismic site response of deep offshore clay deposits," Engineering Geology, Vol. 227, pp.54-68.

Chapter 5

Seismic centrifuge modelling of a gentle slope of layered clay, including a weak layer

This chapter is based on the following reference:

5.1   Introduction

The continental slope in the southern and southeastern regions of Brazil is relatively uniform over long distances, being disturbed only by some widely spaced surface geological features. In the Campos Basin, located on the continental margin of Southeastern Brazil, pelagic and hemipelagic sedimentation are predominant, with an average accumulation rate of 0.064 m / 1,000 years (Kowsmann *et al.* 2016). The deposition of fine materials at such low rates leads to the formation of parallel layers of normally consolidated to lightly overconsolidated, soft cohesive deposits ranging in depth from a few meters to hundreds of meters (Biscontin and Pestana, 2006). The slope inclination in those cases is small with typical values of less than 5 degrees. These slopes are theoretically stable under gravity loads due to strength gains during the low rates of sedimentation of the materials. However, large-scale submarine landslides around the world have occurred in slopes with similarly low gradients (Hühnerbach and Masson, 2004).

In such offshore areas with low sedimentation rates, earthquakes are one of the primary catalysts for submarine landslides (Nadim *et al.*, 2007). In addition, variable rates of deposition of submarine sediments may lead to the generation of weak layers with varying degrees of consolidation (Biscontin *et al.*, 2004). Several studies related to submarine mass movements have suggested the presence of weak layers as one of the causes of the triggering of submarine landslides. (O'Leary, 1991; Haflidason *et al.*, 2003; Bryn *et al.*, 2005a, 2005b; Solheim *et al.*, 2005; Locat and Lee, 2009). Earthquakes of moderate to large magnitudes do not frequently occur along the Brazilian continental margin, however, earthquakes with damage potential have occurred in the past and may occur again (Pirchiner *et al.*, 2015; Garske *et al.*, 2020). Recent studies have focused on the occurrence of hydroplaning and turbidity currents (Acosta *et al.*, 2017; Hotta *et al.*, 2019), on the response of clayey submarine canyons to seismic events representative of Brazilian seismicity (Tarazona *et al.*, 2020) and also on the assessment of seismic hazard on the continental margin of southeastern Brazil (Garske *et al.*, 2020). However, the seismic response of submarine slopes in the Brazilian context is a new field of investigation. This study comprises part of a research project related to the seismic behavior of low-gradient (<5 degrees), soft-clay continental slopes typical of this region.

In the case of submarine slopes, landslides involve large distances relative to the thickness of the soil mass. Therefore, the length of the slide is many times larger than the thickness of the slide. The infinite slope approach to modelling the seismic response of sloping ground in soft clays has been studied by means of numerical models in several studies (Pestana and Nadim, 2000; Biscontin and Pestana, 2006; Rodriguez-Ochoa *et al.*, 2015; Zhou *et al.*, 2017; Dey *et al.*, 2016). However, field, or experimental data regarding the seismic behavior of gentle slopes in soft clays under different ranges of loading are limited. Most of the experimental studies in clays, particularly using centrifuge modeling, have been related to 1D response at different ranges of strain. For example, Afacan *et al.* (2013) performed 1D centrifuge tests in clay using a hinged-plate model container to evaluate the site response at very large strains representative of seismically active regions. In another study, Rayhani and El Naggar (2007) evaluated the seismic response of soft to medium stiff clays of one and two layers using an Equivalent Shear Beam (ESB) model container. More recently, Zhou *et al.* (2017) carried out a series of centrifuge tests on a slightly overconsolidated marine clay deposit employing a Flexible Boundary Container (FSB).

In the case of lateral spreading problems like the seismic behavior of sloping

ground, the use of ESB model containers is unsuitable given that they restrain the lateral displacements of the soil (Madabhushi, 2014). Alternatively, a laminar container can be used for this type of problem. Most of the experience using laminar containers in centrifuge tests is related to liquefaction problems (Elgamal *et al.*, 1996; Taboada and Dobry, 1998; Haigh, 2000; Knappett, 2006). One of the fundamental concerns of the preparation of models in clay is the consolidation of the soil. This requires the use of an impermeable container strong enough to handle the pressures applied to the clay during consolidation. In a laminar container, the soil body is typically placed within a rubber bag or a latex membrane for saturated models. For the construction of a layered profile in clay, an extension is required and the inner rubber bag can be easily damaged during the application of the consolidation pressures, leading to leakage and the generation of additional drainage paths. To sort out these practical issues, it was necessary to develop a new model preparation procedure.

This paper presents an experimental methodology to simulate the seismic behavior of a gentle slope in soft clay including the presence of a weak layer by means of centrifuge modelling. The centrifuge test presented here is part of an experimental program aimed at studying the seismic response of gentle slopes in soft clay. The specific objectives of the present work are: (1) to describe a novel model-preparation technique for simulating a slope of relatively soft clay with an even weaker layer sandwiched between, using a laminar model container used extensively for seismic studies in sands (Lanzano *et al.*, 2012; Brennan *et al.*, 2006b; Tricarico, 2016; Garcia-Torres and Madabhushi, 2019), (2) to present a PIV methodology using an open source software (Blender) as a complementary source of data in terms of displacements and accelerations at different depths in the slope, (3) to discuss the experimental results for use in calibration of numerical and analytical models, and (4) to observe the dynamic behavior of the slope using spectral analysis.

5.2 Dynamic centrifuge modelling

Centrifuge modelling enables the study of complex geotechnical problems using small-scale models, employing centrifugal acceleration to simulate the stress and strains representative of field conditions (Taylor, 1995; Madabhushi, 2014). The dynamic tests in this study were conducted in the 10 m diameter beam centrifuge at the Schofield Centre (University of Cambridge). The earthquake motions were applied using a servo-hydraulic actuator developed by Madabhushi *et al.* (2012). The problem studied consisted of a semi-infinite sloping ground condition in soft

clay. Under these conditions large deformations are expected and therefore a laminar container (Brennan *et al.*, 2006b) was utilized. The box is 500 mm × 250 mm in length and width and the depth is variable, depending on the number of rectangular frames (laminae) used (280 mm for the current centrifuge test).

5.3 Materials and Methods

5.3.1 Materials

The model was made with Speswhite kaolin, a well-documented material with comparative data sets available, widely used in research projects involving physical models (Almeida, 1984; Kim, 1996; Williamson, 2014; Lau, 2015). For the current research, the values reported by Lau (2015), for a Plastic Limit (PL) equal to 30% and a Liquid Limit (LL) equal to 63% (then a Plasticity Index, PI of 33%) were adopted.

5.3.2 Proposed Model Preparation

The centrifuge test performed simulates the behavior of a layered gentle slope in soft clay when subjected to earthquake loading. The model consisted of a three-layer slope with a weak layer, aiming to simulate a strength contrast of about 25 percent between neighboring layers. The consolidation pressures described below (250 kPa and 125 kPa) were selected to reproduce a strength profile typical of marine clays like that encountered in the seabed of the Campos offshore basin, southeastern Brazil. Fagundes *et al.* (2012) described the behavior of marine clays in this region through laboratory and field tests and presented a profile with values ranging between 3 kPa at the surface and 40 kPa at a 20 m depth, approximately the prototype vertical extent as presented in the following sections. Similar consolidation pressures such as those used in the current test have been applied in centrifuge tests in soft clay representative of offshore environments (White *et al.*, 2010; Tarazona *et al.*, 2020). The main difference in the construction of the model presented in this paper is the lower consolidation pressure of 125 kPa in order to consider the presence of a weak layer.

The model soil profile was built from reconstituted clay. The laminar container at the Schofield Centre has been used extensively for liquefaction and lateral spreading problems involving sands. For a model in clay, a different setup was required for the consolidation process. A strongbox, or consolidation container, was designed with the same internal dimensions as the laminar container (500 mm

length × 250 mm width), but deeper (500 mm), aiming to produce samples of the clay between 250 mm and 300 mm in height at the end of consolidation. The sides of the consolidation container can be easily detached, and complete slices of the consolidated clay can be removed with minimal disturbance, enabling the simulation of the target layered soil profile as described below. In order to build the three-layer slope, the model preparation was divided into stages:

1. The kaolin powder was mixed with water at 120% water content employing a clay mixer under vacuum to remove air bubbles from the clay. Once mixed, the slurry was poured into the consolidation container with draining interfaces at the top and base of the clay. A piston was placed on top of the clay slurry and it was left to consolidate for one day under the weight of the piston. The additional consolidation pressures were applied in stages using a computer-controlled consolidation rig.

2. The top and bottom layers of the clay were first consolidated by applying a maximum consolidation pressure of $\sigma'_{v\,\mathrm{max}}$=250 kPa. The load was applied in steps, starting from 0.7 kPa, corresponding to the pressure applied by the piston and increased by doubling the pressures until reaching 250 kPa. The time intervals of each loading step followed the experience of the last forty years using Speswhite kaolin. The consolidation lasted twelve days, and it was stopped when the settlements were stabilized within 48 hours (Figure 5.1a). During the initial stages of consolidation (day 0 to day 4) a combination of consolidation of the vertical stress applied by the consolidation press and suction-induced seepage were used to consolidate the clay slurry and to accelerate the settlements. This methodology has been used for models in clay developed at the Schofield Centre (Garala and Madabhushi, 2019; de Sanctis *et al.*, 2021).

3. The sides of the consolidation container were removed; the resultant block was split by cutting off the top 80 mm and keeping the remaining 150 mm in the same position. The top block was stored and protected to avoid loss of moisture (Figure 5.1b).

4. The sides of the consolidation container were reassembled, and a new layer of the slurry was poured on top of the block of consolidated clay that remained, then, a maximum consolidation pressure of $\sigma'_{v\,\mathrm{max}} = 125$ kPa was applied in stages. The consolidation pressures were applied in ten days in stages from 0.7 kPa doubling the pressures until reaching 125 kPa. (Figure 5.1c and Figure 5.1d).

5. At the end of the consolidation of the second layer, the previously stored top layer was positioned on top, and a $\sigma'_{v\,\mathrm{max}} = 125$ kPa pressure was applied to the

three-layer clay bed for two days to ensure continuity between layers (Figure 5.1e). The continuity between the layers was checked after the centrifuge test by cutting transverse slices of clay, further details are presented in the post-test investigations section of this paper.

6. The applied vertical pressure was removed, and the sides of the consolidation container were again detached. Then the final block of clay was wrapped in a rubber bag to prevent water leakage and to separate the clay and the laminations (Figure 5.1f). Finally, the frames of the laminar container were assembled around the sample.
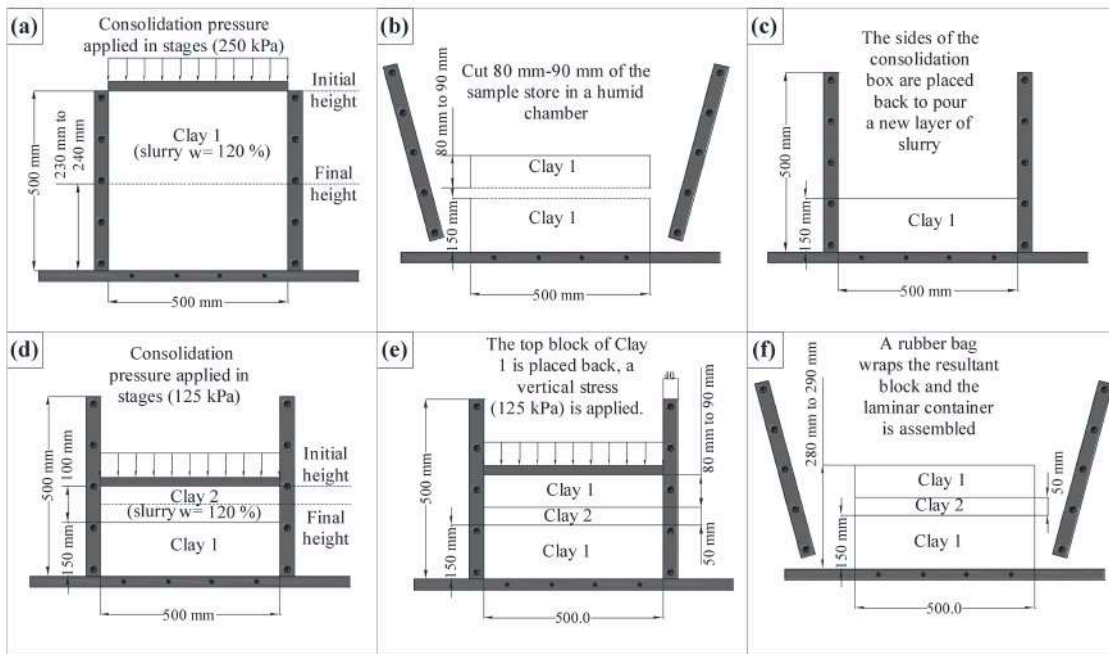
Figure 5.1: Model consolidation stages.

Considering that after unloading the clay, there would be a reduction in the effective stress prior to centrifuge testing commencing, the clay was held under a suction of around -60 kPa. This was done by connecting a vacuum pump to the drains located at the base of the model container (Figure 5.2a) allowing for a continuous application of negative pressure until the moment prior to the centrifugal acceleration of the model in the centrifuge. The applied suction of -60 kPa was below the air entry value to prevent the occurrence of cavitation. A range of pressures of the same order (-60 kPa to -70 kPa) was used by Garala *et al.* 2020 and de Sanctis *et al.* 2021 for the preparation of models in clay during the unloading phase of consolidation. Given the short time in which the suction was applied to the model, no considerable effects were expected in terms of the saturation of the clay.

As part of the experimental setup, water content samples were taken at different depths across the clay profile at the end of the centrifuge test. The average water content and degree of saturation of the clay were around 53% and 100% respectively, confirming that during the centrifuge test the clay was in a saturated condition. For the calculations of the vertical stresses, two saturated unit weights were measured: for the top and bottom layer γ_{sat}=16.9 kN/m^3 and for the weak layer γ_{sat}=16.4 kN/m^3.

5.3.3   Model details: gentle slope

Once assembled to the desired height, the instrumentation was installed in the laminar container. The following electronic instruments were used: (1) piezoelectric accelerometers (model A32 by D.J. Birchall Ltd) to record the dynamic motions at different locations in the soil profile; (2) pore pressure transducers (PPTs, model PDCR-81 manufactured by Druck Ltd.); (3) Linear Variable Differential Transformers (LVDTs, model DC15 manufactured by Solartron Metrology) to record the horizontal displacements during the swing-up of the model and during the application of the dynamic loads and (4) a high-speed camera (MotionBLITZ EoSens mini2 produced by Mikrotron GmbH) to track the displacements of markers installed in the laminae throughout the experiment.

In addition, a support gantry frame was used to fix an actuator above the clay that was used to perform an in-flight T-bar test, and an air hammer (AHD) was placed on the clay surface. The piezo-accelerometers (A1 to A10) and the PPTs (P1 to P4) were installed by excavating boreholes with small pipes, removing the clay and positioning the instruments with a probe for installation at specific depths (Brennan *et al.*, 2006a). Figure 5.2a presents a general view of the model, Figure 5.2b shows the detailed location of the instrumentation and Figure 5.3 displays a view of the model in the servo-hydraulic actuator and the wiring arrangement in the model.
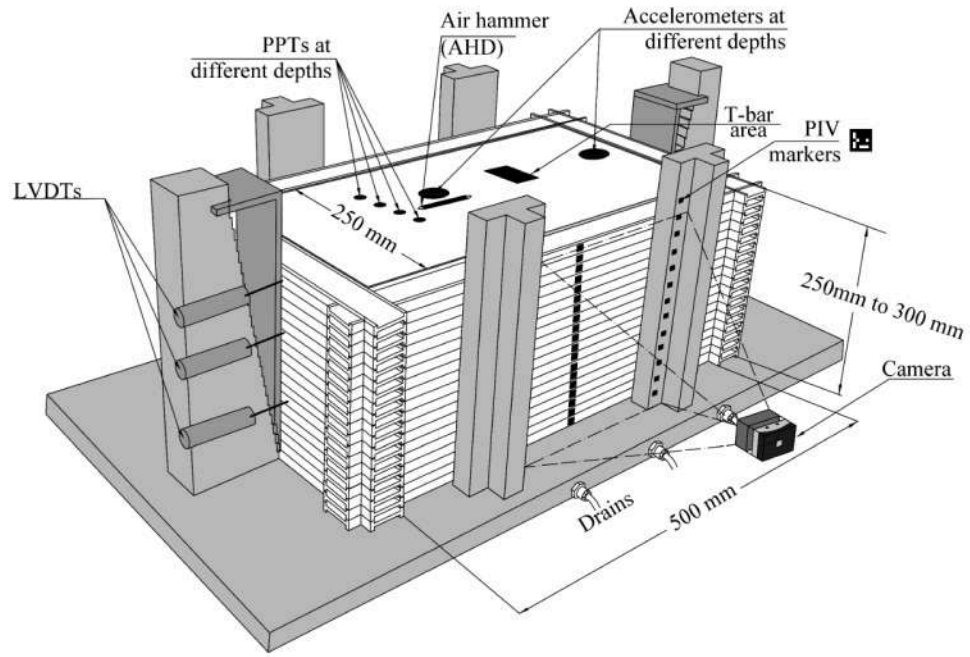
(a)
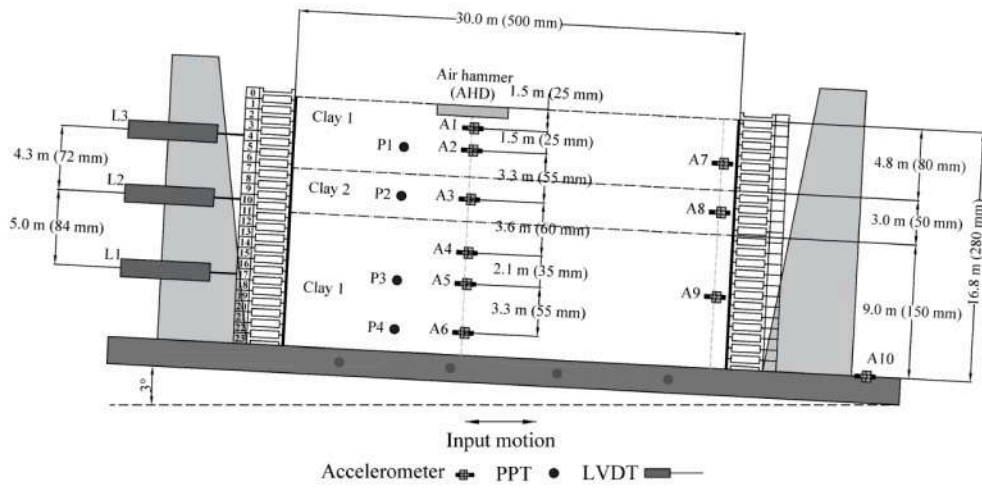
(b)

Figure 5.2: Experimental setup: (a) 3D overview of the model (drawing in model scale); (b) instrumentation layout (model scale in parentheses).

1	PPTs
2	Accelerometers
3	T-bar
4	Gantry
5	High-speed camera
6,7	Lights
8	LVDTs
9	AHD
10,11	Junction box
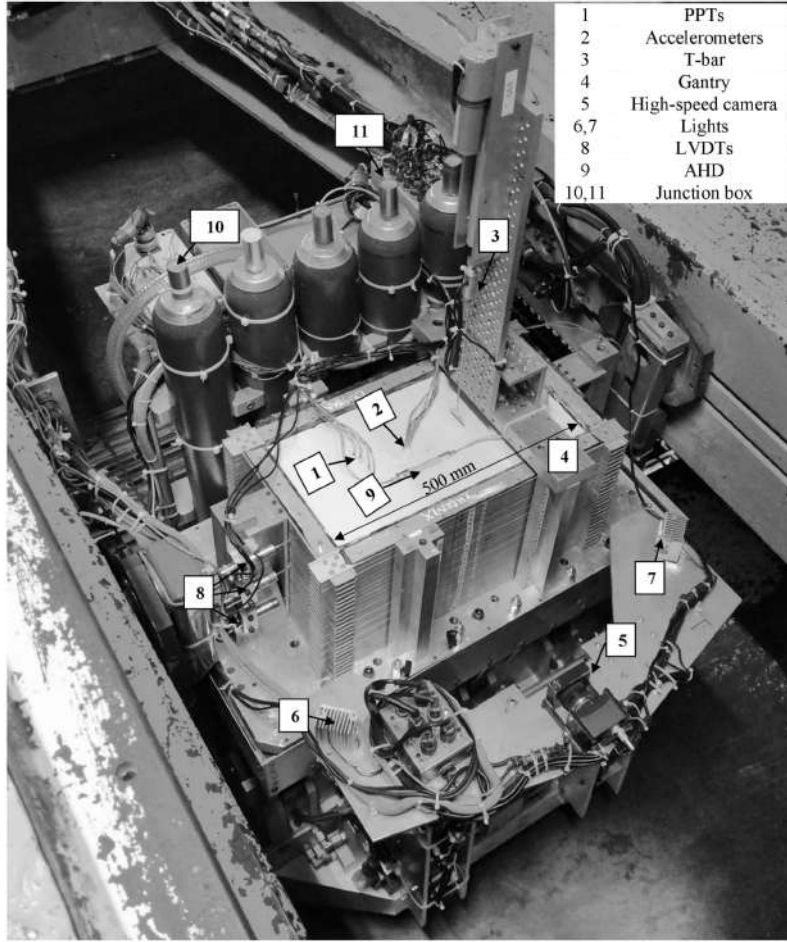
Figure 5.3: View of the model in the servo-hydraulic actuator.

5.3.4 Particle Image Velocimetry (PIV) analysis setup

For the experiment, a high-speed camera developed to record fast processes in confined spaces was employed (MotionBLITZ EoSens mini2 produced by Mikrotron). The resolution of the pictures captured by the camera is linked to the recording frame rate. For example, at a maximum resolution of 1696 by 1710 pixels it is possible to record images at a frame rate of 523 Hz. For the centrifuge test reported here, a resolution of 1504 by 1050 pixels was employed, delivering a frame rate of 953 Hz.

The camera was triggered to record 15 percent of the total frames prior to the trigger via an external signal, and the remaining percentage to record the earthquake itself. The recording time for the dynamic events in the centrifuge is of the order of a few seconds; for the current test 1.4 seconds was sufficient to record a total of 1354 photos (or frames) per earthquake.

Once the laminar container was assembled and the instruments installed, ArUco markers (Garrido-Jurado *et al.*, 2014) were glued to each lamina. Two sets

106

of markers were used, the first set, labelled as Fixed column, (Figure 5.4) was attached to the vertical, rigid columns that act as a boundary and support for the laminar container in the transverse direction. The displacement of the elements of the fixed column is related to the displacement of the shaking table, enabling tracking of the input motion. The second set of markers, labeled as Displacement markers (Figure 5.4), was installed in the laminae of the container and used to track the displacement of the mass of soil at different depths. The three LVDTs installed on the side of the container were also used for comparison with and validation of the displacements tracked by the PIV method.
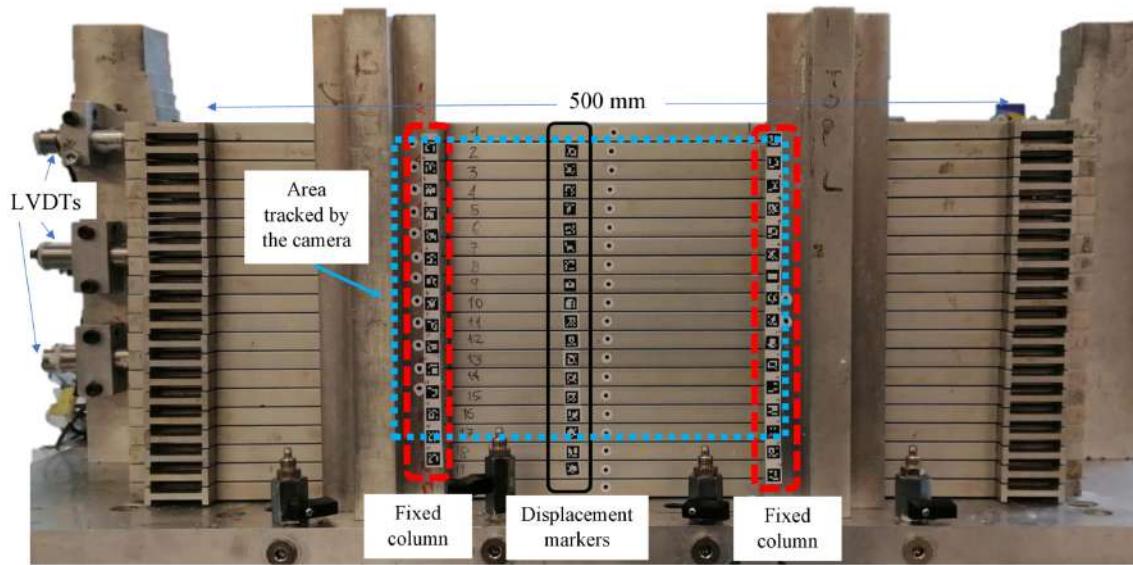
Figure 5.4: Location and sets of markers (dimensions in model scale).

Blender is an open source software package for many purposes related to 2D and 3D animation (Hess, 2010). Among its functionalities, there is a module for motion tracking that enables tracking of markers during a photo or video sequence. Options such as marker size, tracking area, correlation between matched and source image and tracking methodologies are available. Blender uses a tracker with subpixel precision following a brute-force search with subpixel refinement. For the current test, a correlation coefficient of 0.95 and a tracking method called "Location only", which looks for changes in translation of the markers, was used.

The tracking process begins by assigning initial coordinates to the markers to be tracked, in a frame the coordinates are in pixel units in the horizontal and vertical directions. This is performed by defining a pattern area with a size equivalent to the dimensions of the marker. Next, a search area is established in which Blender will look for the position of the marker in the following frames. The definition of the pattern area and the search area is shown in Figure 5.5a. The search

area was assigned to the markers based on their expected displacements during each earthquake motion. This area can be increased in case one of the markers moves beyond the defined range. After tracking the markers, the results were generated in terms of frame number, and the horizontal and vertical coordinates of each marker in pixels. Before the test, a checkerboard was placed in front of the camera in the same plane as the markers in order to associate real coordinates to the coordinates of the markers in the photos (1 pixel was equivalent to approximately 0.18 mm in model scale). Figure 5.5b shows the coordinate system for a photo in pixels and the corresponding equivalence in millimeters.
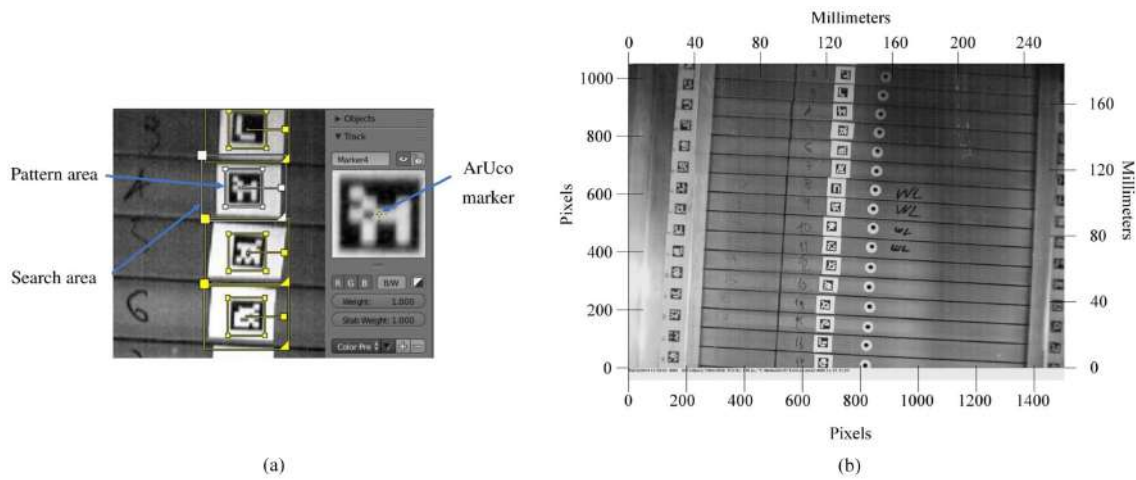
Figure 5.5: Tracking of markers: (a) screenshot of Blender, pattern, and search area for the markers; (b) photo in pixels and scaled in millimeters.

An example of the tracking of one marker is presented in Figure 5.6. The coordinates of each marker (x_i, y_i) after being tracked are in units of pixels and presented frame by frame with a total of 1354 frames tracked in a period of 1.4 s (frame rate 953 Hz) as previously discussed. According to the camera settings and position, an area of 1504 pixels by 1050 pixels covering 15 out of 23 laminations of the model container. The scaling between pixel units and distance units is performed using a known length employing a checkerboard, as mentioned above, then a relationship of a 1-pixel equivalent to approximately 0.18 mm in model scale was obtained. Finally, each coordinate of the marker is expressed in prototype units (X_i, Y_i), the time step is obtained from the sampling frequency and the variation of the horizontal displacement is plotted with time. Considering the displacements occur in the downslope orientation, there was no variation of displacements in the y (vertical) direction (also for the boundary condition imposed by the laminar container), however, the methodology can also be applied to problems in which it is necessary to track displacements in this direction.
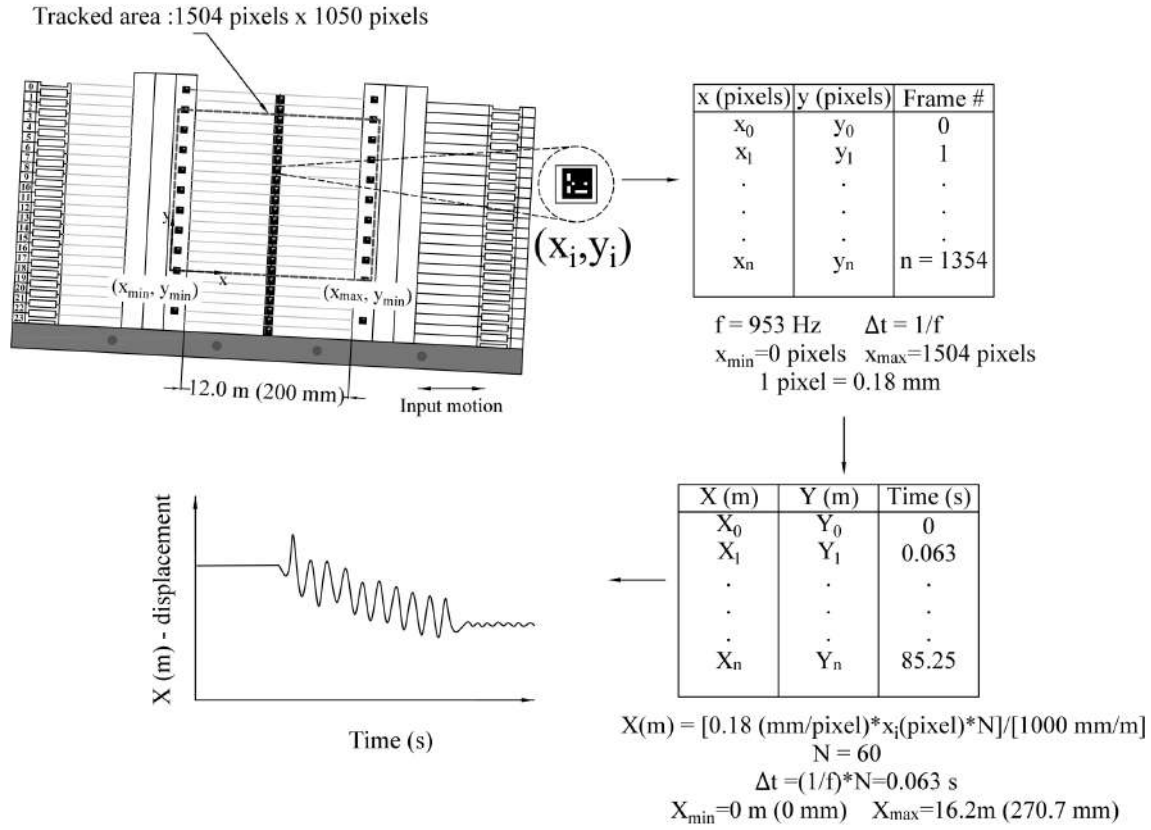
Figure 5.6: Example of tracking of a marker (model units in parenthesis).

5.3.5 Experimental program and testing

To simulate the gentle slope inclination, the model was tilted by 3 degrees using wedges placed along the base of the model. The swing up of the model consisted of increments of 10g until reaching the acceleration level for the test (60g). The bottom drains of the model container were closed during the centrifuge test. Air hammer tests (AHT) were performed at the different stages of the spinning up of the model and between the shaking events to estimate the shear wave velocities within the soil profile in flight. Accelerometers were used to measure the arrival times generated by the air hammer placed on top of the clay (Ghosh and Madabhushi, 2002). Once the target acceleration level was achieved, the model was maintained in flight for 40 minutes before the application of the earthquakes to increase the total stresses and redistribute the pore pressures and effective vertical stresses; a similar methodology was adopted by Garala *et al.* (2020). In the present test program, all centrifuge tests had a similar in-flight time before the application of the earthquakes and all showed similar undrained strength profiles. The following stage consisted of a T-bar penetrometer test (Stewart and Randolph, 1991) and an additional air hammer test. The T-bar used was 40 mm wide with a 4 mm diameter, and was pushed into the clay at a rate of approximately 2 mm/s. The normalized penetration rate, V, is (after Finnie and Randolph, 1994):

$$V = \frac{vD}{C_v} \tag{5.1}$$

where:

v = penetration velocity of the T-bar, 2mm/s

D= diameter of the T-bar, 4 mm.

c_v= coefficient of consolidation of the kaolin, 4.29 mm2/min (0.07 mm^2/s) (Chow $et\ al.$, 2020).

For clays, normalized velocities (V) greater than 10 are likely to be undrained (Oliveira $et\ al.$, 2011; Randolph and Gourvenec, 2011), for the current test V=114, therefore ensuring that the T-bar penetrometer test was performed at an undrained rate.

The results of the in-flight characterization of the clay are presented in Figure 5.7 in terms of effective vertical stresses applied to the model, undrained strength profiles, and shear wave velocity profiles.

Undrained shear strength profile

The measured undrained shear strength (s_u) profile is presented together with an estimate derived from the well-known stress history relationship (Eq. 2; Wroth, 1984):

$$s_u = K\sigma'_v\ (OCR)^m \tag{5.2}$$

where:

K= normalized strength parameter,

$\sigma'_v = (\gamma_{sat} - \gamma_{water}) * z$ = effective vertical stress in kPa,

OCR= $\frac{\sigma'_p}{\sigma'_v}$ = overconsolidation ratio.

m= power constant in the equation.

γ_{sat} = saturated unit weight– 16.9 kN/m^3 (top/bottom layers); 16.4 kN/m^3 (weak layer),

σ'_p = pre-consolidation pressure of the layer – 250 kPa and 125 kPa.

Values of the K and m constants have been reported by several authors (Almeida, 1984; Springman, 1989; Sharma and Bolton, 1996). The theoretical curve was calculated based on the parameters presented by Zhang $et\ al.$ (2011) (K=0.23, m=0.62). The overconsolidation ratio OCR was calculated as the ratio

of the maximum past effective consolidation stresses ($\sigma'_p = 250$ kPa and σ'_p=125 kPa) and the effective vertical stress in flight (σ'_v). The distribution of the effective vertical stresses and pre-consolidation pressures used for the calculation of the OCR are presented in Figure 5.7a. A reasonably good agreement is evident between the experimental and theoretical curves (Figure 5.7b) exhibiting an increase with depth and a reduction in the weaker layer in which a lower pre-consolidation pressure has been applied. The observed contrast of s_u between the weak layer and the neighbouring layers of around 20% lower strength is in accordance with in-situ measured s_u profiles at the offshore Campos Basin, southeastern Brazil (Chapter 2, section 2.4 Figure 2.7) (Soriano *et al*, 2019). There are higher measured values of s_u on top of the clay (between 0 m and 3.6 m) compared with the theoretical curve. This may be due to partial drying of the clay during the swing up and the fact that no superficial water was added to the model in order to avoid sloshing during the earthquake experiments.

Shear wave velocity profile

The shear wave velocities measured by the air hammer were compared with a well-known small-strain stiffness correlation (Equation 5.3) based on the Viggiani and Atkinson (1995) equation:

$$\frac{G_0}{p_r} = A \left(\frac{p\prime}{p_r}\right)^M OCR^k \tag{5.3}$$

where:
G_0 = initial shear modulus in kPa,
p'= mean effective stress in kPa,
p_r = reference pressure equivalent to 1kPa,
OCR= overconsolidation ratio,
A= correlated parameter
k= correlated parameter
M=correlated parameter

The selection of the correlated parameters (A, k , M), was based on the Plasticity Index of the clay (PI=33%). The relationship between the plasticity index and the parameters is presented in Viggiani and Atkinson (1995), for the current research, A=950, k=0.24, and M=0.8. The shear wave velocity (V_s) was calculated in terms of the initial shear modulus (G_0) and the soil density (ρ)

expressed as the total unit weight divided by gravity (Equation 5.4):

$$V_s = \sqrt{\frac{G_o}{\rho}} \tag{5.4}$$

The estimation of the shear wave velocities was based on the travel times between the signals captured by the accelerometers (A1 to A6 in Figure 5.2 b) when the shear waves produced by the air hammer passed through them. To ensure the precision in the recording of the arrival times, it is necessary to have relatively high sampling frequencies. For the current test, a sampling frequency of 30 kHz was used for the air hammer tests. Some uncertainties are involved during air hammer tests (McCullough *et al.*, 2007), such as the location of the instruments, given the permanent deformations that occur during testing (due to swing up and application of earthquakes), therefore, the shear waves may reflect some error.

Despite the uncertainties of the air hammer test, the measured values of the shear wave velocities appear to be in good agreement with the empirical formula (Figure 5.7c). A slight increase in the measured shear wave velocities can also be observed, as the different stages of the test occurred with the lowest values before the re-consolidation of the clay and the highest values after the application of the earthquake EQ4. This implies that there is a hardening of the clay under cyclic loading as the shaking progresses. The fundamental period of the soil profile was 0.5 s. It was estimated by weighted average of shear wave velocity for multiple layer soil using the values from the correlated curve obtained from Equation 5.4, dividing the profile in sub-layers of 0.10 m, and using the following equation (Equation 5.5):

$$T = \frac{4H^2}{\sum_{i=1}^{n} V_i H_i} \tag{5.5}$$

where:
T = fundamental period (s)
H = thickness of the soil profile (m)
V_i = shear wave velocity of the corresponding layer (m/s)
H_i = thickness of the sub-layer (m)
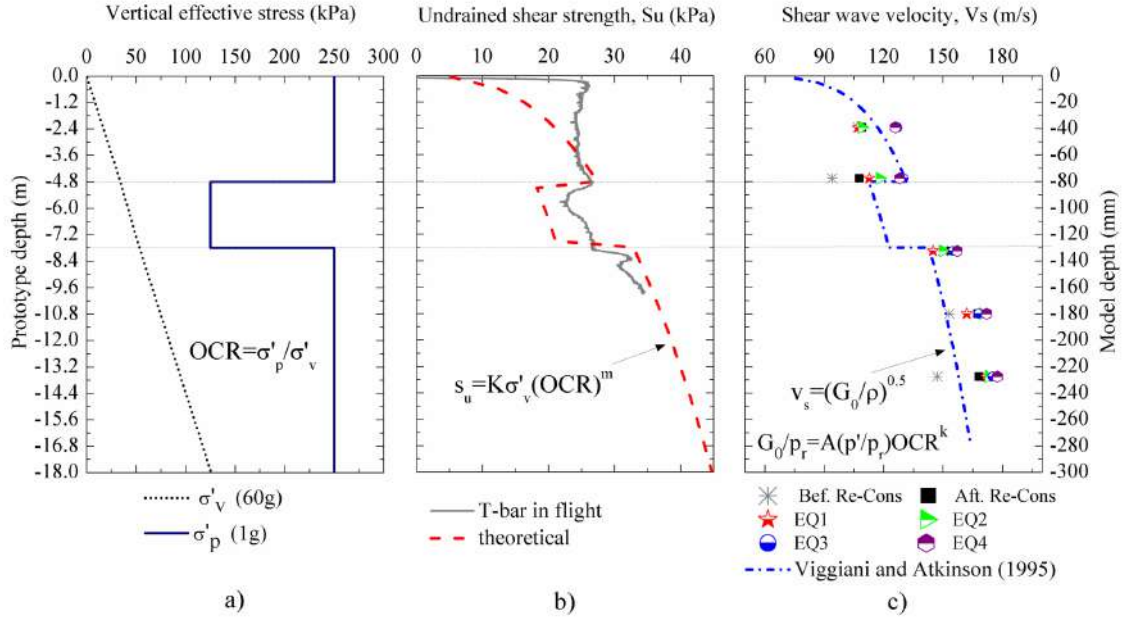
Figure 5.7: Clay model properties: (a) stress history, (b) undrained shear strength profiles, and (c) shear wave velocity profile.

Shaking events

The model was subjected to four earthquakes, three consisting of sinusoidal motions with a driven frequency of 1Hz and the other, a scaled real motion (Kobe earthquake, 1995). During the application of the earthquakes, the instrument data were recorded at a sampling frequency of 6 kHz. Table 5.1 shows the salient characteristics of the earthquakes applied to the model in prototype and model scale. The sequence of the input motions was defined in terms of increasing amplitude. Figure 5.8 presents the acceleration-time histories recorded at the base of the model (accelerometer A10 in Figure 5.2b) or input motions presented in terms of prototype scale.

Table 5.1: Model earthquakes.

Input motion	Type	Frequency (Hz)		Duration (s)		Peak base acceleration (g)	
		Prot.	Model	Prot.	Model	Prot.	Model
EQ1	Sinusoidal	1	60	10	0.17	0.06	3.6
EQ2	Kobe (scaled)	1.4 - 2.4	84.0 - 142.8	4.3	0.07	0.18	10.8
EQ3	Sinusoidal	1	60	10	0.17	0.18	10.8
EQ4	Sinusoidal	1	60	10	0.17	0.37	22.2

113

Figure 5.8: Input motions in prototype scale.

5.4 Test results

5.4.1 Displacement-time histories

The displacement time histories recorded by the LVDTs and calculated by PIV are plotted together with the corresponding input motions in Figure 5.9b and Figure 5.9c. The location of the LVDTs and the corresponding markers used for comparison of the displacement-time histories is presented in Figure 5.9a. For brevity, only the results of earthquakes EQ2 (real scaled) and EQ3 (sinusoidal) are presented in prototype scale. The results show excellent agreement (both series overlap) between the data measured by the LVDTs and the displacements calculated by the PIV methodology incorporated in the Blender software. This validates the use of the ArUco markers for tracking the motions of each of the individual laminae, which is not possible using LVDTs due to their size.

114
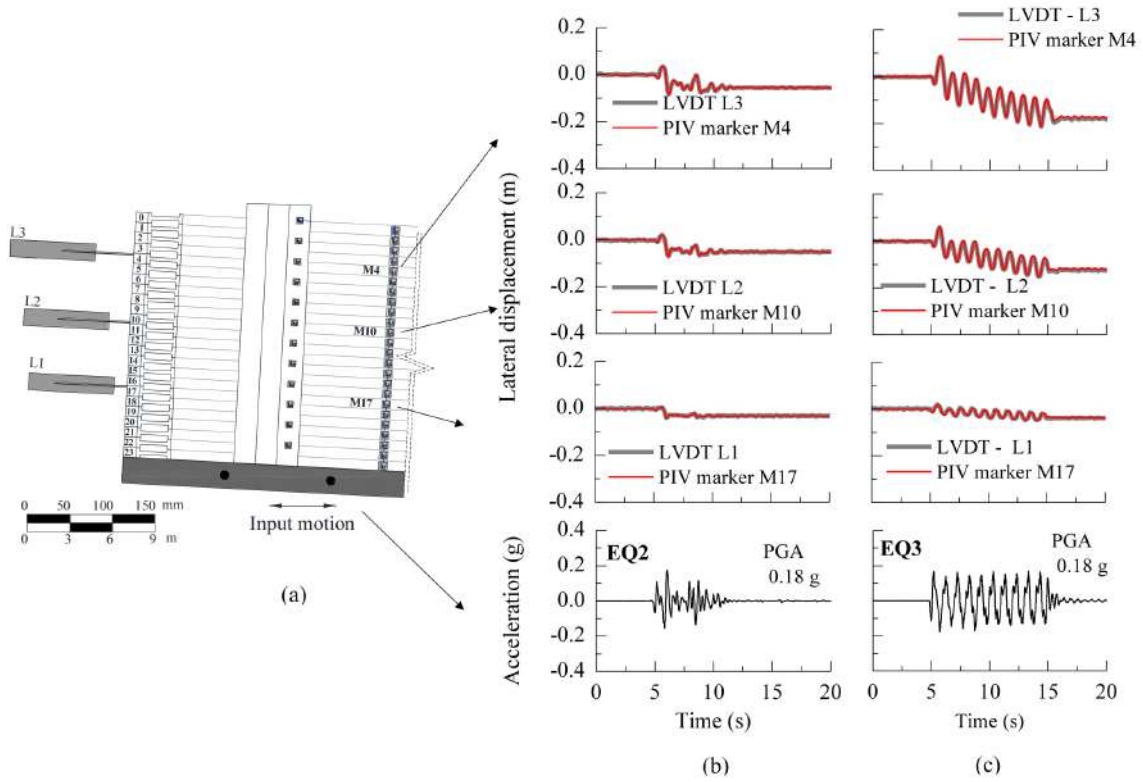
Figure 5.9: Displacement-time histories: (a) location of the LVDTs and markers used for comparison, (b) horizontal displacements during earthquake EQ2, (c) horizontal displacements during earthquake EQ3.

5.4.2 Acceleration time histories

The acceleration time histories and Fast Fourier Transforms (FFT) at different depths for earthquakes EQ2 and EQ3 are presented in Figure 5.10. The results are presented in prototype scale. In addition, from the displacement time histories obtained from the PIV analysis, approximate accelerations at the depths of the corresponding accelerometers were calculated using double differentiation (Figure 5.10a and Figure 5.10c). The raw data from the accelerometers were filtered using a fourth order Butterworth type filter with a bandpass between 5 Hz and 350 Hz in terms of model scale. The selected range of frequencies was defined to remove the low frequencies that produce a drift in the accelerometer signal and the high frequencies associated with electrical noise. The corresponding FFT of the signals at different depths are presented in Figure 5.10b and Figure 5.10d. The FFT results displayed in Figure 5.10d indicate that although earthquake EQ3 was applied as a single frequency (1Hz) sine wave as stated in Table 5.1, the recorded signal is not totally harmonic and other features can be seen in the frequency domain representation. According to Brennan *et al.* (2005), the load applied by a centrifuge earthquake actuator and transferred to the laminar container is not necessarily single frequency. The observed higher harmonics reflect part of the vibration of the shaker and transmitted to the laminar box, and are therefore real loading components and cannot be

considered as noise. This behavior was also observed in the PIV results where the main frequency of the input motions and the higher frequencies were also captured.
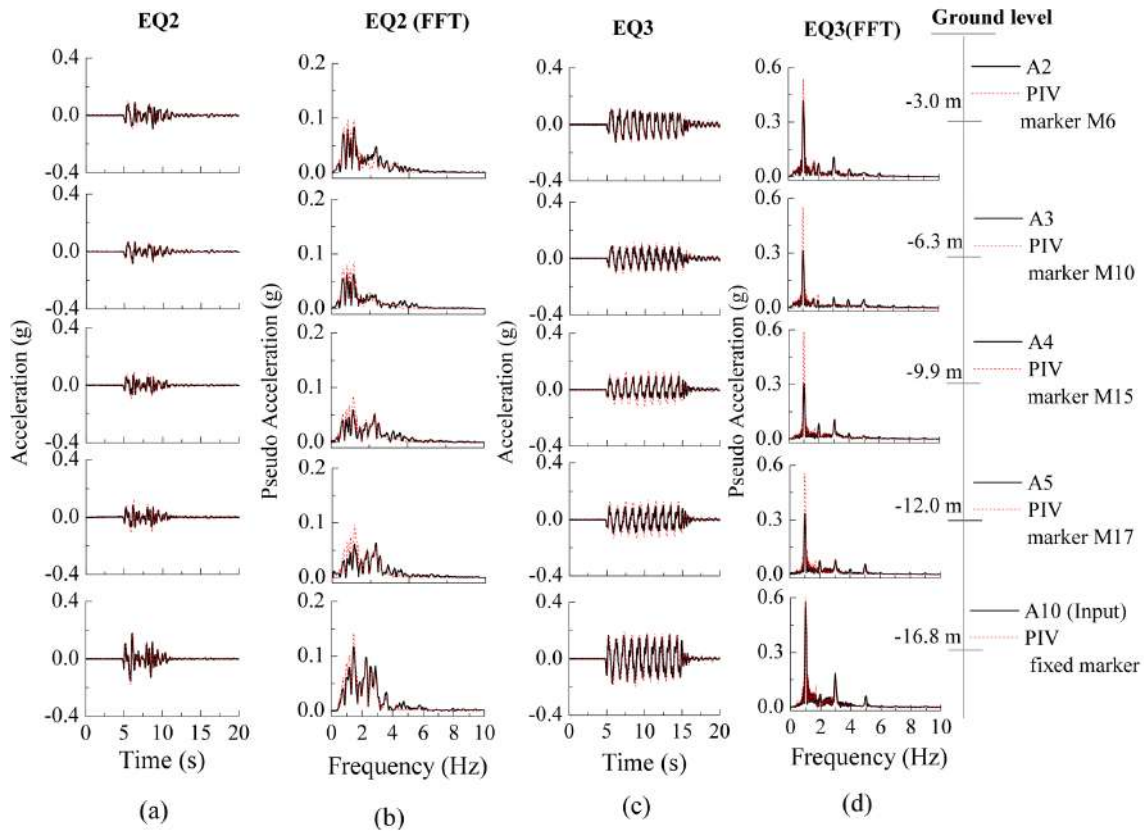
Figure 5.10: Propagation of input motions along the clay: (a) Earthquake EQ 2 accelerations; (b) Earthquake EQ2 Fourier spectra; (c) Earthquake EQ3 accelerations; (d) Earthquake EQ3 Fourier spectra.

5.4.3 Peak ground accelerations and horizontal displacements

The slope response was evaluated by means of maximum displacement profile, Peak Ground Acceleration (PGA) profile, 5%-damped accelerations at the base and near the surface (1.5 m depth) and the ratios of the response spectra. Figure 5.11 presents the peak lateral displacements and PGA profiles obtained after the application of the earthquakes to the model. It must be pointed out that the displacements were plotted for each earthquake by resetting the displacements to zero prior to that earthquake and assuming that the displacement at the base of the slope is zero (net displacements). These displacements are extrapolated in Figure 5.11a as dashed lines below 12 m depth. The values were obtained from the PIV analysis of the markers installed on the laminae (markers M2 to M17 in Figure 5.11) of the container and previously validated with the LVDT measurements (see Figure 5.9). Figure 5.11b shows the PGA variation with depth, with values obtained from two sources: the continuous profile from the PIV using the second derivative of the

116

displacements at each marker depth, and the individual points (identified as "acc.") from the accelerometer data. The results of the PGA profile show a good agreement between the approximation obtained by the PIV calculations and the values measured with the accelerometers. However, a small overestimation of the PGA in the values obtained by the PIV was observed when compared with the accelerometer data. This overestimation could be attributed to the fact that the PIV in the current test was intended to measure the displacements during the application of the earthquakes, and the accelerations from this method were obtained by double differentiation, therefore it is not a direct measurement of the acceleration. Overall, the net displacements show an increase from the bottom to the top, as the earthquake amplitude increased with values ranging between 0.08 m and 0.3 m at the top of the slope in terms of prototype scale. The PGA profiles for earthquakes EQ2, EQ3 and EQ4 exhibit attenuation at depths between 3 m and 10 m in the soil profile.
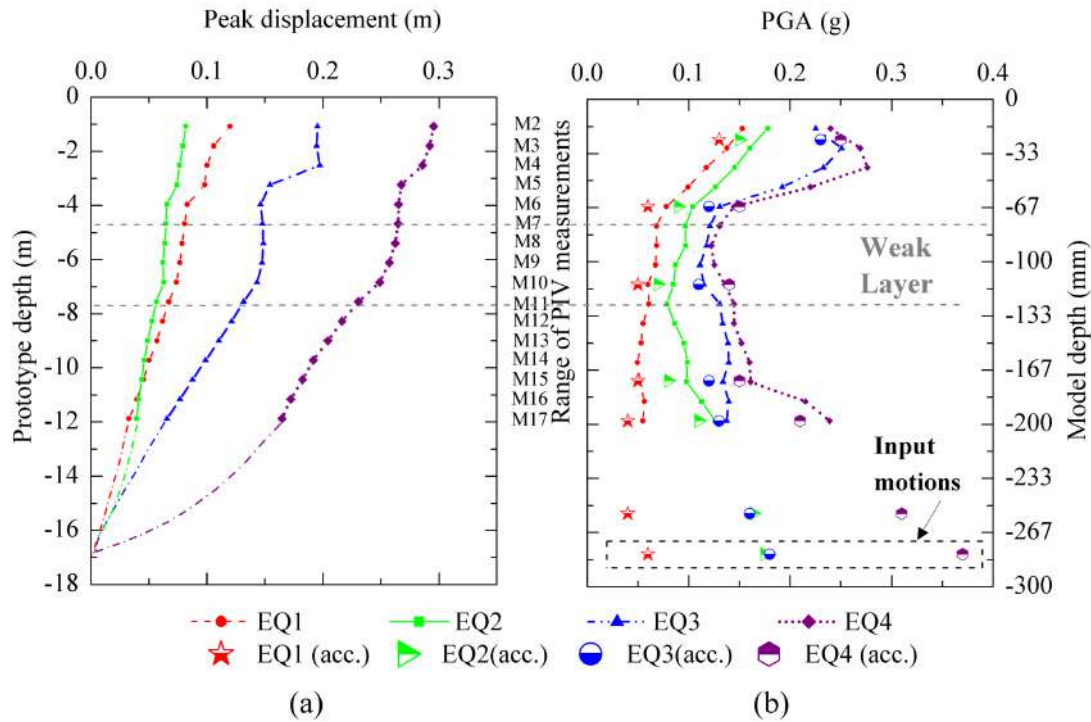
Figure 5.11: Slope response profiles: (a) maximum displacements, (b) PGA.

Figure 5.12a shows the acceleration response spectra of the earthquakes applied to the model at the base and at a depth near the surface (-1.5 m) with a damping ratio of 5% and Figure 5.12b presents the ratio of the response spectra curves. The response spectra ratios exhibit amplifications at the natural period of the soil profile (0.5 s) during earthquakes EQ1 and EQ3 corresponding to sinusoidal loadings, indicating the local site effects on the input motion. For EQ2 the response spectra ratio remained in a range close to 1 for the periods below 1s, followed by amplification at periods greater than 1s. For the largest amplitude earthquake (EQ4), the peak in

the response spectra ratio shifted to a value of 0.7 s followed by an attenuation until 1 s and then a gradual increase, reaching values larger than 1. This shift in the peak of the response spectra ratio for earthquake EQ4 may be explained by nonlinear effects resulting from the reduction in the stiffness of the soil and the increase in damping as the soil softens.
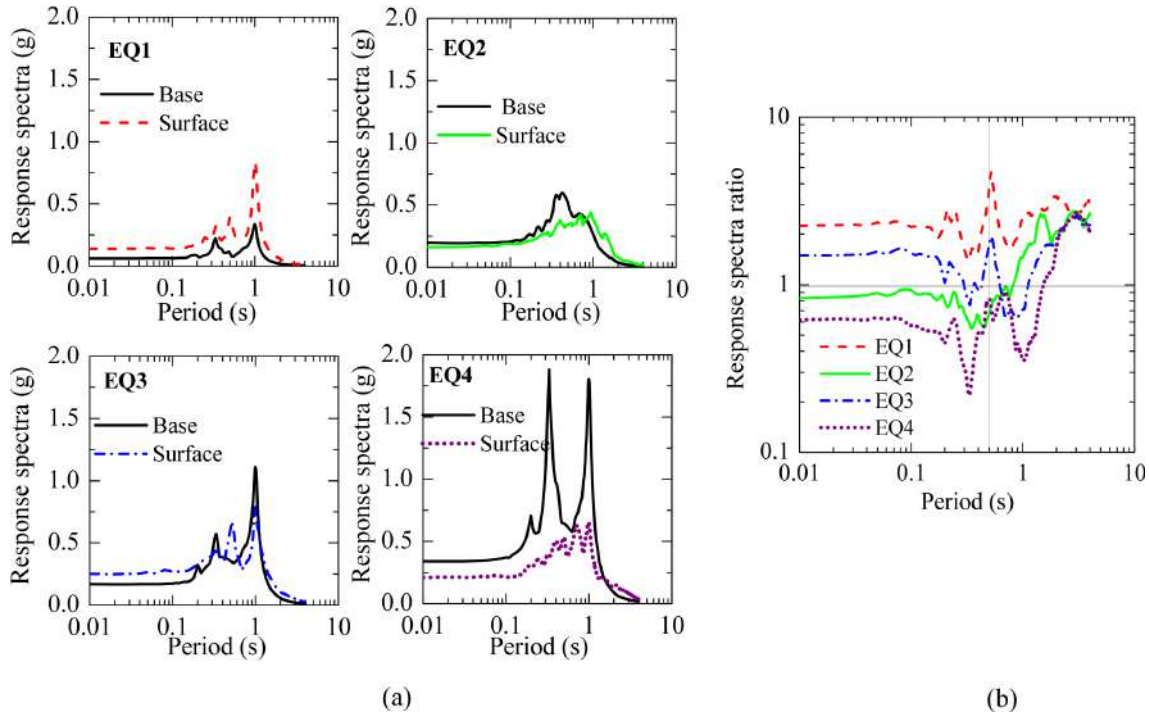
Figure 5.12: (a) acceleration response spectra, (b) response spectra ratio.

Although strength mobilization may occur during the swing up of the model, a snapshot of the strength of the clay at the moment before the application of the shaking events was captured by means of the in-flight characterization tests (T-bar and Air Hammer). Further improvements can be implemented to control the lateral displacements during the swing up, using lateral actuators that laterally support the laminar container with the clay through the swing up process and are released prior to the application of the earthquakes. For the calibration of a numerical model, the selection of the strength parameters must consider the monotonic strengths and the cyclic strengths given by the strain rates applied in centrifuge tests. Strain rate effects significantly increase the strength and stiffness in clays (Afacan *et al.*, 2019; Sathialingam and Kutter, 1989).

5.5   Post-test investigations

A photograph of the model after the test and an overlay of the location of the markers tracked by the camera is shown in Figure 5.13a. An accumulated

displacement is evident on top of the clay at about 10 mm (model scale). An interface line between the clay layers was visible at the periphery of the sample. Thus, to determine the continuity and contact between the layers, a section in the transverse direction was checked. No evidence of discontinuity between the layers was apparent in those transverse sections, therefore, the model soil profile was laterally uniform (Figure 5.13b), indicating a successful sample preparation process.
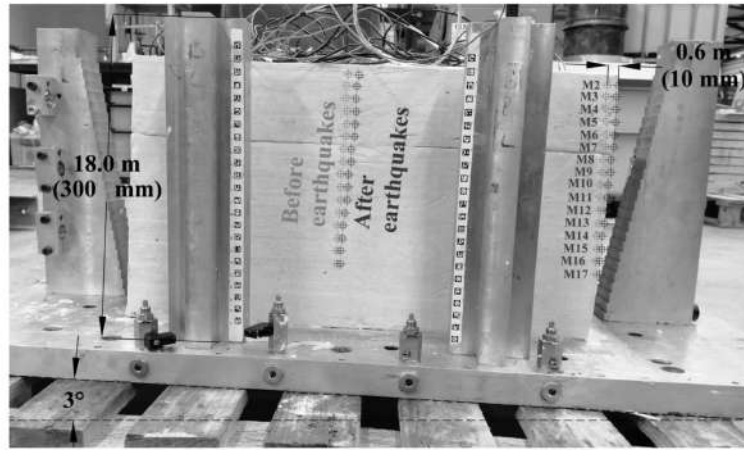
(a)
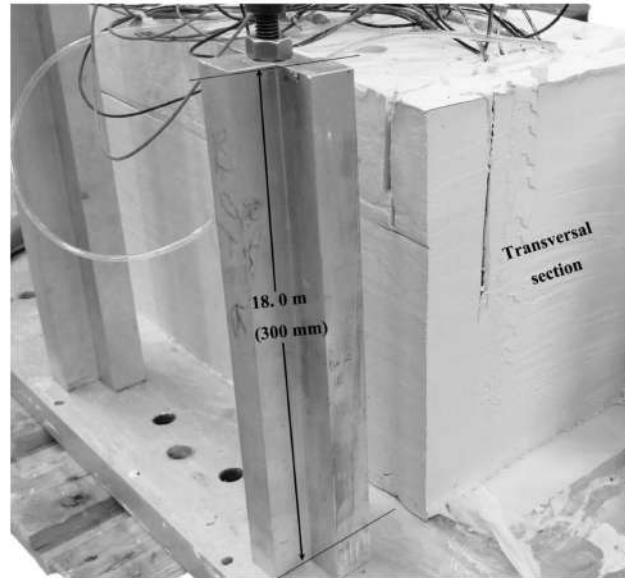
(b)

Figure 5.13: (a) Clay model after centrifuge test (model scale in parentheses), (b) transversal section and contact between layers

5.6 Conclusions and recommendations for similar testing programs

The centrifuge test in this study was performed to develop a model preparation technique for simulating the dynamic behavior of a gentle layered slope in soft clay.

The model was subjected to a series of dynamic motions to investigate the displacement and acceleration behaviors. The main observations from the centrifuge test follow:

- The proposed model preparation technique enabled the simulation of a three-layer soil profile in clay, with a strength contrast between layers achieved by applying different consolidation pressures during the sample preparation process.

- The PIV analysis was used to track the displacements of the model at the different stages of the centrifuge test with particular focus on the application of the dynamic motions. The displacements from the PIV calculations were in good agreement with those measured by the LVDTs, confirming that a similar setup could be applied in comparable testing programs involving the use of laminar containers.

- Measured soil properties for undrained shear strength and shear wave velocity were in reasonable agreement with the empirical predictions.

- The acceleration data at different depths were obtained by direct measurements from the accelerometers and approximated by double differentiation of the PIV displacements. The results were compared in terms of the time histories and the FFT of the signals. Additional frequencies were observed on the sinusoidal motions attributable to the higher vibration modes of the shaker and were transmitted to the laminar container.

- With the validated PIV results, a continuous displacement profile after the applied earthquakes was calculated. The PGA profiles were obtained from the maximum accelerations measured by the accelerometers and from the double derivative of the displacements calculated from the PIV analyses. The results are complementary and show good agreement and could be used for direct comparison with computational analyses.

- The spectral analysis showed amplifications at periods corresponding to the fundamental period of the soil profile during earthquakes EQ2 and EQ3. A shift in the period occurred during the largest amplitude earthquake (EQ4), indicating a nonlinear behavior of the slope profile.

- In addition to the monotonic strengths, given the strain rates applied in dynamic centrifuge tests, cyclic strengths should also be considered for the calibration of numerical models of the problem studied.

- The centrifuge experiment presented in this chapter constitutes a first step on the simulation of clayey soil profiles including weak layers. From several studies, weak layers have been considered as part of the triggering mechanisms of submarine landslides. Subsequent tests from the same experimental program included the simulation of a higher strength contrast between layers by applying lower consolidation pressures aiming to provide additional data on the seismic response of submarine slopes with weak layers.

The results from the centrifuge test provided useful insight into preparation of layered clay-profile models using a laminar container to assess lateral spreading problems. The results can be used for calibration of numerical models and for performing comparisons with existing methods for the calculation of dynamic responses (i.e., Newmark's method).

5.7   Chapter 5 references

ACOSTA, E., TIBANA, S., ALMEIDA, M.S.S., AND SABOYA, F., 2017, "Centrifuge modeling of hydroplaning in submarine slopes," Ocean Engineering, Vol. 129, No.1, pp. 451–458.

AFACAN, K.B., BRANDENBERG , S.J., AND STEWART, P.J., 2013, "Centrifuge modeling studies of site response in soft clay over wide strain range," Journal of Geotechnical and Geoenvironmental Engineering, Vol. 140, No.2, pp. 1-13.

AFACAN, K.B., YNIESTA, S., SHAFIEE, A., STEWART, J., AND BRANDENBERG, S., 2019, "Total Stress Analysis of Soft Clay Ground Response in Centrifuge Models," Journal of Geotechnical and Geoenvironmental Engineering, Vol. 145, No.10.

ALMEIDA, M.S.S., 1984, "Stage constructed embankments on soft clays," PhD thesis, Cambridge University, Cambridge, UK.

BISCONTIN, G., PESTANA, J.M., NADIM, F., 2004, "Seismic triggering of submarine slides in soft cohesive soil deposits,". Marine Geology, Vol. 203, No. 3-4, pp.341-354.

BISCONTIN, G., AND PESTANA, J., 2006, "Factors affecting seismic response of submarine slopes," Natural Hazards and Earth System Science, Vol. 6, No.1, pp. 97-107.

BRENNAN, A. J., THUSYANTHAN, N. I. MADABHUSHI, S. P. G., 2005, "Evaluation of shear modulus and damping in dynamic centrifuge tests," Journal of

Geotechnical and Geoenvironmental Engineering, Vol. 131, No. 12, pp-1488–1498.

BRENNAN, A. J., MADABHUSHI, S. P. G., AND COOPER, P., 2006A, " Dynamic centrifuge testing of suction caissons in soft clay," Proceedings of the 6th International Conference on Physical Modelling in Geotechnics, 6th ICPMG '06, Hong Kong, pp. 625-630.

BRENNAN, A. J., MADABHUSHI, S. P. G., AND HOUGHTON, N. E., 2006B, "Comparing Laminar and Equivalent Shear Beam (ESB) Containers for Dynamic Centrifuge Modeling," Proceedings of the 6th International Conference on Physical Modelling in Geotechnics, 6th ICPMG '06, Hong Kong, pp. 171–176.

BRYN, P., BERG, K., FORSBERG, C.F., SOLHEIM, A., KVALSTAD, T.J., 2005a, "Explaining the Storegga slide," Marine and Petroleum Geology, Vol. 22, pp. 11-19.

BRYN, P., BERG, K., STOKER, M.S., HAFLIDASON, H., SOLHEIM, A., 2005b, "Contourites and their relevance for mass wasting along the Mid-Norwegian Margin," Marine and Petroleum Geology, Vol. 22, pp. 85-96.

CHOW, J.K., WANG, Y., LUI, H.L., AND HUANG, E., 2020, "Determination of consolidation parameters based on the excess pore water pressure measurement using a newly developed U-oedometer," Acta Geotechnica, Vol.15, pp.2665-2680.

DE SANCTIS, L., DI LAORA, R., GARALA, T.K., MADABHUSHI, S.P.G., VIGGIANI, G., FARGNOLI, P., 2021, "Centrifuge modelling of the behaviour of pile groups under vertical eccentric load," Soils and Foundations, Vol. 61(2), pp. 465-479.

DEY, R., HAWLADER, B., PHILLIPS, R., AND SOGA, K., 2016, " Modeling of large deformation behaviour of marine sensitive clays and its application to submarine slope stability analysis," Canadian Geotechnical Journal, Vol. 53, pp. 1138-1155.

ELGAMAL AW, ZEGHAL M, TABOADA V AND DOBRY R, 1996, "Analysis of Site Liquefaction and Lateral Spreading Using Centrifuge Testing Records," Soils and Foundations, Vol. 36, No2, pp. 111-121.

FAGUNDES, D.F., RAMMAH, K.I., ALMEIDA, M.S.S., PEQUENO, J., OLIVEIRA, J.R.M.S., AND GARSKE, R., 2012, "Strength Behaviour Analysis of an Offshore Brazilian Marine Clay." Proceedings of the ASME 2012 31st International Conference on Ocean, Offshore and Arctic Engineering, Rio de Janeiro, Brazil, Vol. 4, pp. 1-9.

FINNIE, I. M. S., AND RANDOLPH, M. F., 1994, "Punch-Though and liquefaction induced failure on shallow foundations on calcareous sediments,"

Proceeding International Conference on Behaviour of Off-Shore Structures – BOSS '94, Boston, Vol. 1, pp. 217-230.

GARALA, T.K., AND MADABHUSHI, S.P.G., 2019, "Seismic behaviour of soft clay and its influence on the response of friction pile foundations," Bull Earthquake Eng Vol. 17, pp. 1919–1939.

GARALA, T. K., MADABHUSHI, G., AND DI LAORA, R., 2020, "Experimental investigation of kinematic pile bending in layered soils using dynamic centrifuge modelling," Geotechnique, pp. 1-16.

GARCÍA-TORRES, S., AND MADABHUSHI, G.S.P., 2019, "Performance of vertical drains in liquefaction mitigation under structures," Bulletin of Earthquake Engineering, Vol. 17, pp. 5849–5866.

GARRIDO-JURADO, S., MUÑOZ-SALINAS, R., MADRID-CUEVAS, F., AND MARÍN-JIMÉNEZ, M., 2014, "Automatic generation and detection of highly reliable fiducial markers under occlusion," Pattern Recognition, Vol. 47, pp. 2280–2292.

GARSKE, R., ASSUMPÇÃO, M., ALMEIDA, M.C.F., ALMEIDA, M.S.S., 2020, "Seismicity and seismic hazard in the Continental Margin of Southeastern Brazil," Journal of Seismology.

GHOSH, B., AND MADABHUSHI, S.P.G., 2002, "An efficient tool for measuring shear wave velocity in the centrifuge." Proceedings of the International Conference on Physical Modeling in Geotechnics: ICPMG'02, pp.119-124.

HAFLIDASON, H., SEJRUP, H. P., BERSTAD, I. M., NYGARD, A., RICHTER, T., LIEN, R. BERG, K., 2003, "A weak layer feature on the northern Storegga slide escarpment," In European margin sediment dynamics, edited by J. Mienert and P. P. E. Weaver, pp. 55–62. Berlin, Germany: Springer.

HAIGH, S. K., GOPAL MADABHUSHI, S. P., SOGA, K., TAJI, Y., AND SHAMOTO, Y., 2000, "Lateral Spreading During Centrifuge Model Earthquakes," ISRM International Symposium, Melbourne, Australia.

HESS, R., 2010, "Blender Foundations: The Essential Guide to Learning Blender 2.6", Focal Press.

HOTTA, M.M., ALMEIDA, M.S.S., PELISSARO, D.T., OLIVEIRA, J.R.M.S., TIBANA, S., GARSKE, R., 2019, "Centrifuge tests for evaluation of submarine-mudflow hydroplaning and turbidity currents," International Journal of Physical Modelling in Geotechnics, Vol. 20, No. 4, pp 239-253.

HÜHNERBACH, V., AND MASSON, D.G., 2004, "Landslides in the North Atlantic and its adjacent seas: an analysis of their morphology, setting and behavior," Marine Geology, Vol. 213, pp. 343-362.

KIM, S. H., 1996, "Model Testing and Analysis of Interactions between Tunnels in Clay," Ph.D. thesis, University of Oxford, Oxford, UK.

KNAPPETT, 2006, "Piled foundations in liquefiable soils: accounting for axial loads," PhD thesis, Cambridge University, Cambridge, UK.

KOWSMANN, R.O, LIMA, A.C, VICALVI, M.A., 2016, "Features indicating geological instability in the continental slope and São Paulo Plateau," in: Geology and Geomorphology. Regional Environmental Characterization of the Campos Basin, Southwest Atlantic, edited by Kowsmann, R.O, pp 71-97, Elsevier Brazil.

LANZANO, G., BILOTTA, E., RUSSO, G., SILVESTRI, F., AND MADAB-HUSHI, S.P.G., 2012, "Centrifuge Modeling of Seismic Loading on Tunnels in Sand," Geotechnical Testing Journal, Vol. 35, No. 6, pp. 854-869.

LAU, B. H. ,2015, "Cyclic behaviour of monopile foundations for offshore wind turbines in clay," PhD thesis, University of Cambridge, Cambridge, UK.

LOCAT, J., LEE, H., 2009, "Submarine mass movements and their consequences: an overview," in: Landslides and Disaster Risk Reduction, edited by Sassa, K., and Canuti, P. pp. 115-142, Springer, Berlin, Heidelberg.

MADABHUSHI, S.P.G., 2014, Centrifuge modelling for civil engineers, CRC Press, Boca Raton.

MADABHUSHI, S.P.G., HAIGH, S.K., HOUGHTON, N.E., AND GOULD, E., 2012, "Development of a servo-hydraulic earthquake actuator for the Cambridge Turner beam centrifuge". International Journal of Physical Modelling in Geotechnics, Vol. 12, pp. 77-88.

MCCULLOUGH, N., DICKENSON, S., SCHLECHTER, S., AND BOLAND, J., 2007,"Centrifuge Seismic Modeling of Pile-Supported Wharves." Geotechnical Testing Journal. Vol. 30, No. 5, pp. 349-359.

NADIM, F., BISCONTIN, G., KAYNIA, A.M., 2007, "Seismic triggering of submarine slides," Offshore Technology Conference, Houston, TX, USA.

O'LEARY, D. W., 1991, "Structure and morphology of submarine slab slides: clues to origin and behaviour," Marine Geotechnology, Vol. 10, pp. 53–69.

OLIVEIRA, J.R.M.S., ALMEIDA, M.S.S., MOTTA, H.P.G., AND ALMEIDA M.C.F, 2011, "Influence of penetration rate on penetrometer resistance," Journal of

Geotechnical and Geoenvironmental Engineering, Vol. 137, pp. 695-703.

PESTANA, J. M. AND NADIM, F., 2000, "Nonlinear site response analysis of submerged slopes", Technical Report UCB/GT/2000-04, University of California, Berkeley, Department of Civil and Environmental Engineering.

PIRCHINER, M., DROUET, S., ASSUMPÇÃO, M., DOURADO, J., FER-REIRA, J., VIEIRA, L., JULIÁ, J., 2015, "PSHAB: Probabilistic Seismic Hazard Analysis for Brazil: A National Hazard Map Building Effort," Proceedings of the 26th International Union of Geodesy and Geophysics General Assembly, Prague, Czech Republic.

RANDOLPH, M., AND GOURVENEC, S., 2011, Offshore Geotechnical Engineering. 1 ed. Oxon, Spon Press.

RAYHANI, M AND EL NAGGAR, M.H., 2007, "Centrifuge modeling of seismic response of layered soft clay," Bulletin of Earthquake Engineering, Vol. 5, No. 4, pp 571-589.

RODRÍGUEZ-OCHOA, R., NADIM, F., CEPEDA, J.M., HICKS, M.A., AND LIU, Z., 2015, " Hazard analysis of seismic submarine slope instability," Georisk: Assessment and Management of Risk for Engineered Systems and Geohazards, Vol. 9, No. 3, pp. 128-147.

SATHIALINGAM, N., AND KUTTER, B., 1989, "The Effects of High Strain Rate and High Frequency Loading on Soil Behavior in Centrifuge Model Tests," NCEL Contract Report.

SHARMA, J.S., AND BOLTON, M.D., 1996, "Centrifuge modeling of an embankment on soft clay reinforced with geogrid," Geotextiles and Geomembranes, Vol. 14, No. 1, pp. 1-17.

SOLHEIM, A., BRYN, P., SEJRUP, H.P., MIENERT, J., BERG, K., 2005, "Ormen Lange e an integrated study for the safe development of a deep-water gas field within the Storegga slide complex, NE Atlantic continental margin; executive summary," Marine and Petroleum Geology, Vol. 22, pp. 1-9.

SORIANO, C., ANDRADE, R.B., MOLLEPAZA, S., ALMEIDA, M.S.S., ALMEIDA, M.C.F., OLIVEIRA, J.R.M., TREJO, P., 2019 "Simulation of a Weak Layered Profile Using Geotechnical Centrifuge," Proceedings of the XVI Pan-American Conference on Soil Mechanics and Geotechnical Engineering (XVI PCSMGE), Cancun, Mexico, pp. 477-484.

SPRINGMAN, S.M., 1989, "Lateral loading on piles due to simulated embankment construction," PhD thesis, Cambridge University, Cambridge, UK.

STEWART, D.P AND RANDOLPH, M.F., 1991, "A new site investigation tool for the centrifuge," Proceedings of the International Conference on Centrifuge Modeling –Centrifuge'91, Boulder, Colorado, pp. 531-538

TABOADA, V.M., DOBRY, R., 1998, "Centrifuge modeling of earthquake induced lateral spreading in sand," Journal of Geotechnical and Geoenvironmental Engineering, Vol. 124, No. 12, pp. 1995-1206.

TARAZONA, S.F.M., ALMEIDA, M.C.F., BRETSCHNEIDER, A., ALMEIDA, M.S.S., ESCOFFIER, S., GARSKE, R., 2020, "Evaluation of seismic site response of submarine clay canyons using centrifuge modelling," International Journal of Physical Modelling in Geotechnics, Vol.20, No. 4 pp. 224-238.

TAYLOR, R.N., 1995, "Centrifuge modelling: principles and scale effects." Geotechnical Centrifuge Technology, Edited by Taylor, R.N., Blackie Academic Professional, pp. 19–33.

TRICARICO, M., MADABHUSHI, G.S.P., AND AVERSA, S., 2016, "Centrifuge modelling of flexible retaining walls subjected to dynamic loading," Soil Dynamics and Earthquake Engineering, Vol. 88, pp. 297-306.

VIGGIANI, G., AND ATKINSON, J.H., 1995, "Stiffness of fine-grained soil at very small strains," Geotechnique, Vol. 45, No. 2, pp. 249-265.

WHITE, D.J., GAUDIN, C., BOYLAN, N., 2010, "Interpretation of T-bar penetrometer tests at shallow embedment and in very soft soils," Canadian Geotechnical Journal, Vol 47, pp218-219.

WILLIAMSON, M., 2014. Tunnelling effect on bored piles in clay. PhD thesis. University of Cambridge, United Kingdom.

WROTH, C.P., 1984, "The Interpretation of in Situ Soil Test," Geotechnique, Vol.34, pp. 449-489.

ZHANG C, WHITE, D., AND RANDOLPH, M., 2011, "Centrifuge modeling of the cyclic lateral response of a rigid pile in soft clay," Journal of Geotechnical and Geoenvironmental Engineering, Vol. 137, No.7, pp. 717–729.

ZHOU, Y-G., CHEN, J., CHEN, Y-M., KUTTER, B., ZHENG, B, WILSON, D., STRINGER, M., AND CLUKEY, E., 2017, " Centrifuge modeling and numerical analysis on seismic site response of deep offshore clay deposits," Engineering Geology, Vol. 227, pp. 54-68.

ZHOU, Y.G., CHEN, J., YU, S., AMIR, M., BO, H., AND YUN-MIN, C, 2017, "Earthquake Response and Sliding Displacement of Submarine Sensitive Clay Slopes." Engineering Geology, Vol. 227, pp. 69–83.

Chapter 6

Numerical modelling of a gentle slope in soft clay

6.1 Introduction

In this chapter, a series of nonlinear ground response analyses are introduced to simulate the behavior of the 3-degree slope model presented in Chapter 4. The numerical simulations were performed in OpenSeesPL (Elgamal and Yang, 2011) using a three-dimensional soil column and a dynamic nonlinear constitutive model (Yang and Elgamal, 2003). The performance of the numerical models was evaluated by comparing the measured response of the slope in terms of lateral displacements and acceleration-time histories. A discussion of the strain rate effects on cohesive soils is also presented in this chapter, suggesting the application of more sophisticated constitutive models. To conclude, the results of a simplified parametric analysis are presented to examine the response a gentle slope in soft clay for various inclination angles.

6.2 Centrifuge test model

The test selected for the calibration of the numerical models explained in this chapter corresponds to the three-degree slope presented in Chapter 4. The centrifuge experiment was performed at an acceleration level of N=60 g simulating a gentle slope with a thickness of clay of 14.3 m on prototype scale. Figure 6.1 displays the experimental setup of the centrifuge test and the location of the instruments as control points for the comparisons of the calculated responses of the numerical models.
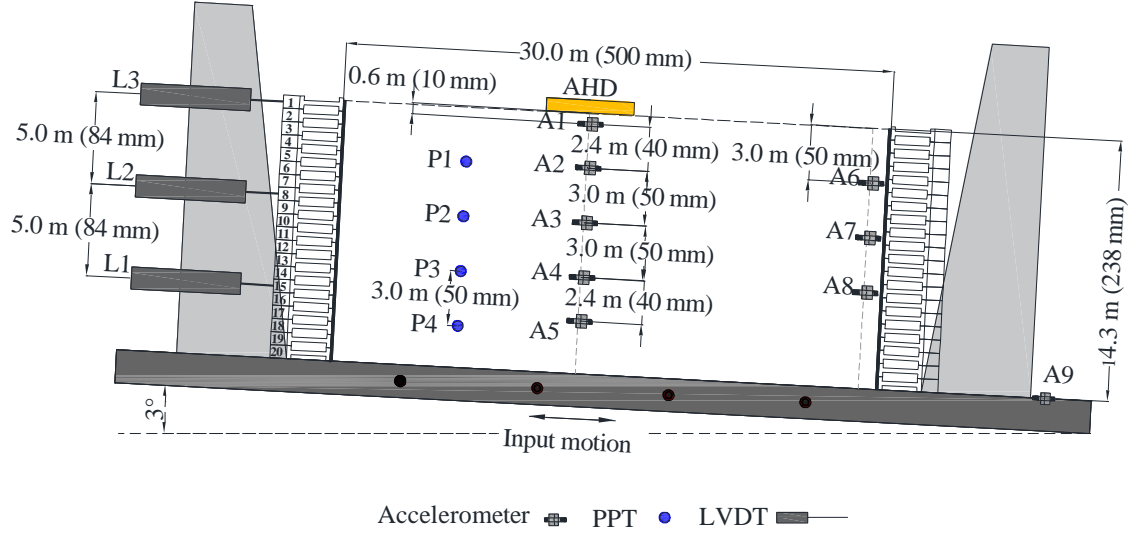
Figure 6.1: Instrumentation layout of three-degrees slope model.

6.3 Numerical modelling methodology

To simulate the response of a gently sloping ground, it was applied the open-source computational interface OpenSeesPL (Elgamal and Yang, 2011), implemented within the finite element code OpenSees (Mazzoni *et al.*, 2009). The Graphical User Interface (GUI) in OpenSeesPL allows the study of various ground modification scenarios including the presence of a group of piles in a soil mass. For liquefaction countermeasures, the simulation of gravel drains, stone columns, and solidification/cementation techniques can also be analyzed. The scenario used in this thesis, allows the simulation of mild infinite slope inclination to estimate accumulated ground deformation during seismic loading.

Given the characteristics of the problem studied of a gentle slope, the model was simplified, and a soil column was used to simulate the soil profile. For that purpose, a shear beam behavior with a boundary condition of equal displacement constraints (x, y, and z) for all the nodes at the same depth was adopted. This technique is less time-consuming than a fully 3D approach. Phillips (2012) developed numerical models to simulate free-field lateral spreading centrifuge tests. Two approaches were adopted, the first consisted of a fully 3D problem considering the model container extents in prototype scale; the second was a shear beam column. Both models provided almost identical results for the simulation of the problem studied, then, the shear beam model was used as the time required for the simulations was less than the required for the full 3D models.

Figure 6.2 presents an example of a soil column used to simulate a layered soil site. The soil column comprehends an extent of 1.0 m in the x and y

directions, and the thickness of the soil elements in the vertical direction is defined by the user. For the analyses, 8-node brick elements were utilized as the simulations are in terms of total stresses. Those elements are based on a trilinear isoparametric formulation and have 3 translational degrees of freedom per node.
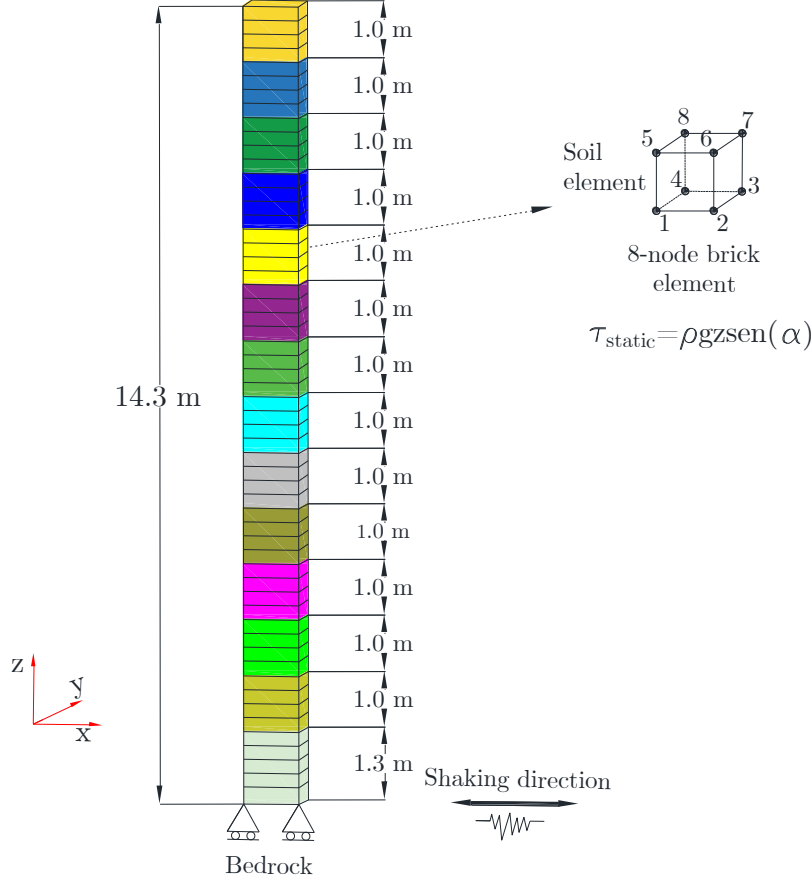
Figure 6.2: Schematic of a 3D column to simulate a layered slope

The element thickness must ensure an adequate number of elements within the wavelength of a shear wave. A range between 8 to 10 elements per wavelength can be set (Kuhlemeyer and Lysmer, 1973; Mullen and Belytschko, 1983). The element size at different depths can be defined in terms of the small-strain shear wave velocity (V_s) and the maximum frequency content f_{max} of the ground motions applied to the models. The minimum wavelength ($\lambda_{min}=V_s/f_{max}$) was then divided by 10 at each depth to define the maximum allowable size of the mesh elements ($h_{max}=\lambda_{min}/10$). For the current numerical centrifuge test: f_{max} =10 Hz, defined from the frequency content of the input motions in terms of prototype scale (Figure 6.3) and V_{smin}=65 m/s from the measured and adjusted profiles (Figure 6.6 and Table 6.1), then λ_{min}=6.5 m and h_{max}=6.5 m/10 =0.65 m. Considering that the the slope to be modelled was relatively shallow, the mesh was refined using finer elements as the maximum allowable size (h_{max}=0.65 m) with no significant computing cost when performing the numerical simulations. Therefore, an element thickness of 0.25

m or 4 brick elements per layer in terms of prototype scale was adopted for the numerical simulations to obtain more data points to compare with the instrumental response of the slope.

6.3.1 Boundary conditions

In OpenSeesPL, there are included diverse boundary conditions, including Shear Beam, Rigid Box, and Periodic Boundary (Elgamal and Yang, 2011). For the numerical analyses presented in this chapter, a Shear Beam condition was selected. In this case, the front and back nodes of the soil column (Figure 6.2) move together in horizontal and vertical directions. Rollers are implemented for lateral and base boundaries for all gravity runs and base nodes are fixed after the first run. The slope inclination is simulated by imposing to the soil column a static driving shear stress component. This static stress can be expressed as:

$$\tau_{static} = \rho g z sen(\alpha) \tag{6.1}$$

where,

ρ=soil density,

$g=$ gravity acceleration (m/s^2),

$z=$ depth (m),

$\alpha=$slope inclination angle (degrees).

6.3.2 Earthquake inputs

In OpenseesPL, input motions can be applied in longitudinal (x in Figure 6.2), transverse (y in Figure 6.2) and vertical (z in Figure 6.2) directions. The ground motion input is associated to the boundary conditions at the bottom of the model (Liang *et al.*, 2017). Two approaches can be adopted:

(i) If the bottom of the model is assumed as a bedrock, the dynamic excitation is applied as an equivalent force-time history to the base of the soil column. The equivalent force-time history, is obtained by integration of the acceleration-time history and converted into a velocity-time history that is multiplied by the mass density (ρ_E) and shear wave velocity (V_{SE}) of the underlying bedrock layer and the area of the base of the soil column (A_E) (Joyner and Chen, 1975). This method requires the definition of a viscous boundary to absorb reflected waves due to setting artificial boundary to simulate the bedrock. The dashpot coefficient $(C = \rho_E V_{sE} A_E)$ is defined by multiplying the rock density (ρ_E),

shear wave velocity of the bedrock (V_{sE}) and the contact area between the soil column and the bedrock (A_E).

(ii) If the bedrock is assumed to be rigid, OpenSeesPL allows the application of the input motion as an acceleration-time history. This condition means the bottom boundary is fixed horizontally and vertically. The software OpenSeesPL has a built-in input motion library that includes near-fault soil surface motions as well as long-duration outcrop motions recorded from earthquakes around the world. User-defined input motions can also be set by loading text files consisting of time-acceleration columns. For the simulation of the centrifuge test, this methodology was utilized.

Figure 6.3 and Figure 6.4 present the acceleration time-histories employed in the numerical analyses; they correspond to the measured accelerations at the base of the model (A9 in Figure 6.1). The measured accelerations were filtered to remove the effects of high and low-frequency noise. As explained in Chapter 4, the input motions consisted of sinusoidal waves with a predominant frequency of 1Hz and varying amplitudes in terms of PGA and real-scaled motions with a broad frequency content (Imperial Valley – EQ2 and Kobe – EQ3).
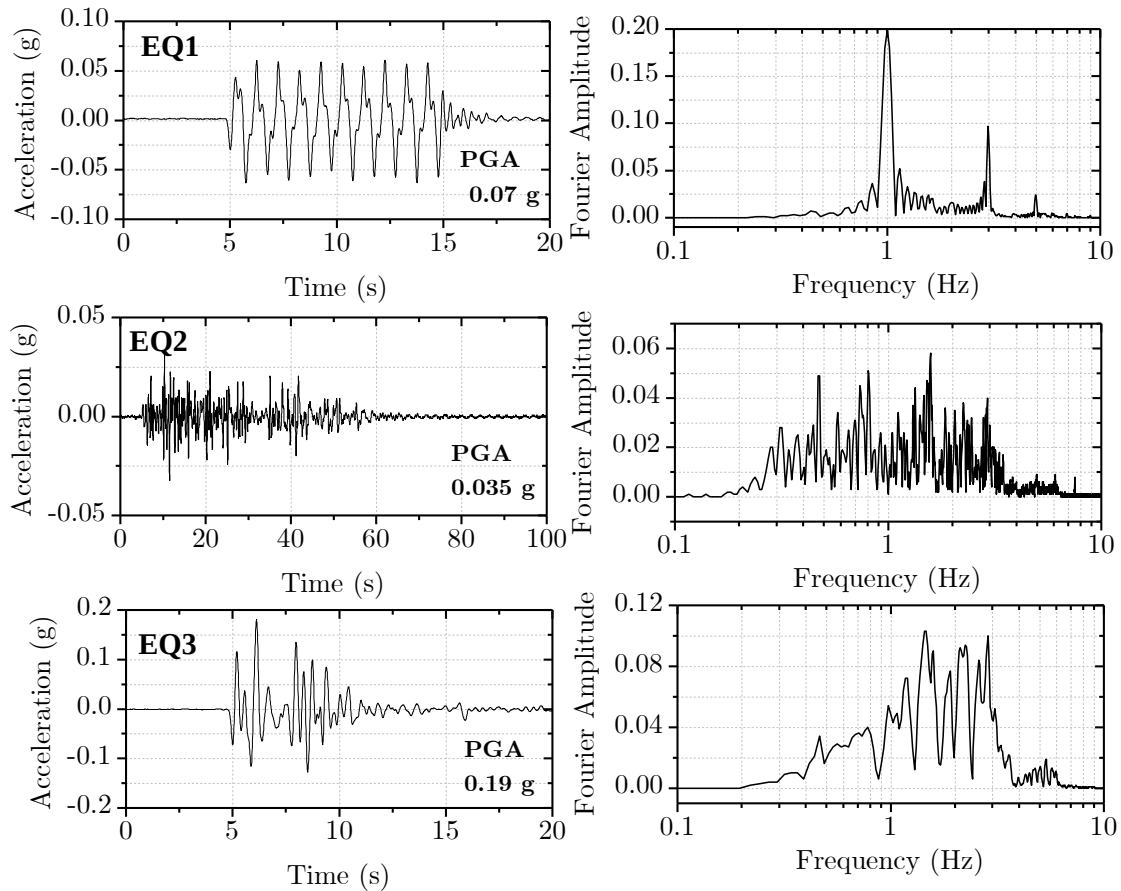
Figure 6.3: Input motions EQ1, EQ2, and EQ3 (accelerometer A9 measurements)

131
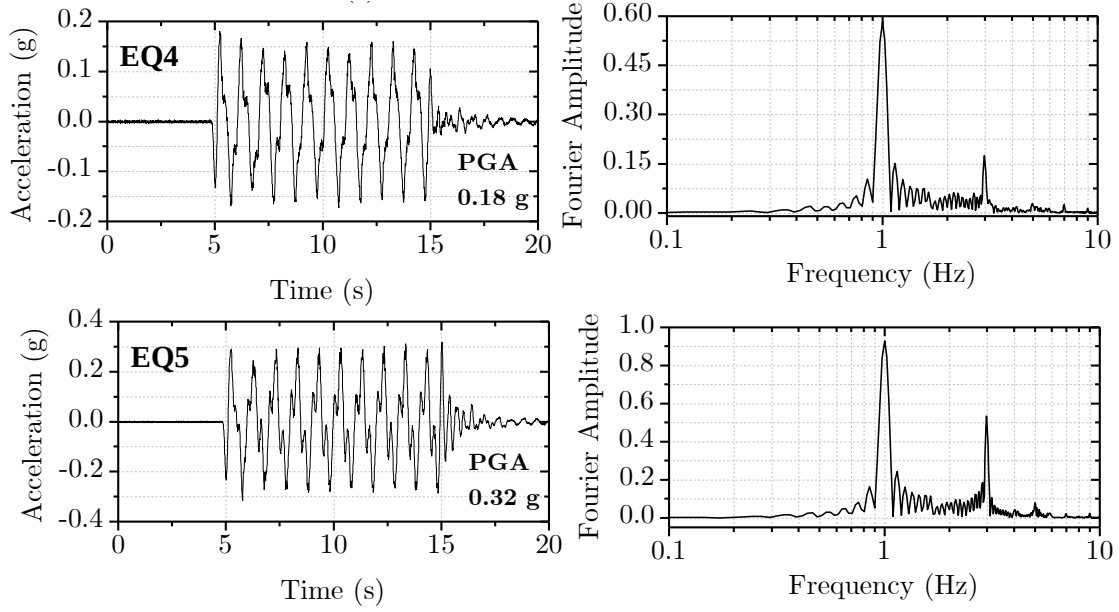
Figure 6.4: Input motions EQ4, and EQ5 (accelerometer A9 measurements)

6.3.3 Soil constitutive model and input parameters

To simulate the dynamic response of the clay inside the laminar box, an accurate constitutive model is required. In this analysis the soil constitutive model for the clay is the *PressureIndependentMultiYield* (PIMY) (Mazzoni *et al.*, 2005). The PIMY model is an elasto-plastic model. The volumetric strain is linear elastic. The model exhibits plasticity in the deviatoric stress-strain response and is not sensitive to confinement (for example, the undrained behavior of clays). The PIMY material model utilizes nested yield surfaces that allows the control of the plastic modulus, then they can be adjusted to comply with a specified backbone curve (Figure 6.5).
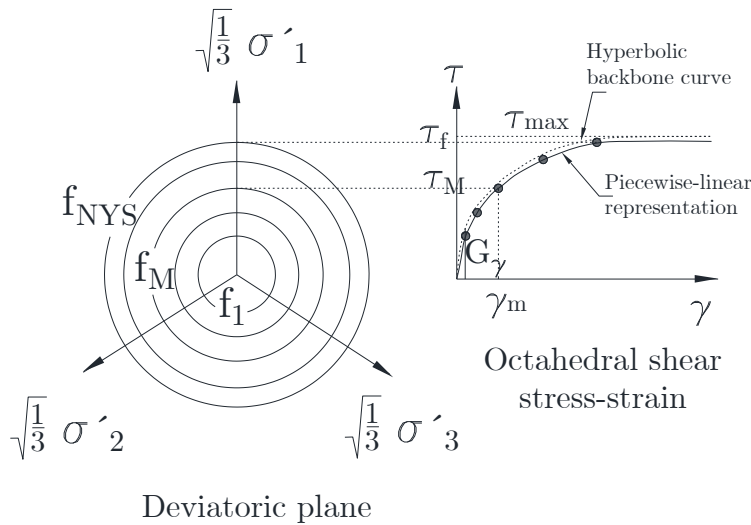
Figure 6.5: Hyperbolic backbone curve for nonlinear shear stress-strain response and piecewise-linear representation in multisurface plasticity (Prevost, 1985; Parra, 1996)

132

OpenseesPL, allows the definition of clay materials by two means, User Defined Clay 1 (U-Clay1) and User Defined Clay 2 (U-clay2):

(i) U-Clay1: the nonlinear stress-strain backbone curve can be defined by the user by specifying a G/G_{max} curve. The number of yield surfaces is defined according to the number of datapoints of the modulus curve. Table 6.1 displays the parameters used in the numerical simulations in this chapter.

Table 6.1: Soil parameters for 3-D soil column U-Clay 1, PIMY material model

Model parameters	Value
Saturated mass density (Mg/m^3)	1.8
Reference pressure (kPa)	100
Pressure dependence coefficient	0
Shear wave velocity (m/s)	65-116 *
Peak shear strain	0.1
Friction angle	0
Cohesion or s_u	9.0-27.0 *

* Range of measured values in the model (see Figure 6.6)

(ii) U-clay2: the backbone curve is adjusted according to the number of yield surfaces defined by the user, the peak shear strain, and the undrained shear strength (automatic surface generation). The parameters requested are the mass density, shear wave velocity, Poisson's ratio (0.49 for soft clay), cohesion, peak shear strain, and number of yield surfaces.

For the analyses presented in this chapter, U-clay1 material was utilized as it allows the definition of user-defined backbone curves. Figure 6.6 shows the undrained shear strength and shear wave velocity profiles discretized for the numerical analyses. As discussed in Chapter 4, the shear wave velocity profile required an adjustment as reflected by the measured transfer function that indicated a smaller natural frequency when compared with the initially calculated. Further details are presented in Section 6.4.1 in this chapter. The adjusted profile is presented in Figure 6.6 with the data points of the Air Hammer Test at the time before the application of the earthquakes as reference.
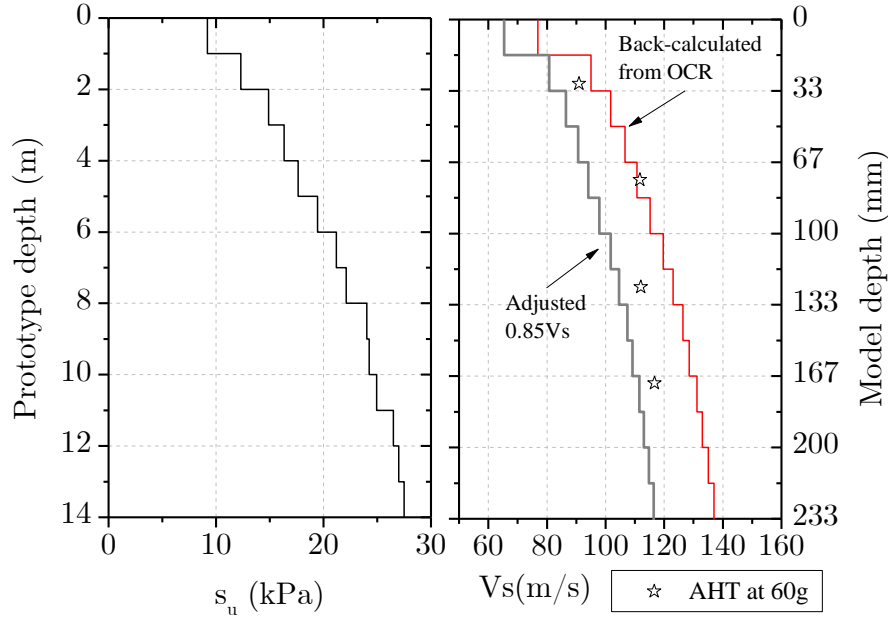
Figure 6.6: Undrained shear strength and shear wave profiles used in the calculations.

Experimental modulus reduction and damping data points were calculated from the measured response of the accelerometers, following the procedure proposed by Zeghal and Elgamal (1994). The data points of the normalized modulus degradation and damping are plotted together with the empirical curves developed by Darendelli (2001) and Vucetic and Dobri (1991) for clays (Figure 6.7). The empirical curves were extended to large strains (10%) by using the General Quadratic Hyperbolic model (GQ/H) (Groholsky *et al.*, 2015) that uses a quadratic equation to satisfy a target shear strength at large strains. The implementation of hysteretic damping is associated with the type of model, particularly by the unload-reload rule. In OpenSees, the PIMY model utilizes Masing´s rules that can lead to high damping values at large strains (Afacan *et al.*, 2019). In the numerical analyses presented in this chapter modifications in the modulus reduction curve were performed to comply with the target undrained shear strength profile and the misfit in hysteretic damping due to the unload-reload rule was accepted. A series of preliminary numerical simulations were performed. In general, the best results in terms of comparisons with the measured horizontal displacements and accelerations were achieved using the Vucetic and Dobri (1991) curve extended to large strains [V&D-GQ/H(PI=33%) as shown in Figure 6.7].
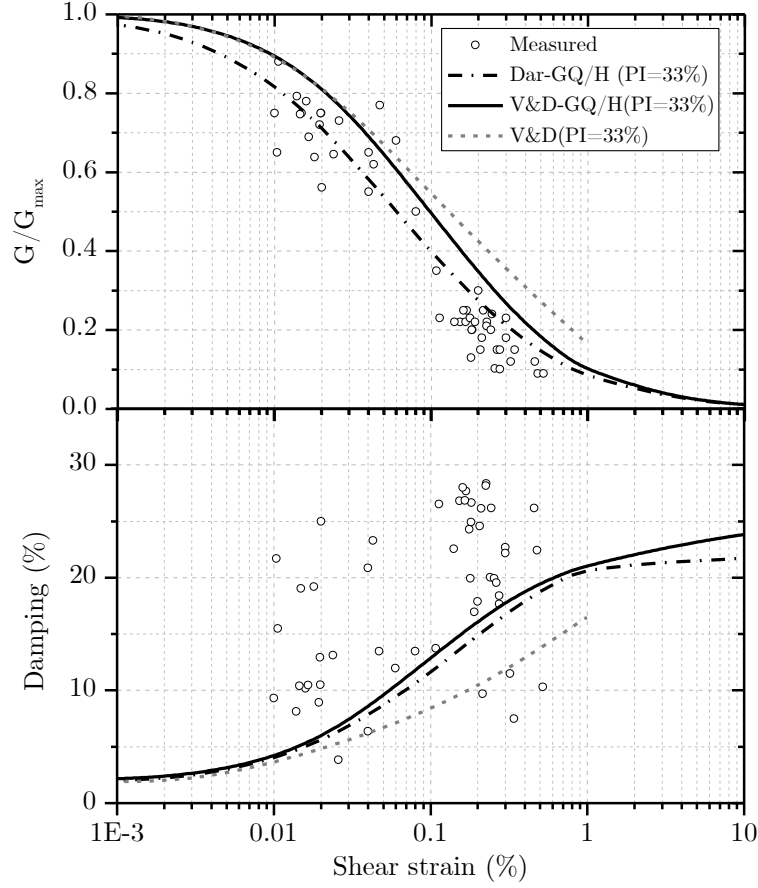
Figure 6.7: Normalized shear modulus and damping data points and empirical curves.

At small cyclic strains, nearly linear behavior can occur, leading to negligible hysteretic damping at these low strain levels. This means that viscous damping has to be added sepparately to consider the small-strain damping observed in soils from laboratory and field studies (Phillips and Hashash, 2009). OpenSees implements the viscous damping (Rayleigh-type damping) assuming that the viscous damping matrix $[C]$ is proportional to the mass matrix $[M]$ and the stiffness matrix $[K]$:

$$[C] = a_0[M] + a_1[K] \tag{6.2}$$

where, a_0 and a_1 are coefficients of Rayleigh damping. The coefficients are frequency dependent and can be expressed in terms of two specific frequencies (ω_m, ω_n) and a corresponding damping ratio (ξ):

$$a_0 = \frac{2\xi\omega_m\omega_n}{\omega_m + \omega_m} \tag{6.3}$$

$$a_1 = \frac{2\xi}{\omega_m + \omega_m} \tag{6.4}$$

In general, for nonlinear seismic ground response analyses ω_n represents the

fundamental frequency of the overall site (Park and Hashash, 2004; Kwok *et al.*, 2007; Phillips and Hashash, 2009). The frequency ω_m can be defined as five times ω_n as suggested by Stewart *et al.* (2008). These criteria were used in the analyses presented in this chapter and a small strain damping ratio (ξ) was set to 5% based on resonant column test results on Speswhite kaolin (Fernandes, 2018; Tarazona, 2019).

6.4 Model validation

The performance of the numerical models was evaluated in terms of the accelerations and horizontal displacements as they were measured in the centrifuge test. Additional analyses were conducted by means of comparisons of spectral accelerations and transfer functions for the lowest amplitude input motion as explained in the following subsection.

6.4.1 Preliminary numerical simulations

An initial numerical model was developed employing the Vs data back-calculated from the OCR profile (red line in Figure 6.6). A comparison of the measured and calculated accelerations was performed using the smallest amplitude input motion, which also had a broad frequency content (EQ2). Further comparisons were performed by means of the 5% damped spectral accelerations at the surface, the amplification ratios and transfer functions calculated from the accelerations at the base and at the surface of the model. Figure 6.8 displays the results of Model 1 using the initial shear wave velocity profile and Model 2, employing an adjusted shear wave velocity profile. The results show that Model 1 presented larger accelerations at the surface (-0.6 m depth) of the slope when compared with the accelerations measured by accelerometer A1 (Figure 6.8a). In addition, it can be observed a shift in the 5% response spectra, in the amplification ratio between the base and the surface (A1 and A9 in Figure 6.8b and 6.8c) and in the calculated transfer function (Figure 6.8d). This means that the shear wave profile required to be adjusted. After several trials, the profile that presented better results was adjusted by reducing 15% of the initial profile (Figure 6.6). The results of this adjusted numerical model (Model 2 in Figure 6.8a to Figure 6.8d) indicated an excellent agreement in terms of the parameters used for comparison: accelerations at the top, 5% response spectra, amplification ratios, and transfer function. From the results of this numerical model, it can be said that the soil characterization from the centrifuge test data can be complemented with the information obtained from the numerical simulations.
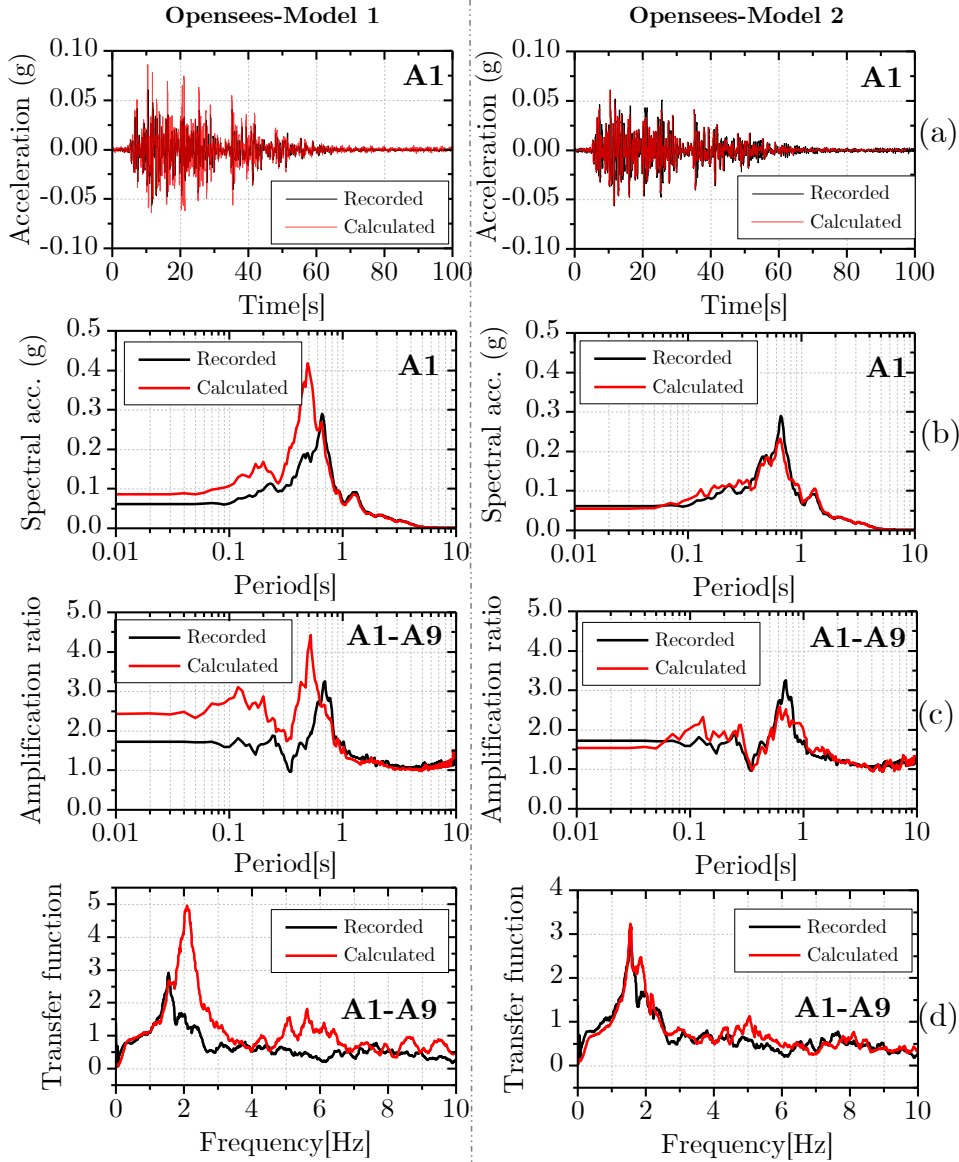
Figure 6.8: Measured and calculated response of the slope: (a) accelerations at model surface (-0.6 m); (b) 5% spectral accelerations at model surface; (c) spectral amplification ratios between the base and the surface of the model; (d) transfer functions between the base and surface of the model.

6.4.2 Displacements

- Sliding block analysis

Preliminary calculations of lateral displacements using Newmark's sliding block analysis (Newmark, 1965) were performed. The method consists of identifying a yielding acceleration, defined as the smallest value of horizontal inertia that would induce slope failure. The yielding acceleration is calculated for a factor of safety of 1.0 against sliding. For the current analyses it is assumed to remain constant during shaking. Figure 6.9 shows a sliding block and the forces that cause downslope slip of a block.
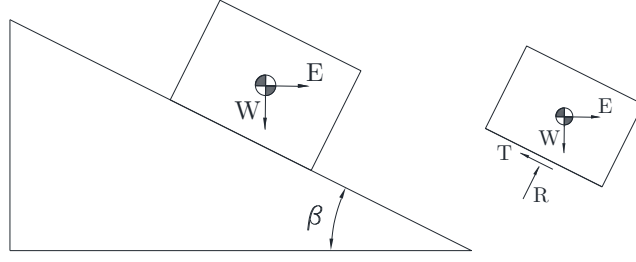
Figure 6.9: Forces for the calculation of the yield acceleration

From Figure 6.9:

$W = mgN$ where W is the weight of the block, m is the mass of the sliding block and N the centrifuge scale factor. $E = ma_y N$ is the inertial force due to acceleration of the block, and β the slope inclination angle.

Finding the value of yield acceleration that will cause downslope slip of the block:

$$F = 1 = \frac{s_u A}{T} \tag{6.5}$$

where,

s_u= undrained shear strength,

A=area of the sliding block

Applying equilibrium parallel to the sliding plane:

$$\sum F_{par} = 0 = mgN sin(\beta) + ma_y N cos(\beta) - T \tag{6.6}$$

$$T = mgN sin(\beta) + ma_y N cos(\beta) \tag{6.7}$$

Solving for a_y:

$$s_u A = T = mgN sin(\beta) + ma_y N cos(\beta) \tag{6.8}$$

$$a_y = \frac{s_u A - mgN sin(\beta)}{mN cos(\beta)} \tag{6.9}$$

For an undrained shear strength s_u of 25 kPa at the base of the slope, a critical acceleration a_y=0.05 g was obtained. Using as input the critical acceleration, assumed constant in the analyses and the consideration of a rigid block, the seismic

displacements for the three degree slope model were calculated as displayed in Figure 6.10 and Figure 6.11. From the results, a reasonable agreement with the recorded displacements at the slope surface can be observed for the low amplitude earthquakes, EQ1 and EQ3. For the larger amplitude earthquakes, EQ3 and EQ4, larger displacements were obtained by Newmark´s method. A similar behavior was observed from the numerical simulations using the monotonic undrained shear strength of the clay as it will be presented below in this section. The results suggest that for the low amplitude earthquakes (EQ1 and EQ3) the assumption of a rigid block gave reasonable results for the prediction of the seismic displacements of the slope. For the large amplitude earthquakes (EQ4 and EQ5), the yielding acceleration employed in the analyses suggest that the earthquakes may produce some hardening of the clay, leading to smaller lateral displacements.
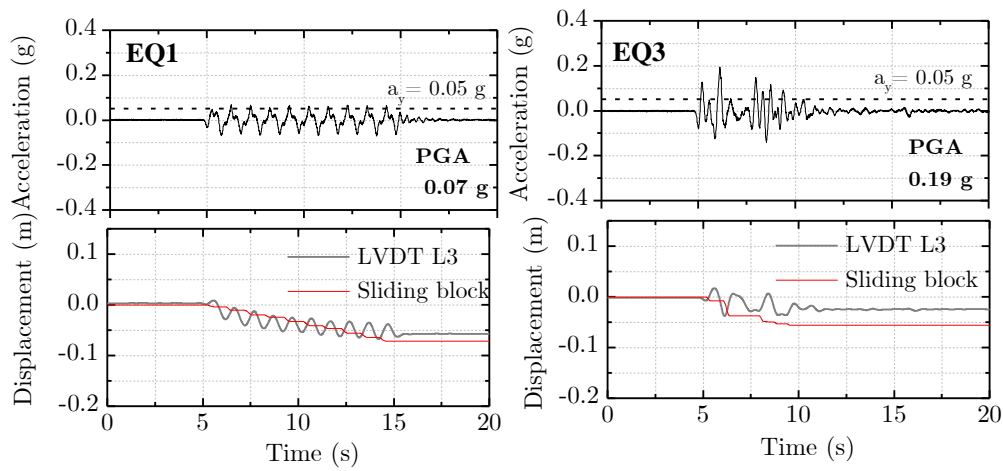
Figure 6.10: Measured and calculated seismic displacements by Newmark´s method for earthquakes EQ1 and EQ3
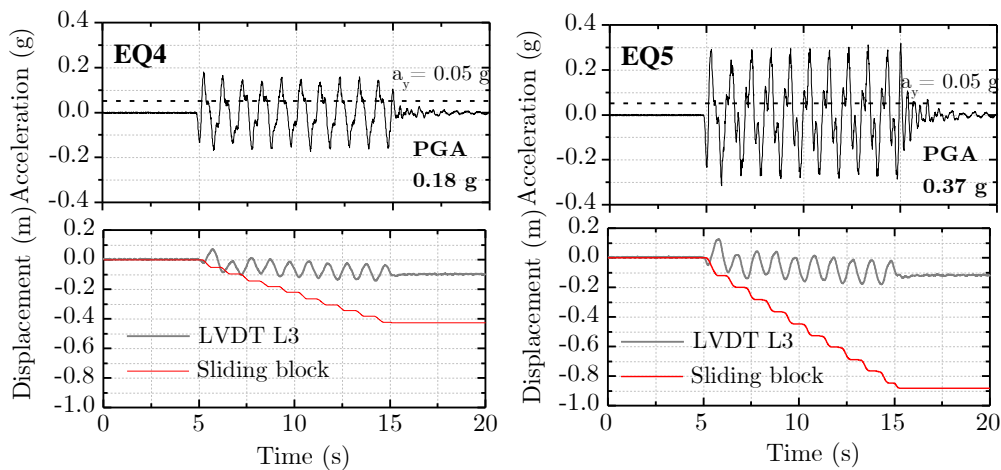
Figure 6.11: Measured and calculated seismic displacements by Newmark´s method for earthquakes EQ4 and EQ5

Using the measured accelerations and corresponding displacements at various depths in the slope, yielding accelerations were back-calculated by applying New-

mark's method. Figure 6.12 shows an schematic of the back calculation of the yielding accelerations to obtain Newmark displacements compatible with the measured values.
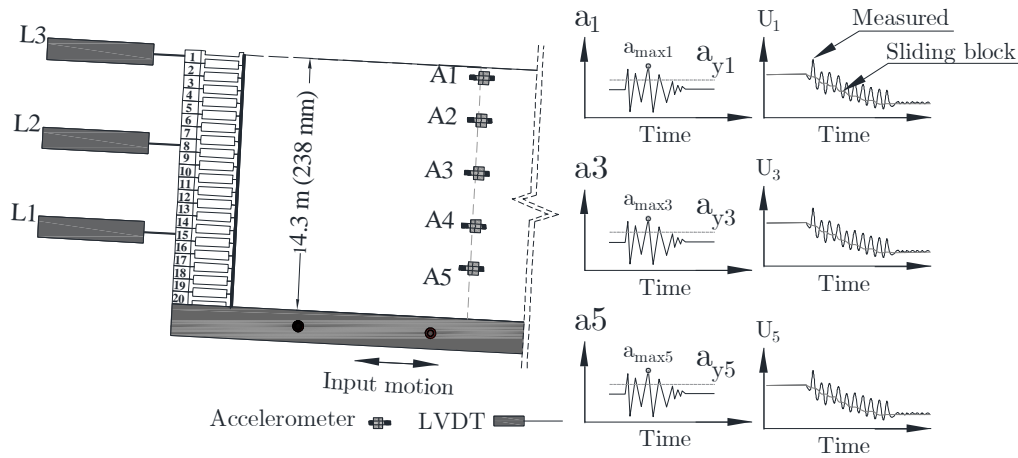
Figure 6.12: Back-calculation of yielding accelerations to obtain measured compatible displacements

Using the Newmark´s method, regression models have been developed for estimating coseismic displacements (Ambraseys and Menu, 1988; Jibson, 1993; Jibson, 2007). The regression models, given its simplicity can be used for preliminary estimation of dynamic slope performance. According to Jibson (2007), the regression models employed for the estimation of Newmark displacements have been developed as a function of: (i) critical acceleration ratio, (ii) critical acceleration ratio and magnitude, and (iii) Arias intensity and critical acceleration ratio. For comparison purposes with the developed regression models and using the available data of the centrifuge experiment, the critical acceleration is employed in this section. The critical acceleration ratio, is defined as the quotient of the critical acceleration (a_y) and the peak acceleration (a_{max}, or PGA) at the corresponding depth of analysis.

Figure 6.13 compares the Newmark displacements obtained for the centrifuge experiment described in this chapter and for comparison the results of the regression models developed by Makdisi and Seed (1978), Ambrasseys and Menu (1988) and Jibson (2007). The results of the centrifuge experiment vary from a lower boundary delimited by the curve of Jibson (2007) to an upper boundary following the curve developed by Makdisi and Seed (1978) for earthquakes with a Magnitude M=7.5. The comparison of the centrifuge test data with the developed regression models suggest that the regression equations should be used carefully and could be employed as a preliminary index of the seismic performance of slopes under seismic loading. For site-specific analyses, rigorous analyses should be conducted.
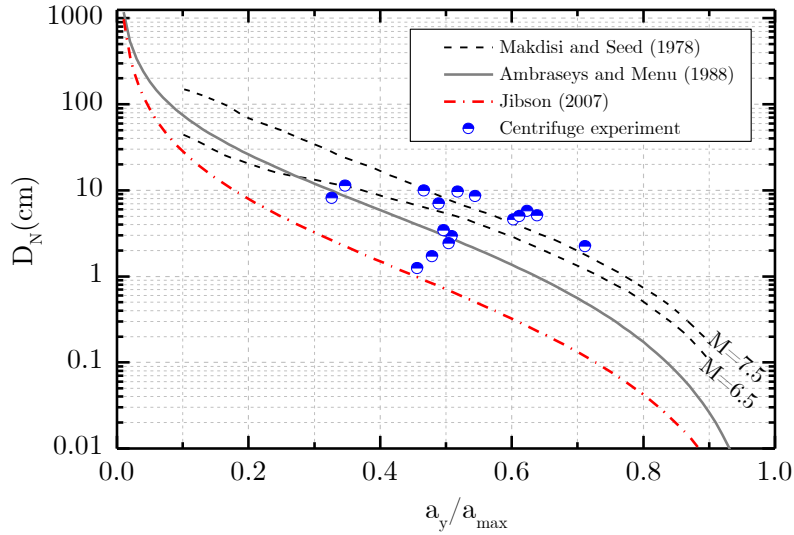
Figure 6.13: Newmark displacements plotted as function of critical acceleration ratio. Results of various studies are shown for comparison.

- Numerical simulation results

As a parameter for the evaluation of the performance of the numerical simulations, lateral displacements were selected. The horizontal displacements were measured by means of LVDTs and PIV, then, an accurate characterization of the displacements was achieved during the centrifuge test. Figure 6.14 to Figure 6.17 display the permanent displacement profiles, defined as the displacements at the end of shaking and the displacement-time histories at two control points (CP.1 and CP.2) at the surface and at mid-depth. Results from EQ2 of lateral relative displacements are not displayed in this section section as no noticeable response was measured considering the low amplitude of this motion. From the profiles and displacement time-histories presented in Figure 6.14 and Figure 6.15, it can be observed a good agreement in the results obtained for earthquakes EQ1 and EQ3. Both models follow the accumulation of displacements in the downslope direction as the shaking occurs.

In contrast, the permanent displacement profiles and relative horizontal displacement time-histories displayed in Figure 6.16 and Figure 6.17 present considerable differences, with larger calculated displacements in both cases. As it will be discussed in the following sections, one approach to satisfy the measured and calculated response could be the consideration of strain rate effects while they produce significant outcomes in increasing the strength and stiffness in clays, particularly in centrifuge testing (Afacan *et al.*, 2019; Sathialingam and Kutter 1989). In addition, the cyclic shear stresses from the earthquakes can cause some hardening of the clay to occur and that may be the reason why the centrifuge

tests are showing smaller lateral movements. For similar testing programs using clay under dynamic loading, it would be useful to perform multiple T-bar tests in flight, an alternative could be the use of actuators that allow the performance of T-bar tests at various locations in the model and if possible between shakings. Other hypothesis that explains the discrepancies of the numerical results could be attributed to limitations of the constitutive model and the numerical modelling approach itself. For future researches the use of more advanced constitutive models is encouraged.

Figure 6.14: Input motion EQ1 recorded and calculated response: (a) permanent lateral displacements; (b) displacement time-histories at two control points.
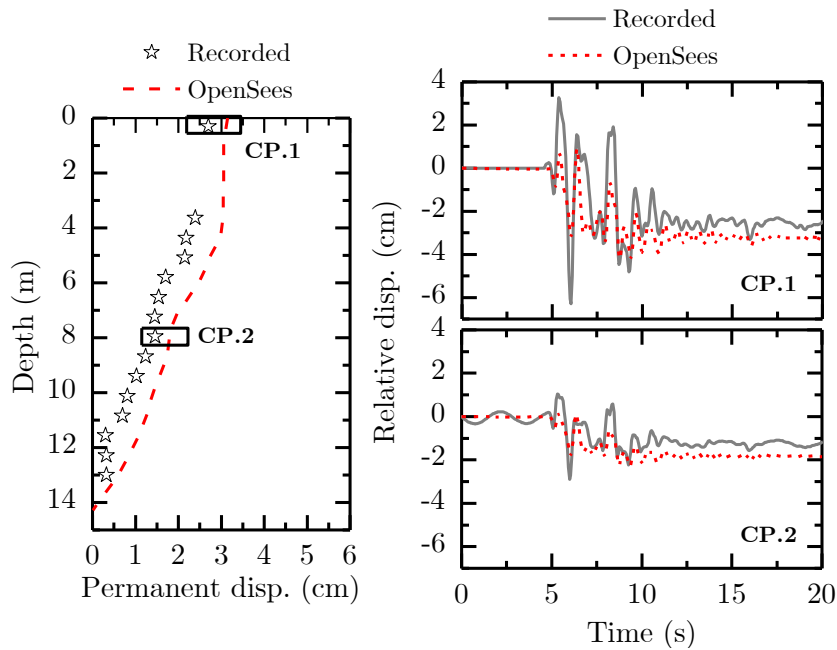
Figure 6.15: Input motion EQ3 recorded and calculated response: (a) permanent lateral displacements; (b) displacement time-histories at two control points.
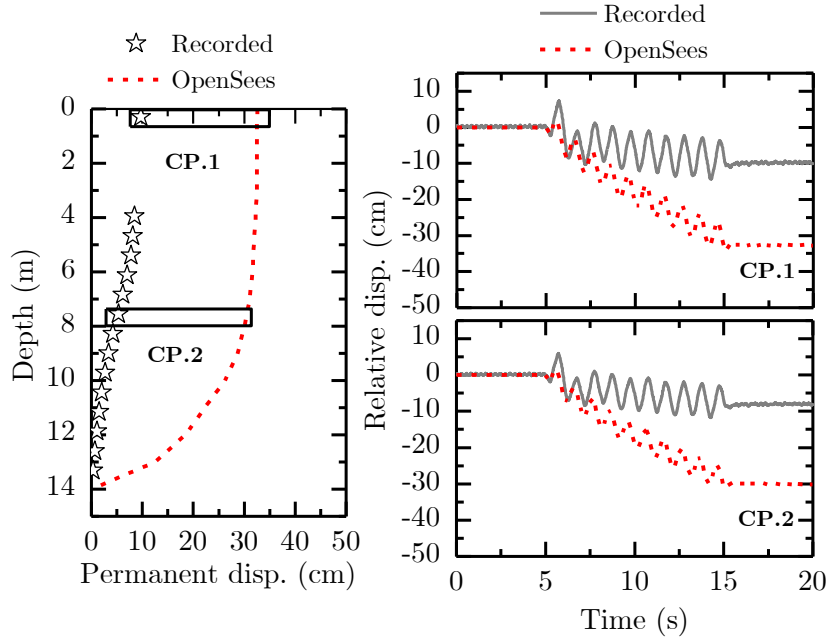
Figure 6.16: Input motion EQ4 recorded and calculated response: (a) permanent lateral displacements; (b) displacement time-histories at two control points.
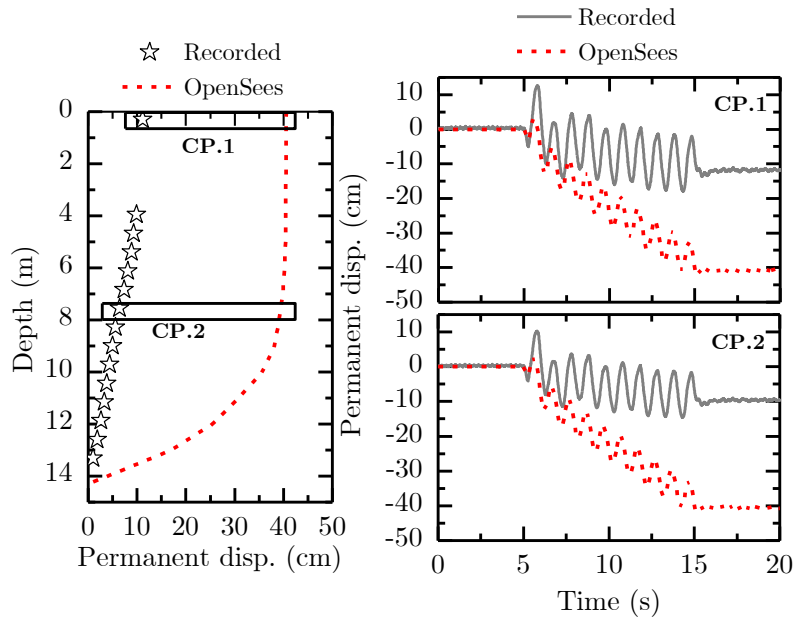
Figure 6.17: Input motion EQ5 recorded and calculated response: (a) permanent lateral displacements; (b) displacement time-histories at two control points.

With the displacement time-histories calculated by the numerical model, an additional comparison was carried out. By double differentiation of the calculated displacements, acceleration time-histories were obtained. Figure 6.18 displays the measured and calculated accelerations at the model surface for the input motions studied. From the results, it can be seen a good match between the accelerations for earthquakes EQ1 and EQ3. For the large amplitude earthquakes, EQ4 and EQ5,

143

larger accelerations were obtained. This trend can also be observed when comparing directly the calculated and measured accelerations and as it will be discussed, the numerical response could be improved by considering corrections to account for strain rate effects.
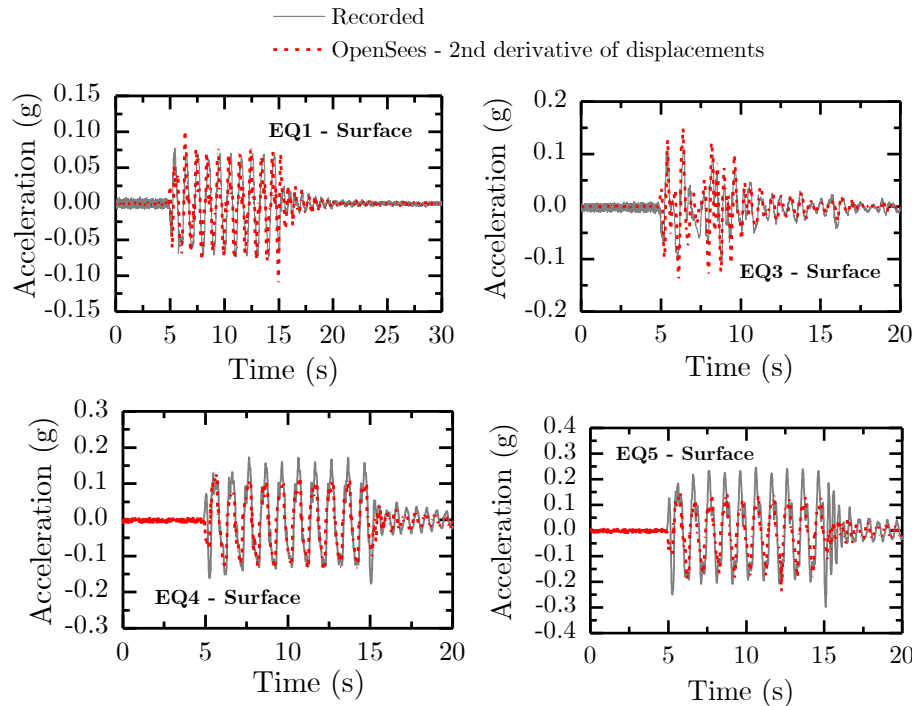
Figure 6.18: Input motion EQ5 recorded and calculated response: (a) permanent lateral displacements; (b) displacement time-histories at two control points.

6.4.3 Acceleration response

Regarding the acceleration response of the measured and calculated data, a first comparison is presented in terms of the Peak Ground Accelerations (PGA) with depth (Figure 6.19). It can be observed a good agreement between the calculated and measured PGA values for earthquakes EQ1, EQ2, and EQ3. However, for earthquakes EQ4 and EQ5, the numerical models seem to overestimate the response of the slope. The calculated and recorded acceleration time-histories and response spectra at the depths of the accelerometers installed in the slope (Accelerometers A1 to A5 in Figure 6.1) for the earthquakes EQ1, EQ3, EQ4, and EQ5 are shown in Figure 6.20 to Figure 6.23. A satisfactory agreement between the recorded and calculated acceleration time histories was achieved for earthquakes EQ1 and EQ3. For earthquakes EQ4 and EQ5, the simulation overestimated the soil accelerations as shown also in the PGA profiles. From the results, the numerical model under the conditions defined seems to perform well for earthquakes EQ1, EQ2, and EQ3. This means that better simulations could be achieved by using more advanced soil constitutive models and high-fidelity numerical simulations. One alternative is the

SANICLAY model (Dafalias *et al.*, 2006), a model aimed for simulating undrained and drained rate-independent behavior of normally consolidated clays and uses well estabilished parameters from the Modified Cam Clay model. A second alternative of constitutive models is the PM4Silt (Boulanger and Ziotopoulou, 2019), developed for representing low-plasticity silts and clays in geotechnical earthquake applications. Finally, for further research, 2D simulations of the problem studied in this thesis is also recommended.
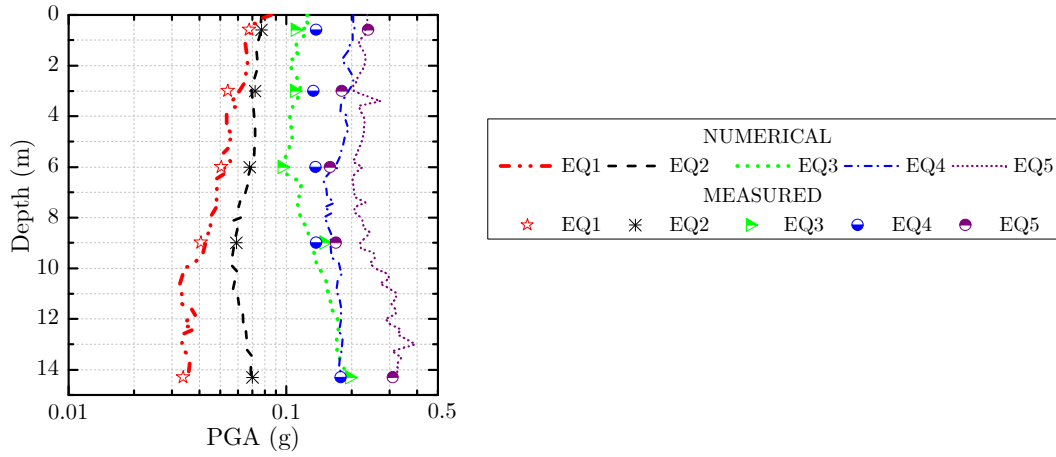
Figure 6.19: Depth profiles of peak acceleration for all shaking events.
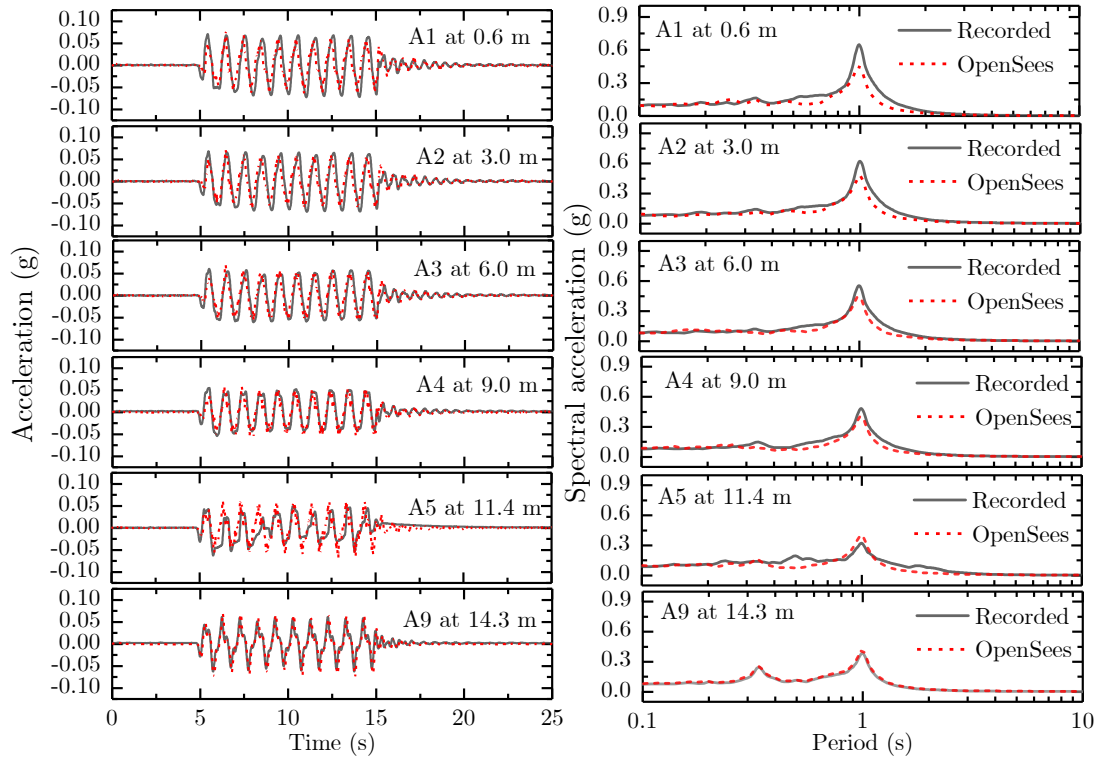
Figure 6.20: Comparison between the centrifuge test and simulation for EQ1: acceleration time-histories and acceleration response spectra.
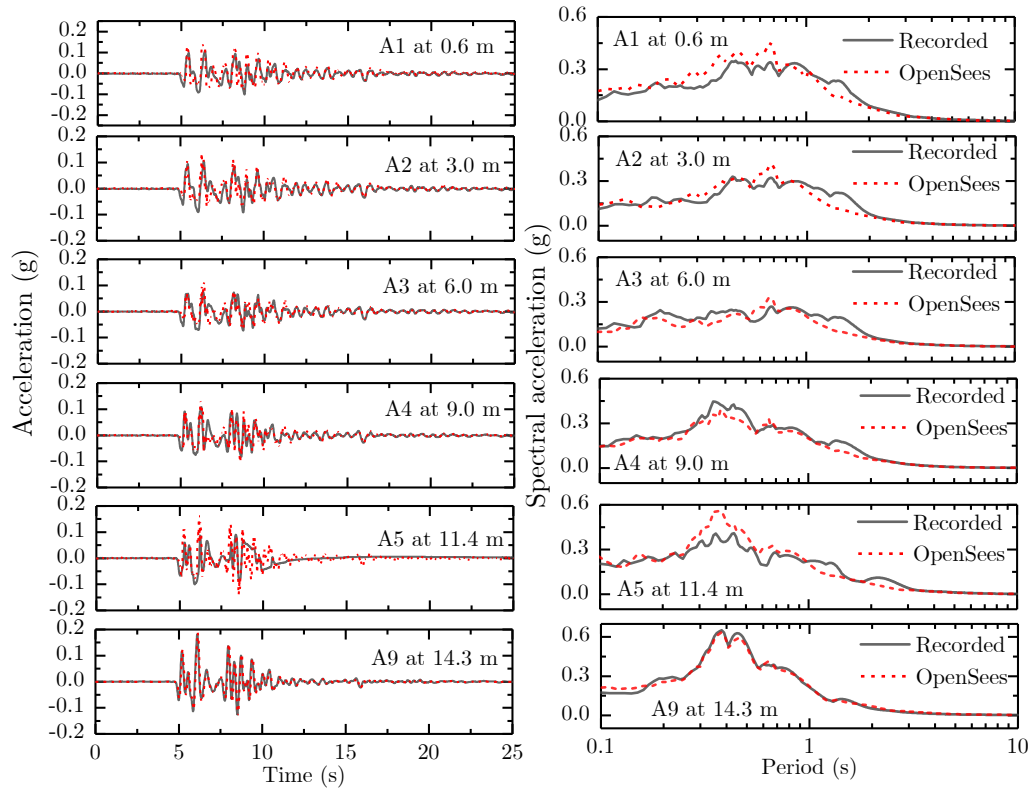
Figure 6.21: Comparison between the centrifuge test and simulation for EQ3: acceleration time-histories and acceleration response spectra.
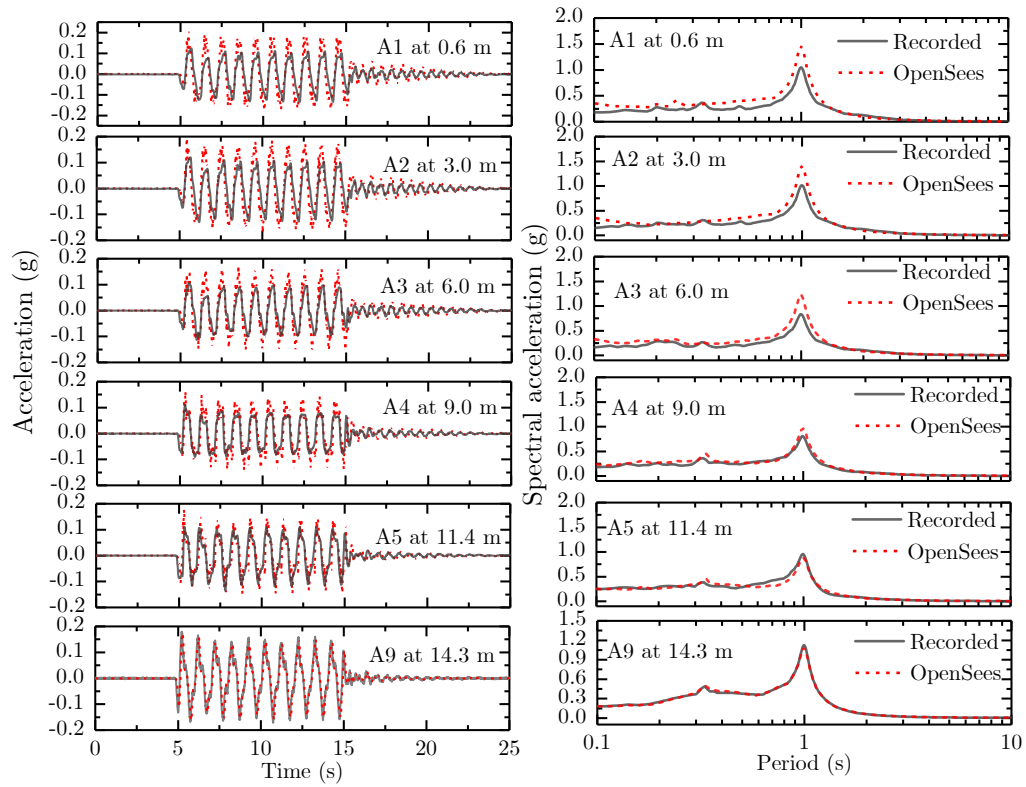
Figure 6.22: Comparison between the centrifuge test and simulation for EQ4: acceleration time-histories and acceleration response spectra.

146
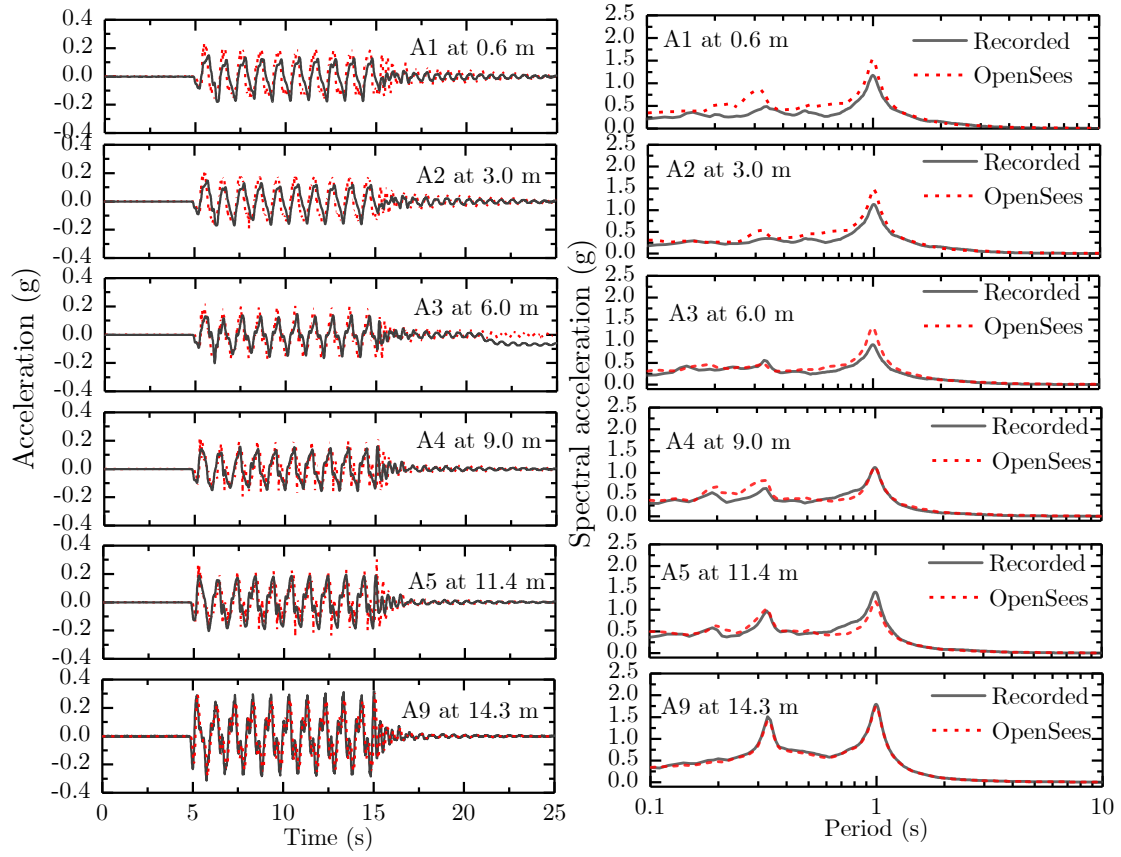
Figure 6.23: Comparison between the centrifuge test and simulation for EQ5: acceleration time-histories and acceleration response spectra.

6.4.4 Correction of shear strength for strain rate effects

As discussed in Chapter 2, the shear strength of the clay is dependent on the strain rate. As discussed by Afacan, 2014, a site response modelling focuses on two fundamental issues:

1) Proper modeling of shear strength, and
2) Correction of shear strength to account for strain rate effects.

To assess the strain rate effects the first stage consisted of the calculation of the strain rates. From the displacements calculated by means of PIV, shear strains and strain rates were calculated in terms of model and prototype scale. Figure 6.24 presents a schematic illustration of the slope profile and the markers used for strain computations.

147
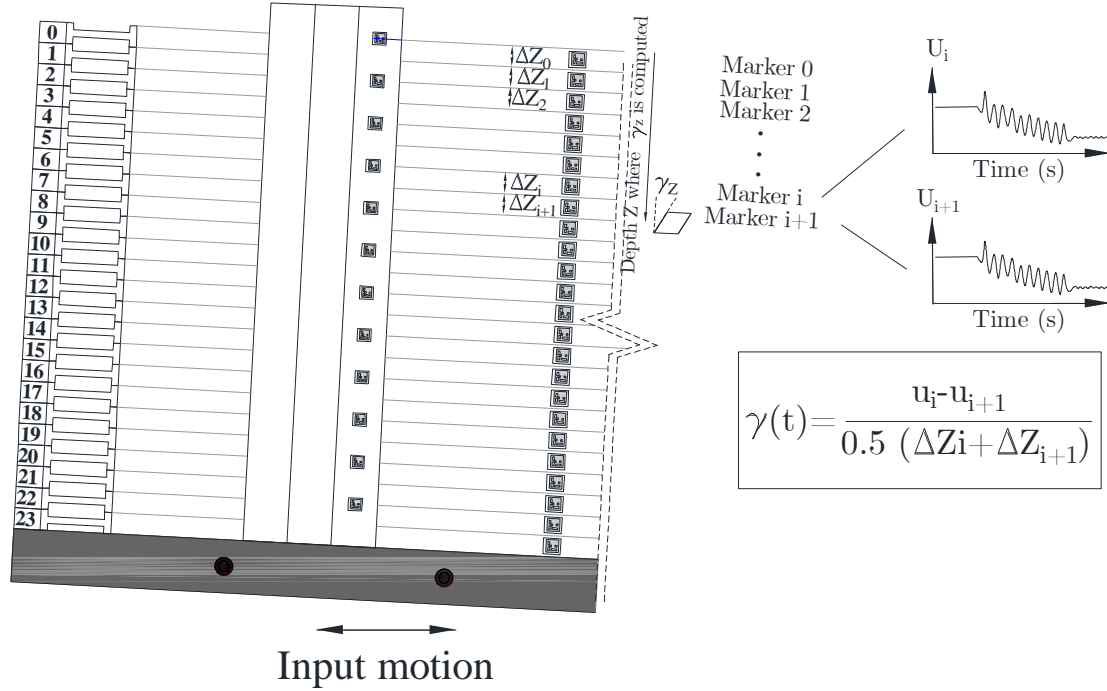
Figure 6.24: Schematic illustration of the slope and the markers used for strain computations.

The PIV measurements covered a range of depths between 4 m and 13 m (protoype scale) or 66 mm and 216 mm (model scale), the strain rates were calculated between pairs of markers as indicated Figure 6.24. The largest shear strain time-histories and shear strain rate time-histories in the range of depths assessed were obtained at 7.2 m depth (prototype scale) or at 120 mm (model scale) for the applied earthquakes. For brevity, the largest strain and strain rate results are shown in Figure 6.25 to Figure 6.28. The results are in model and prototype scale.

The strain rates for the centrifuge test described in this chapter vary from 150 %/s for earthquake EQ1 to 1000%/s for earthquake EQ5, this range agrees with the strain rates reported by Sathialingam and Kutter 1989 for dynamic centrifuge testing. In terms of prototype scale, the strain rates vary from 2.5 %/s to 16.7%/s, meaning that strain rates in the model are N times the strain rates in the prototype. This evidence one of the limitations of geotechnical centrifuge modeling, its inability to satisfy the requirement of both the inertial and strain rate scaling (Taylor, 1995).
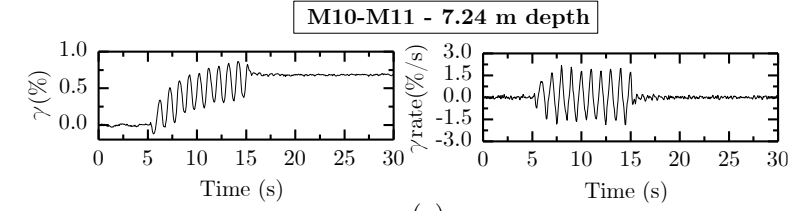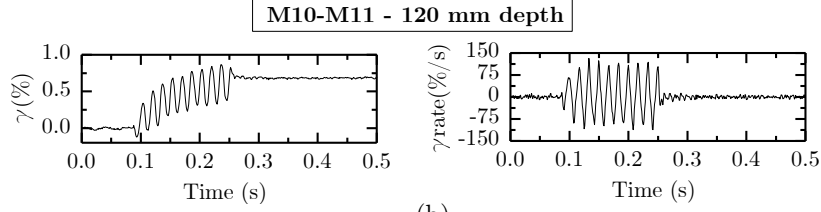
Figure 6.25: Strain-time and strain rate-time histories for earthquake EQ1. (a) Prototype scale; (b)Model scale.
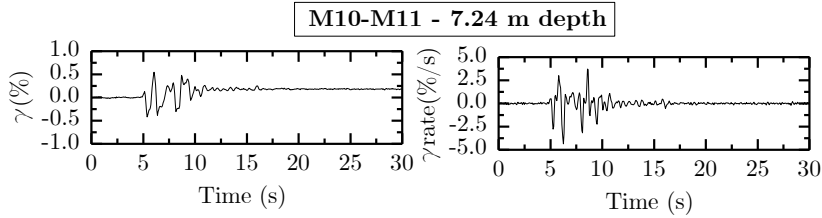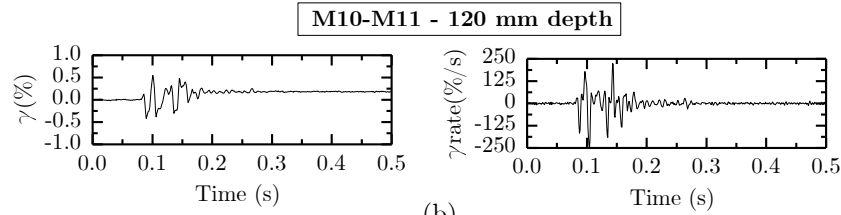
Figure 6.26: Strain-time and strain rate-time histories for earthquake EQ3. (a) Prototype scale; (b)Model scale.
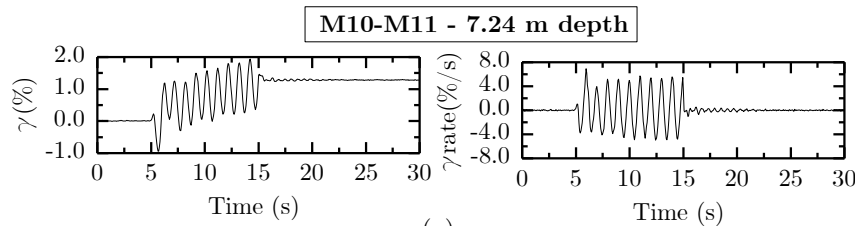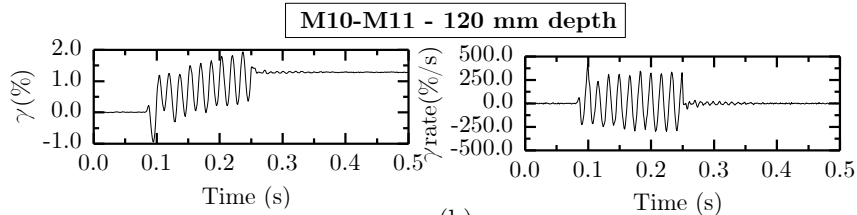
Figure 6.27: Strain-time and strain rate-time histories for earthquake EQ4. (a) Prototype scale; (b)Model scale.
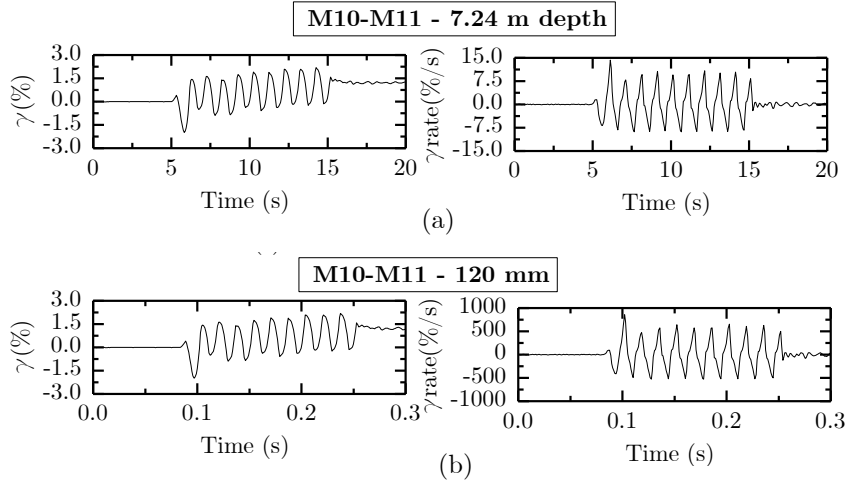
Figure 6.28: Strain-time and strain rate-time histories for earthquake EQ5. (a) Prototype scale; (b)Model scale.

According to the results presented in previous sections in this chapter, the numerical model performed well for the low amplitude earthquakes (EQ1, EQ2, and EQ3). However, for the large-amplitide earthquakes studied here (EQ4 and EQ5), discrepancies between the measured and calculated response were observed, particularly in terms of lateral displacements. Then, for the first group of earthquakes (EQ1, EQ2, and EQ3) it seems that no strain rate corrections were required to properly model the dynamic response of the slope. To account for the strain rate effects, for the large-amplitude earthquakes, for earthquakes EQ4 and EQ5 the undrained shear strength profiles were multiplied by a constant factor aiming to increase the strength of the clay. Using as reference the 10% increase per log cycle line presented in Figure 6.18, an initial factor of 1.5 (or 50% increase) was applied to the undrained shear strength profile for the numerical models subjected to earthquakes EQ4 and EQ5. After several trials, it was found that the factor of 1.4 applied to the initial undrained shear strength profile yielded better results for the simulation of earthquakes EQ4 and EQ5. Then, it can be said that the clay does not have a specific dynamic strength, it has a strength dependent on the earthquake shaking, therefore, it would be consistent to use different strengths depending on the ground motion. Figure 6.29 presents the s_u profiles, consisting of the monotonic profile and the profile with a strength increase to account for strain rate effects. The backbone curve of one layer is also shown as an example of the methodology employed for the correction of the strength and the modulus curves are also displayed.
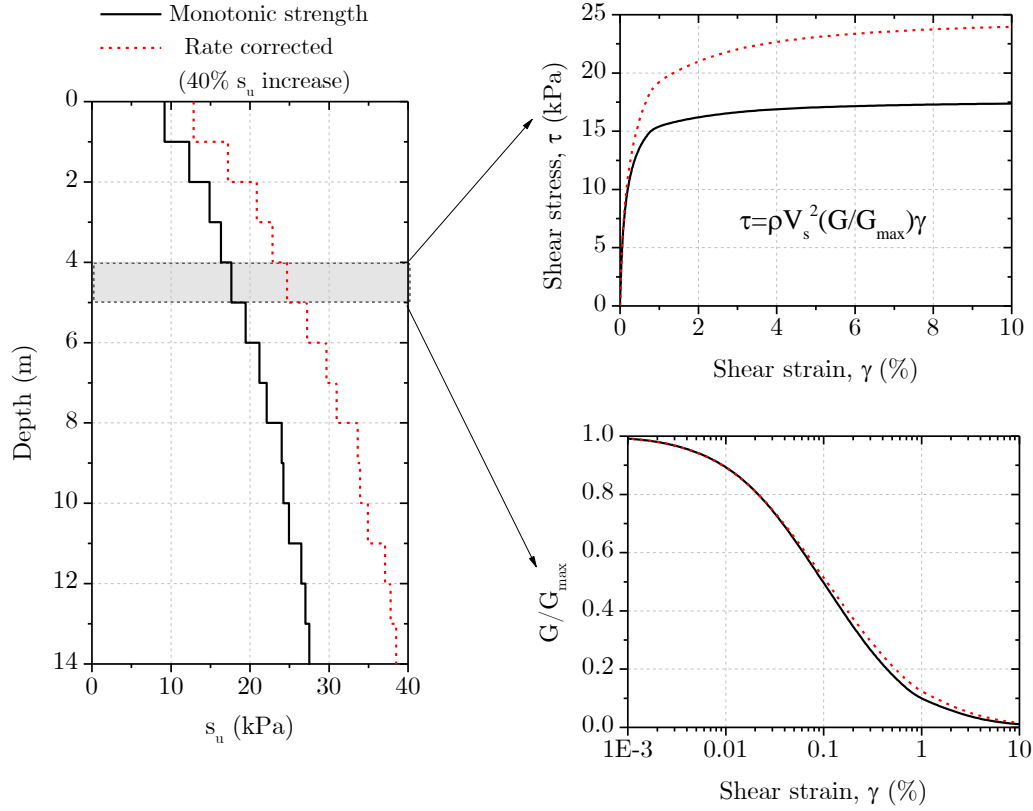
Figure 6.29: Shear strength profiles, and curve fitting example to obtain a target shear strength.

Figure 6.30 and Figure 6.31 present the permanent displacement profiles and displacement time-histories for models in which earthquakes EQ4 and EQ5 were applied. The results show that a poor agreement was achieved between the calculated and measured lateral displacements when using the monotonic undrained shear strength profile, evidencing a limitation of the current numerical approach for the large amplitude input motions (EQ4 and EQ5). Increasing the undrained shear strength by applying strain rate correction improved the response of the model when compared the calculated and measured permanent displacements. However further research is needed to quantify strain rate effects in centrifuge experiments and include them in constitutive modelling.
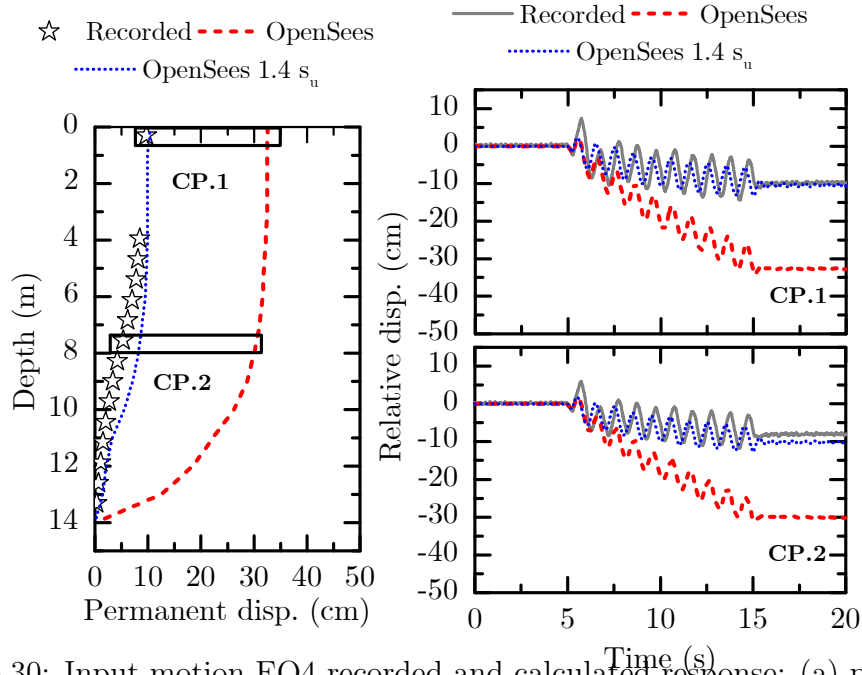
Figure 6.30: Input motion EQ4 recorded and calculated response: (a) permanent lateral displacements; (b) displacement-time histories at two control points.
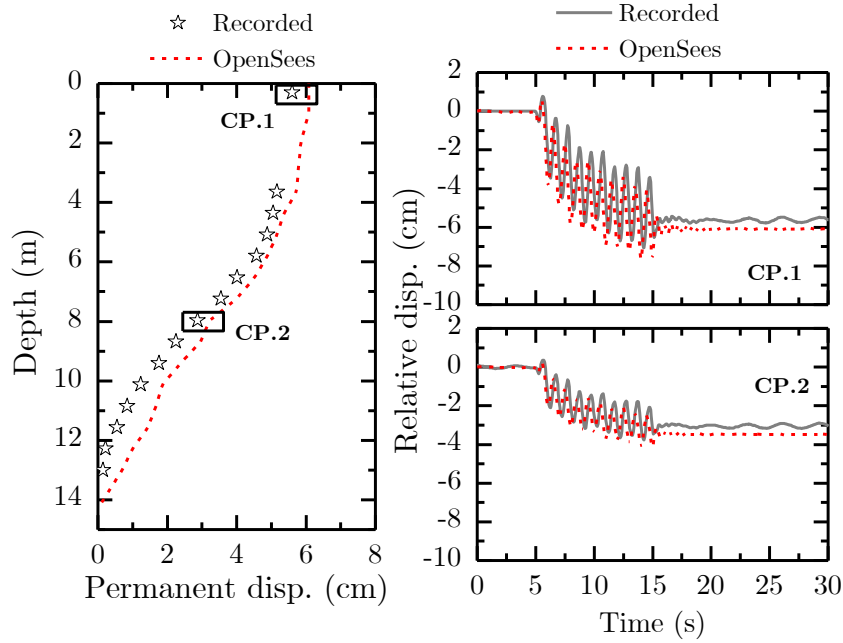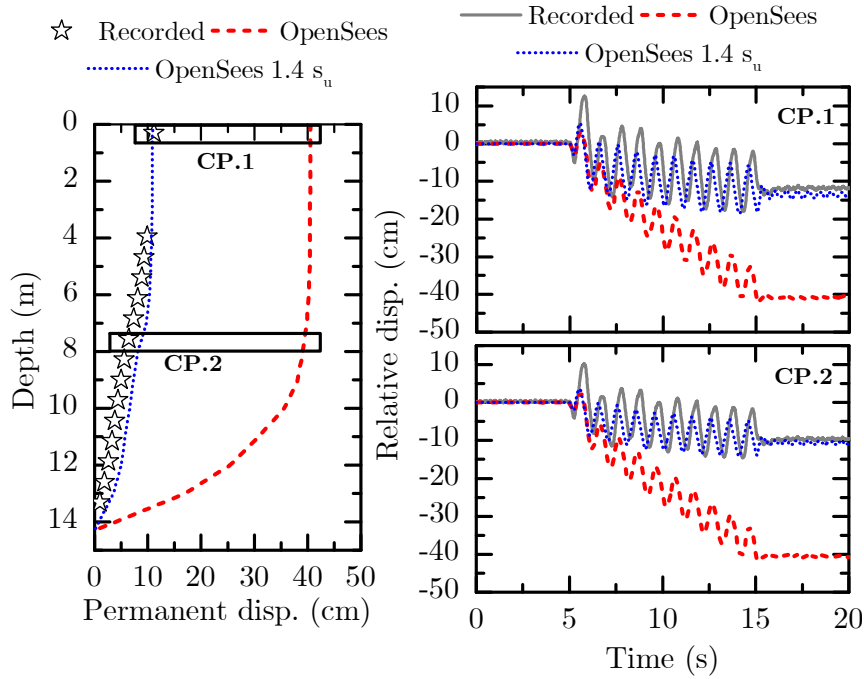

Figure 6.31: Input motion EQ5 recorded and calculated response: (a) permanent lateral displacements; (b) displacement-time histories at two control points.

Regarding the acceleration time-histories and spectral response, the results of the adjusted models are consistent with the recorded data (Figure 6.32 and Figure 6.33). The acceleration time-histories and 5% damped spectral accelerations obtained by the previous model are also displayed. From the results, it can be concluded that the response of the model in terms of the propagation of the accelerations throughout the slope was also properly simulated after the adjustments made in the undrained

shear strength profiles.
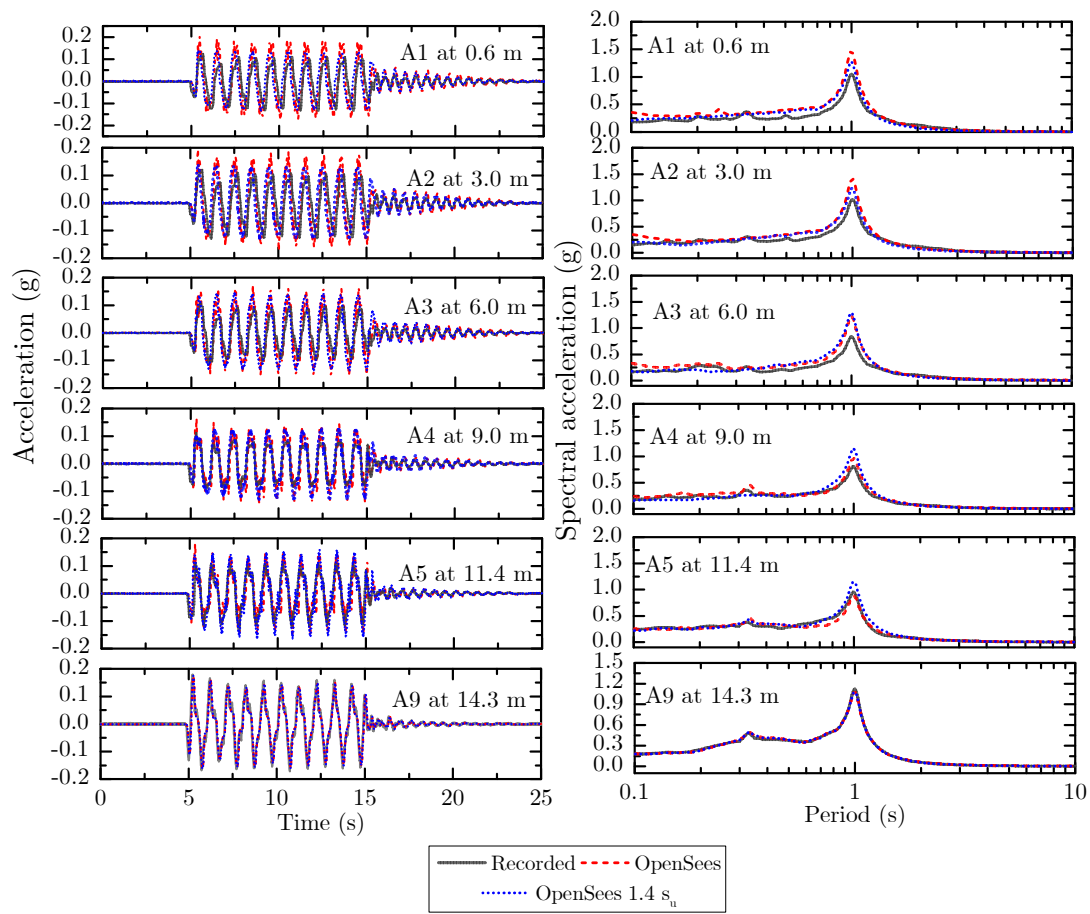
Figure 6.32: Comparison between the centrifuge test and simulation for EQ4: acceleration-time histories and acceleration response spectra.

153
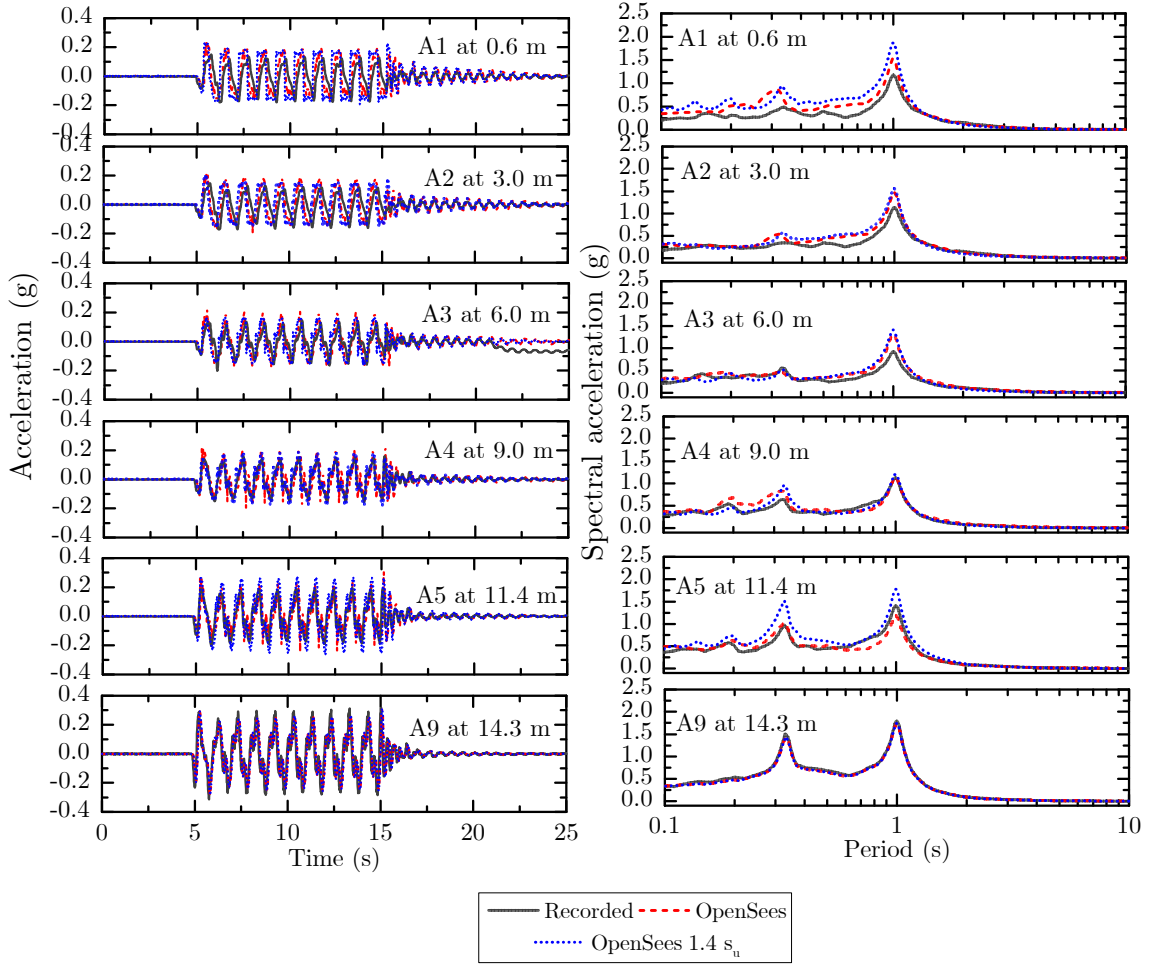
Figure 6.33: Comparison between the centrifuge test and simulation for EQ5: acceleration-time histories and acceleration response spectra.

As the adjustment presented here consisted of applying a scale factor to the undrained shear strength profile, for future researches it is encouraged the application of models that include the strain-rate dependent strength behavior of the clays. For example, the model of Zhu and Randolph (2011) in which the strain-dependent undrained shear strength s_u is expressed as:

$$s_u = s_{u0} \left[1 + \eta \left(\frac{\dot{\gamma}}{\dot{\gamma}_{ref}} \right)^{\beta} \right] = \frac{s_{u,ref}}{(1 + \eta)} \left[1 + \eta \left(\frac{\dot{\gamma}}{\dot{\gamma}_{ref}} \right)^{\beta} \right] \qquad (6.10)$$

where, $\dot{\gamma}_{ref}$ is the reference shear strain rate at which the reference shear strength $s_{u,ref}$ is taken; s_{u0} is the minimum undrained shear strength at zero strain rate; η and β are two parameters identified as viscous property and power law index, respectively.

6.5 Influence of slope angle on the permanent displacements of gentle slopes in clay

Additional numerical simulations were performed to assess the performance of the presented numerical analysis methodology. The output of the numerical models was compared in terms of the displacement time-histories and permanent displacements at the surface. As previously discussed, for the models in which earthquakes EQ1 and EQ3 were applied, the monotonic undrained shear strength was used, then, no strain rate correction was applied, as their performance was adequate for these low amplitude ground motions. For earthquakes EQ4 and EQ5, the strain rate correction, applying a factor equal to 1.4 times the monotonic undrained shear strength profile was considered in the numerical simulations.

Figure 6.34 displays the displacement-time histories for the input motions applied to the validation of numerical model for the slope inclinations, ranging from a flat condition (zero degrees) to six degrees (for comparison with the centrifuge test presented in Chapter 4). The results evidence the effect of the ground inclination on the development and accumulation of lateral displacements in the slope, even by very few degrees. The responses follow a similar trend as presented in Chapter 4 from measured displacements of slopes with three-degrees and six-degrees inclinations.
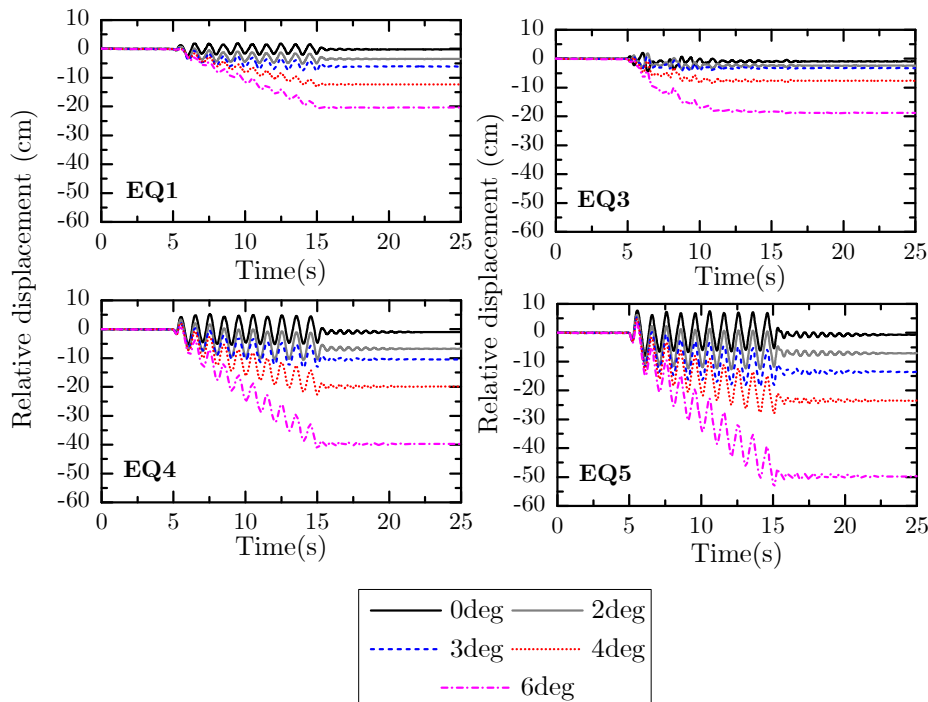
Figure 6.34: Comparison of predicted displacement time-histories for different slope angles.

The results of the comparative response of the models in terms of permanent displacements at the surface are presented in Figure 6.35. The results show a good agreement with the measured values obtained from the three degrees and six degrees experiments (range of measured displacements in Figure 6.35), described in Chapter 4. This means that the numerical modelling approach adopted was able to predict the response of the six-degrees centrifuge test using as baseline the three-degrees calibrated numerical model.
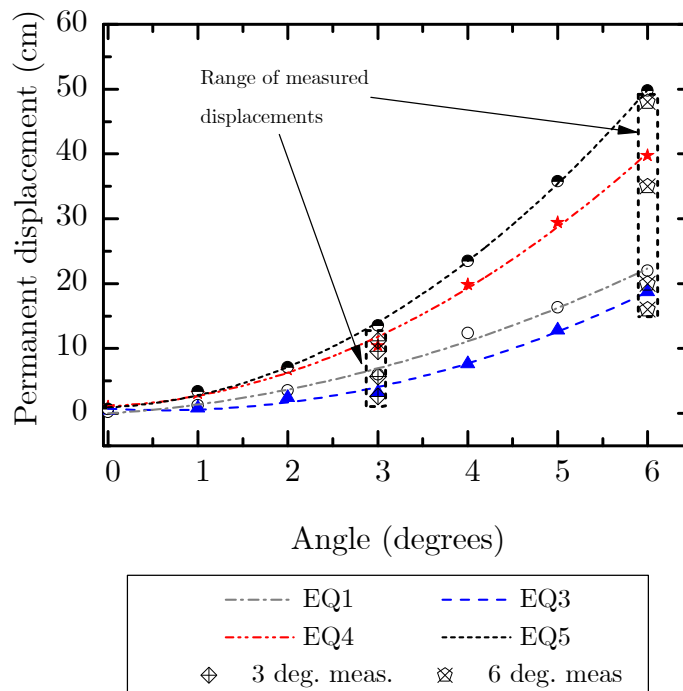
Figure 6.35: Comparison of permanent displacements at the surface for different slope angles.

6.6 Final remarks

Different numerical models were applied to simulate the response of a 3-degree infinite slope. The numerical analyses considered a three-dimensional soil column built on the OpenSees platform. The numerical modeling results were consistent with the experimental results in terms of the accelerations and displacements for the low-amplitude earthquakes (EQ1, EQ2 and EQ3). For the larger amplitude earthquakes (EQ4 and EQ5), additional considerations related to strain rate effects had to be included. In a simplified manner, scale factors were applied to the undrained shear strength profile. This strain rate correction imply that the clay does not exhibit a particular dynamic strength. Instead, its strength depends on the earthquake shaking level. Future research works should implement constitutive

models that include strain rate effects or the possibility to perform numerical simulations at model scale under an increased gravity level to simulate the in-flight strain rates and compare the modeling approaches.

Considering strain rate effects, the modified models for earthquakes EQ4 and EQ5 delivered a better response after the strength increase. To conclude the numerical modeling methodology applied in this chapter, a simplified parametric analysis was performed by varying the slope angle. The slope inclination angles covered in the complementary numerical analyses range from 0 degrees (level ground) to 6 degrees. The calculations of the permanent displacements at the surface are in good agreement with the range of measurements from the 3-degree slope and 6-degree slope. Therefore, the numerical models predicted well the measured displacements.

6.7   Chapter 6 references

AFACAN, K., 2014, "Evaluation of Nonlinear Site Response of Soft Clay Using Centrifuge Models," PhD dissertation, University of California, Los Angeles, USA.

AFACAN, K., YNIESTA, S, SHAFIEE, A., STEWART, J., AND BRANDEN-BERG, S, 2019, "Total Stress Analysis of Soft Clay Ground Response in Centrifuge Models," Journal of Geotechnical and Geoenvironmental Engineering. Vol.145, No.10.

AMBRASEYS, N.N., AND MENU, J.M., 1988, "Earthquake-induced ground displacements," Earthquake Engineering and Structural Dynamics, Vol.16, pp.985-1006.

BOULANGER, R. W., AND ZIOTOPOULOU, K., 2019, "A constitutive model for clays and plastic silts in plane-strain earthquake engineering applications." Soil Dynamics and Earthquake Engineering, Vol.127.

DAFALIAS, Y.F., MANZARI, M.T. AND PAPADIMITRIOU, A.G. ,2006, "SANICLAY: simple anisotropic clay plasticity model," Int. J. Numer. Anal. Meth. Geomech., Vol.30, pp.1231-1257.

DARENDELI, M. B., 2001, Development of a New Family of Normalized Modulus Reduction and Material Damping Curves. Ph.D. thesis, University of Texas, Austin, TX, US

ELGAMAL, A., AND YANG, Z., 2011, "OpenSeesPL: 3D Lateral Pile-Ground Interation User Manual (Beta 1.0)," University of California, San Diego. Department of Structural Engineering.

FERNANDES, F. C., 2018, Ensaios de Coluna Ressonante e de Bender Elements para Medidas de Módulos Cisalhantes em Caulim. MSc. thesis, COPPE-UFRJ, Rio de Janeiro, RJ, BR

GROHOLSKI, D.R., HASHASH, Y.M.A., MUSGROVE, M., HARMON, J., AND KIM, B., 2015, "Evaluation of 1-D non-linear site response analysis using a general quadratic/hyperbolic strength controlled constitutive model," 6th International Conference on Earthquake Geotechnical Engineering, 1–4 November 2015, Christchurch, New Zealand.

JIBSON, R.W., 1993, " Predicting earthquake-induced landslide displacements using Newmark´s sliding block analysis." Transportation Research Record, Vol.1411, pp.9-17.

JIBSON, R.W., 2007, "Regression models for estimating coseismic landslide displacement," Engineering Geology, Vol.91, pp.209-2018.

JOYNER, W.B. AND CHEN, A.T.F., 1975, "Calculation of nonlinear ground response in earthquakes," Bulletin of the Seismological Society of America, Vol.65, No.5, pp.1315-1336.

KONDNER, R. L., 1963, "Hyperbolic stress-strain response: Cohesive soils." Journal of the Soil Mechanics and Foundations Division, Vol.89(SM1), pp.115-143.

KUHLEMEYER, R. AND LYSMER, J., 1973, "Finite element method accuracy for wave propagation Problems," Journal of Soil Mechanics and Foundation Division, ASCE, Vol.95(SM5).

KUTTER, B. L.,1982, "Centrifugal Modeling of the Response of Clay Embankments to Earthquakes," Ph.D Thesis, Cambridge University, England.

KWOK A, STEWART J, HASHASH Y, MATASOVIC N, PYKE R, WANG Z AND YANG Z, 2007, "Use of Exact Solutions of Wave Propagation Problems to Guide Implementation of Nonlinear Seismic Ground Response Analysis Procedures," Journal of Geotechnical and Geoenvironmental Engineering, Vol.133, No.11, pp.1385–1398.

LIANG, F., CHEN, H., AND HUANG, M., 2017, "Accuracy of three-dimensional seismic ground response analysis in time domain using nonlinear numerical simulations,"Earthquake Engineering and Engineering Vibration, Vol.16, No.3, pp.487–498.

MAZZONI, S., MCKENNA, F., AND FENVES, G.L., 2005, "OpenSees command language manual," The Regents of the University of California, Berkeley, 375p.

MAZZONI, S., MCKENNA, F., SCOTT, M.H., AND FENVES, G.L., 2009, "Open System for Earthquake Engineering Simulation, User Command-Language Manual," Pacific Earthquake Engineering Research Center, University of California, Berkeley.

MULLEN, R. AND BELYTSCHKO, T., 1983, "An Analysis of an Unconditionally Stable Explicit Method," Computers and Structures, Vol.16, pp. 691-696.

NEWMARK, N.M., 1965, "Effects of earthquakes on dams and embankments," Geotechnique, Vol.15, pp.139-159.

PARK, D., AND HASHASH, Y., 2004, "Soil Damping Formulation in Nonlinear Time Domain Site Response Analysis," Journal of Earthquake Engineering, Vol.8, No.2, pp.249–274.

PARRA, E.,1996, "Numerical modeling of liquefaction and lateral ground deformation including cyclic mobility and dilation response in soil systems." PhD thesis, Dept. of Civil Engineering, Rensselaer Polytechnic Inst., Troy, N.Y

PHILLIPS, C., 2012, "Dynamic soil modeling in site response and soil-large pile interaction analysis," PhD dissertation, University of Illinois at Urbana-Champaign.

PHILLIPS, C, AND HASHASH, Y., 2009, "Damping formulation for nonlinear 1D site response analyses," Soil Dynamics and Earthquake Engineering. Vol.29, No.7, pp.1143-1158.

PREVOST, J. H. 1985. "A simple plasticity theory for frictional cohesionless soils." Soil Dyn. Earthquake Eng., Vol.4, No.10, pp.9–17.

TARAZONA, S., 2019, "Evaluation of seismic site response of submarine clay canyons: centrifuge modeling,". D.Sc thesis, Federal University of Rio de Janeiro, Rio de Janeiro, Brazil.

TAYLOR, R.N. 1995. Geotechnical Centrifuge Technology. Blackie Academic and Professional.

VUCETIC, M., AND DOBRY, R., 1991, "Effect of Soil Plasticity on Cyclic Response", Journal of Geotechnical Engineering, Vol.117, No.1, pp. 89-107.

YANG, Z. AND ELGAMAL, A. ,2003, Application of unconstrained optimization and sensitivity analysis to calibration of a soil constitutive model. Int. J. Numer. Anal. Meth. Geomech., Vol.27, pp.1277-1297.

ZEGHAL, M., AND ELGAMAL, A.W, 1994, "Analysis of Site Liquefaction Using Earthquake Records", Journal of Geotechnical Engineering, Vol.120, No.6,

pp.996-1017.

ZHU, H.X., AND RANDOLPH, M.F., 2011, "Numerical analysis of a cylinder moving through rate-dependent undrained soil," Ocean Engineering, Vol.38, No.7, pp.943-953.

Chapter 7

Seismic response of submarine gentle slopes in the Offshore Campos Basin, Southeastern Brazil

7.1 Introduction

This chapter presents the methodology and the results of a set of numerical simulations aimed at investigating the seismic response of submarine slopes representative of the Offshore Campos Basin, Southeastern Brazil. Data from subsea bathymetry were employed to identify the predominant geomorphological features in the area of interest. Based on a probabilistic seismic hazard assessment performed for the continental slope of the Campos Basin, a series of acceleration time histories were selected from the Pacific Earthquake Engineering Research (PEER) Ground Motion Database. The soil profile parameters of undrained shear strength and shear wave velocity for the Campos Basin continental slope were obtained from previous studies that developed empirical correlations based on extensive databases of in-situ and laboratory tests. The numerical simulations were performed with OpenSees software following the approach adopted in Chapter 6 for the numerical modeling of the seismic behaviour of a gentle slope in soft clay. A total of 120 numerical simulations was performed considering variations in the depth to bedrock ranging from shallow and deep profiles and variations of the slope angles. The results are summarized in terms of permanent displacements, peak shear strains, and amplification/attenuation of the input ground motions as comparative parameters.

7.2   Area of interest: offshore Campos Basin

The offshore Campos Basin is one of the most prolific oil-producing basins (Cobbold *et al.*, 2001). It is situated in the Southeastern margin, offshore the states of Rio de Janeiro and Espirito Santo, and covers an area of approximately 100,000 km2 (Castro and Picolini, 2015). Figure 7.1 presents a digital elevation model developed of the Campos Basin employing the data of the General Bathymetric Chart of the Oceans (GEBCO). The GEBCO grid provides global coverage of the bathymetry of the oceans and compiles data from various organizations around the world (GEBCO Compilation Group, 2020). The data of the selected area were downloaded in GeoTiff format and processed in Surfer V.13 (Golden Software, Inc.).
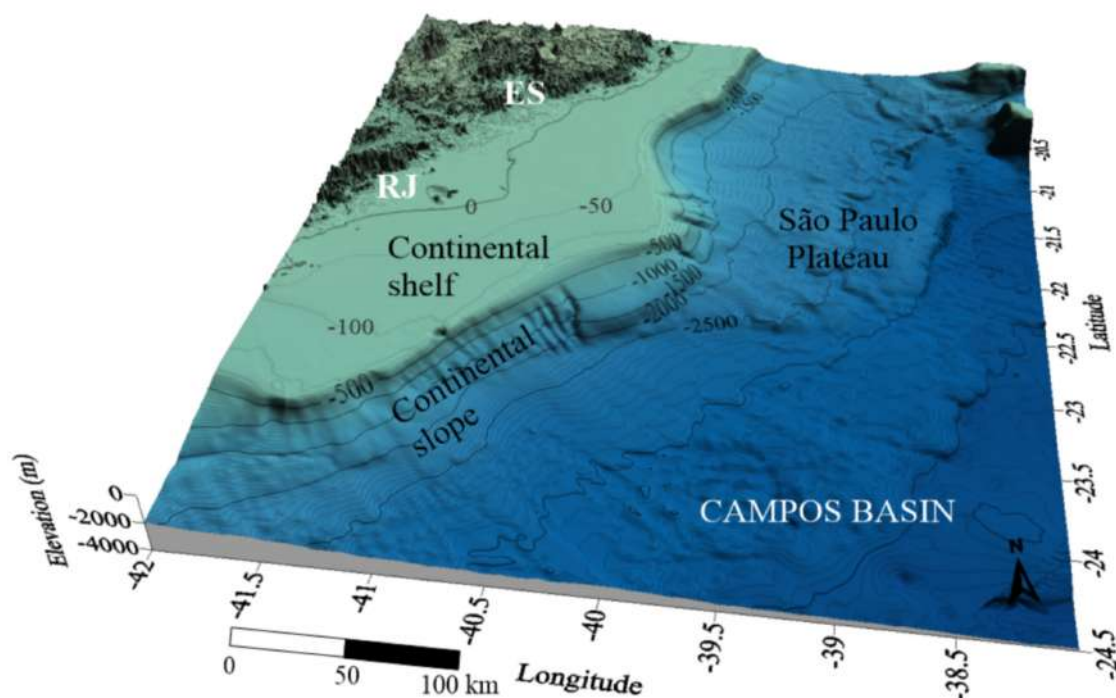
Figure 7.1: A view of the Campos Basin topography (vertical scale exaggerated).

7.2.1   Topography and geomorphology

The Campos Basin is in a passive margin tectonic context (Almeida and Kowsmann, 2015) and is divided into provinces: Continental shelf, Continental slope and São Paulo plateau (Figure 7.1). The Continental slope presents the most significant variation of declivity values, ranging from 0 to 10 degrees (Figure. 7.2a). Relevant geomorphologic features are present in the Continental slope, such as submarine canyons and channels associated with mass wasting processes (Kowsmann *et al.*, 2002) which took place in periods of relatively low sea level (Kowsmann and Viana, 1992). The São Paulo Plateau can be defined as a horizontal area when observed from a regional point of view with declivities from 0 to 2 degrees (Figure 7.2a). A

package of muddy sediments from debris flows and contourites above the salt layer compose this area. Further details related to the geomorphology of the Continental Slope and São Paulo plateau can be encountered in Almeida and Kowsmann, 2015. The continental shelf represents the product of an interaction of sedimentary, hydrodynamic and sea-level variation processes. From the spatial distribution of the slopes, it can be noted a minor variation from 0 degrees to 2 degrees (Figure 7.2b).
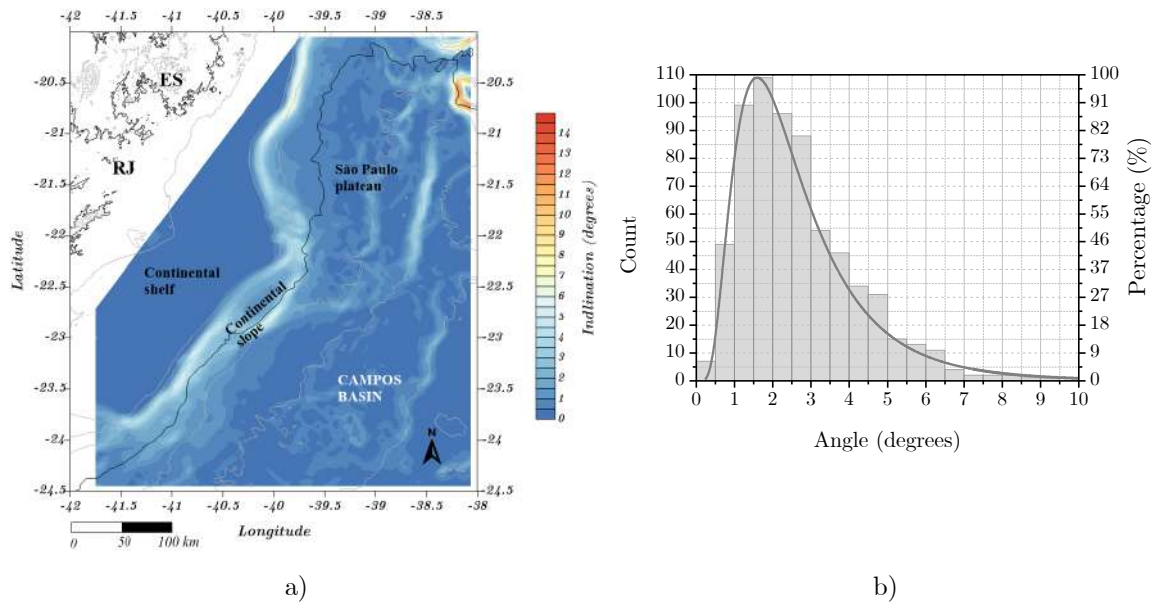
Figure 7.2: (a) Spatial distribution of slopes in the region of interest; (b) histogram of slope distribution across the continental slope.

The area that comprises the Continental Slope and the São Paulo Plateau was divided into three regions (north, central and south) based on their geomorphological characteristics (Almeida and Kowsmann, 2011). The northern region is characterized by a concave profile (Section A-A in Figure 7.3), the highest declivities are encountered in the progression between the Continental Shelf and the Continental slope, then there is a change with inclinations amidst 2 and 3 degrees and the lower slope with gentle declivities (1 degree). The central region presents a convex profile (Section B-B in Figure 7.3) starts with the transition amidst the Continental Shelf and the slope with declivities ranging between 1 and 3 degrees, the highest inclinations are in the transition with the São Paulo Plateau (2 to 6 degrees), this part comprises a series of canyons. The convex shape of the middle slope in the central region could be attributed to the accumulation of mass-movement deposits (Viana *et al*, 1998). The southern region presents a concave profile (section C-C in Figure 7.3), the highest declivities occur in the shelf-slope transition with angles between 1 and 5 degrees with a gradual reduction as the section moves toward the São Paulo

plateau, a relatively horizontal area. Given the level of detail of the bathymetry used in the current study (1km resolution), the geometries of the canyons were partially captured by the Digital Elevation Model generated from the GEBCO data. A comprehensive bathymetric map of the Campos Basin was displayed by Schreiner *et al.* 2015. Given the geomorphology information shown in this section, it can be stated that most of the geometries of the slopes present low gradients in extended areas, then, the continental slope stability analysis can be carried out using the infinite slope approach.
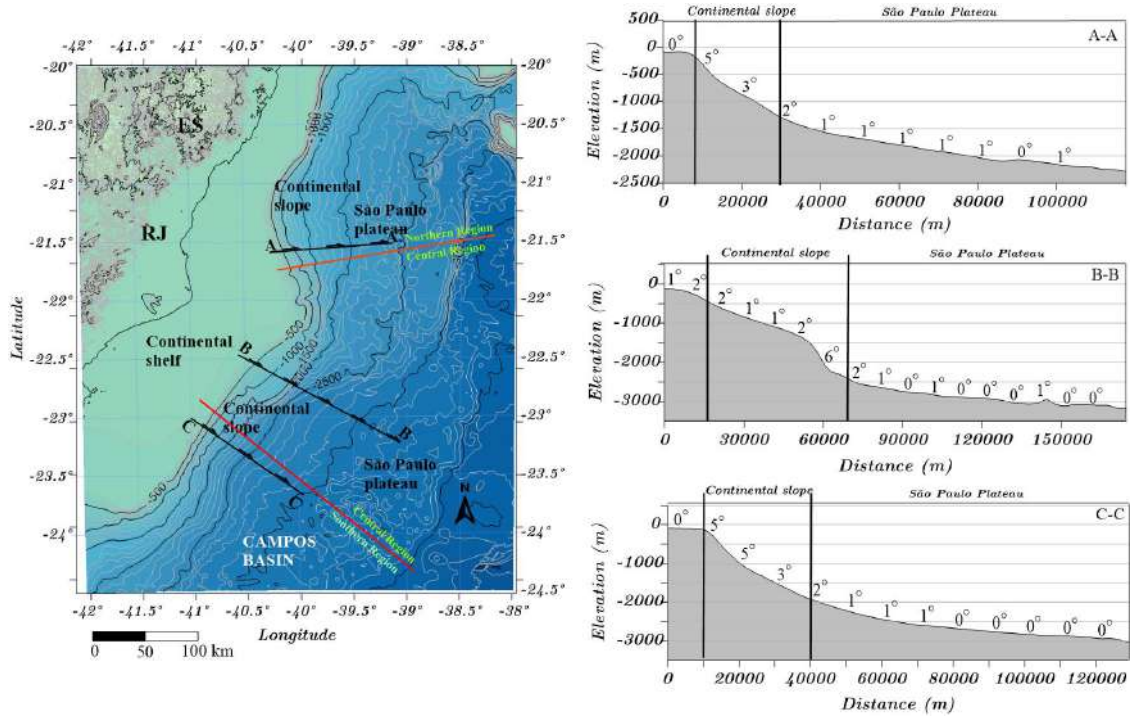
Figure 7.3: Transverse sections, Continental slope, Campos Basin

7.3 Seismic hazards

Given the location of Brazil in an intra-plate area, it is considered a region of low to moderate seismicity. Earthquakes with magnitudes 5 and above have a return period of 4 years (Assumpção *et al.*, 2014) and the limited availability of recordings of strong motions in the region, represent a gap in the knowledge about Brazilian seismicity and the application to the seismic design of offshore structures (monopiles, oil pipelines and foundations). A study performed by Borges *et al.* 2020, compiled historical and recent instrumental seismicity information to develop a mean uniform hazard spectrum, representative of the continental slope of the Campos Basin for various return periods. This represents a starting point in the selection and search of ground motions representative of the seismicity of the area of interest (Campos Basin continental slope). One alternative to obtain ground motions consists of

scaling records from other regions from well-established databases (Yi *et al.*, 2020) a second option incorporates the generation of synthetic accelerograms.

7.3.1 Selection of earthquakes

Considering the limited amount of earthquake records of significant ground motions in intraplate regions, there are alternatives consisting of generating spectrum compatible ground motions or the use of synthetic accelerograms. The first approach will be used in this chapter. For that purpose, the Mean Uniform Hazard Spectra for the continental slope of the Campos Basin developed by Borges *et al.* 2020, two return periods: 475 years and 2475 years were employed as target spectra (Figure 7.4) to cover low amplitude and large amplitude earthquakes.
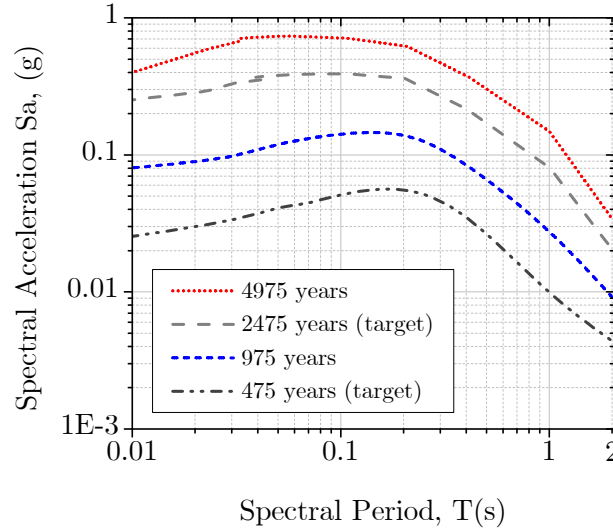
Figure 7.4: Uniform Hazard response spectra of the Offshore Campos Basin (Adapted from Borges *et al.*, 2020).

For the current analyses, the accelerograms were selected from the Pacific Earthquake Engineering Research (PEER) Strong Motion Database. The PEER database consists of two databases: the NGA-East Ground Motion Database and the NGA-West Database (Ancheta *et al.*, 2014). The NGA-West constitutes the largest database of processed recorded ground motions in stable continental regions. The NGA-East includes an extensive set of ground motions recorded worldwide of shallow crustal earthquakes in active tectonic regimes. As Brazil is located within a stable continental intraplate region, it was considered at first instance to employ the NGA-East database. However, from the results of a preliminary search, a limited number of records matched the target Mean Uniform Hazard Spectra. Subsequently, the NGA-West database was used. A similar approach was adopted for the selection of accelerograms in Hong Kong, also an intraplate area of low to

moderate seismicity (Yi *et al.*, 2020).

The tools available in the PEER web application allow the user to define the criteria based on earthquake scenarios and seismological parameters representative of the region of interest: magnitude, fault type, significant duration, distance-to-rupture plane, average shear wave velocity of top 30 m site, and pulse characteristics. The ground motions can also be adjusted to minimize the Mean Squared Error (MSE) and increase the match between the target and recorded (scaled) spectra.

Among the parameters used for scaling earthquake ground motions, the intensity of the earthquakes has been considered in structural response analyses (Anbazhagan *et al.*, 2017). However, intensity alone is not adequate to evaluate the damage potential of an earthquake (Fajfar *et al.*, 1990). For engineering systems with a latent susceptibility of degradation under cyclic loading (for example, landslides, soil profiles prone to liquefaction and structural systems), the seismic demand should include the amplitude and duration of strong shaking within the system (Kempton and Stewart, 2006). The effects of earthquake duration and the potential damage to structural systems have been discussed by Bommer and Martinez-Pereira (1999). For example, if two earthquakes with the same magnitude but different durations are compared, the earthquake with a longer duration will cause more damage to a structure than the earthquake with a shorter duration. In geotechnical systems, the duration of ground motion plays an important role in soil liquefaction and slope stability (Anbazhagan *et al.*, 2017). For instance, the lateral spreading displacements resulting from soil liquefaction are associated with the amplitude and duration of the shaking (Rauch and Martin, 2000). The magnitude of earthquake-induced displacements of soil masses along a slope has been linked to the intensity, frequency content and duration of the ground motion (Bray and Rathe, 1998).

Given the relevance of the duration of the earthquakes on the seismic behavior of geotechnical systems, the following stage consists of applying a predictive relationship for stable continental regions as studied herein. For that purpose, the empirical correlation developed by Lee and Green (2014), was applied to define a range of significant duration as input parameters in the search of records in the PEER-NGA database. Different duration parameters have been proposed in the literature (Bommer and Martinez-Pereira, 1999); the most used are bracketed duration and significant duration. Bracketed duration (D_b) is defined as the time elapsed between the first and last exceedance of a specified threshold acceleration

typically between 0.05 g to 0.1g (Kempton and Stewart, 2006) (Figure 7.5).
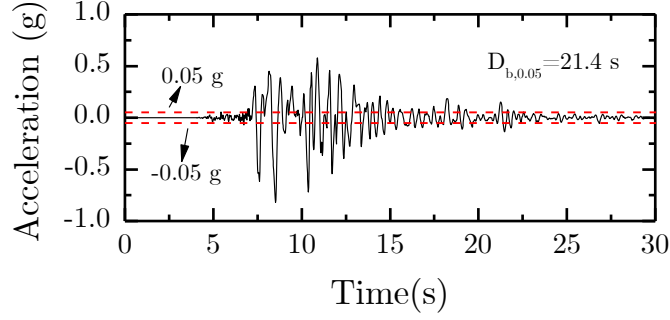
Figure 7.5: Example of bracketed duration of Kobe earthquake (1995), record number P1043.

Significant duration (D_s) is an energy-based parameter. It is defined as the time interval across which a specified amount of energy is dissipated. Energy is expressed as the integral of the square of the ground acceleration, or velocity, or displacement. The integration of the squared aceleration is related to the Arias Intensity (AI) (Arias, 1970), defined as:

$$AI = \frac{\pi}{2g} \int_0^{t_r} a^2(t)dt \qquad (7.1)$$

where $a(t)$ is the acceleration time-history, t_r is the total duration of the accelerogram, and g is the acceleration due to gravity. The build up of energy with time can be represented using Husid plots (Husid, 1969). Two common intervals have been defined in the literature, 5%-75% and 5%-95% of AI (Somerville *et al.*, 1997; Trifunac and Brady, 1975, respectively), denoted as D_{5-75} and D_{5-95}. An example of the Arias intensity for an earthquake with the significant duration parameters is shown in Figure 7.6.
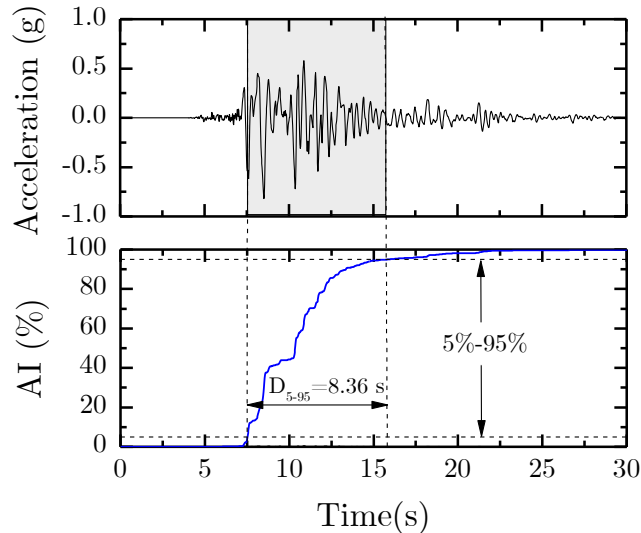
Figure 7.6: Example of significant duration (D_{5-95}) of Kobe earthquake (1995), record number P1043.

167

An empirical correlation proposed by Lee and Green (2014) was developed for stable continental regions, based on a total of 620 sets of horizontal motions: 28 recorded motions and 592 scaled motions (Equation 7.2).

$$lnD_{5-95} = ln \left\{ C_1 + C_2 exp(M-6) + C_3 R + [S_1 + S_2(M-6) + S_3 R] S_S \right\} \quad (7.2)$$

where C_1=2.5, C_2=4.21, C_3=0.14 and S_1=-0.98, S_2=-0,45, S_3=-0,0071 are regression coefficients; M is the moment magnitude; R is the closest distance fault to rupture plane (km); and S_S is a binary number representing local site conditions: SS=0 for rock sites and S_S=1 for soil sites. For the calculations it was considered a rock site (S_S=0). Borges *et al.* 2020 performed a dissagreggation analysis (Bazzurro and Cornell, 1999) to summarize the contributions to the hazard at the site of interest of earthquake sources, magnitude intervals and distance ranges. The most important contibutions to the seismic hazard come from earthquake magnitudes of 4.5 to 5.7 at distances between 40 km and 100 km. Then, by plotting the significant duration (D_{5-95}) with the distance to the rupture plane for stable continental regions (Equation 7.2) for earthquakes of magnitude 4.5 and 5.7 and a range of distances between 40 km and 100 km, a range of significant durations between 9 s and 20 s was estabilished, as displayed in Figure 7.7.
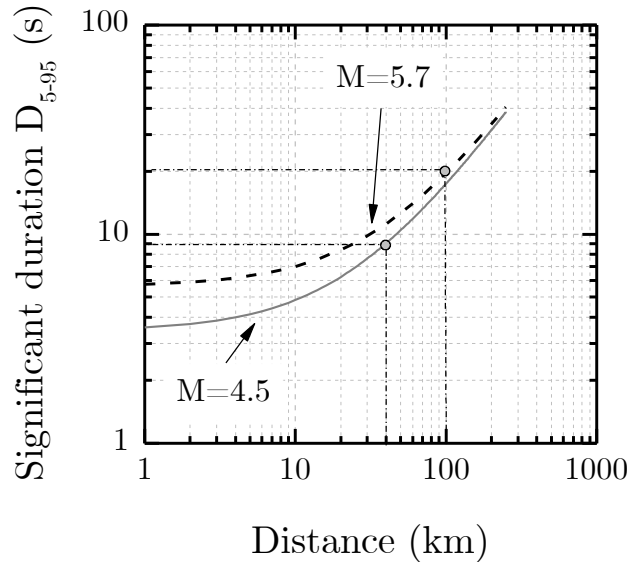
Figure 7.7: D_{5-95} for rock site and two earthquake magnitude scenarios.

Once defined the range of significant duration of the earthquakes and the target spectra for the return periods (475 years and 2475 years), the best matching earthquake motion records were found by the PEER Ground Motion Database Web

Application. Scale factors were applied to the earthquake records over the period of interest and a good match is obtained when the Mean Squared Error of the difference between the spectral accelerations of the recorded motion and the target spectrum is achieved. Five horizontal recorded motions (H1 spectral ordinate in the database) were selected from the PEER-NGA West database and scaled to the target spectra. Each record from the PEER-NGA West catalog has a unique identifier known as Record Sequence Number (RSN). The RSN will be used as identifier for the input motions used in the numerical analyses presented in this chapter. Table 7.1 presents the selected ground motions for the selected target spectrum and Table 7.2 presents the parameters of the selected motions including the scaling factors applied to the original motions. The response spectra of the scaled time histories and the target spectrum are displayed in Figure 7.8.

Table 7.1: Selected spectrum-compatible ground motions

Target spectrum	Earthquake	Station	RSN
2475 years	Northwest Calif-01 1938	Ferndale City Hall	5
	Parkfield 1966	Cholame - Shandon Array #8	31
	San Fernando 1971	Lake Hughes #12	71
	Imperial Valley-06 1979	Superstition Mtn Camera	190
	Mammoth Lakes-02 1980	Long Valley Dam	234
475 years	Northwest Calif-01 1938	Ferndale City Hall	5
	Parkfield 1966	Cholame - Shandon Array #8	31
	San Fernando 1971	Pearblossom Pump	81
	Imperial Valley-06 1979	Plaster City	188
	Livermore-02 1980	Del Valle Dam (Toe)	219

Table 7.2: Parameters of the selected spectrum-compatible ground motions

Target spectrum	Earthquake	RSN	RJB (km)	D5-95 (s)	PGA (g)	Scale Factor
2475 years	Northwest Calif-01 1938	5	52.7	11.6	0.15	1.39
	Parkfield 1966	31	12.9	13.1	0.25	0.79
	San Fernando 1971	71	14.0	12.0	0.38	0.61
	Imperial Valley-06 1979	190	24.6	11.6	0.11	1.82
	Mammoth Lakes-02 1980	234	14.3	10.3	0.10	1.24
475 years	Northwest Calif-01 1938	5	53	12	0.15	0.20
	Parkfield 1966	31	13	13	0.25	0.11
	San Fernando 1971	81	36	14	0.10	0.23
	Imperial Valley-06 1979	188	30	11	0.04	0.45
	Livermore-02 1980	219	10	9	0.04	0.27
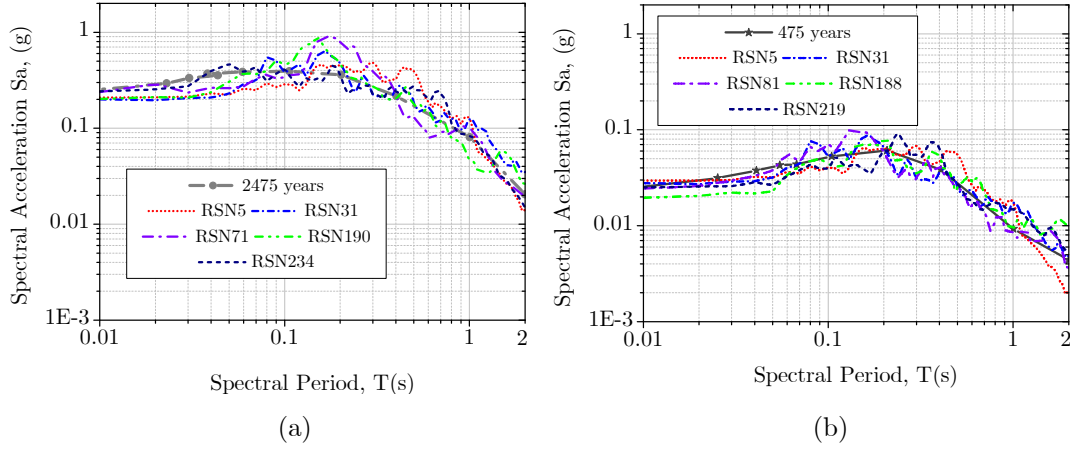
Figure 7.8: Target acceleration spectrum and response spectra of scaled acceleration time histories: (a) 2475 years; (b) 475 years.

Once scaled the selected ground motions, a spectral adjustment was performed. The methodology applied in the current work and implemented in the software SeismoMatch used the wavelets algorithm proposed by Al Atik and Abrahamson (2010). Figure 7.9 and Figure 7.10 display the spectrally matched accelerograms for the return periods selected for the analyses and used as input motions in the numerical studies presented in this chapter.
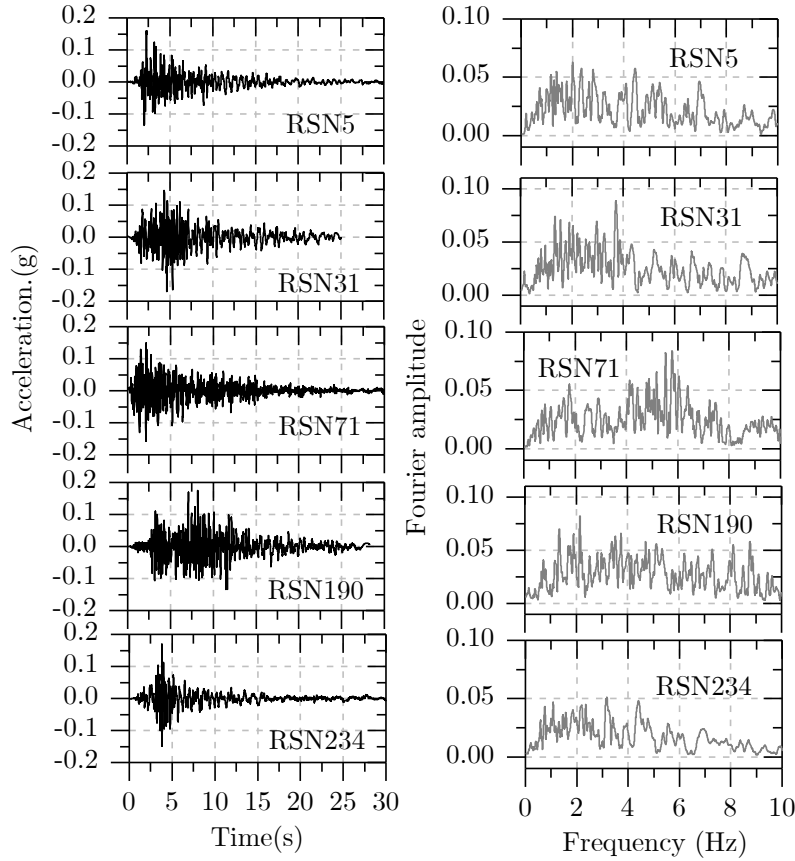
Figure 7.9: Acceleration-time histories for a return period of 475 years.
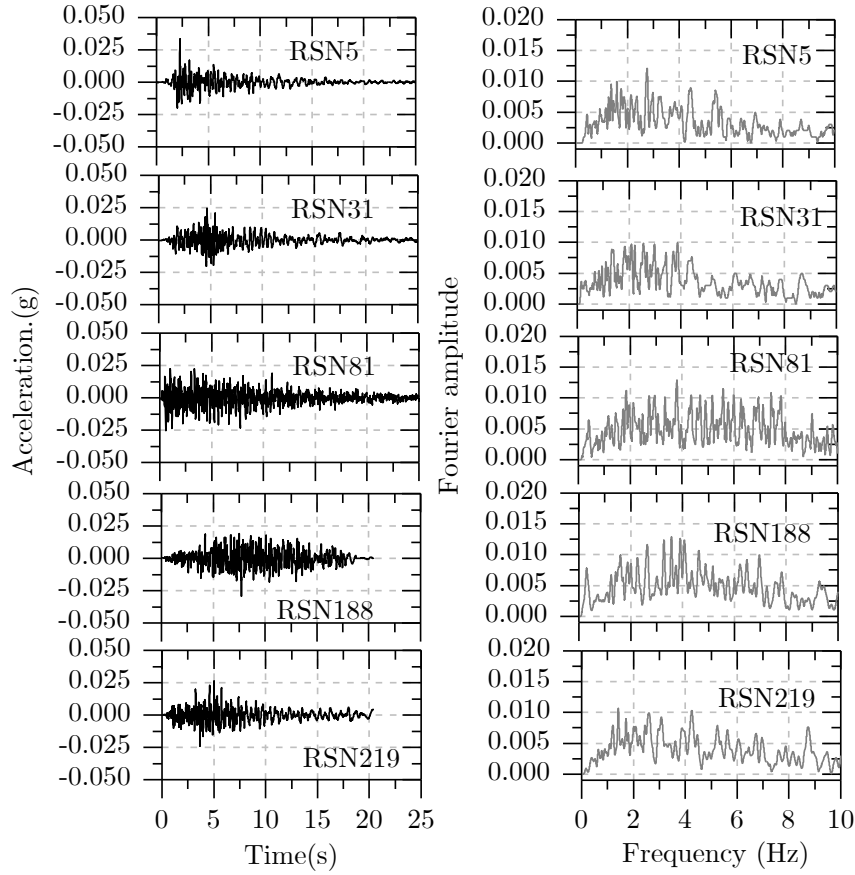
Figure 7.10: Acceleration-time histories for a return period of 2475 years.

7.4 Model input parameters

The objective of the numerical simulations presented in this chapter is to provide insight into the site amplification features for soft marine clay deposits under seismic loads representative of an intraplate region in Southeastern Brazil. The set of numerical analyses performed in this chapter evaluate the seismic behavior of submarine slopes in soft clay and how parameters as the slope inclination and the soil profile thickness affect the response of the system. The numerical modeling approach adopted in the simulation of one of the centrifuge tests presented in Chapter 5 was applied in the parametric studies presented herein. A uniform soil profile was selected as the baseline scenario for the parametric analysis, the undrained shear strength and shear wave velocity profiles were obtained from previous studies on the continental slope of the Campos Basin (Borges *et al.*, 2015; Borges *et al.*, 2020b). Three soil profile thicknesses were selected in the parametric analyses: 20 m, 50 m, and 100 m to cover shallow and deep slope profiles (Figure 7.11). This range of depths agrees with parametric studies for deep offshore clay deposits (Zhou *et al.*, 2017). A range of slopes between 0 degrees and 5 degrees was defined for the numerical simulations, based on the distribution of slopes across the Campos Basin

continental slope (Figure 7.2).

7.4.1   Soil profile and model geometry

The seabed and upper Quaternary sections of the Continental slope and São Paulo Plateau are mostly constituted of pelagic and hemipelagic muds composed of silt and siliciclastic clay deposited by suspension (Caddah *et al.*, 1998). Siliciclastic and carbonate sands are also present in the upper slope, however, their occurrence is significantly limited, and their primary source comes from the Continental shelf (Viana *et al*,1998). With the information related to the topography of the Campos Basin and the global characteristics of the soil deposits in the Continental slope, for the numerical analyses, the slopes to be analysed will be considered uniform and composed of normally consolidated mud.

From previous studies, aimed to assess the Factor of Safety against translational landslides on the continental slope and São Paulo Plateau of the Campos Basin (Borges *et al.*, 2015), the profile of undrained shear strength was defined for this work. The profile presented in Figure 7.11a is based on an extensive database of in-situ and laboratory tests. The variation of the undrained shear strength (s_u) can be presented in a form of an equation:

$$s_u = s_{u0} + z\xi \tag{7.3}$$

where,
s_{u0}=undrained shear strength at the seabed (kPa).
z=depth (m).
ξ=rate of growth of undrained shear strength with depth (kPa/m).

For the current analyses, s_{u0}= 3.0 kPa and ξ=1.728 kPa/m (Borges *et al.*, 2015). The shear wave velocity profiles were obtained from a correlation based on CPTu parameters (Borges *et al.*, 2020b). The equation used in this study (Equation 7.4) was developed based on a series of *in-situ* seismic piezocone penetration tests on the Brazilian continental margin reaching up to 150 m and is expressed in terms of the effective vertical stress:

$$v_s = 34.64\sigma_{v0}'^{\,0.342} \tag{7.4}$$

where,

$\sigma'_{v0}{}^{0.342}$ = effective vertical stress (kPa).

The shear wave velocity profile was calculated using a saturated unit weight $\gamma_{sat} = 17.5 \frac{kN}{m^3}$ according to the values found by Borges *et al.*, 2015 (Figure 7.11b).
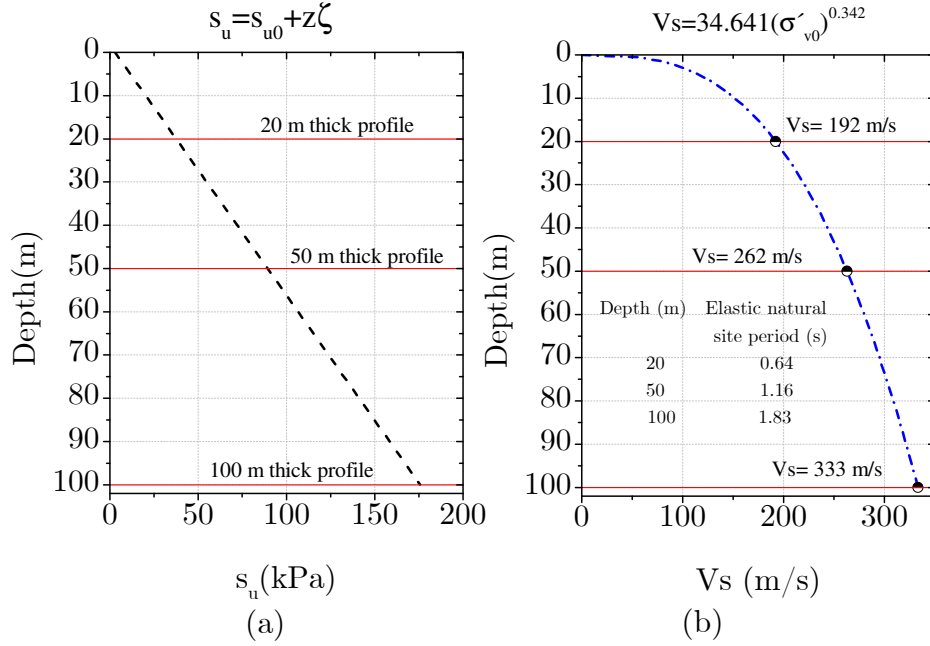
Figure 7.11: Soil profiles of (a) undrained shear strength; (b) shear wave velocity.

7.4.2 Numerical methods and constitutive models

Based on the numerical approach employed to simulate the seismic response of gentle slopes in soft clay by means of centrifuge testing, a series of numerical analyses were performed. The objective was the simulation of the seismic behavior of gentle slopes in soft clay considering the predominant slope angles on the Campos Basin and the geotechnical parameters of the region of interest available in the literature. The numerical models were performed with OpenSees (Mazzoni *et al.*, 2006).

In OpenSees, finite element computational analysis framework, the clay is modeled as a nonlinear hysteretic material with a Von Mises multisurface kinematic plasticity model, called *PressureIndependentMultiYield* (PIMY) (Yang and Elgamal, 2003). The nonlinear shear stress-strain backbone curve is represented by the hyperbolic relation (Kondner, 1963), defined by two material constants: (i) the low-strain shear modulus, and (ii) the ultimate shear strength. The usage of nested yield surfaces by the PIMY material allows the control of the plastic modulus, then they can be adjusted to match a specified modulus reduction curve. For the

173

numerical simulations performed in this chapter, the modulus reduction curves were defined at a first instance utilizing the Vucetic and Dobri (1991) empirical curves for clays (PI=33%). As discussed by Groholski *et al.* (2015), strength corrections need to be performed, as the strength of the soil is underestimated or overestimated in some situations when using reference modulus reduction curves. Figure 7.12 illustrates an example of the modulus reduction and backbone curves defined for 50 m depth (Figure 7.11). It can be observed that the Vucetic and Dobri (1991) reference curves were developed for shear strains of 1%, in addition, the shear strength of the clay was overestimated for the range of strains in which they are valid. This means that strength corrections have to be performed to properly reproduce the large-strain shear strength of the clay. This was achieved by using the General Quadratic/Hyperbolic (GQ/H) model (Groholsky *et al.*, 2015), that uses a quadratic equation to match a target shear strength at large strains (defined as 10%). The shear stresses were calculated from the modulus using the following equation:

$$\tau = \rho V_s^2 \frac{G}{G_{max}} \gamma \tag{7.5}$$

where,

τ= shear stress at a given point (kPa),

V_s=shear wave velocity in the given layer (m/s)

ρ=mass density of the soil

G=shear modulus at a given point (kPa)

G_{max}=small-strain shear modulus

γ=shear strain at a given point
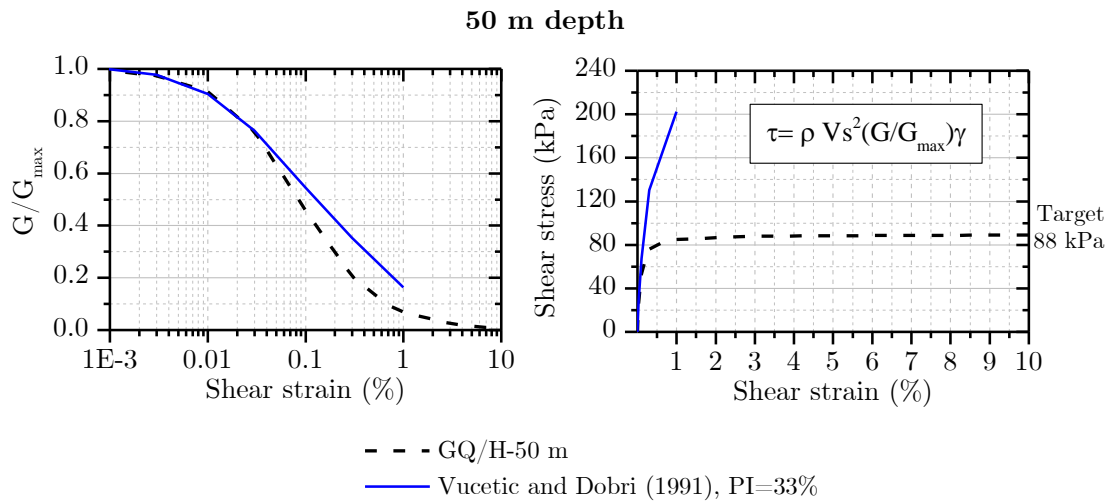
Figure 7.12: Modulus reduction and shear stress curves: GQ/H model and Vucetic and Dobri (1988) for 50 m depth.

Figure 7.13 shows the modulus degradation curves for three depths: 20 m, 50 m and 100 m obtained after applying the GQ/H model to match the target shear strengths. The same procedure was employed for all the remaining layers in the numerical model.
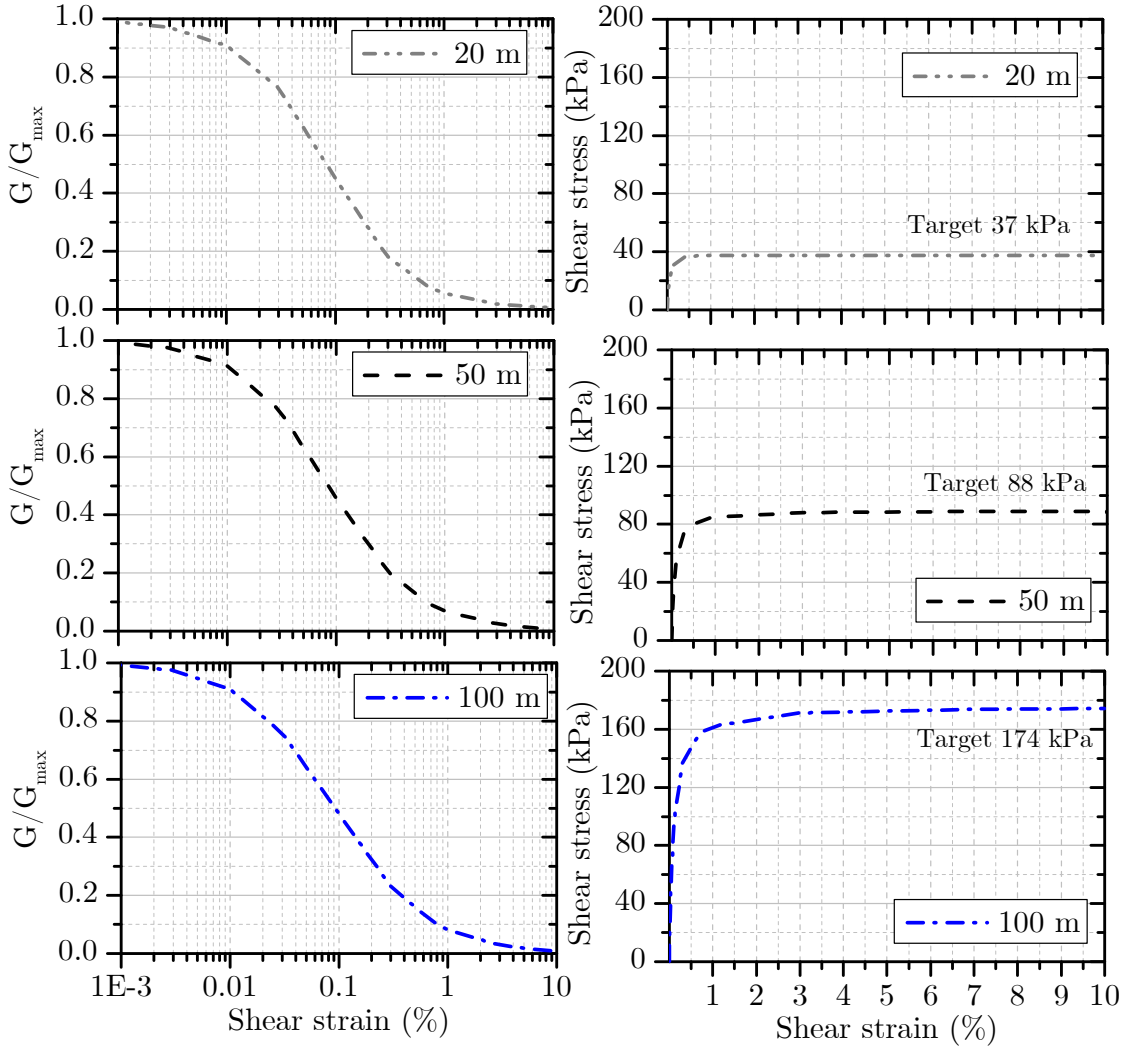
Figure 7.13: Modulus reduction and stress-strain curves at 20 m, 50 m and 100 m depth generated by the GQ/H model.

Using the numerical modeling methodology adopted in Chapter 6, eight-node brick elements were used to build a 3-D shear beam column. To achieve the shear beam boundary condition, the front and back models of the mesh were tied to move simultaneously. The shear wave velocity and undrained shear strength profiles were discretized in sub-layers of 1 m width, the element thickness was set to 0.50 m or two brick elements per layer. The small strain damping was defined for two frequencies: the fundamental frequency of the overall site ω_n and five times ω_n (Stewart *et al.*, 2008). The fundamental frequencies (or elastic site periods) of the

profiles used in the parametric analyses in this chapter are displayed in Figure 7.11. OpenSees allows defining if the ground motions are applied at a rigid boundary or at a flexible boundary. Following the approach presented by Biscontin and Pestana (2006), a rigid boundary was selected to simplify the parametric analyses, as the same amount of energy is applied into the soil profiles independent of the depth of the soil, then direct comparisons of results can be done.

7.5 Effect of slope inclination

The ground inclination represents the most relevant parameter about the slope geometry (Carlton *et al.*, 2016). For the analyses, four model inclinations were selected: level ground (0 degrees), 1 degree, 3 degrees and 5 degrees covering the range of predominant slope angles across the continental slope in the Campos Basin (Figure 7.2). For simplicity, the results of the single uniform layer with 50 m thickness (Figure 7.11) subjected to the 2475 years return period ground motions are presented in this section as a baseline for comparisons.

When the ground is inclined, a static shear stress takes place in the soil, even in gentle slopes (Biscontin, and Pestana., 2006). When an earthquake occurs, this effect is increasingly evident, and an accumulation of displacements and deformations appear in the downslope direction. Figure 7.14 presents the displacement time histories obtained at the surface of the models (1m depth) for the earthquakes corresponding to the 2475 years return period ground motions. The results show an increasing displacement accumulation with an increase in the slope angle. In addition, the difference between the maximum displacement and the permanent or end of shaking displacements decreases as the slope angle is increased, this behavior was reported by Biscontin and Pestana (2006).
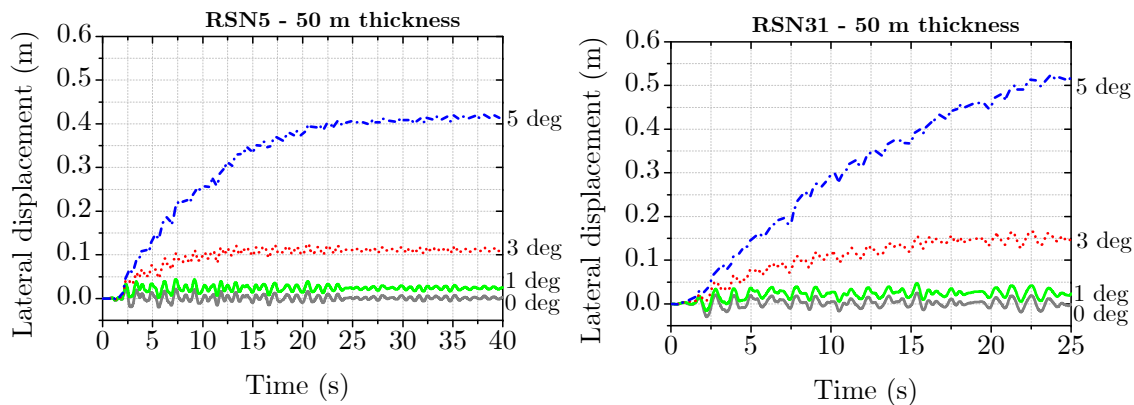
Figure 7.14: Displacement time histories at the surface for different slope angles, for a 50 m thick clay deposit, 2475-year return period input motions.
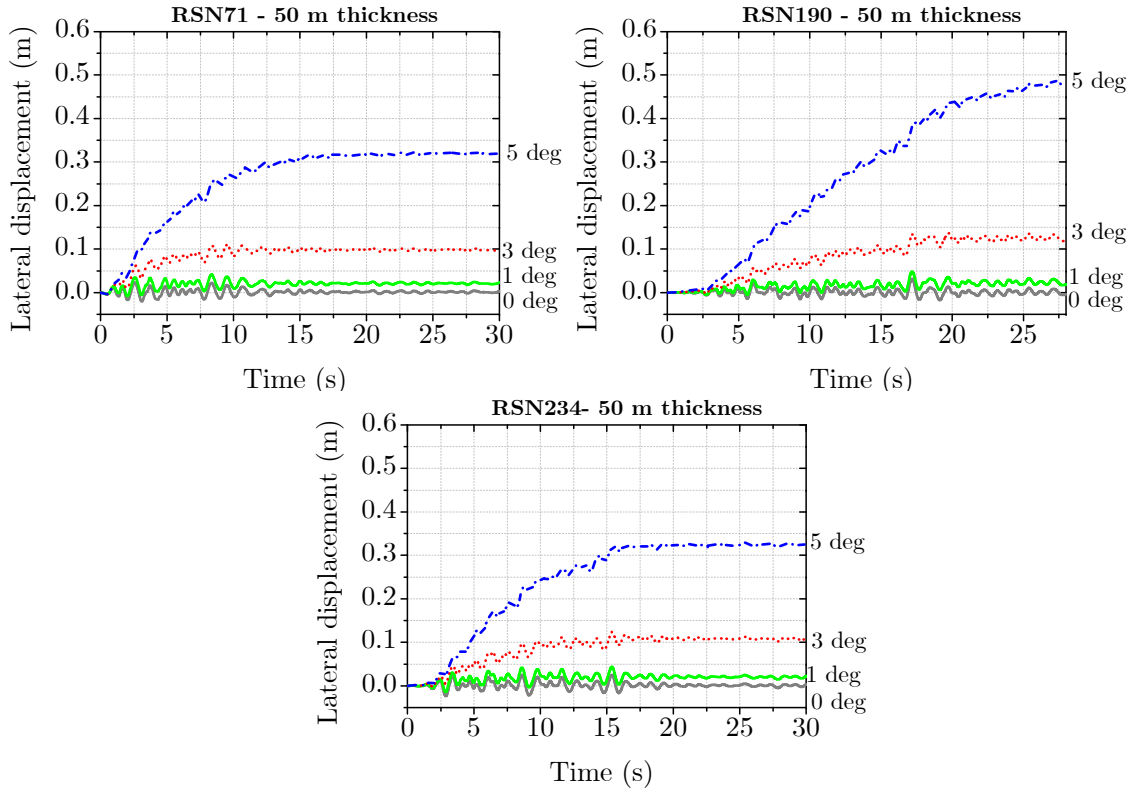
Figure 7.14: Displacement time histories at the surface for different slope angles, for a 50 m thick clay deposit, 2475-year return period input motions (*cont.*).

Figure 7.15 shows the peak shear strain profiles for the ground motions corresponding to the 2475 years return period and for slope angles ranging between 0 degrees and 5 degrees. It can be noted that for the same ground motions, as the slope angle increases, the peak shear strains also rise with localized shear strains accumulations near the surface (between 2.5 m and 5.0 m depth). In addition, the strains at the base of the slope show that the soil mass slides over the bedrock as well as deforming.
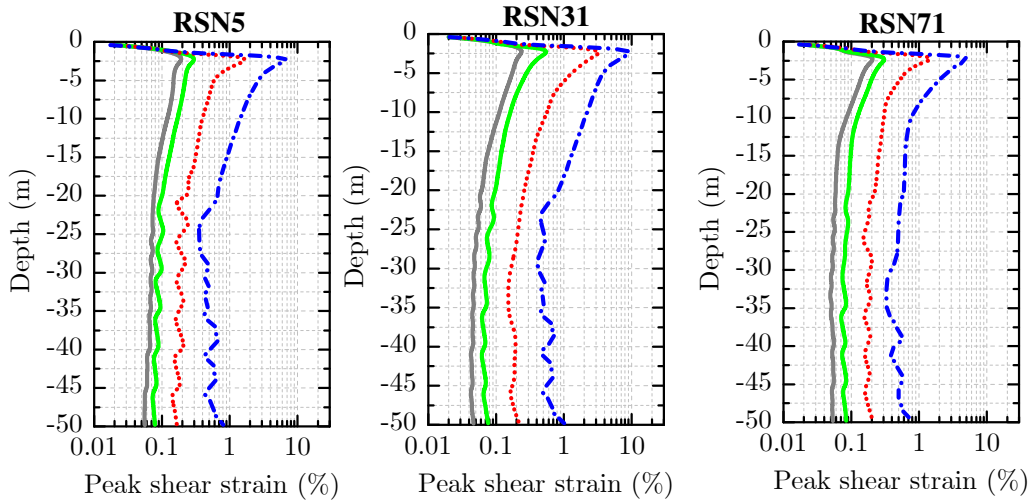
Figure 7.15: Peak shear strain profiles for different slope angles, for a 50 m thickness profile and 2475 years return period input motions.
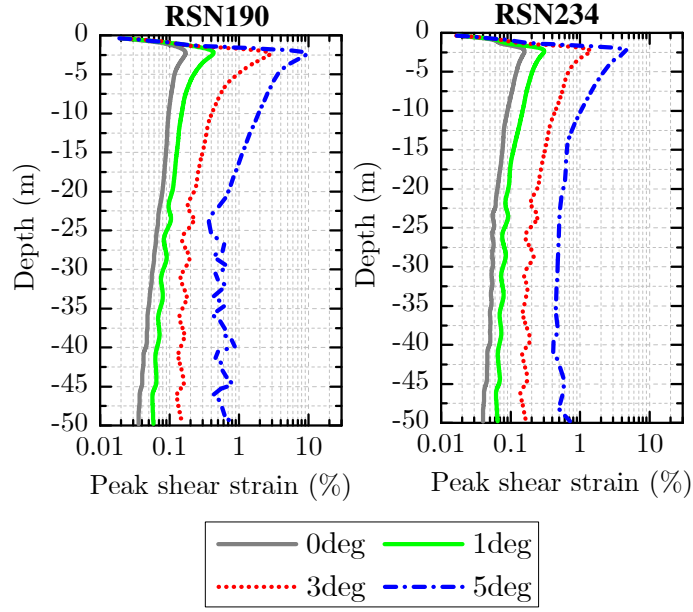
Figure 7.15: Peak shear strain profiles for different slope angles, for a 50 m thickness profile and 2475 years return period input motions (*cont.*).

The acceleration spectra (5% damping) at 1 m depth and the response spectrum ratios between the base and surface accelerations are presented in Figure 7.16 to Figure 7.20. The results highlight a similar trend when comparing the response spectrum ratios: attenuation for periods below 0.3 s and amplification after that, with a peak at a period close to the elastic site period (1.16 s, *see* Figure 7.11). For the 5-degrees slope, the spectral accelerations and response spectrum ratios are smaller than the values of the 0-degrees, 1-degree and 3-degrees slopes for periods larger than 0.2 s to 0.3 s, this offset in the spectral amplification patterns reflects the effects of non linearity and accumulations of permanent deformations in the downslope direction.
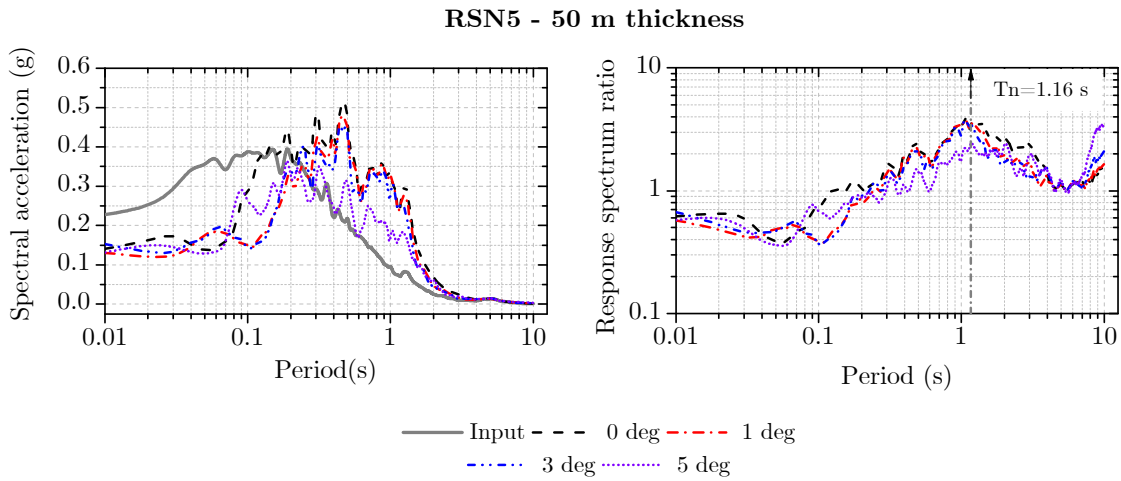
Figure 7.16: Effect of slope angle on acceleration spectra and response spectrum ratio for the 2475 year return period ground motion RSN5.

RSN31 - 50 m thickness
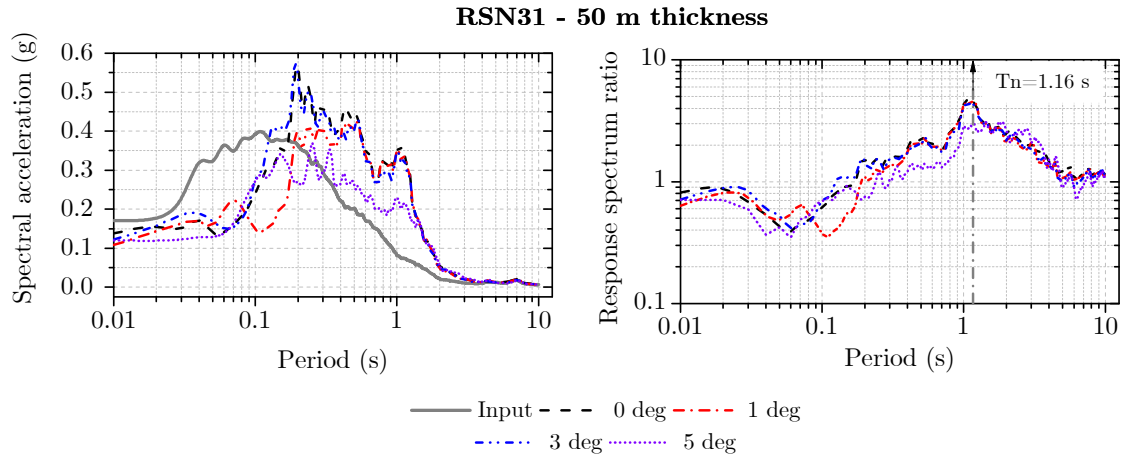
Figure 7.17: Effect of slope angle on acceleration spectra and response spectrum ratio for the 2475 year return period ground motion RSN31.

RSN71 - 50 m thickness
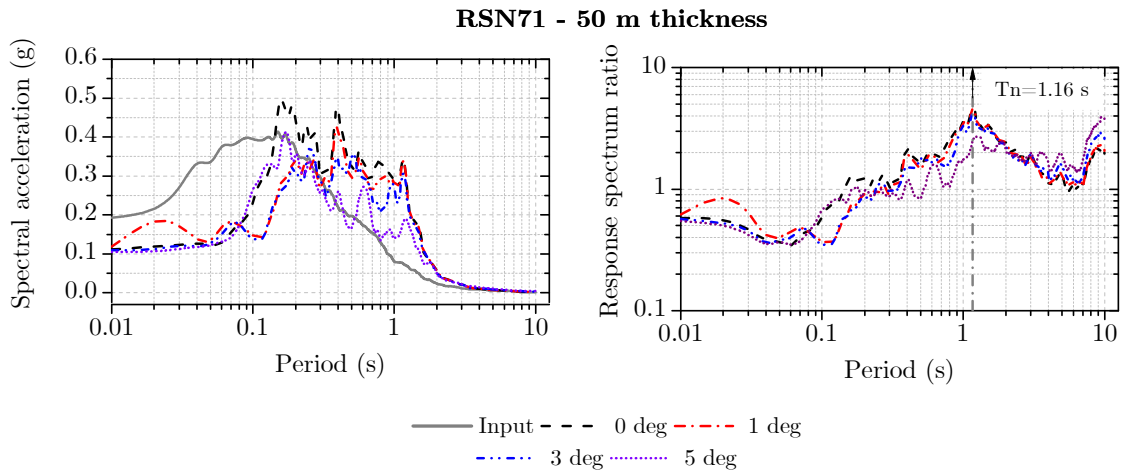
Figure 7.18: Effect of slope angle on acceleration spectra and response spectrum ratio for the 2475 year return period ground motion RSN71.

RSN190 - 50 m thickness
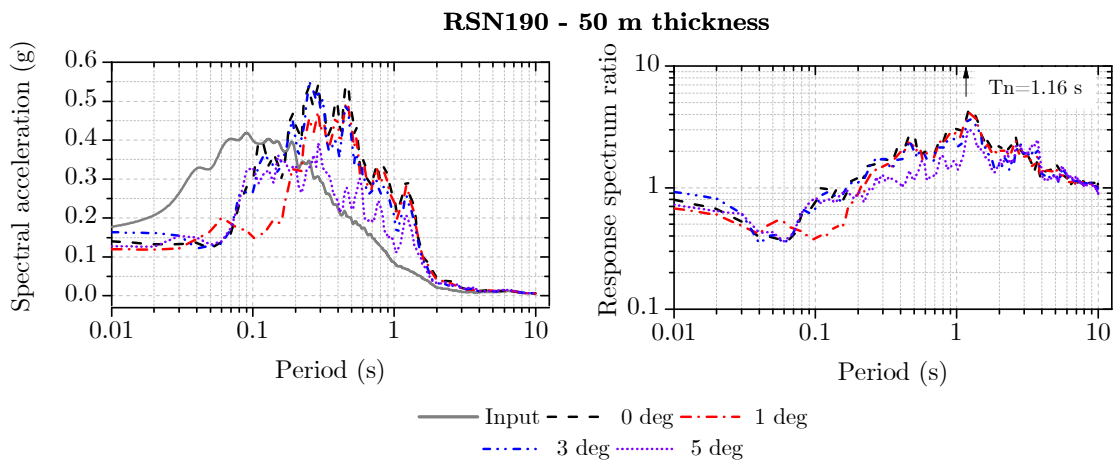
Figure 7.19: Effect of slope angle on acceleration spectra and response spectrum ratio for the 2475 year return period ground motion RSN190.
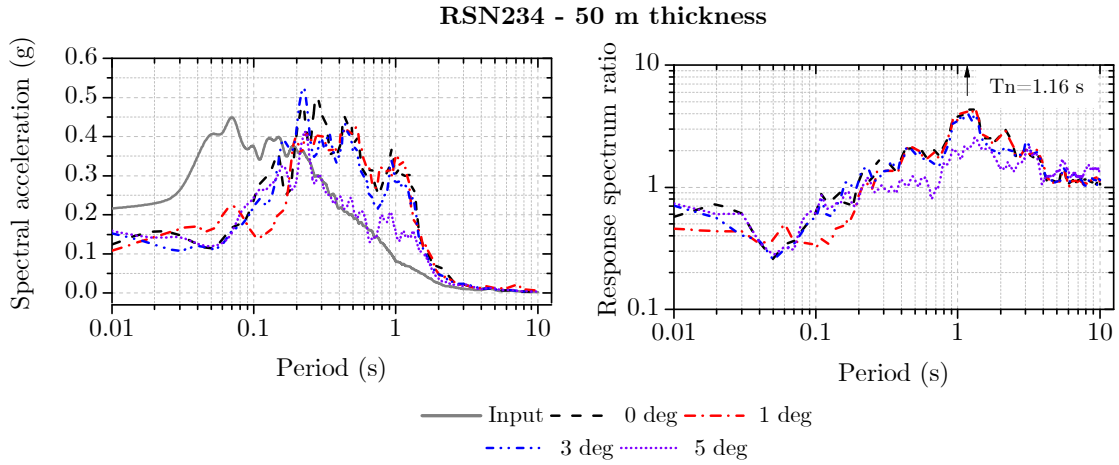
Figure 7.20: Effect of slope angle on acceleration spectra and response spectrum ratio for the 2475 year return period ground motion RSN234.

7.6 Effect of depth to bedrock

Numerical simulations were performed for three depths to bedrock to incorporate a range between shallow and deep soil profiles: 20 m, 50 m and 100 m (Figure 7.11). The purpose of the current set of analyses is to provide a qualitative description of the performance of the slopes. The comparisons are in terms of displacement time histories at the surface, shear strain profiles and spectral accelerations. Figure 7.21 displays the lateral displacement time histories at the surface of the models for the three depths to bedrock selected and for the 5-degrees slopes. It can be observed that the largest displacements correspond to the deepest soil profiles. From the 100 m thickness slopes, a trend of slightly oscillating displacements occurs after the end of the earthquake.
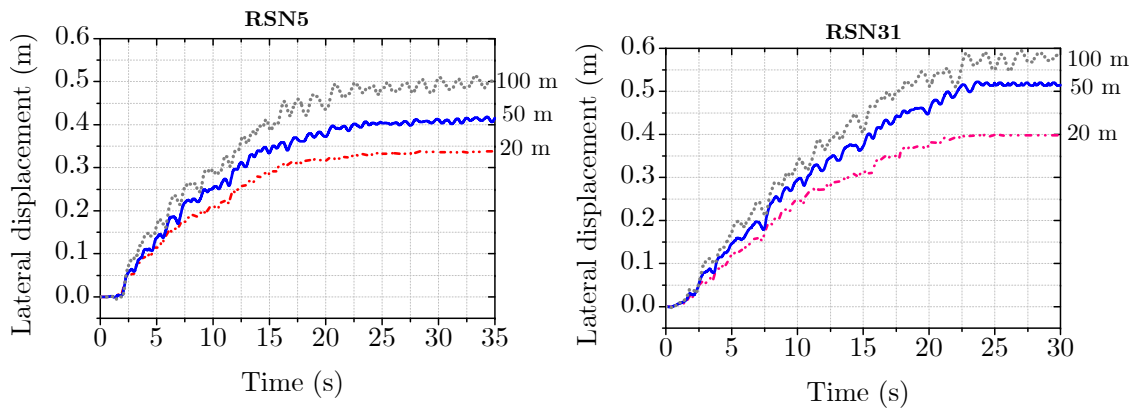
Figure 7.21: Effect of thickness on displacement time histories at the surface of the slopes for the 2475 years return period ground motions: 5-degrees slope.
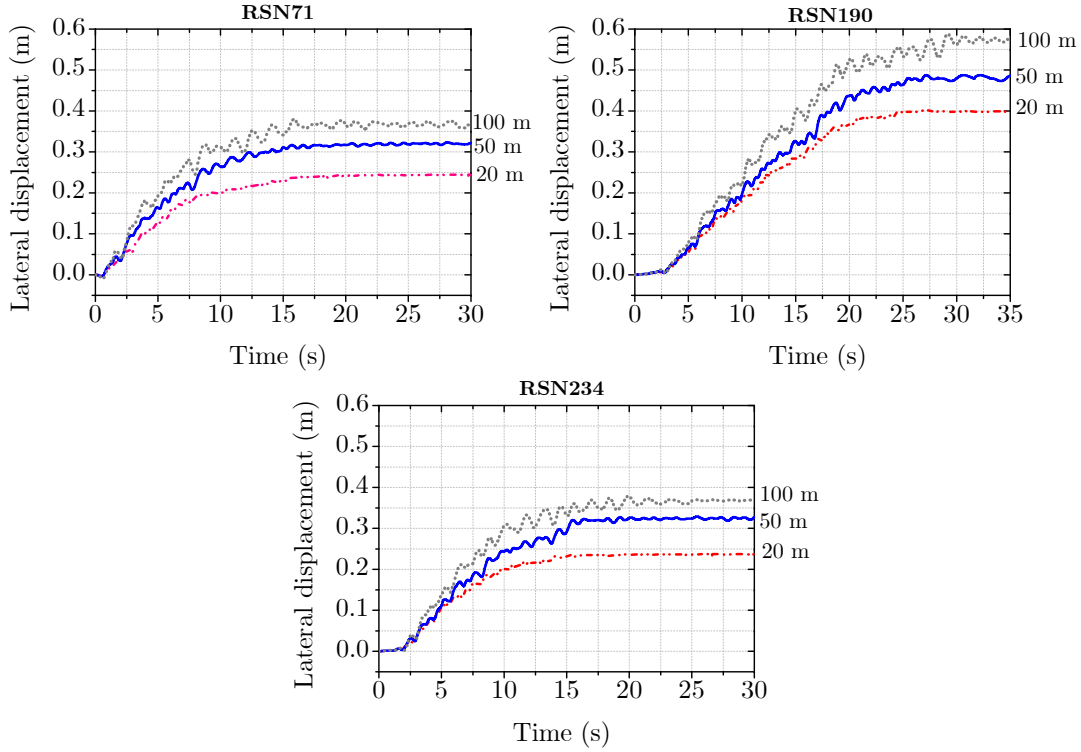
Figure 7.21: Effect of thickness on displacement time histories at the surface of the slopes for the 2475 years return period ground motions: 5-degrees slope (*cont.*).

To compare the peak shear strains the depths were normalized by the total thickness of the soil profiles. The results are presented for the 5-degrees slopes. The results show that the largest strains occur at the shallow slope (20 m thickness) reaching peak shear strains between 8% to 14% for the ground motions studied. The largest strains occurred near the surface of the slopes at normalized depths ranging from 0.01 to 0.1. The profiles displayed in Figure 7.22 evidence the effect of slope thickness on the dissipation of the energy of the earthquake resulting in smaller strains for the deepest slopes. A similar trend of the effects of depth to bedrock in the shear strains has been reported by Biscontin and Pestana (2006).
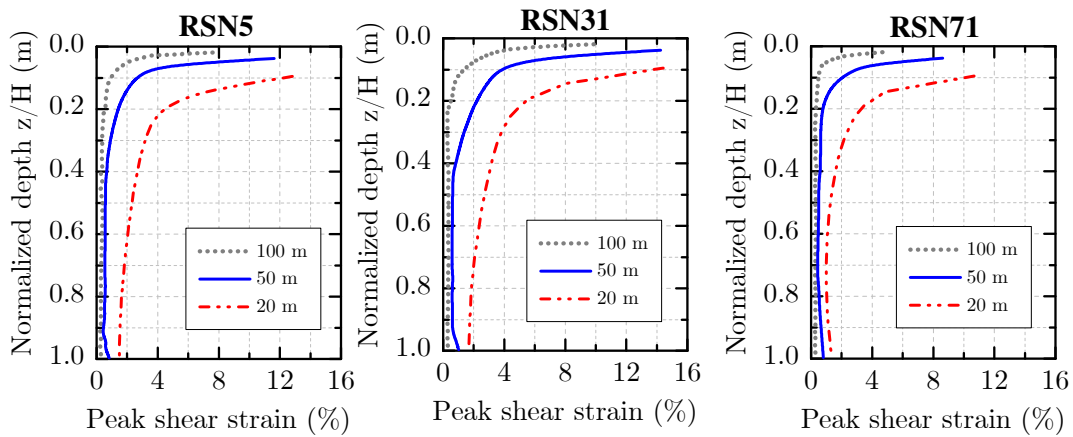
Figure 7.22: Effect of thickness on shear strains on 5° slopes for the 2475 years return period ground motions.

181
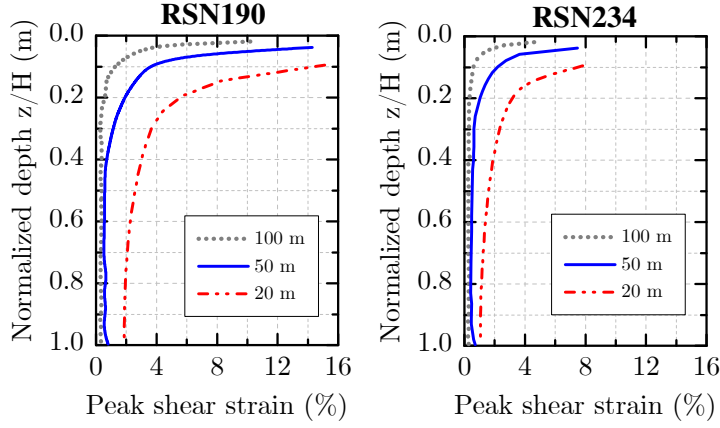
Figure 7.22: Effect of thickness on shear strains on 5° slopes for the 2475 years return period ground motions (*cont.*).

The spectral accelerations and response spectrum ratios are presented in Figure 7.23 to Figure 7.27. In general, a similar trend can be observed with significant attenuation of periods below 0.2 s and amplification for higher periods. For the 100 m depth to bedrock, a peak in the response spectrum ratio can be observed at periods close to the natural elastic site period (1.83 s). This behavior indicates the effects of local site conditions on the propagation of the ground motion through the slope profiles and how they are altered in amplitude and frequency content.
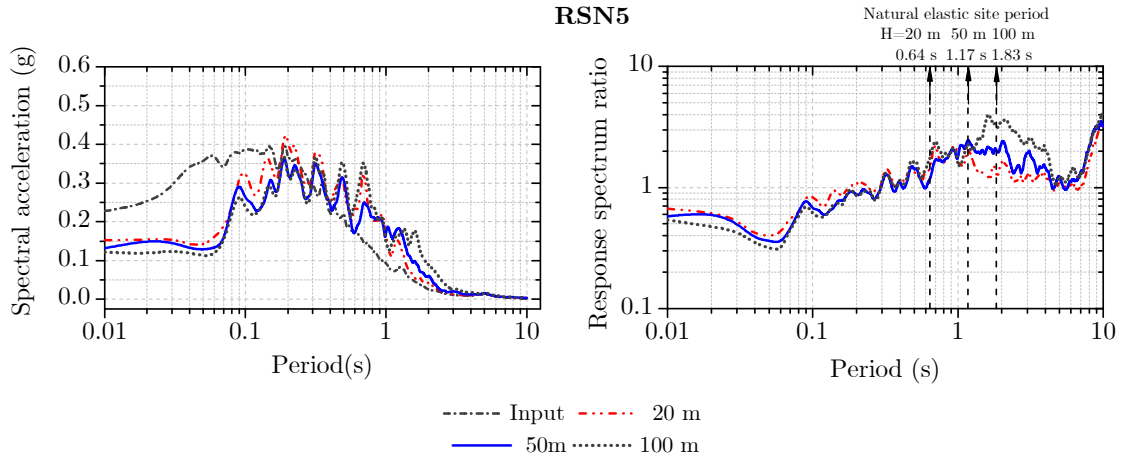
Figure 7.23: Effect of depth to bedrock on acceleration spectra and response spectrum ratio for the 2475 year return period ground motion RSN5.

182
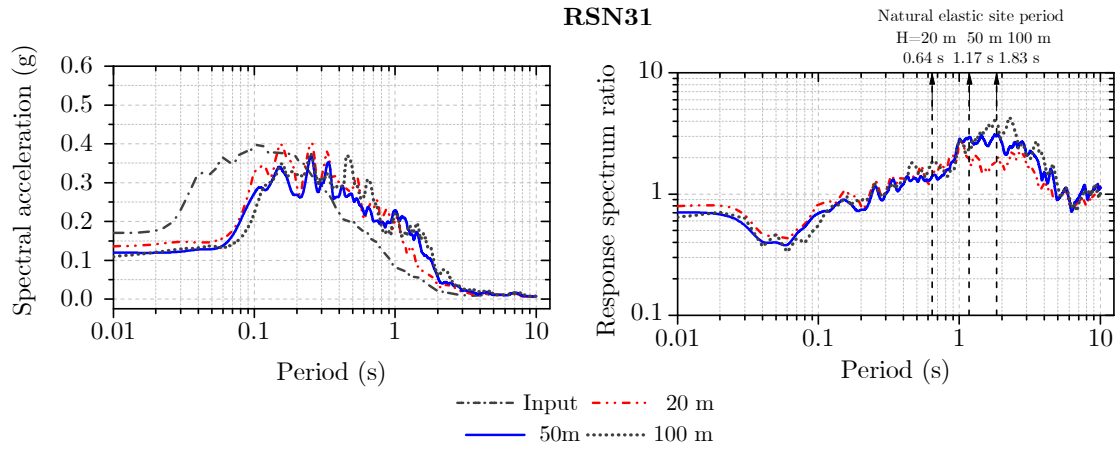
Figure 7.24: Effect of depth to bedrock on acceleration spectra and response spectrum ratio for the 2475 year return period ground motion RSN31.
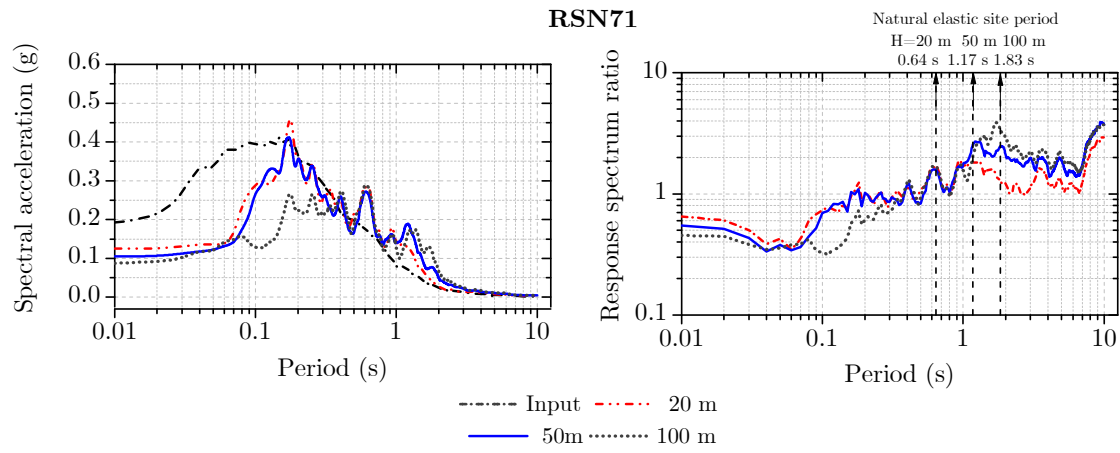
Figure 7.25: Effect of depth to bedrock on acceleration spectra and response spectrum ratio for the 2475 year return period ground motion RSN71.
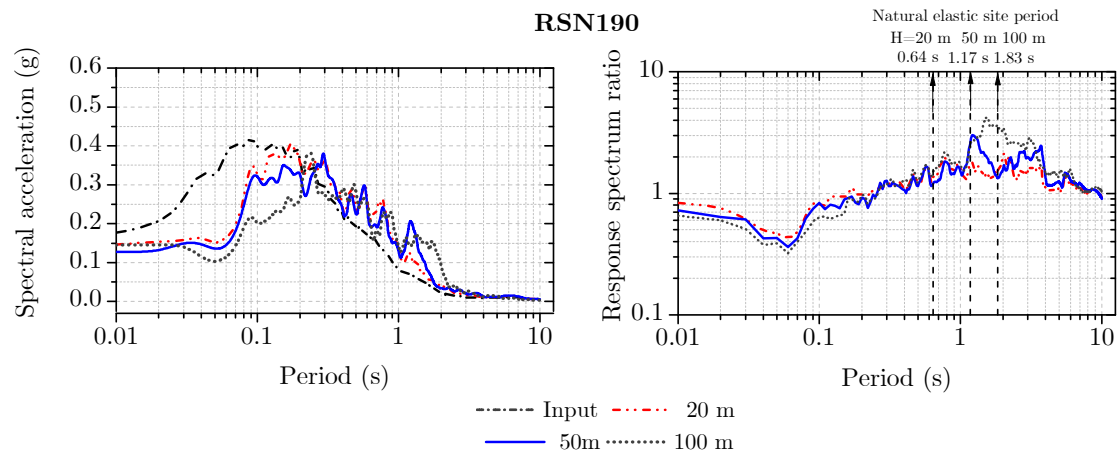
Figure 7.26: Effect of depth to bedrock on acceleration spectra and response spectrum ratio for the 2475 year return period ground motion RSN190.

183
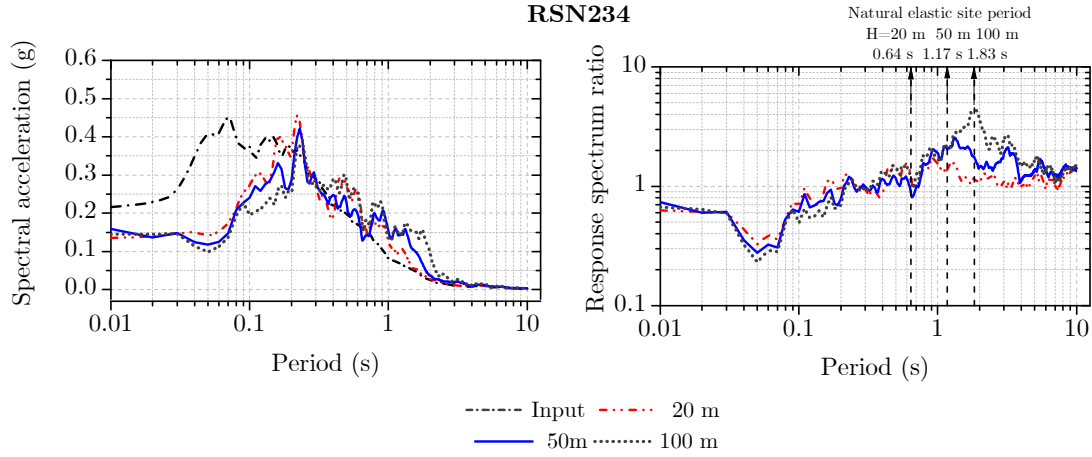
Figure 7.27: Effect of depth to bedrock on acceleration spectra and response spectrum ratio for the 2475 year return period ground motion RSN234.

7.7 Summary of numerical simulations

The results of the numerical analyses for all the ground motions, depth to bedrock and slope inclinations are summarized in terms of permanent displacements, peak shear strains and amplification of ground motions. A total of 120 numerical simulations was performed. Figure 7.28 and Figure 7.29 display the permanent horizontal displacements and peak shear strains for the 2475 years and 475 years return period motions. Altogether, it can be observed an increasing trend of increasing displacements as the inclination of the slope is increased. The ground motions for the return period of 475 years yielded relatively small permanent displacements and shear strains, the peak values of the numerical simulations were around 5 cm and 1.3%, respectively. For the return period of 2475 years, the permanent displacements were approximately 60 cm, and the maximum peak shear strains reached values around 16%. From the shear strains behavior, it can be noted that the largest shear strains occurred at the shallow slope (H=20m) and that trend applied for both return period input ground motions.
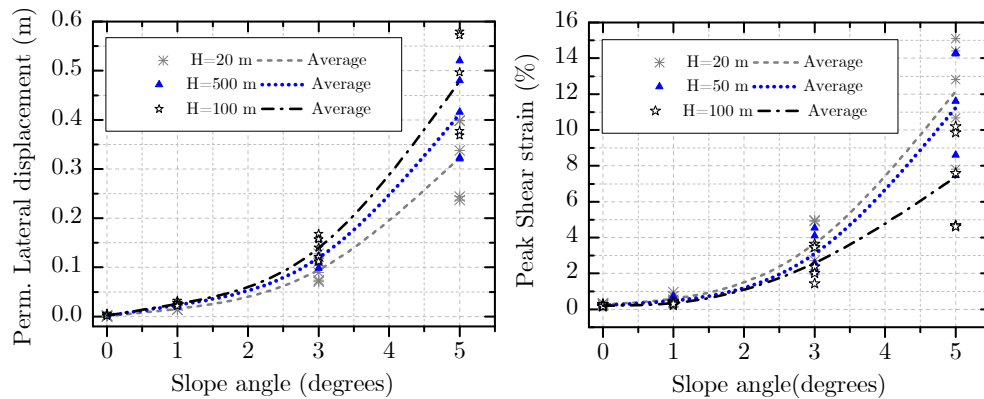
Figure 7.28: Summary of the response of the slopes for different angles and depth to bedrock for 2475 years return period ground motions.

184
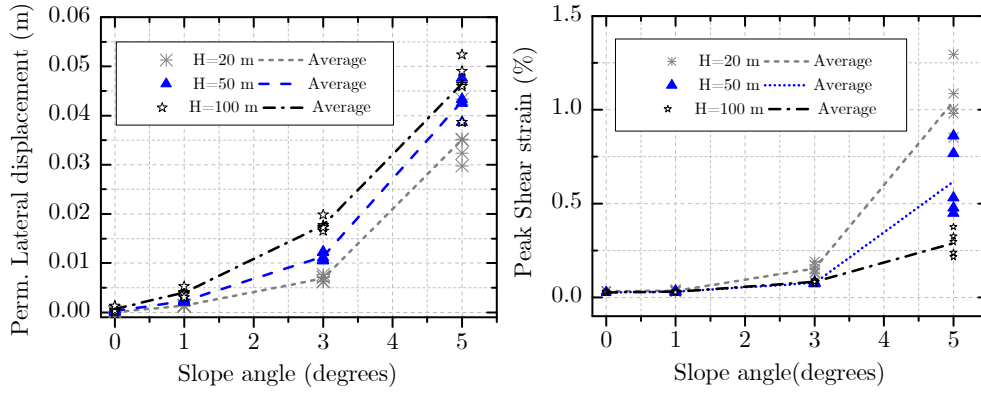
Figure 7.29: Summary of the response of the slopes for different angles and depth to bedrock for 475 years return period ground motions.

Figure 7.30 compares the permanent displacements for the range of parameters studied. It can be seen the difference in orders of magnitude of the response of the slopes depending on the target response spectrum compatible ground motions selected. The results of the analyses presented in this chapter and the methodology applied can be employed for landslide hazard zonation based on the seismic slope displacements using simplified parameters as the soil profile thickness, slope inclination and seismicity of the region of interest.
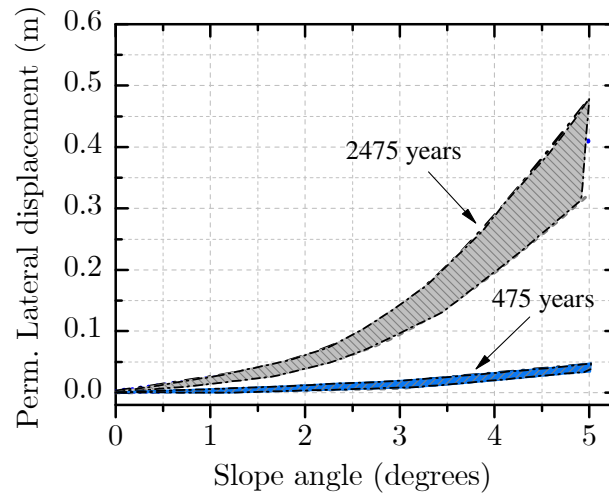
Figure 7.30: Summary of permanent horizontal displacements for the parameters studied.

A comparison with previous findings related to the amplification of PGA from soft soil sites is presented in Figure 7.31. The comparison includes the results predicted by Stewart and Liu, 2000 for Holocene Lacustrine/Marine clays and the PGA amplification from soft soil sites in the San Francisco Bay and Mexico City by Idriss (1990). The results of the numerical simulations exhibit amplification of PGA for the low amplitude ground motions, corresponding to the 475 years return period. For the 2475 years return period ground motions, of larger amplitude, de-amplification of PGA at the base was observed for all the simulations with a trend ranging be-

tween the median and lower bound prediction of amplification/de-amplification of PGA presented by Stewart and Liu, 2000. The results are complemented with the observations from the centrifuge tests presented in Chapter 5 following a trend that agrees well with the numerical simulations. This finding shows the applicability of Speswhite kaolin for the modelling of amplification-deamplification of PGA for offshore geotechnical problems.
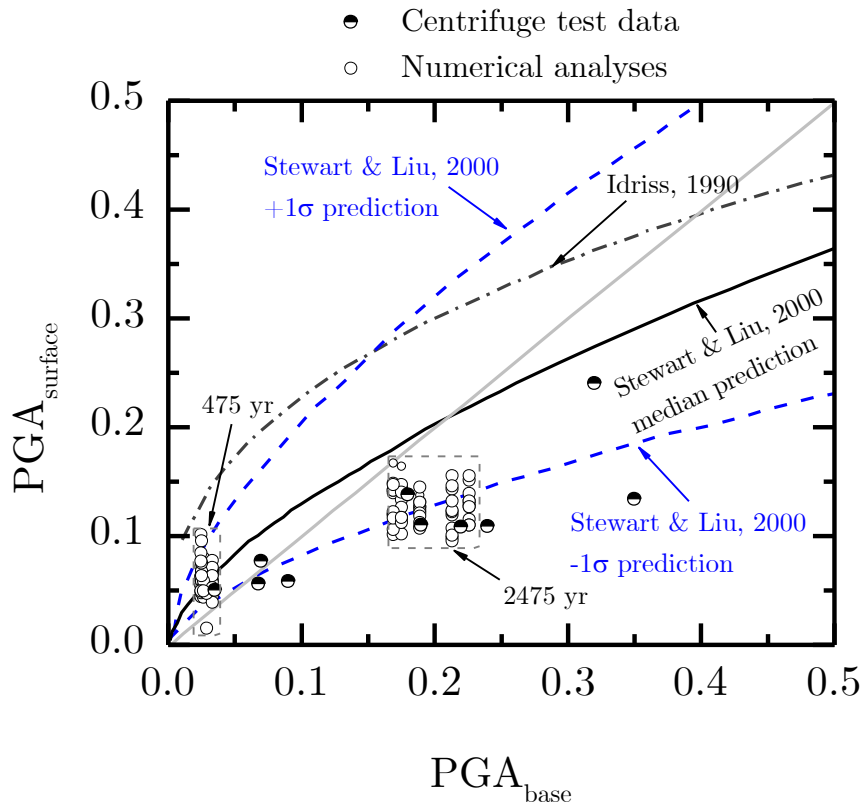
Figure 7.31: Amplification/de-amplification of PGA for the numerical simulations and comparison with previous findings.

7.8 Final remarks

A set of numerical analyses was carried out to investigate the influence of slope inclination and soil thickness on the predicted response of offshore submarine slopes with parameters representative of the offshore conditions in southeastern Brazil. The small strain stiffness and the undrained shear strength were defined by using reference information developed from in-situ tests and characterization available in the literature. The program OpenSees was utilized to perform the numerical simulations.

The main findings are as follows:
- From the bathymetric information obtained for the Campos Basin continental

slope, a predominant presence of gentle slopes with angles less than 5 degrees was observed.

- Even slight slope angles have a remarkable effect on the behavior of the slope response in terms of displacements when subjected to relatively small seismic loads characteristic of intraplate regions. The mechanism is associated with an accumulation of displacements in the downslope direction as the earthquake takes place.

- The thickness of the slope also played a substantial role in the seismic response for the large-amplitude ground motions corresponding to the 2,475-year return period. It was observed that as the depth to bedrock increased, the permanent displacements also increased. However, for the low-amplitude ground motions, differences between the permanent displacements were relatively small as the depth to bedrock increased.

7.9 Chapter 7 references

AL ATIK, L., AND ABRAHAMSON, N.,2010, "An Improved Method for Nonstationary Spectral Matching," Earthquake Spectra, Vol.26, No.3, pp.601–617.

ALMEIDA, A.G., AND KOWSMANN, R.O., 2011, "Caracterização geomorfológica do fundo marinho do talude continental da Bacia de Campos, RJ", 13o Congresso da Associação Brasileira de Estudos do Quaternário, Armação de Búzios, Brasil. São Paulo: Universidade de São Paulo.

ALMEIDA, A.G., AND KOWSMANN, R.O., 2015, "Geomorphology of the continental slope and São Paulo Plateau," In: Kowsmann, R.O., editor. Geology and Geomorphology. Rio de Janeiro: Elsevier. Habitats, Vol.1, pp.33-66.

ANBAZHAGAN, P., NEAZ SHEIKH, M., BAJAJ, K., MARIYA, P.J., MADHURA, H., AND REDDY, G.R., 2017, "Empirical models for the prediction of ground motion duration for intraplate earthquakes," J Seismol. Vol.21, pp.1001–1021.

ANCHETA, T. D., DARRAGH, R. B., STEWART, J. P., SEYHAN, E., SILVA, W. J., CHIOU, B. S.-J., WOODDELL, K. E., GRAVES, R. W., KOTTKE, A. R., BOORE, D. M., KISHIDA, T., AND DONAHUE, J. L., 2014, "NGA-West2 Database," Earthquake Spectra, Vol.30, No.3, pp.989–1005.

ARIAS, A.,1970, "A measure of earthquake intensity," In: Hansen R J (ed) Seismic Design for Nuclear Power Plants,MIT Press, Cambridge, Massachusetts, pp.438–483.

ASSUMPÇÃO, M., FERREIRA, J., BARROS, L., BEZERRA, H., FRANÇA, G., BARBOSA, J., AND DOURADO, J., 2014, "Intraplate seismicity in Brazil," In P. Talwani (Ed.), Intraplate Earthquakes Cambridge: Cambridge University Press., pp.50-71.

BAZZURRO, P., AND CORNELL, C.A., 1999, "Disaggregation of seismic hazard," Bulletin of the Seismological Society of America, Vol.89, No.2, pp.501-520.

BISCONTIN, G., AND PESTANA, J., 2006, "Factors affecting seismic response of submarine slopes," Natural Hazards and Earth System Science, Vol.6, No.1, pp.97-107.

BOMMER, J., AND MARTINEZ-PEREIRA, A., 1999, "The effective duration of earthquake ground motion," J. Earthq. Eng., Vol.3, No.2, pp.127-172.

BORGES, R.G., LIMA, A.C., AND KOWSMANN, R.O. 2015, "Areas susceptible to landsliding on the continental slope," In: Kowsmann, R.O., editor. Geology and Geomorphology. Rio de Janeiro: Elsevier. Habitats, Vol.1, pp.99-136.

BORGES, R.G., ASSUMPÇAO, M.S., ALMEIDA, M.C.F., AND ALMEIDA, M.S.S., 2020, "Seismicity and seismic hazard in the continental margin of southeastern Brazil," J. Seismol, Vol.24, pp. 1205-1224.

BORGES, R., SOUZA JUNIOR, L., ALMEIDA, M.C.F., AND ALMEIDA, M.S.S., 2020b. "Relationship Between Shear Wave Velocity and Piezocone Penetration Tests on the Brazilian Continental Margin," Soils and Rocks. Vol.43, No.2, pp.219-230.

BRAY, J., AND RATHE., E., 1998, "Earthquake induced displacements of solid-waste landfills," J. Geotech. Geoenviron. Eng., Vol.124, No.3, pp.242-253.

CASTRO, R.D., AND PICOLINI, J.P. 2015, "Main features of the Campos Basin regional geology," In: Kowsmann, R.O., editor. Geology and Geomorphology. Rio de Janeiro: Elsevier. Habitats, Vol.1, pp.1-12.

CADDAH, L.F.G., KOWSMANN, R.O., AND VIANA, A.R. 1998, "Slope sedimentary facies associated with Pleistocene and Holocene sea-level changes, Campos Basin, Southeast Brazilian Margin," Sedimentary Geology. Vol.115, No.1/4, pp.159-174.

CARLTON, B., KAYNIA, A.M. AND NADIM, F., 2016, "Some important considerations in analysis of earthquake-induced landslides," Geoenviron Disasters Vol.3, No.11.

COBBOLD, P.R, MEISLING, K.E., AND MOUNT, VAN.S, 2001, "Reactivation of an Obliquely Rifted Margin, Campos and Santos Basins, Southeastern Brazil," AAPG Bulletin, Vol.85, No.11, pp. 1925–1944.

FAJFAR, P., VIDIC, T., AND FISCHINGER, M., 1990, "A measure of earthquake motion capacity to damage medium-period structures," Soil Dyn. Earthq. Eng., Vol 9, pp. 236-242.

GEBCO COMPILATION GROUP,2020, "GEBCO 2020 Grid"

GROHOLSKI, D.R., HASHASH, Y.M.A., MUSGROVE, M., HARMON, J., AND KIM, B., 2015, "Evaluation of 1-D non-linear site response analysis using a general quadratic/hyperbolic strength-controlled constitutive model," 6th International Conference on Earthquake Geotechnical Engineering, 1–4 November 2015, Christchurch, New Zealand.

HUSID, L.R., 1969, "Características de terremotos. Análisis general," Revista del IDIEM Santiago deChile, Vol.8, pp.21–42

IDRISS, I.M.,1990, "Response of soft soil sites during earthquakes," Proc. H. Bolton Seed Memorial Symposium, J. M. Duncan (editor), Vol. 2, pp.273-290.

KEMPTON, J., AND STEWART, J., 2006, "Prediction equations for significant durations of earthquake ground motions considering site and near-source effects," Earthquake Spectra, Vol. 22, pp.985-1013.

KONDNER, R. L.,1963, "Hyperbolic stress-strain response: Cohesive soils." Journal of the Soil Mechanics and Foundations Division, Vol.89(SM1), pp.115-143.

KOWSMANN, R.O., MACHADO, L.C.R., VIANA, A.R., ALMEIDA JR., W., AND VICALVI, M.A., 2002, "Controls on mass-wasting in deep water of the Campos Basin," 34th Offshore Technology Conference; Houston, Texas. Richardson: Society of Petroleum Engineers, pp.1-11.

KOWSMANN, R.O., AND VIANA, A.R., 1992, "Movimentos de massa provocados por cunhas progradantes de nível de mar baixo: exemplo na Bacia de Campos," Boletim de Geociências da Petrobras, Vol.6, No.1/2, pp.99-102.

LEE, J., AND GREEN, R., 2014, "An empirical significan duration relationship for stable continental regions," Bull. Earthq. Eng., Vol.12, pp.217-235.

MAZZONI, S., MCKENNA, F., AND FENVES, G. L., 2006, "Open system for earthquake engineering simulation user manual, Pacific Earthquake Engineering Research Center," University of California, Berkeley.

RAUCH, A., AND MARTIN, J., 2000, "EPOLLS model for predicting average displacements on lateral spreads," J. Geotech. Geoenviron. Eng., Vol.146, No.4, pp.360-371.

SCHREINER, S., MENDONÇA DE SOUZA, M.B.F., MIGLIORELLI, J.P., FIGUEIREDO JR., A.G., PACHECO, C.E.P., VASCONCELOS, S.C., AND SILVA, F.T., 2015, "Bathymetric map of the Campos Basin," In: Kowsmann, R.O., editor. Geology and Geomorphology. Rio de Janeiro: Elsevier. Habitats, Vol.1, pp.67-70.

SOMERVILLE, P., SMITH, N., GRAVES, R., AND ABRAHAMSON, N., 1997, "Modification of Empirical Strong Ground Motion Attenuation Relations to Include the Amplitude and Duration Effects of Rupture Directivity," Seismological Research Letters, Vol.68, No.1, pp.199–222.

STEWART, J.P., KWOK, A.O., HASHASH, Y.M.A, MATASOVIC, N., PYKE, R., WANG, Z., AND YANG, Z., 2008, "Benchmarking of Nonlinear Geotechnical Ground Response Analysis Procedures," Pacific Earthquake Engineering Research Center Report 2008/04.

STEWART, J.P., AND LIU, A.H., 2000, "Ground motion amplification as a function of surface geology," Proc. SMIP2000 Seminar on Utilization of Strong Motion Data, California Strong Motion Instrumentation Program, Sacramento, California, pp.1–22.

TRIFUNAC, M., AND BRADY, A., 1975, "A study on duration of strong earthquake ground motion," Bull. Seismol. Soc. Am., Vol.65, pp.581-626.

VIANA, A.R., FAUGÈRES, J.C., KOWSMANN, R.O., LIMA, J.A., CADDAH, L.F., AND RIZZO, J.G., 1998, "Hydrology, morphology and sedimentology of the Campos Basin continental margin, Offshore Brazil," Sedimentary Geology. Vol.115, No.1/4, pp.133-157.

VUCETIC, M., AND DOBRY, R., 1991, "Effect of Soil Plasticity on Cyclic Response", Journal of Geotechnical Engineering, Vol.117, No.1, pp.89-107.

YANG, Z., AND ELGAMAL, A., 2003, "Application of unconstrained optimization and sensitivity analysis to calibration of a soil constitutive model," Int. J. for Numerical and Analytical Methods in Geomechanics, Vol.27, No.15, pp.1255-1316.

YI, J., LAM, N., TSANG, H.-H., AND AU, F. T., 2020, "Selection of earthquake ground motion accelerograms for structural design in Hong Kong," Advances in Structural Engineering, Vol.23, No.10, pp.2044–2056.

ZHOU, Y.G., CHEN, J., SHE, Y., KAYNIA, A., HUANG,B., AND CHEN,Y-M., 2017, "Earthquake Response and Sliding Displacement of Submarine Sensitive Clay Slopes." Engineering Geology, Vol. 227, pp.69–83

Chapter 8

Conclusions and recommendations for future research studies

8.1 Introduction

This thesis describes the results of a research into the seismic response of gentle slopes in soft clay. Based on the literature review, it was identified a gap in knowledge related to the experimental investigation of submarine slopes with small inclinations (less than 5 degrees) under seismic loading. For the purpose of the investigation, a set of dynamic centrifuge tests and numerical models was carried out. In this chapter, the most significant conclusions will be drawn from the work covered in this thesis and summarized into three major topics: model preparation methodology, results from dynamic centrifuge testing, and outcomes from numerical modeling.

8.2 Model preparation methodology

A model preparation technique was developed for simulating the dynamic response of gentle uniform and layered slopes in soft clay. The models were subjected to a series of dynamic motions to evaluate the response of the slopes in terms of displacements and propagation of accelerations. The main observations from the model preparation of the centrifuge tests are:

- The problem studied, required the selection of a suitable model container. As this research aimed at simulating the response of gentle slopes in soft clay, the model container had to properly reproduce an infinite soil deposit. Among the various containers available at the Schofield Centre, University of Cambridge, the laminar container was selected. Most of the experience using this container has been related to seismic studies throughout sand models. Therefore,

a model preparation methodology had to be developed to consider the use of clay in a laminar container. In order to sort out a series of practical issues associated to perform the consolidation of the clay inside the laminar container, a strongbox with the same dimensions as the laminar container but deeper was employed. A series of stages was presented, including details about the installation of the instruments and of the centrifuge experiments. This information should be valuable for similar testing programs. The in-flight characterization of the uniform slope profiles, built under similar conditions, evidenced the repeatability of the experiments and it allowed direct comparisons of both models in which the difference was the slope inclination.

- The proposed model preparation technique enabled the simulation of uniform and layered soil profiles in clay. In the case of the weak layered model, a strength contrast between layers was achieved by applying different consolidation pressures during the sample preparation process. From the post-test investigations, no discontinuities were observed between the layers, indicating a successful sample preparation process, particularly for this more complex test.

- As a complementary tool to monitor the displacements of the slopes at different depths in the centrifuge experiments, the PIV technique was employed. The specifications of the camera and methodology used to capture images at high frequencies were presented. The usage of ArUco markers ensured a good accuracy in the tracking process of the markers as it was confirmed when the PIV displacements were compared with measurements from the LVDTs. Then, it is recommended to employ this type of markers for similar experiments involving the use of laminar containers. Accelerations were calculated by double differentiation of the displacement time-histories obtained from PIV analysis. A reasonable agreement was also observed between the accelerations calculated from PIV and the recordings of the accelerometers.

8.3   Dynamic centrifuge testing

In this thesis, the results from three centrifuge tests were presented: two tests simulated uniform soil profiles with inclinations of three degrees and six degrees, and one experiment reproduced a three-degrees slope with a weak layer. The principal findings are as follows:

Uniform profile models

- The measured soil properties for undrained shear strength and shear wave velocity were in good agreement with empirical predictions. Shear wave veloc-

ities were obtained by means of Air Hammer testing. The air hammer in clay models is typically placed at the bottom of the model, before the consolidation. However, considering the model preparation methodology the installation of the instruments had to occur at the end of the consolidation of the clay. For the experiments performed, the air hammer was placed at the top of the clay, simulating the conditions of a downhole test. The results obtained were in reasonable agreement with the empirical relationships and both approaches were complementary to achieve a more complete characterization of the dynamic properties of the models. It is worth to point out that there are uncertainties in the air hammer test, mainly associated to the exact locations of the instruments as they are affected by the permanent deformations that occur during the centrifuge experiment.

- Using the recorded accelerations of the model, it was possible to evaluate the model container performance. From previous studies (Brennan *et al.*, 2006) boundary effects have been assessed for models in sand. No information about boundary effects of the laminar model container used for models in clay was available. By means of spectral analysis, 5% damped spectral accelerations at the center of the model and near the walls of the model container were compared. These comparisons made for a low-intensity and a large-intensity ground motion displayed an excellent agreement. This indicated that the laminar model container produced adequate boundary conditions for the simulation of infinite slope models.

- Two models were prepared under similar conditions to evaluate the seismic response of gentle slopes in soft clay and in a uniform profile. Two slope inclinations were investigated, a three-degree slope and a six-degree. The characterization of the models evidenced the repeatability of the experiments and allowed their direct comparison in terms of amplification of PGA and lateral displacements. From the results, it was evident the influence of the slope inclination on the development of lateral displacements. On average, permanent displacements measured from the six-degree slope (0.30 m) were around three times the measured from the three-degree slope (0.09 m). Regarding the amplification of the PGA, comparisons were made with empirical relationships to predict amplification factors as a function of surface geology. The results from the centrifuge tests showed an attenuation pattern of the PGA at the surface as the slope angle and input PGA were increased.

- Pore pressure measurements revealed one limitation of the current experimental program. From the results of the uniform slope profiles, no particular trend

was observed in the pore pressures during the earthquake shakings. One explanation could be associated with the model preparation methodology, as it did not consider placement of the instruments during consolidation in order to prevent damage to the wiring. The pore pressure transducers were installed after consolidation of the clay by excavating small boreholes. After the instruments were positioned at the desired depths the void space was back-filled with slurry. Subsequently, the results suggest not an adequate contact between the clay and the ceramic stone of the pore pressure transducers.

- The results from the dynamic centrifuge tests provided useful information into the seismic response of gentle slopes in soft clay. They represent the opportunity of having measured data in the form of lateral displacements and accelerations at different depths.

Weak layered profile models

- The measured soil properties for undrained shear strength and shear wave velocity obtained during the weak layered profile test, showed a reasonable agreement with the empirical predictions. A strength contrast between soil layers was achieved to simulate the target profile.

- From the weak layered profile experiment, further information was extracted. Approximated accelerations at different depths were obtained by double differentiation of PIV displacements and compared with those from the accelerometers. Additional frequencies were observed from the sinusoidal motions applied to the models, those frequencies are attributed to higher vibration modes of the shaker. The spectral analysis showed amplifications at periods corresponding to the fundamental period of the soil profile during the low-amplitude input ground motions. A shift in the elastic site period was observed during the largest amplitude earthquake applied to the model, indicating a nonlinear behavior of the slope profile.

- The spectral analysis showed amplifications at periods corresponding to the fundamental period of the soil profile during earthquakes EQ2 and EQ3. A shift in the period occurred during the largest amplitude earthquake (EQ4), indicating a nonlinear behavior of the slope profile.

8.4   Numerical modelling of gentle slopes in soft clay

Two series of numerical analyses were performed in this thesis; the first was aimed to simulate one of the centrifuge tests, and a second set comprised parametric

analyses applied to a real scenario. OpenSees was employed to simulate the response of the numerical models. Based on the numerical studies, the following conclusions can be derived:

- The preliminary numerical simulations performed to evaluate the response of the slope subjected to the lowest amplitude and broad frequency input ground motion provided relevant information that allowed the adjustment of the shear wave velocity profile. Comparisons were undertaken in terms of experimental and measured transfer functions, 5% damped spectral accelerations and surface accelerations. By employing in the numerical model the initial shear wave velocity characterization back-calculated from the OCR profile, larger accelerations were observed at the top of the model when compared with the measured records. In addition, a shift between the measured and numerical spectral accelerations and the base to surface transfer function was observed. After several trials, the shear wave velocity profile that yielded better results was the one that consisted of reducing by 15% the initial shear wave velocities. This means that soil characterization from the centrifuge experiments can be complemented with the information from numerical simulations.

- The numerical models of the centrifuge experiment presented in Chapter 6 performed well for the low-amplitude earthquakes. For the large-amplitude shakings, considerable differences were observed in the lateral displacement-time histories and a mismatch between the recorded and calculated accelerations. The results were improved by applying factors to increase the undrained shear strength based on the strain rate effects. One explanation is the strain rates in the model scale are N time the strain rates in the prototype, this means that centrifuge modelling is limited in satisfying strain rate scaling (Taylor, 1995). After applying corrections of the shear strength to account for strain rate effects, the performance of the models for the large amplitude ground motions was considerably improved, showing a more reasonable agreement with the measured response of accelerations and lateral displacements. This means the clay does not exhibit a particular dynamic strength, instead, it has a strength dependent on the earthquake shaking.

- Additional numerical analyses were carried out with the calibrated model based on one of the centrifuge experiments presented in this thesis. The results of the complementary numerical models were in good agreement with the experimental data, particularly in terms of lateral displacements.

- From the case study focused on the Offshore Campos Basin, it was identified a lack of recordings of strong ground motions in the area of interest. As an

alternative, a methodology to obtain spectrum compatible earthquake records was employed based on a recently developed Mean Uniform Hazard Spectra for the continental slope of the Campos Basin (Borges *et al.*, 2020). The PEER NGA-West database was the base for the selection of the earthquake ground motions, as the PEER NGA-East yielded a limited number of recordings based on a preliminary search. From the PEER NGA-West database, significant duration was employed as search criteria for earthquake records. The significant duration for the area of interest was obtained by applying an empirical correlation developed for stable continental regions (Lee and Green, 2014).

- Using the spectrum compatible records, a parametric numerical analysis was performed. Parameters as the undrained shear strength and shear wave velocity profiles were defined based on previous studies aimed to assess the static stability of slopes on the continental slope of the Campos Basin (Borges *et al.*, 2015; Borges *et al.*, 2020b). From the parametric numerical studies applied to conditions representative of the Offshore Campos Basin, other variables as the depth to bedrock and slope inclination were considered. The slope angle indicated a remarkable effect on the behavior of the slopes in terms of displacements and shear strains. The mechanism associated is an accumulation of displacements in the downslope direction, as the earthquake occurs. The depth to bedrock also displayed an effect on the seismic response of gentle slopes. It was observed that as the depth to bedrock was increased, the ´permanent lateral displacements were also raised.

8.5   Recommendations for future research

The seismic behavior of submarine slopes is very complicated, and little or no data from field investigations are available in the literature. This thesis is able to provide a methodology for the preparation of models in soft clay and a database of the seismic behavior of gentle slopes for future research works. Some suggestions for forthcoming studies related to the dynamic response of gentle slopes are:

- To perform centrifuge experiments considering configurations such as the presence of liquefiable sand layers.

- To develop a database of the results of the current testing program and similar dynamic centrifuge investigations using Speswhite kaolin and the previous experience from downhole arrays in field experiments to develop experimental modulus and damping curves. This information could be relevant to calibrate numerical models.

- With the model preparation methodology to include soil profiles in clay in the laminar container, there is a possibility to perform centrifuge tests to incorporate structural elements to evaluate the soil/structure interaction considering sloping grounds. For example, individual piles, pile groups, or pipelines could be installed in such profiles.

- Further improvements need to be evaluated in the PPTs installation methodology to achieve a more adequate response from those instruments.

- Although the numerical simulations showed a good agreement with the centrifuge results. Various aspects could be improved, for instance, the use of more sophisticated constitutive models (Dafalias *et al.*, 2006; Boulanger and Ziotopoulou, 2019). The availability of measured data from gentle slopes in soft clay under seismic loading introduces the possibility to calibrate and evaluate those constitutive models or more advanced numerical approaches.

- Comparisons between defined methodologies to obtain seismic displacements in slopes (i.e. Newmark's method) and the measured response from the centrifuge experiments could be performed.

- To apply the framework presented in this work, related to the seismic hazards in Southeastern Brazil to evaluate the liquefaction potential in submarine gentle slopes and seabed deposits.

8.6   Chapter 8 references

BORGES, R.G., ASSUMPÇAO, M.S., ALMEIDA, M.C.F., ALMEIDA., AND M.S.S., 2020, "Seismicity and seismic hazard in the continental margin of southeastern Brazil," J. Seismol, Vol.24, pp. 1205-1224.

BORGES, R., SOUZA JUNIOR, L., ALMEIDA, M.C.F., AND ALMEIDA, M.S.S., 2020b. "Relationship Between Shear Wave Velocity and Piezocone Penetration Tests on the Brazilian Continental Margin," Soils and Rocks. Vol.43(2), pp.219-230.

BOULANGER, R. W., AND ZIOTOPOULOU, K., 2019, "A constitutive model for clays and plastic silts in plane-strain earthquake engineering applications." Soil Dynamics and Earthquake Engineering, Vol.127.

BRENNAN, A. J., THUSYANTHAN, N. I. AND MADABHUSHI, S. P. G., 2005, "Evaluation of shear modulus and damping in dynamic centrifuge tests," Journal of Geotechnical and Geoenvironmental Engineering, Vol. 131, No. 12, pp-1488–1498.

DAFALIAS, Y.F., MANZARI, M.T. AND PAPADIMITRIOU, A.G. ,2006, "SANICLAY: simple anisotropic clay plasticity model," Int. J. Numer. Anal. Meth. Geomech., Vol.30, pp.1231-1257.

LEE, J., AND GREEN, R., 2014, "An empirical significan duration relationship for stable continental regions," Bull. Earthq. Eng., Vol(12), pp.217-235.

TAYLOR, R.N. 1995. Geotechnical Centrifuge Technology. Blackie Academic and Professional.

Appendix A

Pore pressure measurements during swing up

Figure A.1 presents the excess pore pressures during the swing up of the three-degrees slope model presented in Chapter 4. The data is presented in terms of model scale. The model reached the acceleration level of 60g in minute 18. The consolidation lasted around 40 minutes. From the results, it can be observed a relative stabilization of the pore pressures during the consolidation time.
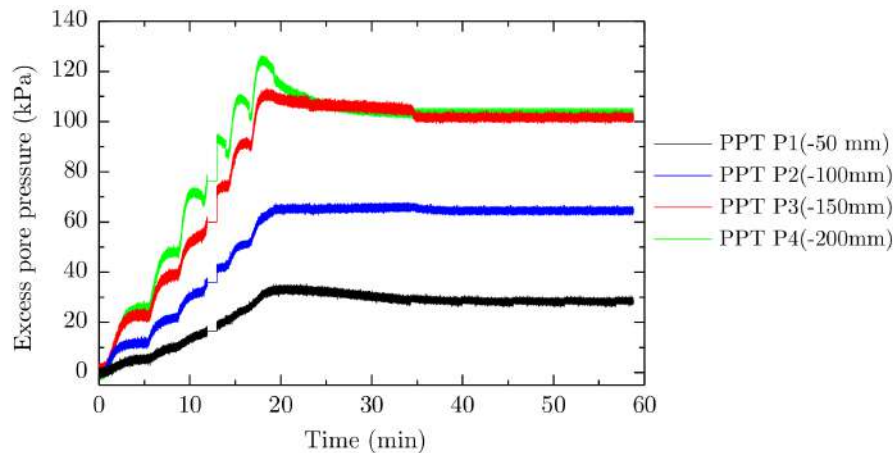
Figure A.1: Excess pore pressures monitoring for the three-degrees model during swing up.

Figure A.2 displays the excess pore pressures during the swing up of the model corresponding to the six-degrees slope. The results are shown in terms of model scale. The model was kept in consolidation for about 40 minutes, similarly to the three-degrees slope model. The order of magnitude of the excess pore pressures is similar for both tests, reaching a maximum value of 130 kPa for the PPT P4, the deepest PPT. The results show that there was not a clear trend of stabilization as the previous experiment (Figure A.1). A complete dissipation of the excess pore pressures represents a challenge in centrifuge testing in clay. For that reason, the

measurement of the undrained shear strength profile by means of the T-bar tests, was the primary criteria to define a snapshot of the state of stresses of the soils tested prior to the application of the earthquakes. The undrained shear strength profiles measured for both tests, built under similar conditions, were consistent. Then, as explained in Chapter 4, a direct comparison of the dynamic response of the three-degrees and six-degrees models was performed to assess the effects of the slope inclination.
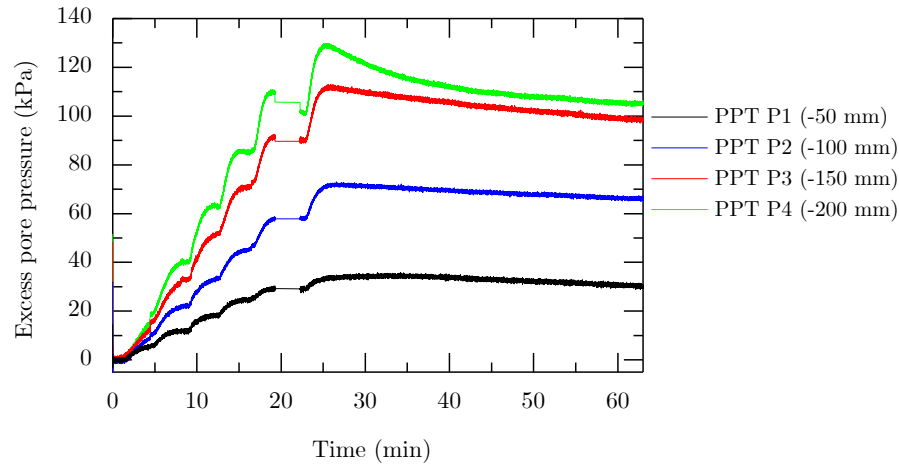
Figure A.2: Excess pore pressures monitoring for the six-degrees model during swing up.

Appendix B

Related publications

INTERNATIONAL SOCIETY FOR SOIL MECHANICS AND GEOTECHNICAL ENGINEERING

Geotechnical Engineering in the XXI Century: Lessons learned and future challenges
N.P. López-Acosta et al. (Eds.)
477

Simulation of a Weak Layered Profile Using Geotechnical Centrifuge

Cristian Yair SORIANO[a], Renan Bezerra de ANDRADE[a], Samuel Felipe MOLLEPAZA[a], Márcio de Souza Soares de ALMEIDA[a], Maria Cascão Ferreira de ALMEIDA[b], José Renato Moreira da Silva de OLIVEIRA[a,1] and Pablo Cesar TREJO[a]

[a]*COPPE, Federal University of Rio de Janeiro, Rio de Janeiro, Brazil*
[b]*ESCOLA POLITÉCNICA, Federal University of Rio de Janeiro, Rio de Janeiro, Brazil*

Abstract. Recent site investigations carried out on submarine slopes at Campos Basin offshore of Rio de Janeiro, Brazil detected the presence of weak subsurface layers, which leads to a contrast in resistance of about 30% between the layers. This research aims to replicate the field conditions by creating a clay profile of a weak layer between two strong layers using a geotechnical centrifuge. Speswhite kaolin was used to simulate the marine soil and a mixture of kaolin-bentonite was used as weak layer. Several consolidation and centrifuge tests were carried out in different proportions to simulate the actual field condition. Addition of bentonite to the Speswhite kaolin was found to increase the compressibility and reduce the soil resistance due to its expansive properties. Finally, a three layered profile was selected to simulate the field condition. Both T-bar and cone penetration tests were carried out to measure contrast in the undrained shear strength due to presence of the weak layer.

Keywords. Submarine slopes, weak layers, geotechnical centrifuge, kaolin-bentonite mixture, undrained shear strength.

1. Introduction

Weak layers can play a major role in the development of many submarine landslides. Locat et al.[1] define a weak layer as a layer (or band) consisting of rock or sediment that has strength potentially or actually sufficiently lower than its adjacent units (strength contrast). Shear strength contrast between weak layers and bordering layers of about 50% is not uncommon [2-4].

The understanding of many aspects of submarine landslides, including the location and deduction of weak layers is commonly based on hypothesis, observation and interpretation [5]. The Storegga slide [6], the Nice airport failure [7]and submarine landslides in the fjords [8, 9] are few cases found in the literature that included direct sampling.

Offshore site investigations carried out in anoffshore Brazilian slope detected the presence of a weak subsurface layer. A borehole was drilled in a region composed mainly of submarine canyons in the continental slope located at the north side of the Campos Basin, close to the limits of the estates of Rio de Janeiro and Espírito Santo. Figure 1 shows the undrained shear strength profile and the evidence of strength

---

[1] Corresponding Author, E-mail: jrmso70@gmail.com

contrast between soil layers. The borehole was executed in a region corresponding to a gentle slope (about 4°). Two types of mud layers were identified at the site. A superficial layer of about 28 m was found over a pre-consolidated older deposits of mud. Figure 1a shows a decrease in the undrained shear strength value (about 30%) between 28 m and 33 m, which proves the existence of a potential weak layer.
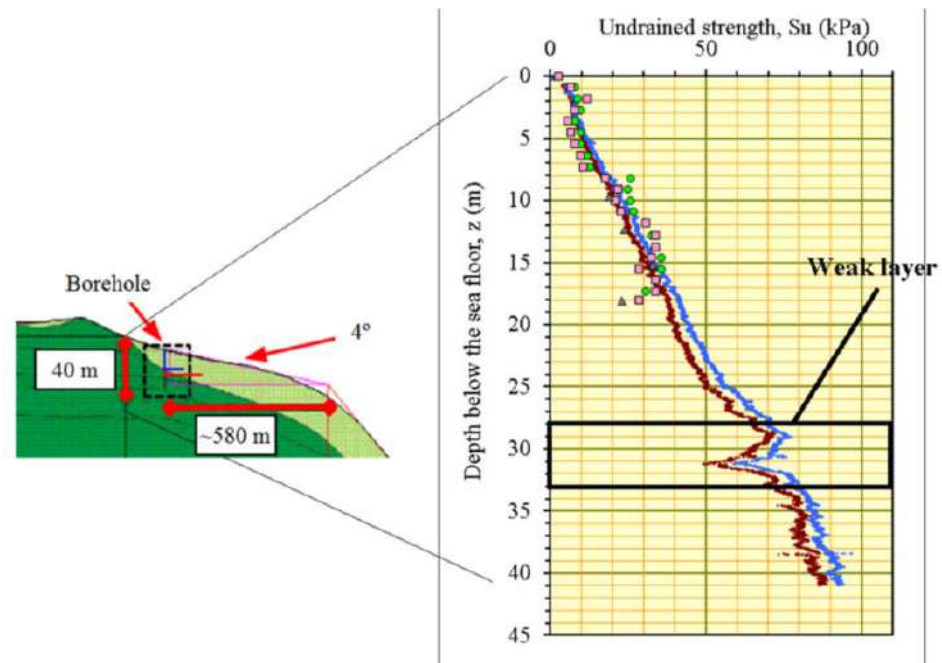
Figure 1. Detail of undrained shear strength profile and evidence of strength contrast between soil layers.

This paper aims to replicate the similar offshore slope at Campos Basin in a geotechnical centrifuge, by creating a clay profile consisting of a weak layer between two stronger layers. Speswhite kaolin was chosen to simulate the marine soil. A mixture of kaolin and bentonite was proposed to simulate the weak layer. The addition of bentonite to the Speswhite kaolin was expected to increase compressibility and reduce soil resistance due to its expansive properties. Four different kaolin-bentonite mixtures were tried in order to determine the mixture that best fits the in-situ condition. Finally, a three layered soil model was tested in the geotechnical beam centrifuge at COPPE/UFRJ to measure the variation of undrained shearstrength with depth by means of T-bar and cone penetration tests.

2. Materials

2.1. Kaolin and Bentonite

The kaolin clay (K) used in the tests is commercially known as Speswhite, which is a highly refined kaolin of ultrafine particle size and high brightness, originated from the southwest of England. This material widely used in research projects involving physical modelling, due to its well documented properties and availability of comparative data sets [10-14].

The bentonite (B) used in the preparation of the mixtures (K+B) with kaolin is an industrial Brazilian sodium montmorillonite commercially known as Brasgel™ [15, 16]. The chemical composition of Brasgel™ bentonite was obtained by performing tests of solubilisation with sulfuric acid. The bentonite is composed of predominantly SiO_2 (silica or silicon dioxide) and Al_2O_3 (aluminum oxide). It also contain iron in the form of Fe_2O_3 (iron III oxide or hematite).

Four different mixtures were prepared according to the following proportions (dry weight basis), as shown in Table 1.

Table 1. Proposed kaolin+bentonite mixtures (dry weight basis).

Mixture	Proportions
M1	95.0 % kaolin (K) + 5.0 % bentonite (B)
M2	92.5 % kaolin (K) + 7.5 % bentonite (B)
M3	90.0 % kaolin (K) + 10.0 % bentonite (B)
M4	90.0 % kaolin (K) + 10.0 % bentonite (B)

Grain size distribution and Atterberg limits tests were performed according to the Brazilian standards. Oedometer tests were performed for virgin kaolin and for the mixtures of kaolin and bentonite. The samples were prepared with a water content equivalent to 1.5 times the Liquid Limit (W_L). Table 2 shows a summary of the geotechnical properties of the materials.

Table 2. Kaolin, bentonite and mixtures soil characterization and oedometer test parameters.

	Sample					
Property	Kaolin (K)	Bentonite (B)	M1	M2	M3	M4
Atterberg limits						
Liquid limit w_L (%)	62	441	65	70	73	84
Plastic limit w_P (%)	23	59	27	31	29	24
Plasticity index PI (%)	39	382	38	39	44	60
Oedometer test						
Water content w (%)	93,0	-	97,5	105,0	109,5	126,0
Initial void ratio e_0	2,43	-	2,54	2,78	2,83	3,37
Compression index Cc	0,44	-	0,51	0,56	0,57	0,73
Compression index $C_C/(1+e_0)$	0,13	-	0,14	0,15	0,15	0,17

2.2. COPPE's Beam Centrifuge

During the first stage of the weak layers research project, centrifuge tests were performed in the mini geotechnical beam centrifuge [17, 18] installed at the Alberto Luiz Coimbra Institute for Graduate Studies and Research in Engineering (COPPE) located in Rio de Janeiro, Brazil.

The mini-beam centrifuge at COPPE has a working radius of 0.66 m and can reach a maximum acceleration of 300 g (9 g-ton at 368 rpm). Figure 2 presents the main dimensions and a photo of the beam centrifuge.
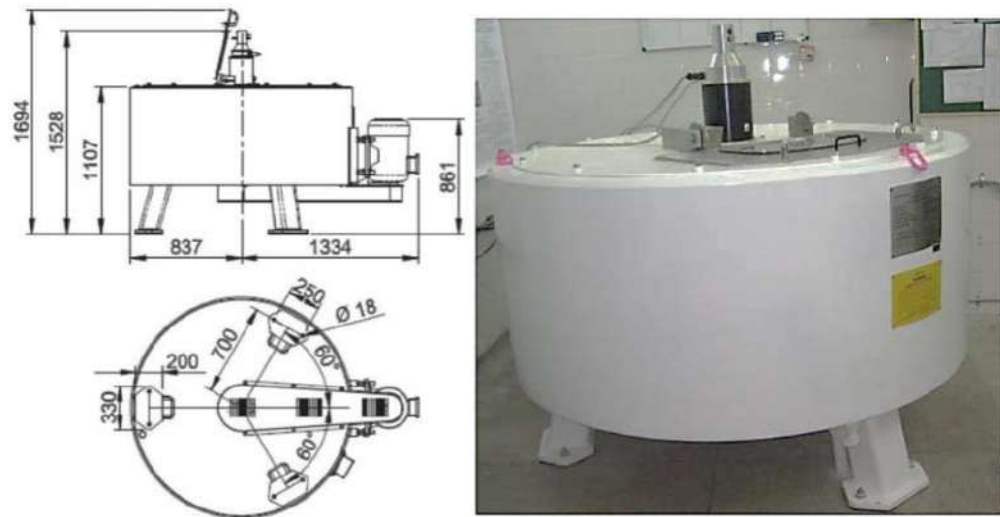
Figure 2. Dimensions and photo of COPPE mini-beam geotechnical centrifuge.

2.3. Centrifuge Equipment

The soil samples used for the centrifuge tests were placed in a 2-D plane strain model container (0.10 m wide, 0.30 m long and 0.18 m high) made from high tensile aluminium.

A mini T-bar penetrometerwas developed to measure continuous shear strength profiles [19]. A mini cone penetrometer having 60° conical tip and 10-mm diameter was also developed for this study. Cone penetration test (CPT) is useful to delineate soil layering, to find the nonhomogeneity within soil layers, and to compare the results with required prototype conditions [20].The dimensions of the T-bar and the mini CPT used in this study are shown in Figures 3a and 3b respectively.
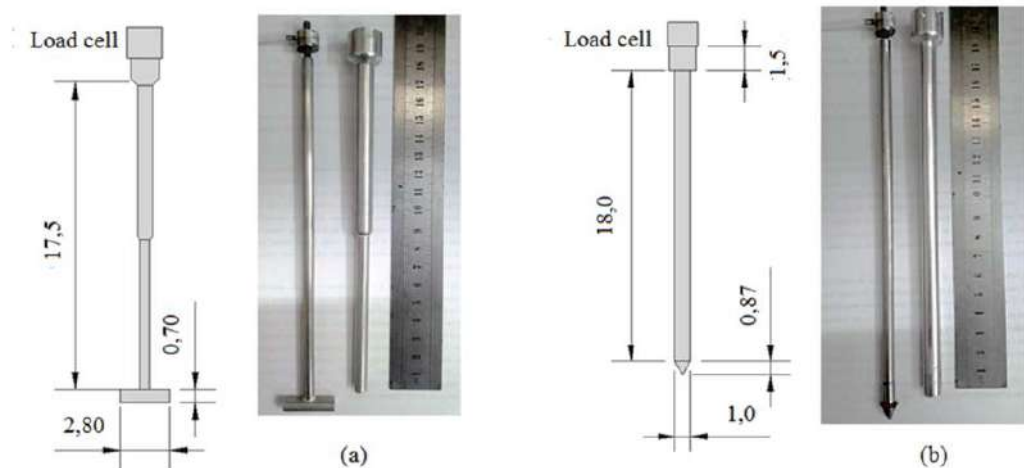
Figure 3. T-bar penetrometer (a) and mini CPT (b) developed for centrifuge tests (dimensions in centimetres).

The undrained shear strength profiles (S_u) are obtained by measuring the vertical force on the load cell installed on top of the T-bar using the Eq.(1) proposed by

Randolph and Housby [21]. The N_b factor recommended by the authors is equal to 10.5 for a bar with average roughness (α=0.5).

$$S_u = \frac{F_v}{N_b DL} \tag{1}$$

where F_v is the measured vertical force, D is the rod diameter (0.7 cm), L is the length of the T-bar (2.8 cm) and N_b=10.5 is the T-bar factor.

3. Methodology

3.1. Model Preparation Technique

The soil sample was composed of three layers. Each layer was placed in the centrifuge container using clay lumps technique. Figure 4 illustrates the clay lumps placed in the model container.

| (a) | (b) |

Figure 4. Centrifuge strong box (a) before and (b) after the clay lumps placing.

A mixture of 90%K and 10%B was chosen to perform the centrifuge tests due to better workability of the mixture. Higher bentonite content (i.e. 15%B) found to produce very soft slurry for the same water content, which collapsed under their own weight. On the other hand, lower percentage of bentonite produced stiffer mixtures reducing their potential effects in simulating the expected strength contrast between the soil layers.

The consolidation of the model was divided into three different stages. First each layer was placed using the clay lumps method, and then they were subjected to a consolidation process as described below. The initial and final height of the model were measured in each step to monitor the settlements during each consolidation phase.

Layer 1: Consists of kaolin with a water content of 1.3 w_L. The initial height of the soil layer before consolidation was 12.2 cm. A steel plate of 1.1 kg was placed on top of the sample to produce a surcharge of 33 kPa to allow the collapse and consolidation of the clay lumps during centrifuge acceleration.The soil sample was subjected to an acceleration of 100 G for 18 hours in the centrifuge.

Layer 2: Composed of a mixture of kaolin and bentonite (90%K+10%B) with a water content of 1.3 w_L. The initial height of the layer before consolidation was 8.4 cm.

The sample was subjected to consolidation under a surcharge of 1.1 kg steel plate at 100G acceleration for 20 hours in the centrifuge.

Layer 3: The top layer was composed of kaolin clay with a water content of 1.3 w_L. The initial height of this layer before consolidation was 9.0 cm. The same method of clay lumps was used to buildthis layer. To achieve the consolidation of the sample, a 1.1 kg steel plate was placed on top of the model and the soil sample was subjected to a 100G acceleration for 24 hours. The second phase of the consolidation was carried out using a 4.2 kg steel plate and subject the soil sample to a 100G acceleration for 24 hours. A total vertical stress of about 138 kPa was applied on top of the sample. An extension piece of the model container made up of acrylic was used to contain the extra height of soil prior to the consolidation.

3.2. Actuation Phase

Model actuation was performed under a centrifuge acceleration of 50G to better simulate the dimensions of the real problem. Two T-bar tests and one Cone Penetration Test were carried out. The positions of the different tests are shown in Figure 5.
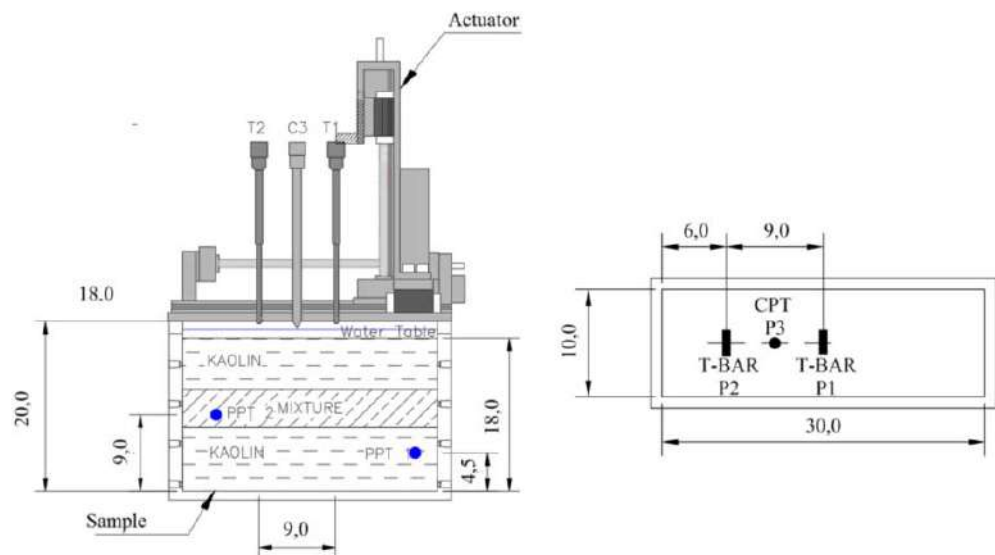
Figure 5. Actuator and location of T-bar and Cone tests.

4. Results and Discussion

Figure 6 presents the undrained shear strength (S_u) profiles of the soil sample. From the figure the location of simulated "weak layer" (mixture of kaolin and bentonite) can be identified. From T-bar test at P1 a drop in undrained shear strength of about 8kPa can be observed between Layer 1 and the weak layer. Shear strength profile from T-bar test at P2 shows a drop of about 4 kPa and a slight variation was observed in case of CPT test. The obtained shear strength contrast was about15% to 30% in case of T-bar tests. This behavior is well compared to the 30% decrease in in-situ S_u value.
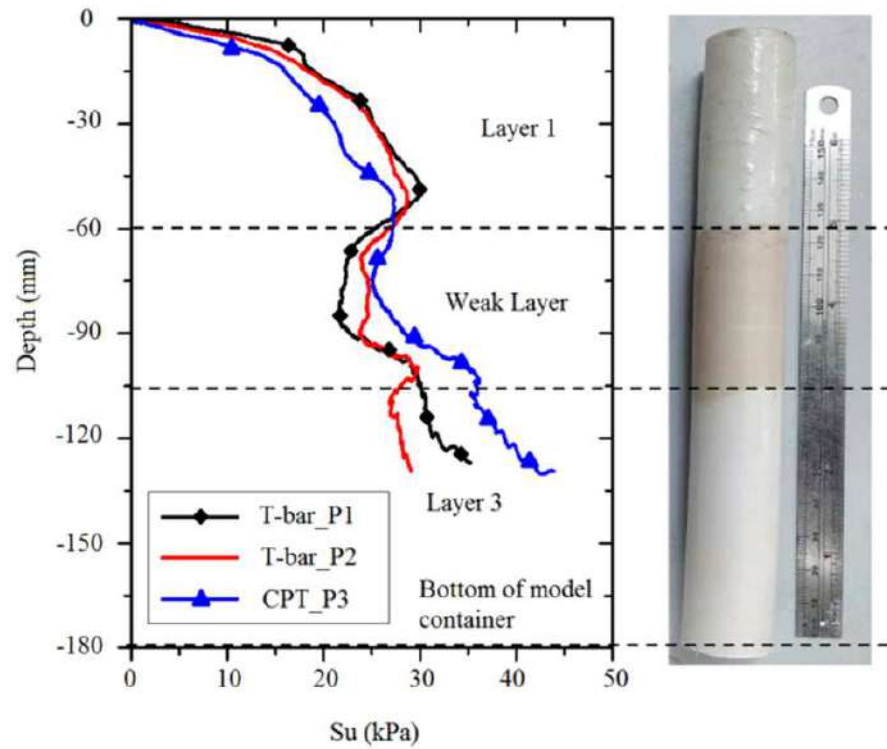
Figure 6. Shear strength profiles using CPT and T-Bar tests.

5. Conclusions

The proposed experimental procedure helps to simulate the contrast in the shear strength profile due to the presence of the weak layer.

The contrast in the shear strength was observed in both T-bar and cone penetration tests.

The reduction in the undrained shear strength due to mixing of bentonite (PI=382%) with kaolin clay (PI=39%) can be explained due to increase in plasticity of the sample (PI=44%). In addition, the bentonite, could have reduced the permeability of the virgin kaolin, leading to a contrast in the degrees of consolidation between the soil layers.

The in-flight consolidation of the model by using the clay lumps technique was found to be time consuming (about 4 days of continuous use of the centrifuge). Alternative 1-g consolidation methods needs to be considered taking into account the procedures, equipment, instrumentation and model container characteristics.

Acknowledgements

References

[1] J. Locat, S. Leroueil, A. Locat and H. Lee, Weak Layers: Their definition and classification from a geotechnical perspective. Submarine Mass Movements and Their Consequences, *Advances in Natural and Technological Hazards Research* 37 (2014), 3-11.

[2] J.S. L'Heureux, O. Longva, A. Steiner, L. Hansen, M. Vardy, M. Vanneste, H. Haflidason, J. Brendryen, T. Kvalstad, C. Forsberg, S. Chand and A. Kopf, Identification of weak layers and their role for the stability of slopes at Finneidfjord, Northern Norway, *Submarine Mass Movements and Their Consequences,* Springer, Netherlands (2012), 321-330.

[3] A. Steiner, J.S. L'Heureux, A. Kopf, M. Vanneste, M. Lange and H. Haflidason, An in-situ free-fall piezocone penetrometer for characterizing soft and sensitive clays at Finneidfjord, northern Norway, *5th International Symposium on Submarine Mass Movements and Their Consequences*, Springer, Dordrecht, Kyoto, Japan (2012), 99-109.

[4] R. Rodríguez-Ochoa, F. Nadim and M.A. Hicks, Influence of weak layers on seismic stability of submarine slopes, *Marine and Petroleum Geology* 65 (2015), 247-268.

[5] D.G. Masson, R.B. Wynn and P.J. Talling, Large landslides on passive continental margins: processes, hypotheses and outstanding questions, *Submarine mass movements and their consequences. Advances in natural and technological hazards research* 28 (2010), 153–165.

[6] T.J. Kvalstad, L. Andresen, C.F. Forsberg, P. Bryn and M. Wangen, The Storegga slide: evaluation of triggering sources and slide mechanics, *Marine and Petroluem Geology* 22 (2005), 245-256.

[7] G. Dan, N. Sultan and B. Savoye, The 1979 nice harbour catastrophe revisited: trigger mechanism inferred from geotechnical measurements and numerical modelling, *Marine Geology* 245 (2007), 40–64.

[8] L. Hansen, J.S. L'Heureux and O. Longva, Turbiditic, clay-rich event beds in fjord-marine deposits caused by landslides in emerging clay deposits – palaeoenvironmental interpretation and role for submarine mass-wasting, *Sedimentology* 58 (2011), 890–915.

[9] C. Levesque, J. Locat, R. Urgeles and S. Leroueil, Preliminary overview of the morphology in the Saguenay Fjord with a particular look at mass movements, *Proceedings of the 57th Canadian geotechnical conference* 6, Quebec (2004), 23–30.

[10] R.J. Mair, Centrifugal Modelling of Tunnel Construction in Soft Clay, *Ph.D. thesis, University of Cambridge*, Cambridge, UK (1979).

[11] J.P. Love, Model Testing of Geogrids in Unpaved Roads, *Ph.D. thesis, University of Oxford*, Oxford, UK (1984).

[12] M.S.S. Almeida, Stage constructed embankments on soft clays", *Ph.D. Thesis, University of Cambridge*, Cambridge, UK (1984).

[13] S.H. Kim, Model Testing and Analysis of Interactions between Tunnels in Clay", *Ph.D. thesis, University of Oxford*, Oxford, UK (1996).

[14] M. Williamson, Tunnelling effect on bored piles in clay", *Ph.D. thesis. University of Cambridge*, Cambridge, UK (2014).

[15] R. Ferraz, Acoplamento dos Processos do Adensamento e do Transporte de Contaminantes em Solos Compressíveis, *Ph.D. thesis, COPPE/UFRJ*, Brazil (2006).

[16] T.L.C. Morandini and A.L. Leite, Characterization and Hydraulic Conductivity of some Tropical Soils Samples and Bentonite Mixtures for CCL Purposes, *Engineering Geology* 196 (1) (2015), 251-267.

[17] M.S.S. Almeida, M.C.F. Almeida and J.R.M.S. Oliveira, Twenty years of Centrifuge Modeling at the Federal University of Rio de Janeiro, *3rd European Conference on Physical Modelling in Geotechnics Eurofuge*, Nantes (2016).

[18] M.S.S. Almeida, M.C.F. Almeida, P.C. Trejo, K.H. Rammah, J.A. Lukiantchuki, M.P.P. Guimarães, and J.R.M.S. Oliveira The geotechnical beam centrifuge at COPPE centrifuge laboratory, Perth, *Physical Modelling in Geotechnics*, London (2014).

[19] D.P. Stewart and M.F. Randolph, A new site Investigation tool for the centrifuge, *Proceedings International Conference on Centrifuge Modelling – Centrifuge '91*, Boulder, Colorado (1991), 531-538.

[20] M.D. Bolton, M.W. Gui, J. Garnier, J.F. Corte, G. Bagge, J. Laue and R. Renzi, Centrifuge cone penetration tests in sand, *Géotechnique*, 49 (4) (1999), 543–552.

[21] D.P. Stewart and M.F. Randolph, A new site Investigation tool for the centrifuge, *Proceedings International Conference on Centrifuge Modelling – Centrifuge '91*, Boulder, Colorado (1991), 531-538.

Cristian Soriano,[1] Maria Cascão Ferreira de Almeida,[2] S. P. Gopal
Madabhushi,[3] Sam Stanier,[4] Marcio de Souza Soares de Almeida,[5]
Huida Liu,[6] and Ricardo Garske Borges[7]

Seismic Centrifuge Modeling of a Gentle Slope of Layered Clay, including a Weak Layer

581

212

Cristian Soriano,[1] Maria Cascão Ferreira de Almeida,[2] S. P. Gopal Madabhushi,[3] Sam Stanier,[4] Marcio de Souza Soares de Almeida,[5] Huida Liu,[6] and Ricardo Garske Borges[7]

Seismic Centrifuge Modeling of a Gentle Slope of Layered Clay, including a Weak Layer

C23

Reference

[1] Graduate School of Engineering, COPPE, Federal University of Rio de Janeiro, Avenida Pedro - Calmon Cidade Universitaria, Rio de Janeiro 21941596, Brazil (Corresponding author), e-mail: cysorianoc@coc.ufrj.br, https://orcid.org/0000-0001-9530-0185

[2] Polytechnic School of Engineering – Poli, Federal University of Rio de Janeiro, Avenida Pedro Calmon Cidade Universitaria, Rio de Janeiro 21941596, Brazil, https://orcid.org/0000-0002-3133-6098

[3] Department of Engineering, University of Cambridge, Trumpington St., Cambridge CB2 1PZ, UK, https://orcid.org/0000-0003-4031-8761

ABSTRACT

This article presents a model preparation methodology for simulating the seismic behavior of a gentle slope in clay with the presence of a soft, weak layer employing centrifuge testing. The model consisted of a three-layered slope of relatively soft clay with a 3° inclination, representative of Brazilian marine subsoils. In-flight characterization of the undrained shear strength and shear wave velocity profiles were achieved through T-bar penetrometer and air hammer tests. The model was subjected to a series of earthquake simulations at different amplitudes, and the response was tracked with accelerometers and displacement transducers. Additional data were obtained using a particle image velocimetry (PIV) methodology also described in this work. The results show that the proposed model preparation methodology enables the simulation of the strength contrast between the weak and relatively stronger surrounding layers using a laminar container. The additional displacement and acceleration data obtained from the PIV were in good agreement with the corresponding displacement transducer and accelerometer measurements. From the spectral analysis, a shift in the fundamental period was observed as the strain amplitude was increased, suggesting that strain rate effects mobilize higher stresses and a strength rate correction should be considered for the calibration of numerical models and comparison with existing methods for calculation of dynamic displacements in slopes.

Keywords

seismic response, centrifuge modeling, soft clay, submarine slope, weak layer

1

[4] Centre for Offshore Foundations, University of Western Australia, M053, Civil Engineering Building, Crawley, Western Australia 6009447571092, Australia, 🄳 https://orcid.org/0000-0001-5671-2902

[5] Graduate School of Engineering, COPPE, Federal University of Rio de Janeiro, Avenida Pedro Calmon - Cidade Universitaria, Rio de Janeiro 2194159, Brazil, 🄳 https://orcid.org/0000-0003-2230-397X

[6] China Construction Infrastructure Co., Ltd., Chegongzhuang St., Xicheng District, Beijing 100044, China

[7] Petrobras, Research and Development Center – CENPES, Av. Horácio Macedo, 950 - Cidade Universitária da Universidade Federal do Rio de Janeiro, Rio de Janeiro 21941915, Brazil, 🄳 https://orcid.org/0000-0001-7623-0337

Introduction

31

The continental slope in the southern and southeastern regions of Brazil is relatively uniform over long distances, being disturbed only by some widely spaced surface geological features. In the Campos Basin, located on the continental margin of Southeastern Brazil, pelagic and hemipelagic sedimentation are predominant, with an average accumulation rate of 0.064 m/1,000 years (Kowsmann, Lima, and Vicalvi 2016). The deposition of fine materials at such low rates leads to the formation of parallel layers of normally consolidated to lightly overconsolidated, soft cohesive deposits ranging in depth from a few meters to hundreds of meters (Biscontin and Pestana 2006). The slope inclination in those cases is small with typical values of less than 5°. These slopes are theoretically stable under gravity loads because of strength gains during the low rates of sedimentation of the materials. However, large-scale submarine landslides around the world have occurred in slopes with similarly low gradients (Hühnerbach and Masson 2004).

In such offshore areas with low sedimentation rates, earthquakes are one of the primary catalysts for submarine landslides (Nadim, Biscontin, and Kaynia, n.d.). In addition, variable rates of deposition of submarine sediments may lead to the generation of weak layers with varying degrees of consolidation (Biscontin, Pestana, and Nadim 2004). Several studies related to submarine mass movements have suggested the presence of weak layers as one of the causes of the triggering of submarine landslides (O'Leary 1991; Haflidason et al. 2003; Bryn et al. 2005a, 2005b; Solheim et al. 2005; Locat and Lee 2009).

Earthquakes of moderate to large magnitudes do not frequently occur along the Brazilian continental margin; however, earthquakes with damage potential have occurred in the past and may occur again (Pirchiner et al., n.d.; Garske et al. 2020). Recent studies have focused on the occurrence of hydroplaning and turbidity currents (Acosta et al. 2017; Hotta et al. 2020), on the response of clayey submarine canyons to seismic events representative of Brazilian seismicity (Tarazona et al. 2020), and also on the assessment of seismic hazard on the continental margin of southeastern Brazil (Garske et al. 2020). However, the seismic response of submarine slopes in the Brazilian context is a new field of investigation. This study comprises part of a research project related to the seismic behavior of low-gradient (<5°), soft-clay continental slopes typical of this region.

In the case of submarine slopes, landslides involve large distances relative to the thickness of the soil mass. Therefore, the length of the slide is many times larger than the thickness of the slide. The infinite slope approach to modeling the seismic response of sloping ground in soft clays has been studied by means of numerical models in several studies (Pestana and Nadim 2000; Biscontin and Pestana 2006; Rodríguez-Ochoa et al. 2015; Zhou et al. 2017; Dey et al. 2016). However, field or experimental data regarding the seismic behavior of gentle slopes in soft clays under different ranges of loading are limited. Most of the experimental studies in clays, particularly using centrifuge modeling, have been related to one-dimensional (1D) response at different ranges of strain. For example, Afacan et al. (2014) performed 1D centrifuge tests in clay using a hinged-plate model container to evaluate the site response at very large strains representative of seismically active regions. In another study, Rayhani and El Naggar (2007) evaluated the seismic response of soft to medium stiff clays of one and two layers using an equivalent shear beam (ESB) model container. More recently, Zhou et al. (2017) carried out a series of centrifuge tests on a slightly overconsolidated marine clay deposit employing a flexible boundary container.

In the case of lateral spreading problems like the seismic behavior of sloping ground, the use of ESB model containers is unsuitable given that they restrain the lateral

displacements of the soil (Madabhushi 2014). Alternatively, a laminar container can be used for this type of   78
problem. Most of the experience using laminar containers in centrifuge tests is related to liquefaction problems   79
(Elgamal et al. 1996; Taboada and Dobry 1998; Haigh et al. 2000; Knappett 2006).   80

One of the fundamental concerns of the preparation of models in clay is the consolidation of the soil. This   81
requires the use of an impermeable container strong enough to handle the pressures applied to the clay during   82
consolidation. In a laminar container, the soil body is typically placed within a rubber bag or a latex membrane for   83
saturated models. For the construction of a layered profile in clay, an extension is required, and the inner rubber   84
bag can be easily damaged during the application of the consolidation pressures, leading to leakage and the gen-   85
eration of additional drainage paths. To sort out these practical issues, it was necessary to develop a new model   86
preparation procedure.   87

This article presents an experimental methodology to simulate the seismic behavior of a gentle slope in soft   88
clay including the presence of a weak layer by means of centrifuge modeling. The centrifuge test presented here is   89
part of an experimental program aimed at studying the seismic response of gentle slopes in soft clay. The specific   90
objectives of the present work are (1) to describe a novel model-preparation technique for simulating a slope of   91
relatively soft clay with an even weaker layer sandwiched between, using a laminar model container used ex-   92
tensively for seismic studies in sands (Lanzano et al. 2012; Brennan et al. 2006b; Tricarico, Madabhushi, and   93
Aversa 2016; García-Torres and Madabhushi 2019), (2) to present a particle image velocimetry (PIV) method-   94
ology using an open source software (Blender) as a complementary source of data in terms of displacements and   95
accelerations at different depths in the slope, (3) to discuss the experimental results for use in calibration of   96
numerical and analytical models, and (4) to observe the dynamic behavior of the slope using spectral analysis.   97

Dynamic Centrifuge Modeling   98

Centrifuge modeling enables the study of complex geotechnical problems using small-scale models, employing   99
centrifugal acceleration to simulate the stress and strains representative of field conditions (Taylor 1995;   100
Madabhushi 2014). The dynamic tests in this study were conducted in the 10-m-diameter beam centrifuge   101
at the Schofield Centre (University of Cambridge). The earthquake motions were applied using a servo-hydraulic   102
actuator developed by Madabhushi et al. (2012). The problem studied consisted of a semi-infinite sloping ground   103
condition in soft clay. Under these conditions, large deformations are expected and therefore a laminar container   104
(Brennan et al. 2006b) was used. The box is 500 by 250 mm in length and width, and the depth is variable,   105
depending on the number of rectangular frames (laminae) used (280 mm for the current centrifuge test).   106

Materials and Methods   107

MATERIALS   108
The model was made with Speswhite kaolin, a well-documented material with comparative data sets available and   109
widely used in research projects involving physical models (Almeida 1984; Kim 1996; Williamson 2014; Lau   110
2015). For the current research, the values reported by Lau (2015), for a plastic limit (PL) equal to 30 %   111
and a liquid limit (LL) equal to 63 % (then a plasticity index [PI] of 33 %) were adopted.   112

PROPOSED MODEL PREPARATION   113
The centrifuge test performed simulates the behavior of a layered gentle slope in soft clay when subjected to   114
earthquake loading. The model consisted of a three-layer slope with a weak layer, aiming to simulate a strength   115
contrast of about 25 % between neighboring layers. The consolidation pressures described below (250 and   116
125 kPa) were selected to reproduce a strength profile typical of marine clays like that encountered in the seabed 117
of the Campos offshore basin, southeastern Brazil. Fagundes et al. (2012) described the behavior of marine clays in 118
this region through laboratory and field tests and presented a profile with values ranging between 3 kPa at the   119
surface and 40 kPa at a 20-m depth, approximately the prototype vertical extent as presented in the following   120

sections. Similar consolidation pressures such as those used in the current test have been applied in centrifuge   121
tests in soft clay representative of offshore environments (White, Gaudin, and Boylan 2010; Tarazona et al. 2020).   122
The main difference in the construction of the model presented in this article is the lower consolidation pressure   123
of 125 kPa in order to consider the presence of a weak layer.   124

    The model soil profile was built from reconstituted clay. The laminar container at the Schofield Centre has   125
been used extensively for liquefaction and lateral spreading problems involving sands. For a model in clay, a   126
different setup was required for the consolidation process. A strongbox, or consolidation container, was designed   127
with the same internal dimensions as the laminar container (500-mm length by 250-mm width), but deeper   128
(500 mm), aiming to produce samples of the clay between 250 and 300 mm in height at the end of consolidation.   129
The sides of the consolidation container can be easily detached, and complete slices of the consolidated clay can be   130
removed with minimal disturbance, enabling the simulation of the target layered soil profile as described below.   131

    In order to build the three-layer slope, the model preparation was divided into stages: 132

(1) the kaolin powder was mixed with water at 120 % water content employing a clay mixer under vacuum to   133
    remove air bubbles from the clay. Once mixed, the slurry was poured into the consolidation container with   134
    draining interfaces at the top and base of the clay. A piston was placed on top of the clay slurry and it was   135
    left to consolidate for one day under the weight of the piston. The additional consolidation pressures were   136
    applied in stages using a computer-controlled consolidation rig.   137

(2) The top and bottom layers of the clay were first consolidated by applying a maximum consolidation   138
    pressure of $\sigma'_{v\,\max} = 250$ kPa. The load was applied in steps, starting from 0.7 kPa, corresponding to   139
    the pressure applied by the piston and increased by doubling the pressures until reaching 250 kPa.   140
    The time intervals of each loading step followed the experience of the last 40 years using Speswhite kaolin.   141
    The consolidation lasted twelve days, and it was stopped when the settlements were stabilized within 48 h   142
    (fig. 1A). During the initial stages of consolidation (day 0 to day 4), a combination of consolidation of the   143
    vertical stress applied by the consolidation press and suction-induced seepage were used to consolidate the   144

FIG. 1 Model consolidation stages.

clay slurry and to accelerate the settlements. This methodology has been used for models in clay developed 145
at the Schofield Centre (Garala and Madabhushi 2019; de Sanctis et al. 2021). 146

(3) The sides of the consolidation container were removed; the resultant block was split by cutting off the top 147
80 mm and keeping the remaining 150 mm in the same position. The top block was stored and protected 148
to avoid loss of moisture (fig. 1B). 149

(4) The sides of the consolidation container were reassembled, and a new layer of the slurry was poured on top 150
of the block of consolidated clay that remained, then, a maximum consolidation pressure of $\sigma'_{v\,\mathrm{max}} =$ 151
125 kPa was applied in stages. The consolidation pressures were applied in 10 days in stages from 152
0.7 kPa doubling the pressures until reaching 125 kPa (fig. 1C and 1D). 153

(5) At the end of the consolidation of the second layer, the previously stored top layer was positioned on top, 154
and a $\sigma'_{v\,\mathrm{max}} = 125$ kPa pressure was applied to the three-layer clay bed for two days to ensure continuity 155
between layers (fig. 1E). The continuity between the layers was checked after the centrifuge test by cutting 156
transverse slices of clay, further details are presented in the post-test investigations section of this article. 157

(6) The applied vertical pressure was removed, and the sides of the consolidation container were again detached. 158
Then the final block of clay was wrapped in a rubber bag to prevent water leakage and to separate the clay 159
and the laminations (fig. 1F). Finally, the frames of the laminar container were assembled around the sample. 160

Considering that after unloading the clay, there would be a reduction in the effective stress prior to centrifuge 161
testing commencing, the clay was held under a suction of around −60 kPa. This was done by connecting a vacuum 162
pump to the drains located at the base of the model container (fig. 2A), allowing for a continuous application of 163
negative pressure until the moment prior to the centrifugal acceleration of the model in the centrifuge. The ap- 164
plied suction of −60 kPa was below the air entry value to prevent the occurrence of cavitation. A range of pres- 165
sures of the same order (−60 to −70 kPa) was used by Garala, Madabhushi, and Di Laora 2020 and de Sanctis et al. 166
2021 for the preparation of models in clay during the unloading phase of consolidation. Given the short time in 167
which the suction was applied to the model, no considerable effects were expected in terms of the saturation of the 168
clay. As part of the experimental setup, water content samples were taken at different depths across the clay profile 169
at the end of the centrifuge test. The average water content and degree of saturation of the clay were around 53 % 170
and 100 %, respectively, confirming that during the centrifuge test the clay was in a saturated condition. For the 171
calculations of the vertical stresses, two saturated unit weights were measured: for the top and bottom layer 172
$\gamma_{sat} = 16.9$ kN/m³ and for the weak layer $\gamma_{sat} = 16.4$ kN/m³. 173

MODEL DETAILS: GENTLE SLOPE   174

Once assembled to the desired height, the instrumentation was installed in the laminar container. The following 175
electronic instruments were used: (1) piezoelectric accelerometers (model A32 by D. J. Birchall Ltd.) to record the 176
dynamic motions at different locations in the soil profile; (2) pore pressure transducers (PPTs, model PDCR-81 177
manufactured by Druck Ltd.); (3) linear variable differential transformers (LVDTs, model DC15 manufactured by 178
Solartron Metrology) to record the horizontal displacements during the swing-up of the model and during the 179
application of the dynamic loads and (4) a high-speed camera (MotionBLITZ EoSens mini 2 produced by 180
Mikrotron GmbH) to track the displacements of markers installed in the laminae throughout the experiment. 181
In addition, a support gantry frame was used to fix an actuator above the clay that was used to perform an in-flight 182
T-bar test, and an air hammer (AHD) was placed on the clay surface. The piezo-accelerometers (A1 to A10) and **AQ5**
the PPTs (P1 to P4) were installed by excavating boreholes with small pipes, removing the clay and positioning 184
the instruments with a probe for installation at specific depths (Brennan et al. 2006a). **Figure 2A** presents a 185
general view of the model, **figure 2B** shows the detailed location of the instrumentation, and **figure 3** displays 186
a view of the model in the servo-hydraulic actuator and the wiring arrangement in the model. 187

PIV ANALYSIS SETUP   188

For the experiment, a high-speed camera developed to record fast processes in confined spaces was employed 189
(MotionBLITZ EoSens mini 2 produced by Mikrotron). The resolution of the pictures captured by the camera is 190

FIG. 2 Experimental setup: (*A*) 3D overview of the model (drawing in model scale) and (*B*) instrumentation layout (model scale in parentheses).
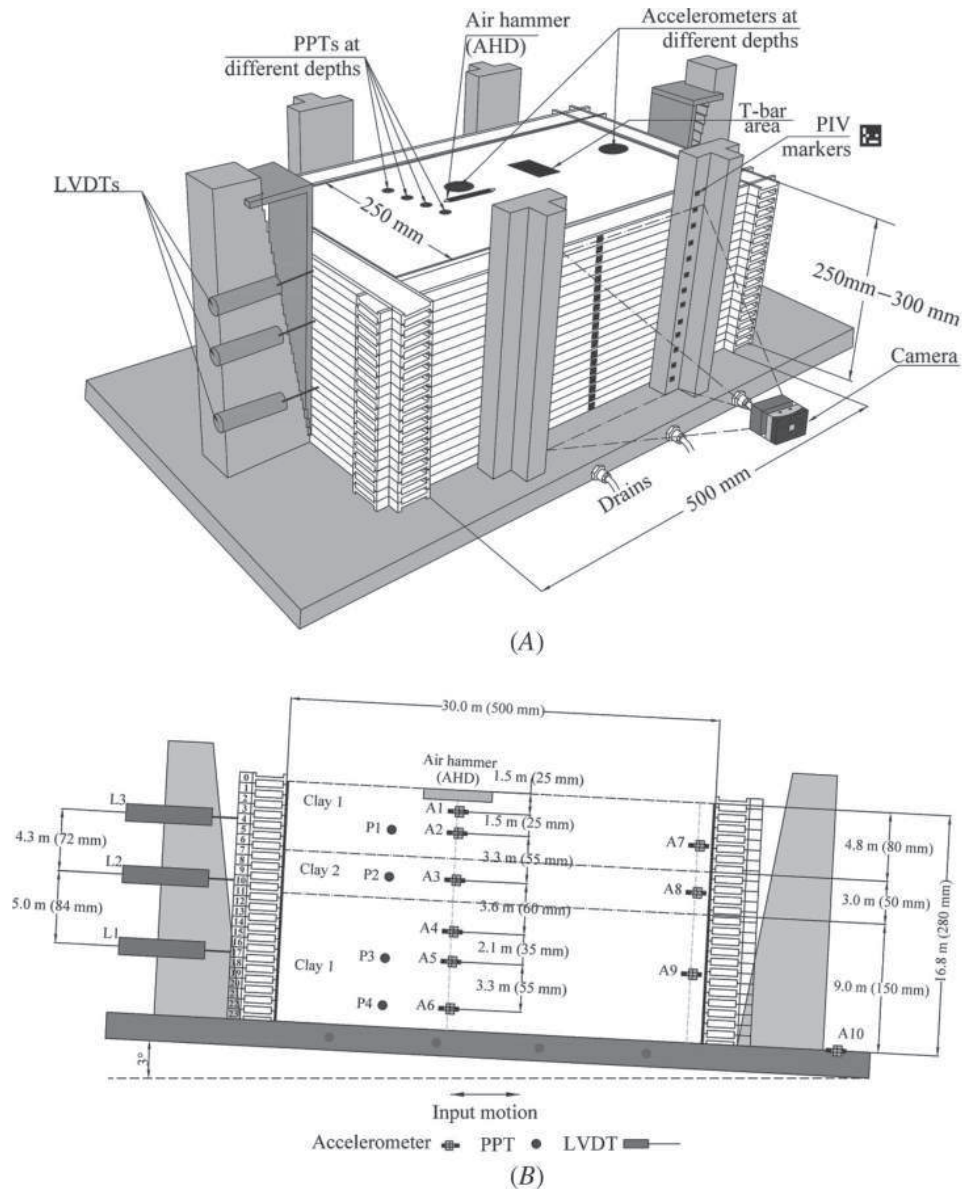
(A)

(B)

linked to the recording frame rate. For example, at a maximum resolution of 1,696 by 1,710 pixels, it is possible to record images at a frame rate of 523 Hz. For the centrifuge test reported here, a resolution of 1,504 by 1,050 pixels was employed, delivering a frame rate of 953 Hz.

The camera was triggered to record 15 % of the total frames prior to the trigger via an external signal, and the remaining percentage to record the earthquake itself. The recording time for the dynamic events in the centrifuge is of the order of a few seconds; for the current test, 1.4 s was sufficient to record a total of 1,354 photos (or frames) per earthquake.

Once the laminar container was assembled and the instruments were installed, ArUco markers (Garrido-Jurado et al. 2014) were glued to each lamina. Two sets of markers were used, the first set, which was labelled as

1	PPTs
2	Accelerometers
3	T-bar
4	Gantry
5	High-speed camera
6,7	Lights
8	LVDTs
9	AHD
10,11	Junction box
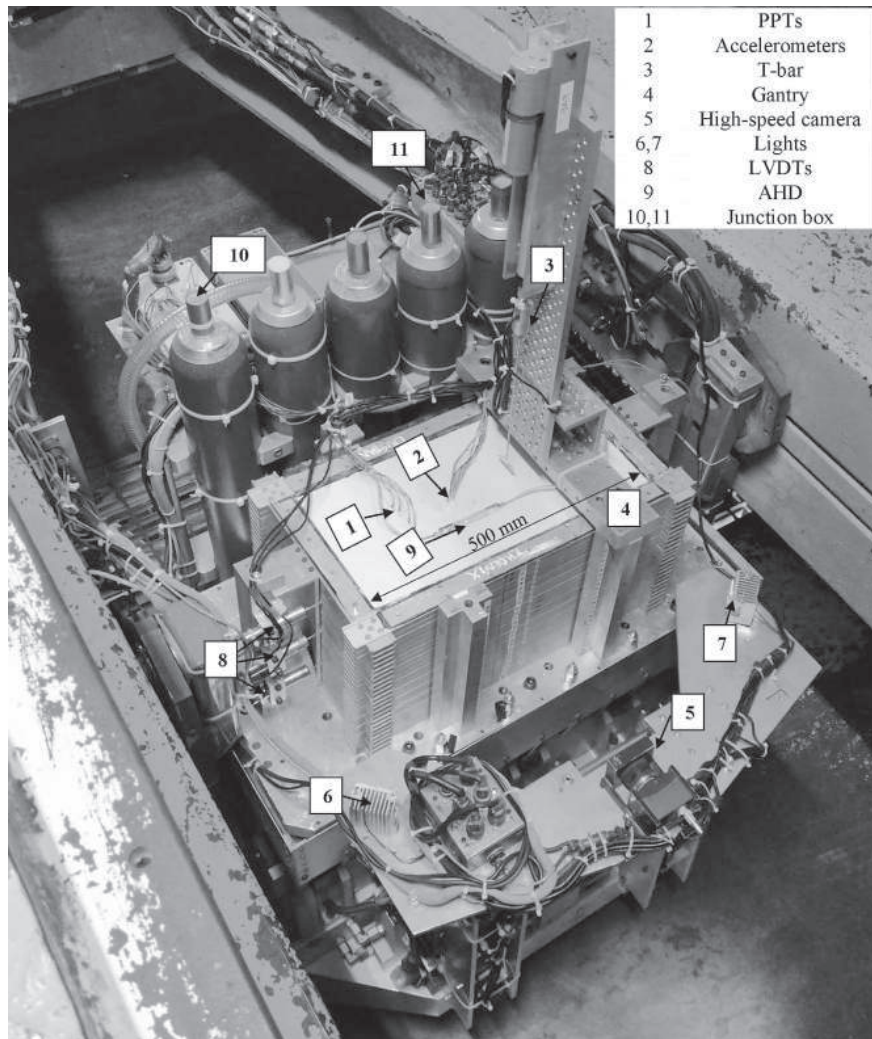
fixed column (fig. 4), was attached to the vertical, rigid columns that act as a boundary and support for the laminar container in the transverse direction. The displacement of the elements of the fixed column is related to the displacement of the shaking table, enabling tracking of the input motion. The second set of markers, labeled as displacement markers (fig. 4), was installed in the laminae of the container and used to track the displacement of the mass of soil at different depths. The three LVDTs installed on the side of the container were also used for comparison with and validation of the displacements tracked by the PIV method.

Blender is an open source software package for many purposes related to 2D and 3D animation (Hess 2010). Among its functionalities, there is a module for motion tracking that enables tracking of markers during a photo or video sequence. Options such as marker size, tracking area, correlation between matched and source image, and tracking methodologies are available. Blender uses a tracker with subpixel precision following a brute-force search with subpixel refinement. For the current test, a correlation coefficient of 0.95 and a tracking method called "location only," which looks for changes in translation of the markers, was used.

The tracking process begins by assigning initial coordinates to the markers to be tracked; in a frame the coordinates are in pixel units in the horizontal and vertical directions. This is performed by defining a pattern area

FIG. 4   Location and sets of markers (dimensions in model scale).
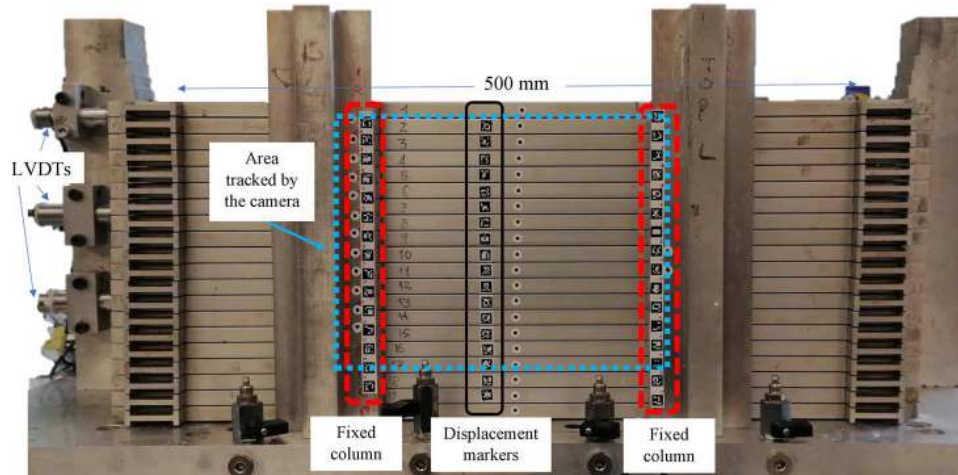
with a size equivalent to the dimensions of the marker. Next, a search area is established in which Blender will   214
look for the position of the marker in the following frames. The definition of the pattern area and the search area   215
is shown in **figure 5A**. The search area was assigned to the markers based on their expected displacements during   216
each earthquake motion. This area can be increased in case one of the markers moves beyond the defined range.   217
After tracking the markers, the results were generated in terms of frame number, and the horizontal and vertical   218
coordinates of each marker in pixels. Before the test, a checkerboard was placed in front of the camera in the same   219
plane as the markers in order to associate real coordinates to the coordinates of the markers in the photos (1 pixel   220
was equivalent to approximately 0.18 mm in model scale). **Figure 5B** shows the coordinate system for a photo in   221
pixels and the corresponding equivalence in millimeters.   222

An example of the tracking of one marker is presented in **figure 6**. The coordinates of each marker (x_i, y_i)   223
after being tracked are in units of pixels and presented frame by frame with a total of 1,354 frames tracked in a   224
period of 1.4 s (frame rate 953 Hz) as previously discussed. According to the camera settings and position, an area   225
of 1,504 by 1,050 pixels covering 15 out of 23 laminations of the model container. The scaling between pixel units   226

FIG. 5   Tracking of markers: (A) screenshot of Blender, pattern, and search area for the markers; (B) photo in pixels and scaled in millimeters.
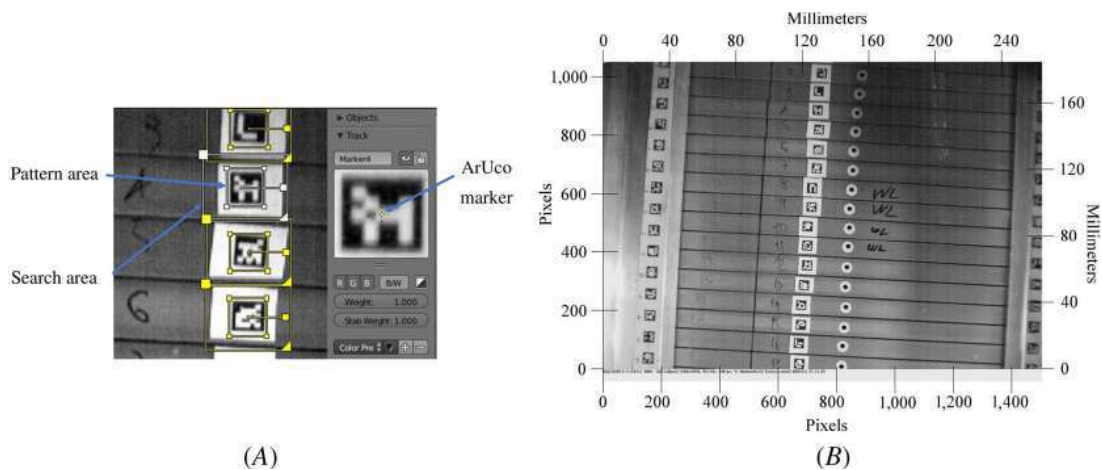
FIG. 6 Example of tracking of a marker (model units in parenthesis).

and distance units is performed using a known length employing a checkerboard, as mentioned above, then a 227
relationship of a 1-pixel equivalent to approximately 0.18 mm in model scale was obtained. Finally, each coor- 228
dinate of the marker is expressed in prototype units (X_i, Y_i), the time step is obtained from the sampling frequency, 229
and the variation of the horizontal displacement is plotted with time. Considering the displacements occur in the 230
downslope orientation, there was no variation of displacements in the y (vertical) direction (also for the boundary 231
condition imposed by the laminar container); however, the methodology can also be applied to problems in which 232
it is necessary to track displacements in this direction.   233

Experimental Program and Testing   234

To simulate the gentle slope inclination, the model was tilted by 3° using wedges placed along the base of the 235
model. The swing up of the model consisted of increments of 10 g until reaching the acceleration level for the 236
test (60 g). The bottom drains of the model container were closed during the centrifuge test. Air hammer tests 237
(AHTs) were performed at the different stages of the spinning up of the model and between the shaking events 238
to estimate the shear wave velocities within the soil profile in flight. Accelerometers were used to measure the 239
arrival times generated by the air hammer placed on top of the clay (Ghosh and Madabhushi 2002). Once the 240
target acceleration level was achieved, the model was maintained inflight for 40 min before the application of 241
the earthquakes to increase the total stresses and redistribute the pore pressures and effective vertical stresses; 242
a similar methodology was adopted by Garala, Madabhushi, and Di Laora 2020. In the present test program, 243
all centrifuge tests had a similar inflight time before the application of the earthquakes, and all showed similar 244
undrained strength profiles. The following stage consisted of a T-bar penetrometer test (Stewart and Randolph 245
1991) and an additional AHT. The T-bar used was 40 mm wide with a 4 mm diameter and was pushed into the 246
clay at a rate of approximately 2 mm/s. The normalized penetration rate, V, is (after Finnie and Randolph 247
1994).   248

FIG. 7 Clay model properties: (*A*) stress history, (*B*) undrained shear strength profiles, and (*C*) shear wave velocity profile.

$$V = \frac{\nu D}{C_{\nu}} \qquad (1)$$

where: 249
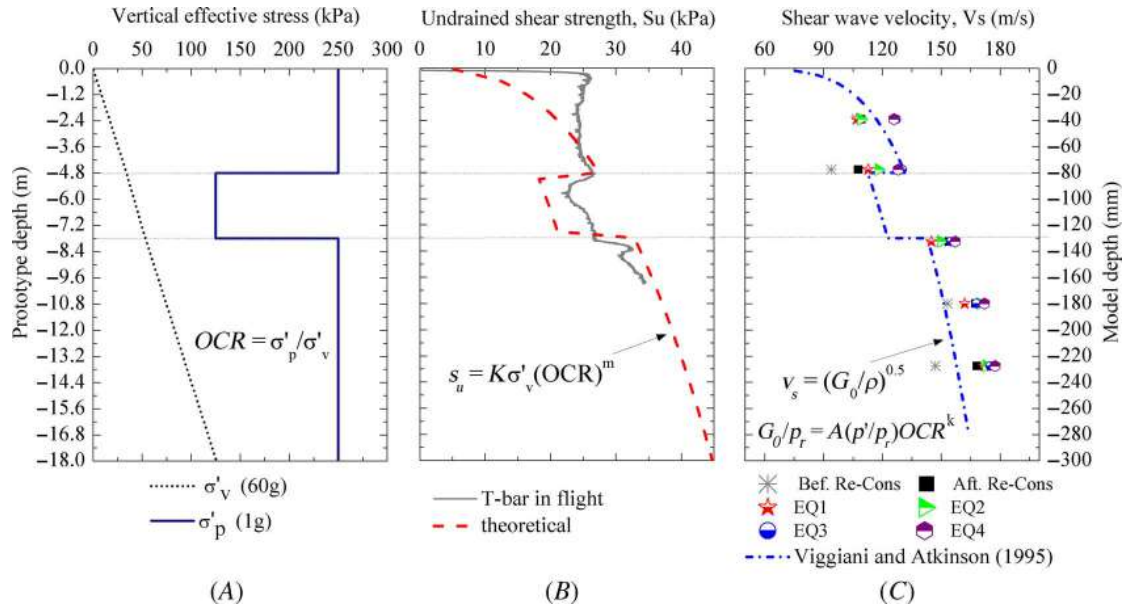
ν = penetration velocity of the T-bar, 2 mm/s;   250

D = diameter of the T-bar, 4 mm; and   251

c_{ν} = coefficient of consolidation of the kaolin, 4.29 mm²/min (0.07 mm²/s) (Chow et al. 2020).   252

For clays, normalized velocities (*V*) greater than 10 are likely to be undrained (Oliveira et al. 2011; Randolph 253
and Gourvenec 2011), for the current test *V* = 114, therefore ensuring that the T-bar penetrometer test was per- 254
formed at an undrained rate.   255

The results of the in-flight characterization of the clay are presented in **figure 7** in terms of effective vertical 256
stresses applied to the model, undrained strength profiles, and shear wave velocity profiles.   257

UNDRAINED SHEAR STRENGTH PROFILE   258

The measured undrained shear strength (*s_u*) profile is presented together with an estimate derived from the well- 259
known stress history relationship (equation (2); Wroth 1984):   260

$$S_u = K\sigma'_{\nu}(OCR)^m \qquad (2)$$

where: 261

K = normalized strength parameter;   262

$\sigma'_{\nu} = (\gamma_{sat} - \gamma_{water})^{\ast}Z$ = effective vertical stress in kPa;   263

$OCR = \sigma'_p/\sigma'_v$ = overconsolidation ratio;   264

m = power constant in the equation;   265

γ_{sat} = saturated unit weight – 16.9 kN/m³ (top/bottom layers); 16.4 kN/m³ (weak layer); and   266

σ'_p = pre-consolidation pressure of the layer – 250 kPa and 125 kPa.   267

Values of the *K* and *m* constants have been reported by several authors (Almeida 1984; Springman 1989; 268
Sharma and Bolton 1996). The theoretical curve was calculated based on the parameters presented by Zhang, 269

White, and Randolph (2011) ($K = 0.23$, $m = 0.62$). The overconsolidation ratio (OCR) was calculated as the ratio   270
of the maximum past effective consolidation stresses ($\sigma'_p = 250$ kPa and $\sigma'_p = 125$ kPa) and the effective vertical   271
stress in flight (σ'_v). The distribution of the effective vertical stresses and pre-consolidation pressures used for the   272
calculation of the OCR are presented in **figure 7A**. A reasonably good agreement is evident between the exper-   273
imental and theoretical curves (**fig. 7B**) exhibiting an increase with depth and a reduction in the weaker layer in   274
which a lower pre-consolidation pressure has been applied. The observed contrast of s_u between the weak layer   275
and the neighbouring layers of around 20 % lower strength is in accordance with in-situ measured s_u profiles   276
(Soriano et al., n.d.). There are higher measured values of s_u on top of the clay (between 0 and 3.6 m) compared   277
with the theoretical curve. This may be due to partial drying of the clay during the swing up and the fact that no   278
surficial water was added to the model in order to avoid sloshing during the earthquake experiments.   279

SHEAR WAVE VELOCITY PROFILE   280

The shear wave velocities measured by the air hammer were compared with a well-known small-strain stiffness   281
correlation (equation (3)) based on the Viggiani and Atkinson (1995) equation: 282

$$\frac{G_0}{p_r} = A \left(\frac{p'}{p_r} \right)^M OCR^k \tag{3}$$

where: 283

$\quad G_0 =$ initial shear modulus in kPa;   284
$\quad p' =$ mean effective stress in kPa;   285
$\quad p_r =$ reference pressure equivalent to 1 kPa;   286
$OCR =$ overconsolidation ratio;   287
$\quad A =$ correlated parameter;   288
$\quad k =$ correlated parameter; and   289
$\quad M =$ correlated parameter.   290

The selection of the correlated parameters (A, k, M) was based on the PI of the clay (PI = 33 %). The relation-   291
ship between the PI and the parameters is presented in Viggiani and Atkinson (1995); for the current research,   292
$A = 950$, $k = 0.24$, and $M = 0.8$. The shear wave velocity (V_s) was calculated in terms of the initial shear modulus   293
(G_0) and the soil density (ρ) expressed as the total unit weight divided by gravity (equation (4)):   294

$$V_S = \sqrt{\frac{G_o}{\rho}} \tag{4}$$

The estimation of the shear wave velocities was based on the travel times between the signals captured by the   295
accelerometers (A1 to A6 in **fig. 2B**) when the shear waves produced by the air hammer passed through them. To   296
ensure the precision in the recording of the arrival times, it is necessary to have relatively high sampling frequen-   297
cies. For the current test, a sampling frequency of 30 kHz was used for the AHTs. Some uncertainties are involved   298
during AHTs (McCullough et al. 2007), such as the location of the instruments, given the permanent deforma-   299
tions that occur during testing (due to swing up and application of earthquakes); therefore, the shear waves may   300
reflect some error. Despite the uncertainties of the AHT, the measured values of the shear wave velocities appear   301
to be in good agreement with the empirical formula (**fig. 7C**). A slight increase in the measured shear wave   302
velocities can also be observed, as the different stages of the test occurred with the lowest values before the re-   303
consolidation of the clay and the highest values after the application of the earthquake EQ4. This implies that   304
there is a hardening of the clay under cyclic loading as the shaking progresses. The fundamental period of the soil   305
profile was 0.5 s. It was estimated by weighted average of shear wave velocity for multiple layer soil using the   306
values from the correlated curve obtained from equation (4), dividing the profile in sublayers of 0.10 m, and using   307
the following equation (equation 5):   308

$$T = \frac{4H^2}{\sum_{i=1}^{n} V_i H_i}$$

(5)

where: 309
    T = fundamental period (s);   310
    H = thickness of the soil profile (m);   311
    V_i = shear wave velocity of the corresponding layer (m/s); and 312
    H_i = thickness of the sublayer (m).   313

SHAKING EVENTS   314

The model was subjected to four earthquakes, three consisting of sinusoidal motions with a driven frequency of 315
1 Hz and the other, a scaled real motion (Kobe earthquake, 1995). During the application of the earthquakes, the 316
instrument data were recorded at a sampling frequency of 6 kHz. **Table 1** shows the salient characteristics of the 317
earthquakes applied to the model in prototype and model scale. The sequence of the input motions was defined in 318

TABLE 1
Model earthquakes

Input Motion	Type	Frequency, Hz		Duration, s		Peak Base Acceleration, g	
		Prot.	Model	Prot.	Model	Prot.	Model
EQ1	Sinusoidal	1	60	10	0.17	0.06	3.6
EQ2	Kobe (scaled)	1.4–2.4	84.0–142.8	4.3	0.07	0.18	10.8
EQ3	Sinusoidal	1	60	10	0.17	0.18	10.8
EQ4	Sinusoidal	1	60	10	0.17	0.37	22.2

Note: Prot. = Prototype.

FIG. 8

Input motions in
prototype scale.
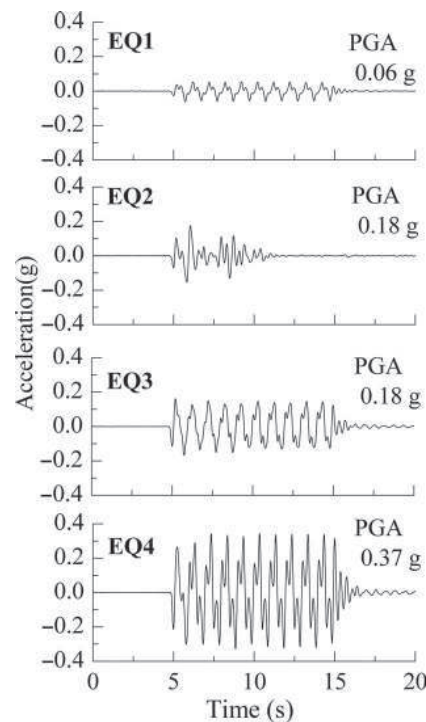
terms of increasing amplitude. **Figure 8** presents the acceleration-time histories recorded at the base of the model 319
(accelerometer A10 in **fig. 2B**) or input motions presented in terms of prototype scale. 320

Test Results
321

DISPLACEMENT-TIME HISTORIES
322

The displacement time histories recorded by the LVDTs and calculated by PIV are plotted together with the 323
corresponding input motions in **figure 9B** and **9C**. The location of the LVDTs and the corresponding markers 324
used for comparison of the displacement-time histories is presented in **figure 9A**. For brevity, only the results of 325
earthquakes EQ2 (real scaled) and EQ3 (sinusoidal) are presented in prototype scale. The results show excellent 326
agreement (both series overlap) between the data measured by the LVDTs and the displacements calculated by the 327
PIV methodology incorporated in the Blender software. This validates the use of the ArUco markers for tracking 328
the motions of each of the individual laminae, which is not possible using LVDTs because of their size. 329

ACCELERATION TIME HISTORIES
330

The acceleration time histories and fast Fourier transforms (FFTs) at different depths for earthquakes EQ2 and 331
EQ3 are presented in **figure 10**. The results are presented in prototype scale. In addition, from the displacement 332
time histories obtained from the PIV analysis, approximate accelerations at the depths of the corresponding 333
accelerometers were calculated using double differentiation (**fig. 10A** and **10C**). The raw data from the accel- 334
erometers were filtered using a fourth-order Butterworth-type filter with a bandpass between 5 and 350 Hz in 335
terms of model scale. The selected range of frequencies was defined to remove the low frequencies that produce a 336
drift in the accelerometer signal and the high frequencies associated with electrical noise. The corresponding FFTs 337

FIG. 9 Displacement-time histories: (*A*) location of the LVDTs and markers used for comparison, (*B*) horizontal
displacements during earthquake EQ2, and (*C*) horizontal displacements during earthquake EQ3.
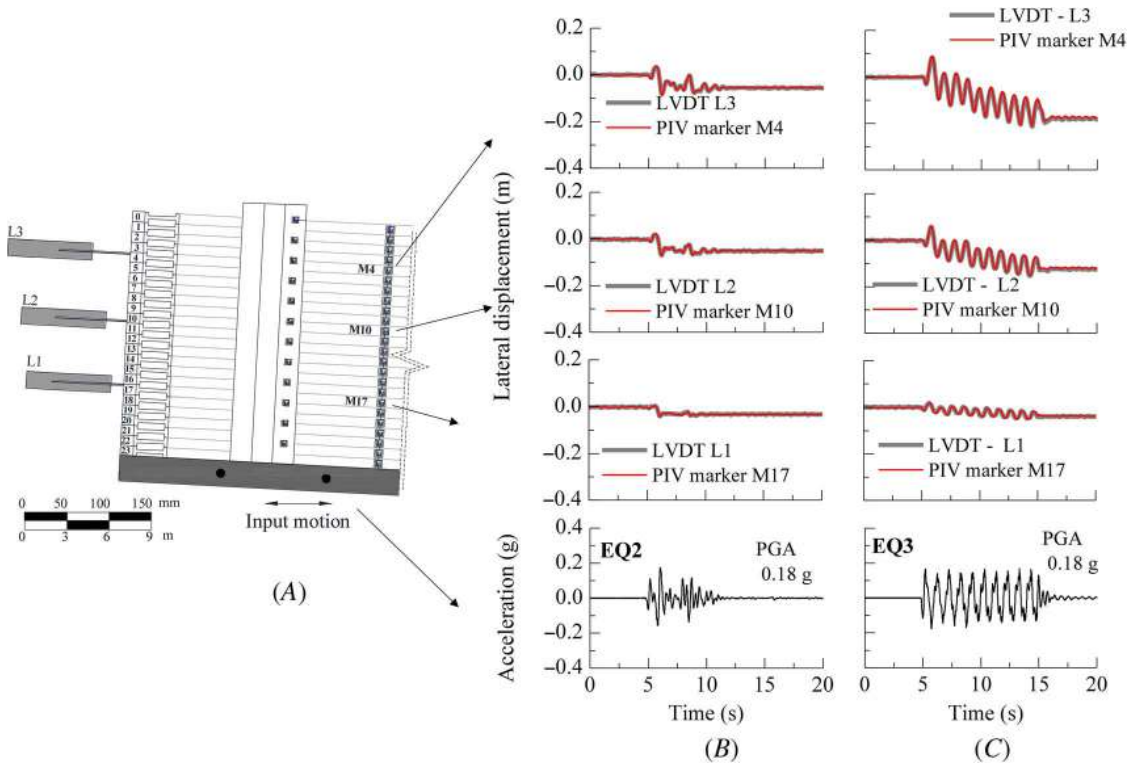
FIG. 10 Propagation of input motions along the clay: (*A*) earthquake EQ 2 accelerations, (*B*) earthquake EQ2 Fourier spectra, (*C*) earthquake EQ3 accelerations, and (*D*) earthquake EQ3 Fourier spectra.
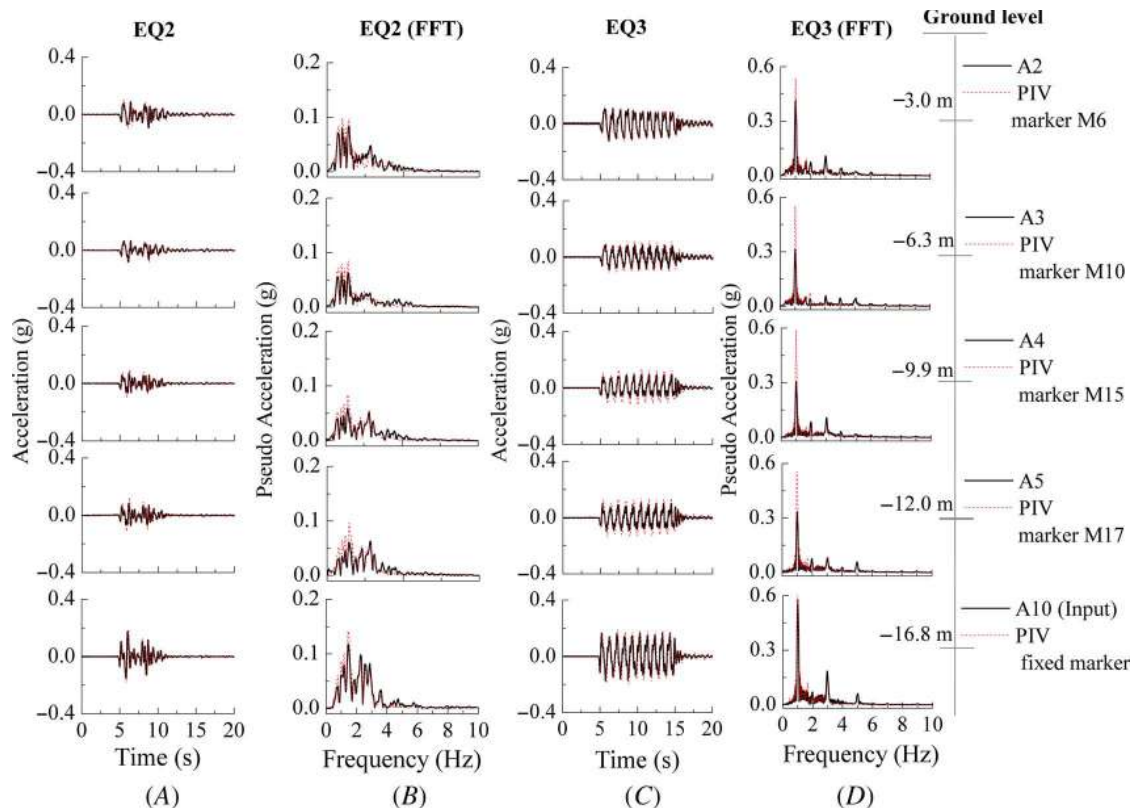
of the signals at different depths are presented in **figure 10*B*** and **10*D***. The FFT results displayed in **figure 10*D*** 338
indicate that although earthquake EQ3 was applied as a single frequency (1 Hz) sine wave as stated in **Table 1**, the 339
recorded signal is not totally harmonic and other features can be seen in the frequency domain representation. 340
According to Brennan, Thusyanthan, and Madabhushi (2005), the load applied by a centrifuge earthquake ac- 341
tuator and transferred to the laminar container is not necessarily single frequency. The observed higher harmon- 342
ics reflect part of the vibration of the shaker and transmitted to the laminar box and are therefore real loading 343
components and cannot be considered as noise. This behavior was also observed in the PIV results where the 344
main frequency of the input motions and the higher frequencies were also captured. 345

PEAK GROUND ACCELERATIONS AND HORIZONTAL DISPLACEMENTS 346

The slope response was evaluated by means of maximum displacement profile, peak ground acceleration (PGA) 347
profile, 5 %-damped accelerations at the base and near the surface (1.5-m depth), and the ratios of the response 348
spectra. **Figure 11** presents the peak lateral displacements and PGA profiles obtained after the application of the 349
earthquakes to the model. It must be pointed out that the displacements were plotted for each earthquake by 350
resetting the displacements to zero prior to that earthquake and assuming that the displacement at the base of 351
the slope is zero (net displacements). These displacements are extrapolated in **figure 11*A*** as dashed lines below a 352
12-m depth. The values were obtained from the PIV analysis of the markers installed on the laminae (markers 353
M2 to M17 in **fig. 11**) of the container and previously validated with the LVDT measurements (see **fig. 9**). 354
Figure 11*B* shows the PGA variation with depth, with values obtained from two sources: the continuous profile 355
from the PIV using the second derivative of the displacements at each marker depth and the individual points 356

FIG. 11 Slope response profiles: (*A*) maximum displacements and (*B*) PGA.
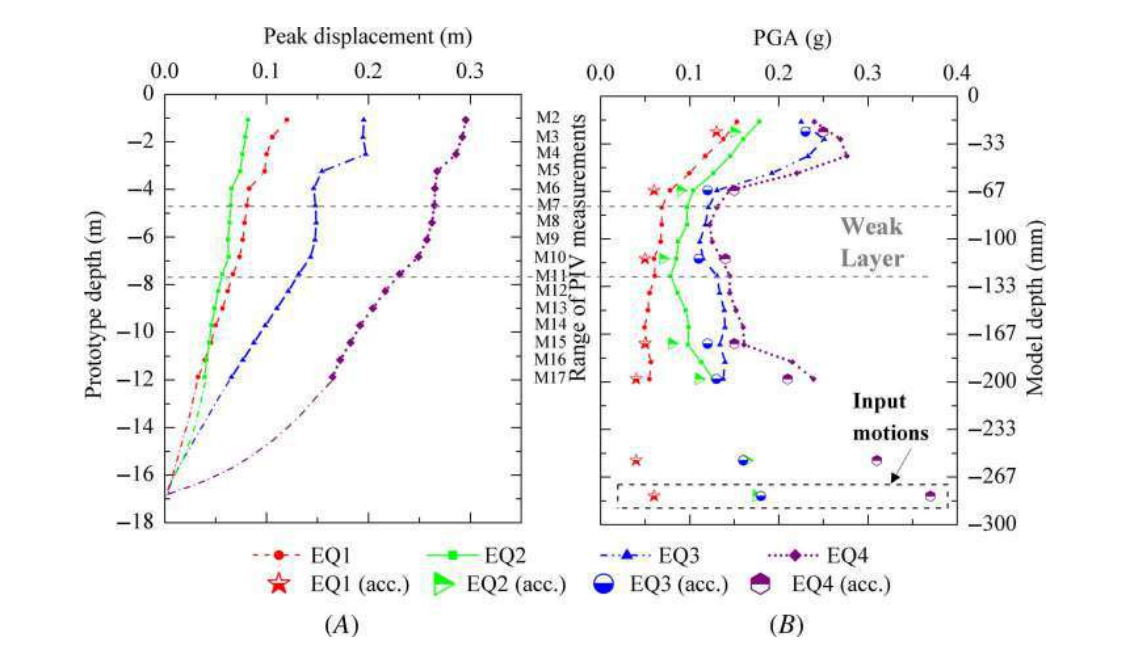
(identified as "acc.") from the accelerometer data. The results of the PGA profile show a good agreement be-   357
tween the approximation obtained by the PIV calculations and the values measured with the accelerometers.   358
However, a small overestimation of the PGA in the values obtained by the PIV was observed when compared   359
with the accelerometer data. This overestimation could be attributed to the fact that the PIV in the current test   360

FIG. 12 (*A*) Acceleration response spectra and (*B*) response spectra ratio.
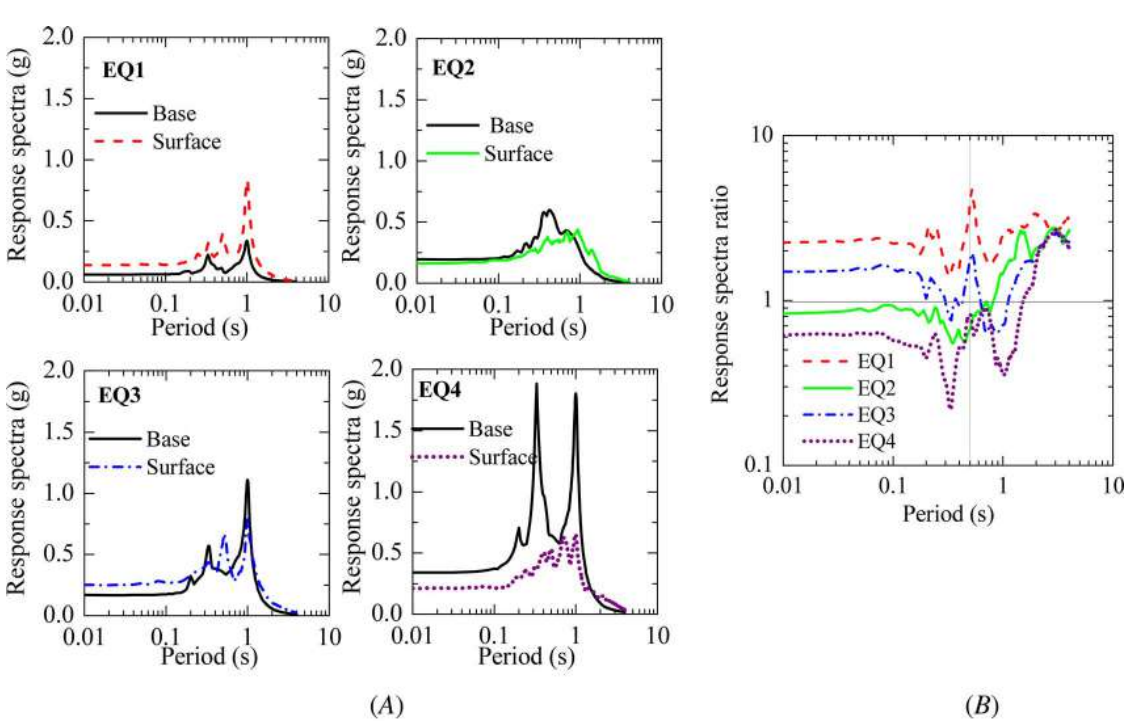
FIG. 13

(*A*) Clay model after centrifuge test (model scale in parentheses) and (*B*) transversal section and contact between layers.

(A)

(B)

was intended to measure the displacements during the application of the earthquakes, and the accelerations 361
from this method were obtained by double differentiation; therefore, it is not a direct measurement of the 362
acceleration. Overall, the net displacements show an increase from the bottom to the top, as the earthquake 363
amplitude increased with values ranging between 0.08 and 0.3 m at the top of the slope in terms of prototype 364
scale. The PGA profiles for earthquakes EQ2, EQ3, and EQ4 exhibit attenuation at depths between 3 and 10 m 365
in the soil profile. 366

Figure 12*A* shows the acceleration response spectra of the earthquakes applied to the model at the base and 367
at a depth near the surface (−1.5 m) with a damping ratio of 5 %, and **figure 12*B*** presents the ratio of the response 368
spectra curves. The response spectra ratios exhibit amplifications at the natural period of the soil profile (0.5 s) 369
during earthquakes EQ1 and EQ3 corresponding to sinusoidal loadings, indicating the local site effects on the 370
input motion. For EQ2, the response spectra ratio remained in a range close to 1 for the periods below 1 s, 371
followed by amplification at periods greater than 1 s. For the largest amplitude earthquake (EQ4), the peak 372
in the response spectra ratio shifted to a value of 0.7 s followed by an attenuation until 1 s and then a gradual 373
increase, reaching values larger than 1. This shift in the peak of the response spectra ratio for earthquake EQ4 may 374
be explained by nonlinear effects resulting from the reduction in the stiffness of the soil and the increase in 375
damping as the soil softens. 376

Although strength mobilization may occur during the swing up of the model, a snapshot of the strength of 377
the clay at the moment before the application of the shaking events was captured by means of the in-flight char- 378
acterization tests (T-bar and air hammer). Further improvements can be implemented to control the lateral dis- 379
placements during the swing up, using lateral actuators that laterally support the laminar container with the clay 380
through the swing up process and are released prior to the application of the earthquakes. For the calibration of a 381
numerical model, the selection of the strength parameters must consider the monotonic strengths and the cyclic 382
strengths given by the strain rates applied in centrifuge tests. Strain rate effects significantly increase the strength 383
and stiffness in clays (Afacan et al. 2019; Sathialingam and Kutter 1989). 384

POST-TEST INVESTIGATIONS 385

A photograph of the model after the test and an overlay of the location of the markers tracked by the camera is 386
shown in figure 13A. An accumulated displacement is evident on top of the clay at about 10 mm (model scale). 387
An interface line between the clay layers was visible at the periphery of the sample. Thus, to determine the con- 388
tinuity and contact between the layers, a section in the transverse direction was checked. No evidence of dis- 389
continuity between the layers was apparent in those transverse sections; therefore, the model soil profile was 390
laterally uniform (fig. 13B), indicating a successful sample preparation process. 391

Conclusions and Recommendations for Similar Testing Programs

392
393

The centrifuge test in this study was performed to develop a model preparation technique for simulating the 394
dynamic behavior of a gentle layered slope in soft clay. The model was subjected to a series of dynamic motions 395
to investigate the displacement and acceleration behaviors. The main observations from the centrifuge test follow: 396

- The proposed model preparation technique enabled the simulation of a three-layer soil profile in clay, with 397
  a strength contrast between layers achieved by applying different consolidation pressures during the sample 398
  preparation process. 399
- The PIV analysis was used to track the displacements of the model at the different stages of the centrifuge 400
  test with particular focus on the application of the dynamic motions. The displacements from the PIV 401
  calculations were in good agreement with those measured by the LVDTs, confirming that a similar setup 402
  could be applied in comparable testing programs involving the use of laminar containers. 403
- Measured soil properties for undrained shear strength and shear wave velocity were in reasonable agree- 404
  ment with the empirical predictions. 405
- The acceleration data at different depths were obtained by direct measurements from the accelerometers 406
  and approximated by double differentiation of the PIV displacements. The results were compared in terms 407
  of the time histories and the FFT of the signals. Additional frequencies were observed on the sinusoidal 408
  motions attributable to the higher vibration modes of the shaker and were transmitted to the laminar 409
  container. 410
- With the validated PIV results, a continuous displacement profile after the applied earthquakes was calcu- 411
  lated. The PGA profiles were obtained from the maximum accelerations measured by the accelerometers 412
  and from the double derivative of the displacements calculated from the PIV analyses. The results are 413
  complementary and show good agreement and could be used for direct comparison with computational 414
  analyses. 415
- The spectral analysis showed amplifications at periods corresponding to the fundamental period of the soil 416
  profile during earthquakes EQ2 and EQ3. A shift in the period occurred during the largest amplitude 417
  earthquake (EQ4), indicating a nonlinear behavior of the slope profile. 418
- In addition to the monotonic strengths, given the strain rates applied in dynamic centrifuge tests, cyclic 419
  strengths should also be considered for the calibration of numerical models of the problem studied. 420

The results from the centrifuge test provided useful insight into preparation of layered clay-profile models 421
using a laminar container to assess lateral spreading problems. The results can be used for calibration of numerical 422
models and for performing comparisons with existing methods for the calculation of dynamic responses (i.e., 423
Newmark's method). 424

References   432

Acosta, E., S. Tibana, M. S. S. Almeida, and F. Saboya. 2017. "Centrifuge Modeling of Hydroplaning in Submarine Slopes." 433
    Ocean Engineering 129, no. 1 (January): 451–458. https://doi.org/10.1016/j.oceaneng.2016.10.047 434
Afacan, K. B., S. J. Brandenberg, and P. J. Stewart. 2014. "Centrifuge Modeling Studies of Site Response in Soft Clay over Wide 435
    Strain Range." *Journal of Geotechnical and Geoenvironmental Engineering* 140, no. 2 (February): 1–13. https://doi.org/10. 436
    1061/(ASCE)GT.1943-5606.0001014 437
Afacan, K. B., S. Yniesta, A. Shafiee, J. Stewart, and S. Brandenberg. 2019. "Total Stress Analysis of Soft Clay Ground Response 438
    in Centrifuge Models." *Journal of Geotechnical and Geoenvironmental Engineering* 145, no. 10 (October): https://doi.org/10. 439
    1061/(ASCE)GT.1943-5606.0002115 **AQ6**
Almeida, M. S. S. "Stage Constructed Embankments on Soft Clays." PhD diss., Cambridge University, 1984. 441
Biscontin, G. and J. Pestana. 2006. "Factors Affecting Seismic Response of Submarine Slopes." *Natural Hazards and Earth* 442
    System Science 6, no. 1 (January): 97–107. https://doi.org/10.5194/nhess-6-97-2006 443
Biscontin, G., J. M. Pestana, and F. Nadim. 2004. "Seismic Triggering of Submarine Slides in Soft Cohesive Soil Deposits." 444
    Marine Geology 203, nos. 3–4 (January): 341–354. https://doi.org/10.1016/S0025-3227(03)00314-1 445
Brennan, A. J., S. P. G. Madabhushi, and P. Cooper. 2006a. "Dynamic Centrifuge Testing of Suction Caissons in Soft Clay." 446
    Paper presented at the Sixth International Conference on Physical Modelling in Geotechnics, Hong Kong, August 4–6, 2006. 447
Brennan, A. J., S. P. G. Madabhushi, and N. E. Houghton. 2006b. "Comparing Laminar and Equivalent Shear Beam (ESB) 448
    Containers for Dynamic Centrifuge Modeling." *Paper presented at the Sixth International Conference on Physical Modelling* 449
    in Geotechnics, Hong Kong, August 4–6, 2006. 450
Brennan, A. J., N. I. Thusyanthan, and S. P. G. Madabhushi. 2005. "Evaluation of Shear Modulus and Damping in Dynamic 451
    Centrifuge Tests." *Journal of Geotechnical and Geoenvironmental Engineering* 131, no. 12 (December): 1488–1498. https:// 452
    doi.org/10.1061/(ASCE)1090-0241(2005)131:12(1488) 453
Bryn, P., K. Berg, C. F. Forsberg, A. Solheim, and T. J. Kvalstad. 2005a. "Explaining the Storegga Slide." *Marine and Petroleum* 454
    Geology 22, nos. 1–2 (January/February): 11–19. https://doi.org/10.1016/j.marpetgeo.2004.12.003 455
Bryn, P., K. Berg, M. S. Stoker, H. Haflidason, and A. Solheim. 2005b. "Contourites and Their Relevance for Mass Wasting 456
    along the Mid-Norwegian Margin." *Marine and Petroleum Geology* 22, nos. 1–2 (January/February): 85–96. https://doi.org/ 457
    10.1016/j.marpetgeo.2004.10.012 458
Chow, J. K., Y. Wang, H. L. Lui, and E. Huang. 2020. "Determination of Consolidation Parameters Based on the Excess Pore 459
    Water Pressure Measurement Using a Newly Developed U-oedometer." *Acta Geotechnica* 15 (February): 2665–2680. 460
    https://doi.org/10.1007/s11440-020-00914-y 461
De Sanctis, L., R. Di Laora, T. K. Garala, S. P. G. Madabhushi, G. Viggiani, and P. Fargnoli. 2021. "Centrifuge Modelling of the 462
    Behaviour of Pile Groups under Vertical Eccentric Load." *Soils and Foundations* 61, no. 2 (April): 465–479. https://doi.org/ 463
    10.1016/j.sandf.2021.01.006 464
Dey, R., B. Hawlader, R. Phillips, and K. Soga. 2016. "Modeling of Large Deformation Behaviour of Marine Sensitive Clays and 465
    Its Application to Submarine Slope Stability Analysis." *Canadian Geotechnical Journal* 53, no. 7 (July): 1138–1155. https:// 466
    doi.org/10.1139/cgj-2015-0176 467
Elgamal, A. W., M. Zeghal, V. Taboada, and R. Dobry. 1996. "Analysis of Site Liquefaction and Lateral Spreading Using 468
    Centrifuge Testing Records." *Soils and Foundations* 36, no. 2 (June): 111–121. https://doi.org/10.3208/sandf.36.2_111 469
Fagundes, D. F., K. I. Rammah, M. S. S. Almeida, J. Pequeno, J. R. M. S. Oliveira, and R. Garske. 2012. "Strength Behaviour 470
    Analysis of an Offshore Brazilian Marine Clay." In *Proceedings of the ASME 2012 31st International Conference on Ocean,* 471
    Offshore and Arctic Engineering, OMAE2012-83008. New York, NY: American Society of Mechanical Engineers. 472
Finnie, I. M. S. and M. F. Randolph. 1994. "Punch-through and Liquefaction Induced Failure on Shallow Foundations on 473
    Calcareous Sediments." *In Seventh International Conference on the Behaviour of Offshore Structures*, 217–230. Boston, 474
    MA: Pergamon. 475

Garala, T. K. and S. P. G. Madabhushi. 2019. "Seismic Behaviour of Soft Clay and Its Influence on the Response of Friction Pile Foundations." *Bulletin of Earthquake Engineering* 17 (November): 1919–1939, https://doi.org/10.1007/s10518-018-0508-4

Garala, T. K., S. P. G. Madabhushi, and R. Di Laora. 2020. "Experimental Investigation of Kinematic Pile Bending in Layered Soils Using Dynamic Centrifuge Modelling." *Geotechnique. Published ahead of print*, December 14, 2020. https://doi.org/10.1680/jgeot.19.p.185

García-Torres, S. and G. S. P. Madabhushi. 2019. "Performance of Vertical Drains in Liquefaction Mitigation under Structures." *Bulletin of Earthquake Engineering* 17 (September): 5849–5866. https://doi.org/10.1007/s10518-019-00717-x

Garrido-Jurado, S., R. Muñoz-Salinas, F. Madrid-Cuevas, and M. Marín-Jiménez. 2014. "Automatic Generation and Detection of Highly Reliable Fiducial Markers under Occlusion." *Pattern Recognition* 47, no. 6 (June): 2280–2292. https://doi.org/10.1016/j.patcog.2014.01.005

Garske, R., M. Assumpção, M. C. F. Almeida, and M. S. S. Almeida. 2020. "Seismicity and Seismic Hazard in the Continental Margin of Southeastern Brazil." *Journal of Seismology* 24 (July): 1205–1224. https://doi.org/10.1007/s10950-020-09941-4

Ghosh, B. and S. P. G. Madabhushi. 2002. "An Efficient Tool for Measuring Shear Wave Velocity in the Centrifuge." In *Physical Modelling in Geotechnics—ICPMG '02*, edited by P. Guo, R. Phillips, and R. Popescu, 119–124. BogaRaton, FL: CRC Press.

Haflidason, H., H. P. Sejrup, I. M. Berstad, A. Nygard, T. Richter, R. Lien, and K. Berg. 2003. "A Weak Layer Feature on the Northern Storegga Slide Escarpment." In *European Margin Sediment Dynamics*, edited by J.Mienert and P. P. E. Weaver, 55–62. Berlin, Germany: Springer.

Haigh, S. K., S. P. G. Madabhushi, K. Soga, Y. Taji, and Y.Shamoto. n.d. "Lateral Spreading During Centrifuge Model Earthquakes." *Paper presented at ISRM International Symposium*, Melbourne, Australia, November 19–24, 2000.

Hess, R. 2010. *Blender Foundations: The Essential Guide to Learning Blender 2.6*. Waltham, MA: Focal Press.

Hotta, M. M., M. S. S. Almeida, D. T. Pelissaro, J. R. M. S. Oliveira, S. Tibana, and R. Garske. 2020. "Centrifuge Tests For Evaluation Of Submarine-Mudflow Hydroplaning And Turbidity Currents." *International Journal of Physical Modelling in Geotechnics* 20, no. 4 (July): 239–253. https://doi.org/10.1680/jphmg.18.00081

Hühnerbach, V. and D. G. Masson. 2004. "Landslides in the North Atlantic and Its Adjacent Seas: An Analysis of Their Morphology, Setting and Behavior." *Marine Geology* 213, nos. 1–4 (December): 343–362. https://doi:10.1016/j.margeo.2004.10.013, https://doi.org/10.1016/j.margeo.2004.10.013

Kim, S. H. "Model Testing and Analysis of Interactions between Tunnels in Clay." PhD diss., University of Oxford, 1996.

Knappett, J. A. "Piled Foundations in Liquefiable Soils: Accounting for Axial Loads." PhD diss., Cambridge University, 2006.

Kowsmann, R. O, A. C. Lima, and M. A. Vicalvi. 2016. "Features Indicating Geological Instability in the Continental Slope and São Paulo Plateau." *In Geology and Geomorphology. Regional Environmental Characterization of the Campos Basin, Southwest Atlantic*, edited by R. O. Kowsmann, 71–97. Amsterdam, the Netherlands: Elsevier. https://doi.org/10.1016/B978-85-352-8444-7.50012-3

Lanzano, G., E. Bilotta, G. Russo, F. Silvestri, and S. P. G. Madabhushi. 2012. "Centrifuge Modeling of Seismic Loading on Tunnels in Sand." *Geotechnical Testing Journal* 35, no. 6 (November): 854–869. https://doi.org/10.1520/GTJ104348

Lau, B. H. "Cyclic Behaviour of Monopile Foundations for Offshore Wind Turbines in Clay." PhD diss., University of Cambridge, 2015.

Locat, J. and H. Lee. 2009. "Submarine Mass Movements and Their Consequences: An Overview." *In Landslides and Disaster Risk Reduction*, edited by K. Sassa and P. Canuti, 115–142. Berlin, Germany: Springer. https://doi.org/10.1007/978-3-540-69970-5_6

Madabhushi, S. P. G. 2014. *Centrifuge Modelling for Civil Engineers*. Boca Raton, FL: CRC Press.

Madabhushi, S. P. G., S. K. Haigh, N. E. Houghton, and E. Gould. 2012. "Development of a Servo-hydraulic Earthquake Actuator for the Cambridge Turner Beam Centrifuge." *International Journal of Physical Modelling in Geotechnics* 12, no. 2 (June): 77–88. https://doi.org/10.1680/ijpmg.11.00013

McCullough, N., S. Dickenson, S. Schlechter, and J. Boland. 2007. "Centrifuge Seismic Modeling of Pile-Supported Wharves." *Geotechnical Testing Journal* 30, no. 5 (September): 349–359. https://doi.org/10.1520/GTJ14066

Nadim, F., G. Biscontin, and A. M. Kaynia. n.d. "Seismic Triggering of Submarine Slides." *Paper presented at the Offshore Technology Conference*, Houston, TX, April 30–May 3, 2007.

O'Leary, D. W. 1991. "Structure and Morphology of Submarine Slab Slides: Clues to Origin and Behaviour." *Marine Geotechnology* 10, nos. 1–2 (December): 53–69. https://doi.org/10.1080/10641199109379882

Oliveira, J. R. M. S., M. S. S. Almeida, H. P. G. Motta, and M. C. F. Almeida. 2011. "Influence of Penetration Rate on Penetrometer Resistance." *Journal of Geotechnical and Geoenvironmental Engineering* 137, no. 7 (July): 695–703. https://doi.org/10.1061/(ASCE)GT.1943-5606.0000480

Pestana, J. M. and F. Nadim. 2000. *Nonlinear Site Response Analysis of Submerged Slopes*, Technical Report UCB/GT/2000-04. Berkeley, CA: University of California, Berkeley.

Pirchiner, M., S. Drouet, M. Assumpção, J. Dourado, J. Ferreira, L. Vieira, and J. Juliá. n.d. "PSHAB: Probabilistic Seismic Hazard Analysis for Brazil: A National Hazard Map Building Effort." Paper presented at the 26th International Union of Geodesy and Geophysics General Assembly, Prague, Czech Republic, June 22-July 2, 2015.

Randolph, M. and S. Gourvenec. 2011. *Offshore Geotechnical Engineering*, 1 ed. Boca Raton, FL: CRC Press.

Rayhani, M. and M. H. El Naggar. 2007. "Centrifuge Modeling of Seismic Response of Layered Soft Clay." *Bulletin of Earthquake Engineering* 5, no. 4 (September): 571–589. https://doi.org/10.1007/s10518-007-9047-0

Rodríguez-Ochoa, R., F. Nadim, J. M. Cepeda, M. A. Hicks, and Z. Liu. 2015. "Hazard Analysis of Seismic Submarine Slope Instability." *Georisk: Assessment and Management of Risk for Engineered Systems and Geohazards* 9, no. 3 (August): 128–147. https://doi.org/10.1080/17499518.2015.1051546

Sathialingam, N. and B. Kutter. 1989. *The Effects of High Strain Rate and High Frequency Loading on Soil Behavior in Centrifuge Model Tests*, NCEL Contract Report CR 89.011. Port Hueneme, CA: Naval Civil Engineering Laboratory.

Sharma, J. S. and M. D. Bolton. 1996. "Centrifuge Modeling of an Embankment on Soft Clay Reinforced with Geogrid." *Geotextiles and Geomembranes* 14, no. 1 (January): 1–17. https://doi.org/10.1016/0266-1144(96)00003-9

Solheim, A., P. Bryn, H. P. Sejrup, J. Mienert, and K. Berg. 2005. "Ormen Lange—An Integrated Study for the Safe Development of a Deep-water Gas Field within the Storegga Slide Complex, NE Atlantic Continental Margin; Executive Summary." *Marine and Petroleum Geology* 22, nos. 1–2 (January/February): 1–9. https://doi.org/10.1016/j.marpetgeo.2004.10.001

Soriano, C., R. B. Andrade, S. Mollepaza, M. S. S. Almeida, M. C. F. Almeida, J. R. M. Oliveira, and P. Trejo. n.d. "Simulation of a Weak Layered Profile Using Geotechnical Centrifuge." *Paper presented at the XVI Pan-American Conference on Soil Mechanics and Geotechnical Engineering*, Cancun, Mexico, November 17–20, 2019.

Springman, S. M. "Lateral Loading on Piles due to Simulated Embankment Construction." PhD diss., Cambridge University, 1989.

Stewart, D. P. and M. F. Randolph. 1991. "A New Site Investigation Tool for the Centrifuge." In *Centrifuge 91: Proceedings of the International Conference on Centrifuge Modeling*. Boca Raton, FL: CRC Press, 531–538.

Taboada, V. M. and R. Dobry. 1998. "Centrifuge Modeling of Earthquake Induced Lateral Spreading in Sand." *Journal of Geotechnical and Geoenvironmental Engineering* 124, no. 12 (December): 1995–1206. https://doi.org/10.1061/(ASCE)1090-0241(1998)124:12(1195)

Tarazona, S. F. M., M. C. F. Almeida, A. Bretschneider, M. S. S. Almeida, S. Escoffier, and R. Garske. 2020. "Evaluation Of Seismic Site Response Of Submarine Clay Canyons Using Centrifuge Modelling." *International Journal of Physical Modelling in Geotechnics* 20, no. 4 (July): 224–238. https://doi.org/10.1680/jphmg.18.00084

Taylor, R. N. 1995. "Centrifuge Modelling: Principles and Scale Effects." In *Geotechnical Centrifuge Technology*, edited by R. N. Taylor. Boca Raton, FL: CRC Press, 19–33.

Tricarico, M., S. P. G. Madabhushi, and S. Aversa. 2016. "Centrifuge Modelling of Flexible Retaining Walls Subjected to Dynamic Loading." *Soil Dynamics and Earthquake Engineering* 88 (September): 297–306. https://doi.org/10.1016/j.soildyn.2016.06.013

Viggiani, G. and J. H. Atkinson. 1995. "Stiffness of Fine-grained Soil at Very Small Strains." *Geotechnique* 45, no. 2 (June): 249–265. https://doi.org/10.1680/geot.1995.45.2.249

White, D. J., C. Gaudin, and N. Boylan. 2010. "Interpretation of T-bar Penetrometer Tests at Shallow Embedment and in Very Soft Soils." *Canadian Geotechnical Journal* 47 (February): 218–219. https://doi.org/10.1139/T09-096

Williamson, M. "Tunnelling Effect on Bored Piles in Clay." PhD diss., University of Cambridge, 2014.

Wroth, C. P. 1984. "The Interpretation of In Situ Soil Tests." *Geotechnique* 34, no. 4 (December): 449–489. https://doi.org/10.1680/geot.1984.34.4.449

Zhang, C., D. White, and M. Randolph. 2011. "Centrifuge Modeling of the Cyclic Lateral Response of a Rigid Pile in Soft Clay." *Journal of Geotechnical and Geoenvironmental Engineering* 137, no. 7 (July): 717–729. https://doi.org/10.1061/(ASCE)GT.1943-5606.0000482

Zhou, Y.-G., J. Chen, Y.-M. Chen, B. L. Kutter, B.-L. Zheng, D. W. Wilson, M. E. Stringer, and E. C. Clukey. 2017a. "Centrifuge Modeling and Numerical Analysis on Seismic Site Response of Deep Offshore Clay Deposits." *Engineering Geology* 227 (September): 54–68. https://doi.org/10.1016/j.enggeo.2017.01.008

Zhou, Y.-G., J. Chen, Y. She, A. M. Kaynia, B. Huang, and Y.-M. Chen. 2017b. "Earthquake Response and Sliding Displacement of Submarine Sensitive Clay Slopes." *Engineering Geology* 227 (September): 69–83. https://doi.org/10.1016/j.enggeo.2017.05.004

Selection of earthquake ground motion accelerograms for the continental margin of Southeastern Brazil

Cristian Yair Soriano Camelo [a], Samuel Felipe Mollepaza Tarazona [a], Maria Cascão Ferreira de Almeida [b],
Márcio de Souza Soares de Almeida [a] & Ricardo Garske Borges [c]

[a] Graduate School of Engineering – COPPE/UFRJ, Río de Janeiro, Brazil. cysorianoc@coc.ufrj.br, samuelfelipe@coc.ufrj.br, almeida@coc.ufrj.br
[b] Polytechnic School of Engineering, – Poli /UFRJ, Río de Janeiro, Brazil. mariacascao@poli.ufrj.br
[c] Petrobras Research and Development Center – CENPES, Río de Janeiro, Brazil. ricardogarskeborges@gmail.com

Abstract

Brazil is in an intraplate area of low to moderate seismicity, this means that few or no records of strong ground motions are available. Part of the site response analysis and seismic design of structures require the use of acceleration time-histories compatible with a specified target response spectrum. This study aims to utilize methodologies based on the use of existing earthquake records from a well-known database and synthetic accelerograms to obtain ground motions representative of the Brazilian Southeast Region, particularly in the offshore Campos Basin. Information from a probabilistic seismic hazard assessment performed in the interest area was employed as input to the methodologies applied in terms of target response spectrum and the dominant earthquake scenarios. Besides, the acceleration time-histories of two relatively recent earthquakes that occurred in the Brazilian Southeast were used to apply one of the approaches to obtain a synthetic spectrum compatible accelerogram.

Keywords: artificial accelerograms; earthquake accelerogram; ground motion; spectral matching.

Selección de acelerogramas sísmicos para la margen continental de la región Sudeste de Brasil

Resumen

Brasil se encuentra en una región intra-placa de baja a moderada sismicidad, esto quiere decir que hay una limitada disponibilidad de registros de acelerogramas representativos de la región. Parte de un estudio de respuesta local o del diseño sísmico de estructuras requiere del uso de registros aceleración-tiempo que sean compatibles con un espectro de diseño. El presente trabajo tiene como objetivo la aplicación de metodologías para obtener acelerogramas representativos de la región sudeste brasilera, en particular en la región *offshore* de la cuenca de Campos. Se utilizó la información del análisis probabilístico del riesgo sísmico desarrollado para la región de interés en este estudio para obtener el espectro de respuesta de diseño y para definir los escenarios sísmicos que generan mayor influencia. Adicionalmente, se utilizó la información de acelerogramas registrados a partir de dos sismos relativamente recientes ocurridos en la región sudeste brasilera, para la aplicación de una de las metodologías de obtención de acelerogramas sintéticos.

Palabras clave: acelerogramas artificiales; acelerogramas; sismos; ajuste espectral.

1. Introduction

Brazil is in a large mid-plate region considered one of the least seismically active continental areas in the world. Earthquakes with maximum magnitudes 5 and above occur with a return period of 4 years [1]. This means that recordings of strong ground motions in the region are scarce. As alternative to obtain earthquakes to be applied in the seismic design of structures or site response analyses in such intraplate regions, different methodologies can be applied [32].

This paper aims to obtain a series of accelerograms representative of the earthquake scenarios in a region located

in Southeastern Brazil, specifically in the Campos Basin Continental Slope, offshore of the State of Rio de Janeiro. The dominant earthquake scenarios and mean uniform hazard spectra used in this work for the region of interest were developed by [5]. Three methodologies were employed to obtain spectrum-compatible accelerograms. The first approach consisted of the use of real accelerograms obtained from the Pacific Earthquake Engineering Research (PEER-NGA) database [58] and the application of spectral matching procedures. A second methodology of developing synthetic accelerograms generated from seismological source models [45,46]. And a third alternative, also based on synthetic accelerograms, using envelope shapes adjusted from real records of accelerograms in Brazil [3,57].

1.1 Seismic hazard in Southeastern Brazil

Based on the distribution of seismicity, the main active seismic areas in Brazil were delineated by [1] as follows: (1) Southern part of the Guyana shield and middle Amazon basin; (2) a North-South-trending zone along the Eastern border of the Amazon craton; (3) Northern part of the Borborena Province, in Northeastern Brazil around the Potiguar marginal basin; (4) the Porto dos Gauchos seismic zone; (5) a NE-SW zone in the Tocantins province possibly continuing towards the Pantanal Basin; (6) Southern Minas Gerais zone, in and around the southern tip of the São Francisco craton; and (7) the Southeast offshore zone with activity concentrated along the continental slope from the Pelotas Basin in the south to the Campos basin from 33°S to 20°S [2,3]. The Campos Basin represents an important pole in Brazilian economy and is one of the most prolific Brazilian oil-producing basins [4]. Given the importance of the Campos Basin, moderate seismicity in the oceanic portion of the Southeast region (magnitude 5 every 10-30 years and potential occurrences of magnitude up to 7) represent a hazard to the design of offshore infrastructure developments. The area of interest for the analyses presented in this work correspond to the continental margin of Southeastern Brazil. Specifically, the Campos Basin Continental Slope [6], offshore the state of Rio de Janeiro (Fig. 1).
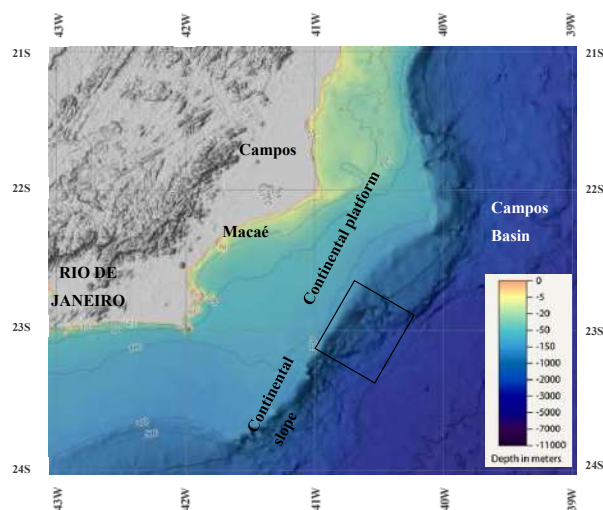
Two main sources of stress are associated in the seismicity pattern in the Brazilian Atlantic coast. A regional component of compressive stresses and a local component due to density contrast between continental/oceanic crusts and lithospheric flexure due to sediment load in the continental shelf [2]. The overall structural style in Campos Basin is detached, with a detachment surface at the base of the Aptian salt [7]. Below the detachment, the main structural features are horsts and grabens limited by steep normal faults [8,9]. The stress regime is variable with depth. Extensional regimes at depths of less than 1,500 m, transtensional regimes at depths ranging from 1,500 to 3,500 m, and strike-slip, for depths greater than 3,500 m [10].

1.2 Earthquake catalog

Brazilian earthquake data from historical and relatively recent instrumental records have been compiled through the earthquake catalog provided by the Seismology Center of the Institute of Astronomy Geophysics and Atmospheric Sciences of the University of São Paulo (IAG/USP). Further details on the earthquake catalog are presented [11]. Fig. 2 presents the location of the epicentres and magnitudes of the historical earthquakes covering a period from November 1720 to December 2019. It can be observed from Fig. 2 a concentration of epicenters in the Campos Basin, roughly across the continental slope [5].

2. Selection of earthquake ground motion accelerograms

For seismic hazard assessment, the definition of the ground motions represents a significant role. The most complete way to represent the ground motion is through seismograms that describe the variation with time of the accelerations, velocity, and displacements. It is usually displayed the variation of the accelerations with time (accelerogram), the velocities and displacements are obtained by integration.

Figure 1. Location of the site of interest (dark square).
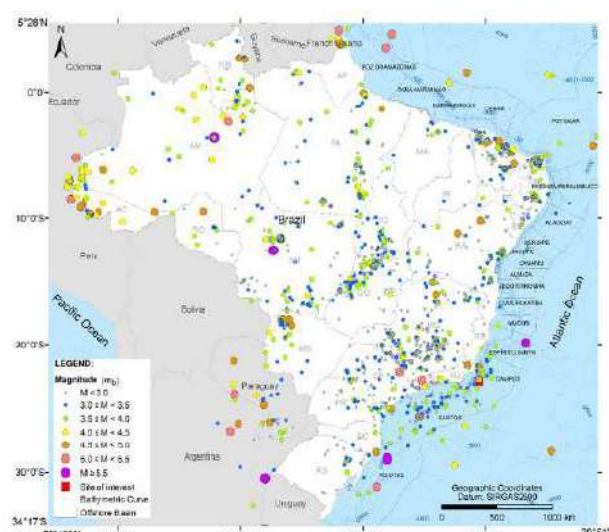Source: The authors.

Figure 2. Historical and instrumental seismic activity from 1720 to 2019.
Source: [5]

One common challenge of many intraplate regions is the limited amount of significant earthquake records due to the infrequent occurrence of these events. When two of the largest Brazilian earthquakes occurred in 1955 (m_b 6.2 on January 31 and m_b 6.1 on March 1) no Brazilian stations were operating [11]. Early instrumental data in the Brazilian earthquake catalog were obtained from international agencies (USGS and ISC) and using stations from other countries. Only in the late 1960s with the installation and in the 1970s instrumental records begin in earnest [12]. Further details related to the history of the seismological stations in Brazil can be found in [13]. The most recent boost in the seismological research in Brazil started in 2011 with the operation of the Brazilian Seismographic Network [11]. Given the scarcity of recorded accelerograms, an alternative to obtaining strong motion data consist of scaling and matching ground motions from other regions with local seismic hazard response spectra [14] or the generation of spectrum compatible accelerograms [15-18].

The accelerogram generation methods can be divided into the following categories: (1) deterministic methods, implementing a superposition of harmonic waves to match a target response spectrum [19]; (2) wavelet-based techniques [20-23]; (3) stochastic methods that consider the accelerogram as a Gaussian process [24-26]. In this work, three methodologies will be employed to obtain spectrum compatible ground motions. For the analyses, the Mean Uniform Hazard Response Spectra for the site of interest at the continental slope of the Campos Basin for a return period of 975 years was used as target spectrum (Fig. 3).

2.1 Method 1: seismic records from database

The first approach consisted of using recorded accelerograms from the Pacific Earthquake Engineering Research (PEER) Strong Motion Database. The PEER database consists of two databases: the NGA-East Ground Motion Database and the NGA-West Database [58]. The first constitutes the largest database of processed recorded ground motions in Stable Continental Regions (SRCs).
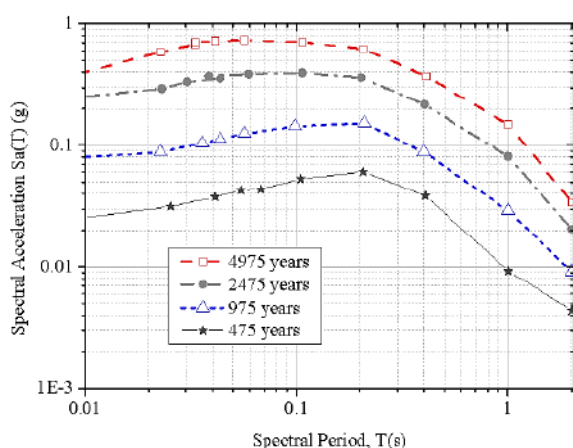

Figure 3. Uniform Hazard Response spectra for the site of interest at the continental slope of the Campos Basin for various return periods.
Source: Adapted from [5].

The second includes a very large set of ground motions recorded worldwide of shallow crustal earthquakes in active tectonic regimes. As Brazil is located within a stable continental intraplate region, it was considered at a first instance to use the NGA-East database. However, from the results of a preliminary search, no records satisfied the criteria discussed in the following section. Then, the NGA-West database was used. A similar approach was used for the selection of earthquake ground accelerograms in Hong Kong, also an intraplate area of low to moderate seismicity [14].

2.1.1 Search and selection criteria

The PEER web application allows the user to load a target spectrum and a series of criteria to select the earthquakes (magnitude, fault type, significant duration, distance to rupture plane, average shear wave velocity of top 30 meters' site, and pulse characteristics). The ground motions can also be adjusted to reduce the Mean Squared Error (MSE) and increase the match between the target and recorded (scaled) spectra. A maximum limit for the scale factor of 2.0 was defined for the records that satisfied the search criteria. This value for the scale factor of 2.0 was proposed by [27].

From a disaggregation analysis, it is possible to obtain the contribution of different earthquake scenarios at the site of interest. The parameters considered are the magnitude intervals and distance ranges [28-30]. The moment magnitude and the source-to-site distance are two variables commonly used in the selection of accelerograms. The most relevant geophysical parameter for the selection of records is earthquake magnitude, as it strongly influences frequency content and duration of the motion [31]. Regarding the source-to-site distance, these effects have not been clearly established. Boomer and Acevedo [32] proposed that, in performing the selection of real records, the search window based on the magnitude should be as narrow as possible, and in terms of the distance, the range can be extended. [31] recommended the selection of records from events within 0.25 units of the target magnitude. [33] proposed select the time series, using records within 0.5 magnitude units of the design earthquake. For the current analyses, a search window in the earthquake's magnitude of ±0.5 M_w was adopted, a similar range was used by [14]. The primary reason was that using a narrower search window yielded less or no results when consulting the records from the PEER-NGA East database.

For the area of interest at the offshore Campos Basin, the most significant contribution comes from magnitudes 4.5 to 5.1 M_w at distances between 40 and 100 km. Regarding large earthquakes (magnitudes up to 5.7 M_w) it was defined a contribution at distances up to 200 km [5]. There are few events accurately located in the Brazilian earthquake catalog, and the source-to-site distance estimated was at less than about 15 km. In addition, [2] reported an average distance of 10 km for oceanic source zones. Subsequently, the minimum distance used for the search criteria was reduced from 40 to 10 km. Given the stress regime in the Campos Basin, the failure mechanism considered reverse and normal faults, however, to include larger amplitude motions reverse and reverse/oblique faults were accounted in the search criteria. The target site rock condition of the uppermost 30 m of the earth crust ($v_{s,30}$) was defined for $v_{s,30}$ values higher than 800 m/s. With those criteria, three earthquake scenarios were defined, and the search parameters are shown in Table 1.

230

Table 1.
Parameters for the selection of accelerograms

Earthquake scenario	M_w=4.5	M_w=5.1	M_w=5.7
Distance, d (km)	10<d<100	10<d<100	d>100
Magnitude, M_w	4<M_w<5	4.5<M_w<6.0	5.2<M_w<6.2
$V_{s,30}$ (m/s)		> 800	
Fault type		Reverse, reverse/oblique/normal/strike slip	

Source: the authors

Table 2.
Accelerograms selected from PEER NGA-West 2 Ground Motion Database

Record Sequence number (RSN)	Event	Year	Station	Mag.
23	San Francisco	1957	Golden Gate Park	5.28
98	Hollister-03	1974	Gilroy Array #1	5.14
146	Coyote Lake	1979	Gilroy Array #1	5.74
643	Whittier Narrows-01	1987	LA - Wonderland Ave	5.99
680	Whittier Narrows-01	1987	Pasadena - CIT Kresge Lab	5.99
703	Whittier Narrows-01	1987	Vasquez Rocks Park	5.99
1649	Sierra Madre	1991	Vasquez Rocks Park	5.61
1709	Northridge-06	1994	LA - Griffith Park Observatory	5.28
1715	Northridge-06	1994	LA - Wonderland Ave	5.28
4083	Parkfield-02, CA	2004	Parkfield - Turkey Flat #1	6
4312	Umbria-03, Italy	1984	Gubbio	5.6
2805	Chi-Chi, Taiwan-04	1999	KAU003	6.2

Source: the authors

Table 3.
Accelerograms selected from PEER NGA-West 2 Ground Motion Database (part 2)

Record Sequence number (RSN)	Mechanism	Rrup(km)	Vs30(m/s)	Scale Factor
23	Reverse	11.0	874.7	0.90
98	strike slip	10.5	1428.1	1.24
146	strike slip	10.7	1428.1	0.60
643	Reverse Oblique	27.6	1222.5	1.49
680	Reverse Oblique	18.1	969.1	0.55
703	Reverse Oblique	50.4	996.4	1.36
1649	Reverse	39.8	996.4	1.17
1709	Reverse	21.7	1015.9	1.34
1715	Reverse	17.1	1222.5	1.91
4083	strike slip	5.3	907.0	0.29
4312	Normal	15.7	922.0	0.99
2805	strike slip	116.2	913.8	3.70

Source: the authors

The search results are shown in Table 2, 3, a total of twelve records were found. The response spectra of the scaled ground motions are presented in Fig. 4 including the geometric mean of the results. The process of searching and scaling the accelerograms returned a series of results that on average are compatible with the target response spectrum.

From Fig. 4, it can be observed that the scaled records either exceed or are equal to the design spectra only over a certain period range. In addition, the second part of the

application of the methodology consists of modifying the time series and makes them compatible with the target response spectra at all spectral periods is the spectral matching. The use of spectrum compatible time series for the seismic design of structures has been discussed by [33]. On one hand, spectrum compatible time series represent more than one earthquake and may be considered unrealistic when compared to typical earthquake response spectra. On the other hand, spectrum compatible time series has the advantage to reduce the number of time series necessary for an Engineering analysis [34], and the variability in spectral amplitude is considerably shortened.

Various methodologies have been proposed to obtain spectrum compatible time series [56,35,37-39]. Three basic approaches for spectral matching have been adopted in the different methods [33]: frequency-domain method, frequency-domain method with Random Vibration Theory (RVT), and time-domain method. The third approach is generally more complicated, however, produces a good convergence [40,41]. [42] implemented in RSPMatch program the Lilahanand and Tseng algorithm, a method based on the spectral matching in the time-domain. The adjustment wavelets used, however, produced drifts in the displacement and velocity time series and baseline corrections were required. The method was revised by [43] using new wavelets, to eliminate the drift in the adjustment wavelets to produce time series that do not require baseline correction.

The methodology applied in the current work and implemented in the software SeismoMatch [22] used the wavelets algorithm proposed by [33]. It has the advantage of matching the pseudo-acceleration response spectra of the time series with the target spectra, it does not introduce additional energy into the ground motion, preserves the characteristics of the original ground motion and eliminates the drift in the velocity and displacement time series.

As an example of the matching process in terms of the target response spectra, Fourier spectra, and Arias intensity, two earthquakes from Table 2 were selected. Arias Intensity (energy content) was included in the comparison of the
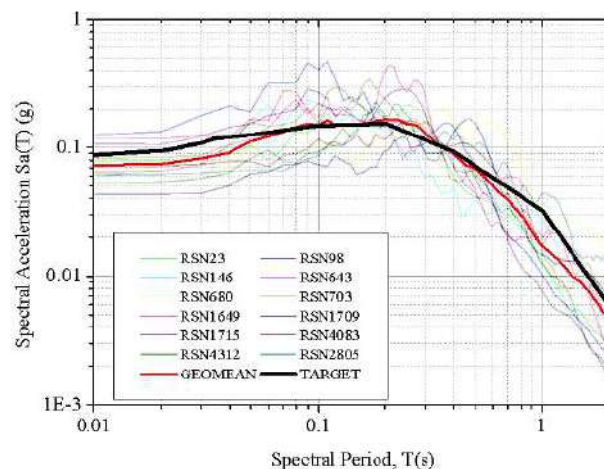

Figure 4. 5% response spectra for the scaled accelerograms and target spectra.
Source: the authors.

matched records, considering its importance in seismic hazard analysis [44]. Fig. 5 shows the acceleration time-histories, Fourier spectra and Arias Intensities of the recorded and matched time series of earthquakes RSN 23 and RSN 4803. The Fourier amplitude maintains the characteristics of the initial time series. In addition, a good agreement was observed between the normalized Arias intensities of the initial (measured) and the modified (spectrally matched) time series. The same procedure was employed for all the records shown in Tables 2,3 and the spectral matching results are presented in Fig. 6.

From this methodology, it can be stated that nowadays it is relatively straightforward to have access to extensive databases of real strong-motion records. And the criteria for selecting the records are available in the literature [32] to obtain results representative of the seismicity of the area of interest. The spectrum compatible accelerograms obtained presented a satisfactory agreement also in terms of the frequency content and energy when compared to the original records.

2.2 Method 2: synthetic accelerograms

The second alternative consisted of the generation of artificial accelerograms based on the adaptation of a random process to a target spectrum. One of the most complete methodologies for obtaining ground motions is the specific barrier model developed by [45,46]. The model has been implemented and calibrated with extended databases of response spectral amplitudes from earthquakes of intraplate areas, interplate regions and regions of tectonic extension [47]. The advantage of this model is the use of relatively few parameters to generate records: (1) tectonic regime, (2) magnitude, (3) distance, and (4) soil/rock type. The method has been implemented

Figure 6. Response spectra of matched accelerograms.
Source: the authors.

in the software SeismoArtif [48], in which the generation of the synthetic accelerogram starts from a Gaussian white noise that is multiplied by the [49] envelope shape and then adapted to a target spectrum using the Fourier Transform Method [50].

Fig. 7 presents a comparison between the Peak Ground Accelerations (PGA) obtained from the synthetic accelerograms versus distance and the curve obtained from the Ground Motion Prediction Equation (GMPE) developed by [51] and modified by [52], for the stable continental region in Central and Eastern North America (curve for a scaling factor equal to 1.00 in Fig. 7). Considering that Brazil is in an intraplate setting of low attenuation, [5] adopted [51] and [52] GMPE for the probabilistic hazard assessment in the continental margin of Southeastern Brazil. Additional curves were generated using Scaling Factors (SF) to cover the range of possible seismic attenuation in Brazil (SF = 0.4, 0.75, 1.00, 1.33). From Fig. 7, it can be observed a good agreement in terms of the PGA values obtained from the synthetic accelerograms and the curves obtained from GMPE.
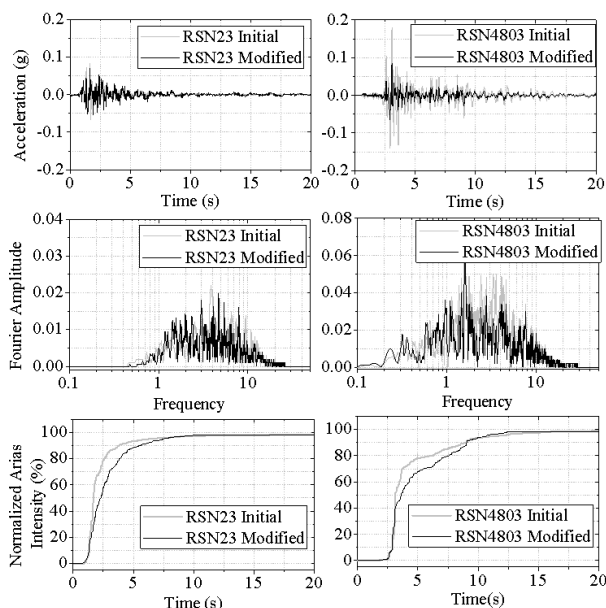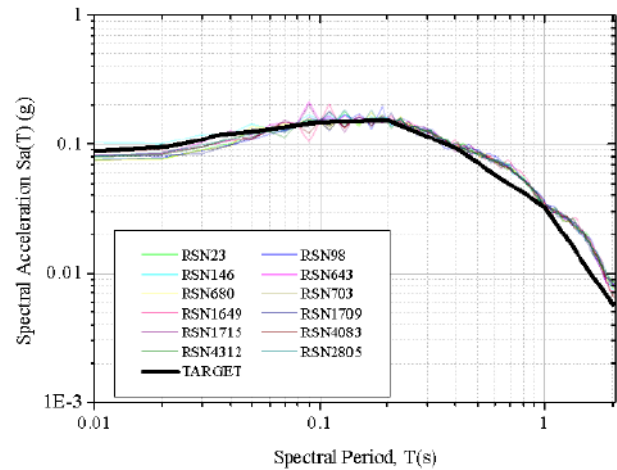

Figure 5. Example of matched accelerograms: acceleration time-histories, Fourier amplitude and normalized Arias intensity.
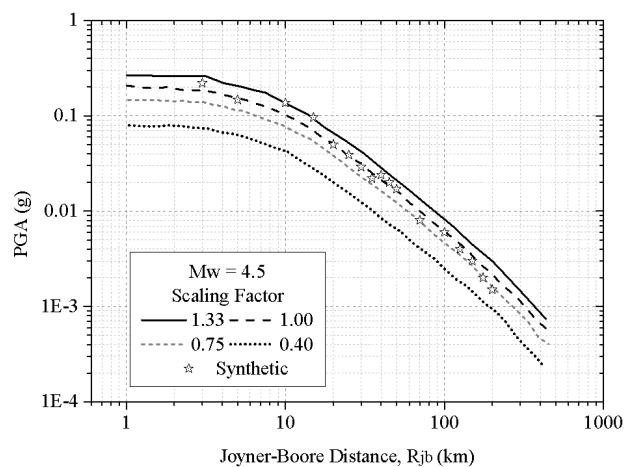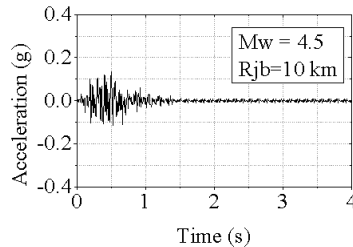Source: the authors

Figure 7. Peak Ground Accelerations with distance: comparison between GMPE and synthetic accelerograms for a 4.5 M_w earthquake.
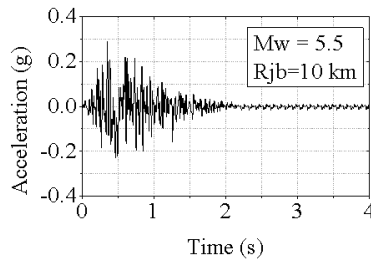Source: the authors.

232

Table 4.
Earthquake scenarios for the generation of synthetic accelerograms

Earthquake Scenario	M_w=4.5	M_w=5.1	M_w=5.7
Distance (km)	10,50,100	10,50,100	100,200,400
Soil category		Very hard rock	
Regime		Intraplate	

Source: the authors

Figure 8. Example of a synthetic accelerogram using the specific barrier model (Mw=4.5).
Source: the authors.

Figure 9. Example of a synthetic accelerograms using the specific barrier model (Mw=5.5).
Source: the authors.

A series of artificial accelerograms were obtained using the criteria of the disaggregation analysis for earthquake scenarios as presented in Tables 1 and 4 presents in detail the criteria adopted for the generation of the synthetic accelerograms. Figs. 8 and 9 show examples of synthetic acceleration time-histories for two earthquakes of magnitudes 4.5 and 5.5 M_w, for a rupture distance of 10 km.
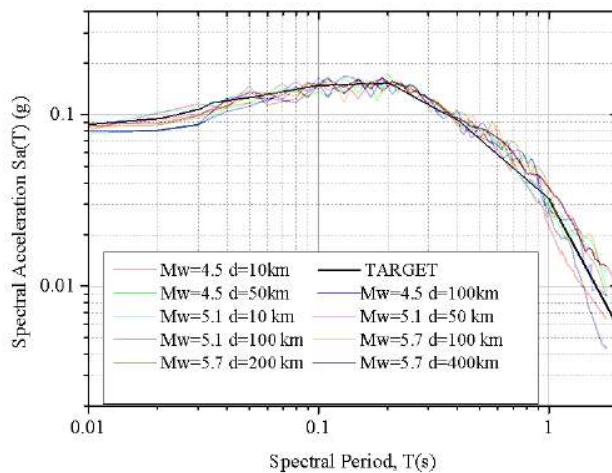

Figure 10. Response spectra of matched synthetic accelerograms.
Source: the authors.

Once obtained the synthetic accelerograms, the following stage consisted of performing a spectral matching based on the target spectra. The results are presented in Fig. 10. The algorithm was able to converge for all the synthetic accelerograms with slight variations for periods larger than one second.

2.3 Method 3: synthetic accelerograms using shape functions

A third approach to obtain synthetic accelerograms consisted of modifying a starting random process using an envelope shape [53-55,49] and a Power Spectral Density Function (PDSF). The method was proposed by [56], and it starts with the generation of steady-state motions (sinusoidal waves) with phase angles in the interval (0, 2π) and amplitudes given by the PSDF (eq. 1).

$$a(t) = q(t) \sum_{i=1}^{n} A_i \sin(\omega_i t + \Phi_i) \qquad (1)$$

Where $q(t)$ is an envelope shape (or intensity function) that allows to resemble a real accelerogram; A_i, ω_i and Φ_i are respectively the amplitude, frequency, and the phase angle if the i_{th} sinusoidal wave. The generated ground motion is adapted to the target response spectrum using the Fourier Transform Method.

For the current analysis, it was adjusted an exponential envelope shape [54] defined by three parameters: duration, constants that modify the shape of the envelope (α and β) and a parameter (A) that is function of the α and β coefficients. Fig. 11 shows a representation of the envelope shape and the parameters involved in the calculation.

Given the lack of earthquake records in the continental margin of Southeastern Brazil by Ocean Bottom Seismometers (OBS's), two earthquakes of particular interest were selected to obtain measured envelope shapes. The first earthquake selected occurred on May 19th, 2012, in the town of Montes Claros, Brazil, a region in which seismicity is not a recent occurrence [57]. The second earthquake occurred on April 23rd, 2008, 125 km South of the city of São Vicente, on the coast of São Paulo State. Both earthquakes were recorded by many stations of the Brazilian seismic network
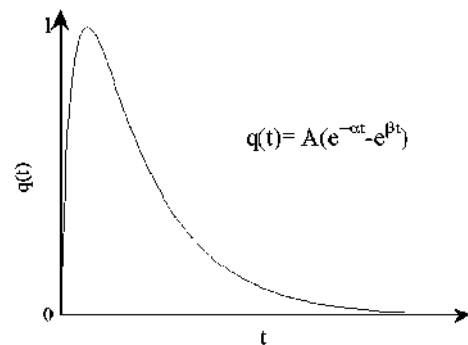

Figure 11. Envelope shape definition.
Source: the authors

233

Table 5.
Earthquakes recorded in Southeastern Brazil.

Earthquake			Epicenter		
Earthquake	Date	Magnitude (Mw)	Latitude	Longitude	Focal depth (km)
Montes Claros	19/12/2012	3.2	-16.69	-43.87	1.4
São Vicente	23/04/2008	5.6	-25.7	-45.41	17

Source: the authors

Table6.
Earthquakes and stations that recorded the events.

Earthquake			Station		
Earthquake	Date	Magnitude (Mw)	Station	Latitude	Longitude
Montes Claros	19/12/2012	3.2	MCI9-BL	-16.7	-43.89
São Vicente	23/04/2008	5.6	ESAR-BL	-23.02	-44.44

Source: the authors

and well-detailed information about the mentioned seismic events was presented by [3] and [57]. Tables 5 and 6 show information about the selected events and the location of the stations that registered the accelerograms used for the analysis.

Figs. 12 and 13 present the acceleration time-histories and the associated envelope shapes of the recorded motions. It can be observed that low accelerations were recorded from the São Vicente earthquake, this is due to the distance between the station and the epicenter (around 313.8 km). The Montes Claros earthquake, on the other hand, was recorded by a station located at 1.44 km of the epicenter, then, relatively higher accelerations can be observed.

Using the envelope shapes of the two recorded accelerograms, the coefficients α and β were defined to match an approximate envelope shape for the generation of the synthetic accelerogram (Fig. 14). The synthetic accelerogram and the response spectra are shown in Fig. 15.

Figure 13. Recorded earthquakes and envelope shapes: Montes Claros (2012) earthquake.
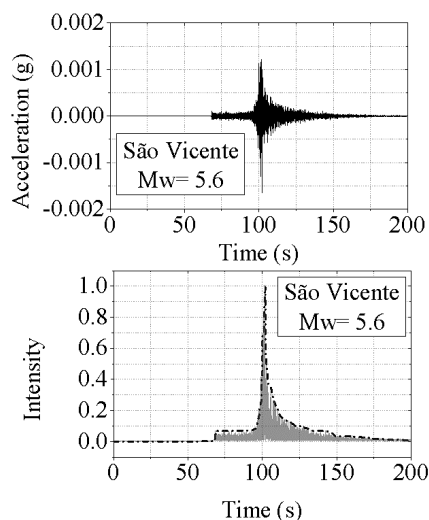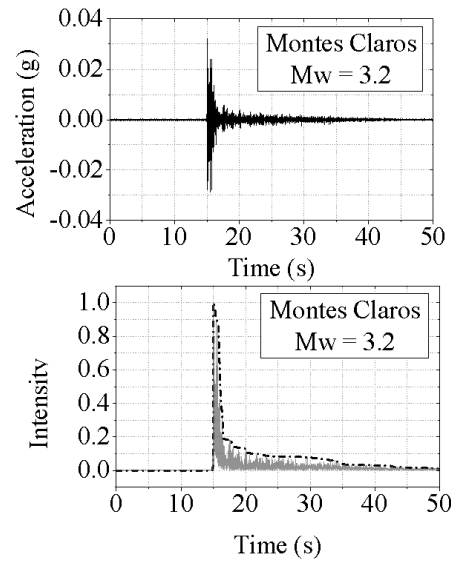Source: the authors.

Figure 14. Adjusted envelope shape.
Source: the authors.

Figure 12. Recorded earthquakes and envelope shapes: São Vicente (2008) earthquake.
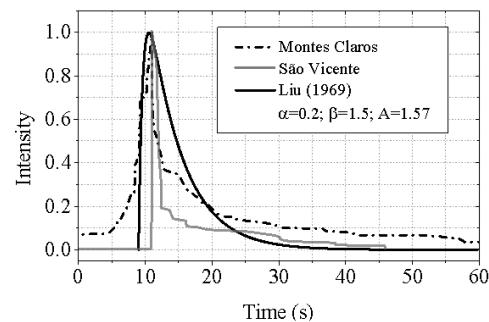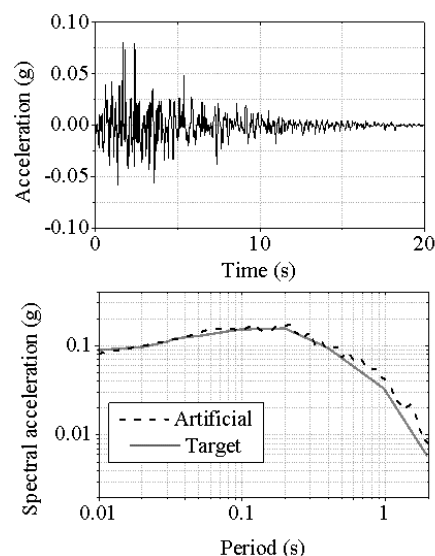Source: the authors.

Figure 15. Artificial accelerogram using the adjusted envelope shape.
Source: the authors.

234

3. Conclusions

This study presented three approaches to acquire spectrum-compatible accelerograms aimed to be applied for site response analyses or seismic design of structures in an area located in the Southeast region Brazil, specifically in the offshore Campos Basin. The first method presented, based on real accelerograms enables the obtention of accelerograms that are spectrum and energy-compatible accelerograms when compared with the historical records obtained from the PEER-NGA database. The second approach, based on seismological characteristics of the zone of interest, produced a good agreement in terms of Peak Ground Accelerations with distance obtained from the GMPE adopted for a stable continental region in Central and Eastern North America and adapted for the continental margin of Southeastern Brazil. The third alternative presented used information from real records in Southeastern Brazil, and well documented in the literature [3,57], to generate a synthetic accelerogram utilizing an adjusted shape function to capture the characteristics of real ground motions.

Further analyses can be performed in the future with more data from earthquakes that occurred in Brazil: to refine the parameters for the generation of synthetic accelerograms or to adjust real records compatible also with the energy and frequency content.

Acknowledgements

References

[1] Assumpção, M., Ferreira, J., Barros, L., Bezerra, H., França, G., Barbosa, J. and Dourado, E., Intraplate seismicity in Brazil. In: Talwani, P., Ed., Intraplate Earthquakes Cambridge University Press., Cambridge, U.K., 2014, pp. 50-71. DOI: 10.1017/CBO9781139628921.004.

[2] Assumpção, M., Seismicity and stresses in the Brazilian passive margin. Bull Seismol Soc Am., 88(1), pp. 160-169, 1998a.

[3] Assumpção, M., Dourado, J.C., Ribotta, L.C., Mohriak, W.U., Dias, F.L. and Barbosa, J.R., The São Vicente earthquake of 2008 April and seismicity in the continental shelf off SE Brazil: further evidence for flexural stresses. Geophys J. Int., 187(3), pp. 1076-1088, 2011. DOI: 10.1111/j.1365-246X.2011.05198.x.

[4] Cobbold, P.R, Meisling, K.E. and Mount, Van.S., Reactivation of an obliquely rifted margin, Campos and Santos Basins, Southeastern Brazil. AAPG Bulletin, 85(11), pp. 1925-1944, 2001. DOI: 10.1306/8626D0B3-173B-11D7-8645000102C1865D.

[5] Borges, R.G., Assumpçao, M.S., Almeida, M.C.F., Almeida. and M.S.S., Seismicity and seismic hazard in the continental margin of southeastern Brazil, J. Seismol., 24, pp. 1205-1224, 2020. DOI: 10.1007/s10950-020-09941-4.

[6] Amante, C. and Eakins B.W., ETOPO1 1 Arc-minute global relief model: procedures, data sources and analysis. NOAA Technical Memorandum NESDIS NGDC-24. National Geophysical Data Center, NOAA, 2009. DOI: 10.7289/V5C8276M

[7] Fetter, M., The role of basement tectonic reactivation on the structural evolution of Campos Basin, offshore Brazil: evidence from 3D seismic analysis and section restoration. Marine and Petroleum Geology, 26, pp. 873-886, 2009. DOI: 10.1016/j.marpetgeo.2008.06.005.

[8] Dias, J.L., Scarton, J.C., Guardado, L.R., Esteves, F.R. and Carminatti, M., Aspectos da evolução tectono-sedimentar e da ocorrência de hidrocarbonetos na Bacia de Campos. In: Raja-Gabaglia, G.P., Milani, E.J., Eds., Origem e Evolução de Bacias Sedimentares. Petrobras, Rio de Janeiro, 1990, pp. 333-360.

[9] Chang, H.K., Kowsmann, R.O., Figueiredo, A.M.F. and Bender, A.A., Tectonics and stratigraphy of the East Brazil Rift system: an overview.

Tectonophysics, 213, pp. 97-138, 1992. DOI: 10.1016/0040-1951(92)90253-3

[10] Lima-Neto F.F. and Beneduzi, C., Using leakoff tests and acoustic logging to estimate insitu stresses at deep waters - Campos Basin. Extended Abstracts Volume, in: American Association of Petroleum Geologists International Conference & Exhibition, Rio de Janeiro, Brazil, 1998, pp. 224-225.

[11] Bianchi, M.B., Assumpção, M., Rocha, M.P., Carvalho, J.M., Azevedo, P.A., Fontes, S.L., Dias, F.L., Ferreira, J.M., Nascimento, A.F., Ferreira, M.V. and Costa, I.S.L., The Brazilian seismographic network (RSBR): improving seismic monitoring in Brazil. Seismol. Res. Lett., 89(2A), pp. 452-457, 2018. DOI: 10.1785 /0220170227

[12] Almeida, A.A.D., Assumpção, M., Bommer, J.J., Drouet, S., Riccomini, C. and Prates, C.L.M., Probabilistic seismic hazard analysis for a nuclear power plant site in southeast Brazil, J. Seismol., 23, pp. 1-23, 2019. DOI: 10.1007/s10950-018-9755-8.

[13] Bianchi, M., Assumpção, M., Detzel, H., Carvalho, J.M., Rocha, M.P., Drouet, S., Fontes, S., Ferreira, J., Nascimento, M.A. and Veloso, J.A.V., The Brazilian seismographic network: historical overview and current status. Bull. Int. Seismol., Cent. 49, (1/6), pp. 70-90, 2015. DOI: 10.5281/zenodo.998851

[14] Yi, J., Lam, N., Tsang, H.-H. and Au, F.T., Selection of earthquake ground motion accelerograms for structural design in Hong Kong. Advances in Structural Engineering, 23(10), pp. 2044-2056, 2020. DOI: 10.1177/1369433220906926

[15] Ahmadi G., Generation of artificial time-histories compatible with given response spectra: a review. SM Arch., 4(3), pp. 207-239, 1979.

[16] Lam, N., Wilson, J. and Hutchinson, G., Generation of synthetic earthquake accelerograms using seismological modelling: a review. Journal of Earthquake Engineering, 4(3), pp. 321-354. DOI: 10.1080/13632460009350374

[17] Iervolino I. and Cornell, A.C., Record selection for nonlinear seismic analysis of structures. Earthq Spectra, 21(3), pp. 685-713, 2005. DOI: 10.1193/1.1990199

[18] Ferreira, F., Moutinho, C., Cunha, Á. and Caetano, E., An artificial accelerogram generator code written in Matlab. Engineering Reports, 2(3), art. e12129, 2020. DOI: 10.1002/eng2.12129

[19] Barenberg, M.E., Inelastic response of a spectrum-compatible artificial accelerogram. Earthq Spectra., 5(3), pp.477-493, 1989. DOI: 10.1193/1.1585536

[20] Giaralis, A. and Spanos, P.D., Wavelets based response spectrum compatible synthesis of accelerograms - Eurocode application (EC8). Soil Dyn. Earthq. Eng., 29, pp. 219-235, 2009. DOI: 10.1016/j.soildyn.2007.12.002

[21] Hancock, J., Watson-Lamprey, J. and Abrahamson, N.A., An improved method of matching response spectra of recorded earthquake ground motion using wavelets. J. Earthq. Eng., 10, pp. 67-89, 2006. DOI: 10.1080/13632460609350629

[22] Seismosoft. SeismoMatch - A computer program for generation of artificial accelerograms, [online]. 2020. Available at: https://seismosoft.com/

[23] Mukherjee, S. and Gupta, V., Wavelet-based characterization of design ground motions. Earthquake Engineering & Structural Dynamics. 31, pp. 1173-1190, 2002. DOI: 10.1002/eqe.155.

[24] Vanmarcke, E.H. and Gasparini, D.A., Simulated earthquake groundmotions. Proceedings of the 4th International Conference on SMIRT, K1/9, San Francisco, CA, USA, 1977.

[25] Taylor, C.A., EQSIM. A program for generating spectrum compatible earthquake ground acceleration time histories. Reference Manual. Bristol Earthquake Engineering Data Acquisition and Processing System, UK, 1989.

[26] Cacciola, P., A stochastic approach for generating spectrum compatible fully nonstationary earthquakes. Comput Struct, 88, pp. 889-901, 2010. DOI: 10.1016/j.compstruc.2010.04.009.

[27] Vanmarcke, E.H., Representation of earthquake ground motion: scaled accelerograms and equivalent response spectra, State-of-the-art for assessing earthquake hazards in the United States, Report 14, Miscellaneous Paper, S-73-1. US Army Corps of Engineers, Vicksburg, Mississippi, USA, 1979.

[28] Kramer, S.L., Geotechnical earthquake engineering. Prentice-Hall, New Jersey, USA, 1996.

[29] Bazzurro, P. and Cornell, C.A., Disaggregation of seismic hazard. Bull Seismol. Soc. Am., 89(2), pp. 501-520, 1999.

[30] Abrahamson, N.A., State of the practice of seismic hazard evaluation. In: Paper presented at the International Society for Rock Mechanics and Rock Engineering Symposium, Melbourne, Australia, November 19-24, 2000.

[31] Stewart, J.P., Chiou, S.-J., Bray, J.D., Graves, R.W., Somerville, P.G. and Abrahamson, N.A., Ground motion evaluation procedures for performance-based design, PEER Report 2001/09, Pacifc Earthquake Engineering Research Center, University of California, Berkeley, USA, 2001.

[32] Bommer, J.J. and Acevedo, A.B., The use of real earthquake accelerograms as input to dynamic analysis. Journal of Earthquake Engineering, 8(1), pp. 43-91, 2004. DOI: 10.1080/13632460409350521

[33] Al-Atik, L. and Abrahamson, N., An improved method for nonstationary spectral matching. Earthquake Spectra, 26(3), pp.601-617, 2010. DOI: 10.1193/1.3459159

[34] Bazzurro, P. and Luco, N., Do scaled and spectrum-matched near-source records produce biased nonlinear structural responses? In: Proc. of the 8th U.S. National Conf. on Earthquake Engin., San Francisco, California, USA, 2006.

[35] Kaul, M.K., Spectrum-consistent time-history generation, ASCE J. Eng. Mech. EM4, pp.781-788, 1978. DOI: 0.1061/JMCEA3.0002379

[36] Gasparini, D.A. and Vanmarcke, E H., Simulated earthquake motions compatible with prescribed response spectra, Evaluation of Seismic Safety of Buildings Report No. 2, Department of Civil Engineering, MIT, Cambridge, Massachusetts, USA, 1979.

[37] Iyengar, R.N, and Rao, P., Generation of spectrum compatible accelerograms. Earthq. Eng. Struct. Dyn., 7(3), pp. 253-263, 1979. DOI: 10.1002/eqe.4290070305

[38] Cacciola, P., Colajanni, P. and Muscolino, G., Combination of modal responses consistent with seismic input representation. J. Struct. Eng., 130(1), 2004. DOI: 10.1061/(ASCE)0733-9445(2004)130:1(47)

[39] Zentner, I. and Poirion, F., Enrichment of seismic ground motion databases using Karhunen-Loe`ve expansion. Earthq. Eng. Struct. Dyn., 41(14), pp. 1945-1957, 2012. DOI: 10.1002/eqe.2166

[40] Lilhanand, K. and Tseng, W.S., Generation of synthetic time histories compatible with multiple-damping response spectra, SMiRT-9, Lausanne, K2/10, 1987.

[41] Lilhanand, K. and Tseng, W.S., Development and application of realistic earthquake time histories compatible with multiple damping response spectra, in: Ninth World Conf. Earth. Engin., Tokyo, Japan, (2), 1988, pp. 819-824.

[42] Abrahamson, N.A., Non-stationary spectral matching, Seismol. Res. Lett., 63, art. 30, 1992.

[43] Hancock, J., Watson-Lamprey, J., Abrahamson, N.A., Bommer, J.J., Markatis, A., McCoy, E. and Mendis, R., An improved method of matching response spectra of recorded earthquake ground motion using wavelets, J. Earthquake Eng., 10, pp. 67-89, 2006. DOI: 10.1080/13632460609350629

[44] Stafford, P.J., Berrill, J.B. and Pettinga, J.R., New predictive equations for Arias intensity from crustal earthquakes in New Zealand. J Seismol., 13(1), pp. 31-52, 2009a. DOI: 10.1007/s10950-008-9114-2

[45] Papageorgiou, A.S. and Aki, K., A Specific barrier model for the quantitative description of inhomogeneous faulting and the prediction of strong ground motion. Description of the model, Bull. Seism. Soc. Am., 73, pp. 693-722, 1983a.

[46] Papageorgiou, A.S. and Aki, K., Scaling law of far-field spectra based on observed parameters of the specific barrier model. PAGEOPH 123, pp. 353-374 ,1985. DOI: 10.1007/BF00880736

[47] Hallodorsson, B. and Papageorgiou, A.S., Calibration of the specific barrier model to earthquakes of different tectonic regions Bull. Seismol. Soc. Am., 95(4), pp. 1276-1300, 2005. DOI: 10.1785/0120040157.

[48] Seismosoft. SeismoArtif - A computer program for generation of artificial accelerograms, [online]. 2020. Available at: https://seismosoft.com/

[49] Saragoni, G.R. and Hart, G.C., Simulation of artificial earthquakes. Earthq. Eng. Struct. Dyn., 2(3), pp.249-267, 1974. DOI: 10.1002/eqe.4290020305.

[50] Mucciarelli, M., Masi A., Gallipoli, M.R., Harabaglia, P., Vona, M., Ponzo, F. and Dolce, M., Analysis of RC building dynamic response and soil-building resonance based on data recorded during a damaging earthquake. Bull. Seismol. Soc. Am., 94(5), pp.1943-1953, 2004. DOI: 10.1785/012003186.

[51] Toro, G.R., Abrahamson, N.A. and Schneider, J.F., Model of strong ground motions from earthquakes in central and eastern North America: best estimates and uncertainties Seismological Research Letters, 68(1), pp. 41-57, 1997. DOI: 10.1785/gssrl.68.1.41.

[52] Toro, G.R., Modification of the Toro et al. (1997) attenuation equations for large magnitudes and short distances. Risk Engineering, Inc.,2002.

[53] Hou, S., Earthquake simulation models and their applications. Tech. Rep., Department of civil engineering, Massachusetts Institute of Technology, USA, 1968.

[54] Liu, S.C., Autocorrelation, and power spectral density functions of the parkfield earthquake of june 27, 1966. Bull Seismol. Soc. Am., 59(4), pp.1475-1493, 1969.

[55] Jennings, P.C., Housner, G.W. and Tsai, N.C., Simulated earthquake motions. Tech. Rep., EERL California Institute of Technology, USA, 1968.

[56] Gasparini, D.A. and Vanmarcke, E.H., Simulated earthquake motions compatible with prescribed response spectra. Research Report R76-4. Department of Civil Engineering, Massachusetts Institute of Technology, Cambridge, MA, USA, 1976.

[57] Agurto-Detzel, H., Assumpção, M., Ciardelli, C., Farrapo, D., Barros, L.V. and França, G., The 2012-2013 Montes Claros earthquake series in the São Francisco Craton, Brazil: new evidence for non-uniform intraplate stresses in mid-plate South America, Geophysical Journal International, 200(1), pp. 216-226, 2015. DOI: 10.1093/gji/ggu333.

[58] Ancheta, T.D., Darragh, R.B., Stewart, J.P., Seyhan, E., Silva, W.J., Chiou, B.S.-J., Wooddell, K.E., Graves, R.W., Kottke, A.R., Boore, D.M., Kishida, T. and Donahue, J.L., NGA-West2 Database. Earthquake Spectra, 30(3), pp. 989-1005, 2014. DOI: 10.1193/070913EQS197M

C. Soriano, received the BSc. Eng. in Civil Engineering in 2011 from the Universidad Nacional de Colombia, Bogotá, Colombia. He also holds a MSc. in Civil Engineering from the Graduate School of Engineering of the Federal University of Rio de Janeiro, Brazil. Currently, he is a DSc. student in Civil Engineering with emphasis in Geotechnical Engineering at the Graduate School of Engineering of the Federal University of Rio de Janeiro, Brazil.
ORCID: 0000-0001-9530-0185

S. Tarazona, graduated in 2007 from Universidad Católica de Santa María in Peru. He holds a MSc. in Civil Engineering from the Pontifical Catholic University of Rio de Janeiro Brazil, and a DSc. from Graduate School of Engineering of the Federal University of Rio de Janeiro, Brazil. Currently, he is a researcher at COPPE/UFRJ Multidisciplinary Centrifuge Modeling Laboratory (LM²C) with interests related to the identification of the static and dynamic liquefaction triggers of tailings dams.
ORCID: 0000-0001-5268-6487

M.C.F. Almeida, has a BSc. Eng. in Civil Engineering and Structures from the Federal University of Rio de Janeiro, Brazil, in 1975, a MSc. in Civil Engineering Structures from the Polytechnic of Central London, U.K., in 1984, and a PhD. in Civil Engineering Structures from UFRJ, Brazil, in 1997. She is currently an adjunct professor 3 from UFRJ, Brazil. She has experience in the field of civil engineering, with emphasis on static and dynamic structural analysis, acting mainly on the following themes: structural analysis, cracking, reinforced concrete, soil-structure interaction, seismic analysis, seismic risk analysis with Brazilian data, and technical standards.
ORCID: 0000-0002-3133-6098

M.S.S. Almeida, is currently a full professor in geotechnical engineering at COPPE-UFRJ in Brazil. He did his undergraduate study in 1974 at the Civil Engineering Department of the School of Engineering, Federal University of Rio de Janeiro; and his MSc. from the same university in 1977. Prof. Almeida obtained his PhD. from Cambridge University, U.K., on stage constructed embankment in soft clays. He was a visiting researcher in many universities: Oxford University (1986-1989); Cambridge University (1993-1996); University of Western Australia (2002); LCPC, France (2011), and ETH, Switzerland (2012). He was also a postdoctoral research fellow at ISMES, Italy and NGI, Oslo, Norway in 1991-1992.
ORCID: 0000-0003-2230-397X

R.G. Borges, is BSc. in 2001 from the Lutheran University of Brazil. He holds MSc and DSc degrees in Civil Engineering from the Federal University of Rio de Janeiro, Brazil. He is currently a researcher at the Petrobras Research and Development Center (CENPES). He has experience in the fields of seismic hazards, soil-structure interaction, submarine slope stability physical modelling in geotechnical centrifuge, and salt rock Geomechanics.
ORCID: 0000-0001-7623-0337